Measuring adhesion between particles

Jiankai Yang

Department of Chemical and Biological Engineering

The University of Sheffield

PhD Thesis

March 2018

Submitted in partial fulfilment for the DPhil degree

Under the supervision of:

Prof. Agba D. Salman

Prof. Michael J. Hounslow

Abstract

Given that catalyst layer is used to carry automotive catalysts in catalytic converters, the strength of a catalyst layer is important for the durability of catalytic converters. However catalyst layer in service is found to suffer from both cohesive and adhesive failure for which the current literature does not have separate method of strength measurement. This thesis then developed methods to separately measure the cohesive and the adhesive strength of a catalytic layer (made of γ-alumina particles) based on the unit of stress. Measurement of the cohesive strength was based on tensile strength of a tablet made of the same material as the catalyst layer; the adhesive strength was determined from a scraping technique.

The cohesive strength obtained was found to vary with particle size, pH of suspension and drying rate of the suspension. A bimodal particle size distribution was found to improve the cohesive strength due to tighter particle packing. A combination of free movement for particles and longer exposure to a drying environment was also found to improve the cohesive strength. The underlying reason was determined to be in close agreement with the DLVO theory. At very high pHs, it was believed that γ-alumina particles can form a more structured material, immobilising them during drying. Furthermore, γ-alumina particles prepared by wet-milling were found to result in stronger cohesive strength compared with those obtained from dry-milling. The adhesive strength of the catalyst layer was found to be influenced by surface roughness profile of substrates, pH of the γ-alumina suspension and porosity of substrates (in the case of alumina substrate). Influence of the pH of the suspension was determined to be related to particle mobility, being similar to the cohesive strength study.

A second consideration in granular catalyst support is that the current literature does not determine whether structural failure of the support occurs between primary particles or within primary particles. In this thesis, the primary particles used were micrometre sized boehmite powder (the same powder used for substrate in the adhesive strength study); these primary particles are already agglomerates of nanometre sized crystals and polycrystalline aggregates. A method to directly quantify the strength of such primary agglomerates was developed; strength data obtained were supported by other indirect methods. It was determined that granular catalyst support produced from weak primary agglomerates may have structural failure both within and between primary agglomerates while support produced from strong primary agglomerates tend to have the failure between the agglomerates.

Acknowledgement

I would first like to sincerely thank my supervisor, Prof Agba Salman. The door to Prof Salman's office was always open whenever I ran into trouble or wanted a discussion about my research or writing.

I would also like to thank all of my industrial supervisors, Dr Patricia Blanco-García, Miss Elizabeth M. Holt and Dr Alison Wagland who kindly offered their time for discussion and communication during the progress of the project. Without their passionate participation and input, the project could not have been successfully conducted. In particular, I would like give my earnest gratitude to Dr Patricia Blanco-García who always helped me in preparing the suspension, hosting me in Johnson Matthey and reviewed my thesis.

I am also truly grateful for the technicians in our workshop who have machined various apparatus for the work and fixed equipment especially in times of urgency.

I would also like to thank everyone in the PPG group. They provided me with mental strength to finish my work especially in times of my medical conditions. They were coming to visit me and preparing food for me day by day. Special thanks also go to Aquino who worked together with me during a lot of nights in the lab.

Finally, I must express my heartfelt gratitude to my parents and parents-in-law, my wife and my dear friends for providing me with unfailing support and continuous encouragement throughout my years of study and through the process of researching and writing this thesis. This accomplishment would not have been possible without them. Thank you.

Publication

Jiankai Yang, Elizabeth M. Holt, Patricia Blanco-García, Alison Wagland, Michael J. Hounslow, Agba D. Salman, A novel technique for quantifying the cohesive strength of washcoat, Chemical Engineering Research and Design, Volume 110, 2016.

Pages 108-113,Jiankai Yang, Elizabeth M. Holt, Karen Huang, Patricia Blanco-García, Alison Wagland, Michael J. Hounslow, Agba D. Salman, Cohesive strength measurement of catalyst layer: Uniform drying and on-line monitoring, Chemical Engineering Research and Design, 2018.

Dedication

This thesis is dedicated to my parents and my parents-in-law, Guoliang Yang, Yan Wang,

Xuemei Yuan, Dungui Ji,

my wife, Wenwen Ji,

my grandparents, Longmei Liu, Guozhen Wang,

my aunt and uncle, Jie Wang, Long Xu

and my brother, Yifan Xu

Table of Contents

List of Figures

List of Tables

Chapter 1 Introduction

1.1 Catalyst layer

1.1.1 The emergence of catalytic converters by emission control legislations

During the process of industrialisation, the lifestyle of human beings was significantly transformed. Horse driven carriages were completely replaced by petrol powered vehicles. Handmade products were mostly substituted by factory manufactured ones facilitated by massive production. This dramatic advancement in human civilisation was realised by the wide use of fossil fuel.

However a major problem was inevitably associated with this advancement, which has become a popular topic these days, i.e. air pollution. Increasing number of vehicles has been reported to be responsible for this problem, causing acid rain and smog in large cities [1]. The severity of this issue has caught significant attention from many governments in the world; starting from 1970's, several developed countries such as America, Europe and Japan have already begun to introduce emission control regulations, and from 1990's onwards, even a number of developing nations such as India and Brazil initialised their legislation of transport emission control (Figure 1.1).
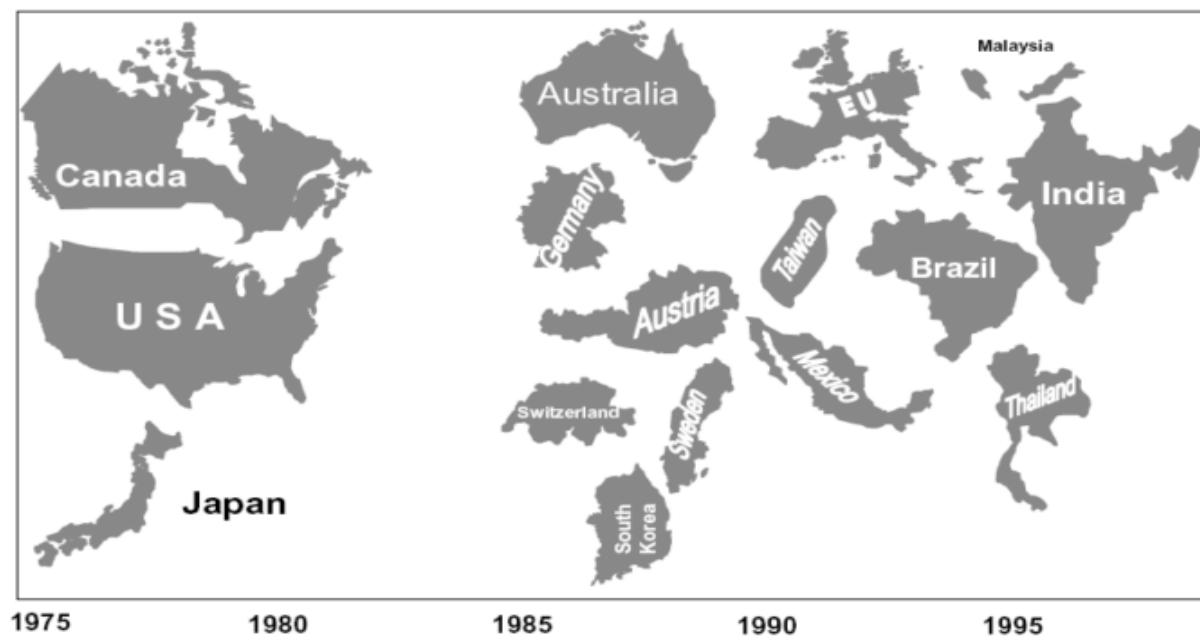
Figure 1.1 The introduction of emission control regulations in the world [2]

Powered by the pressure of incoming emission standards, in the late 1960's, the car manufacturing industry and the catalyst industry commenced some early research work together to develop an afterburner converter in order to reduce emission [3]. In 1975, the world's first car fitted with a catalytic converter was made in America, and ever since that, emission control regulations worldwide have become increasingly stringent, mostly led by wealthy regions such as America (Figure 1.2) and Europe, urging the capabilities of catalytic converters to be continuously improved [2].
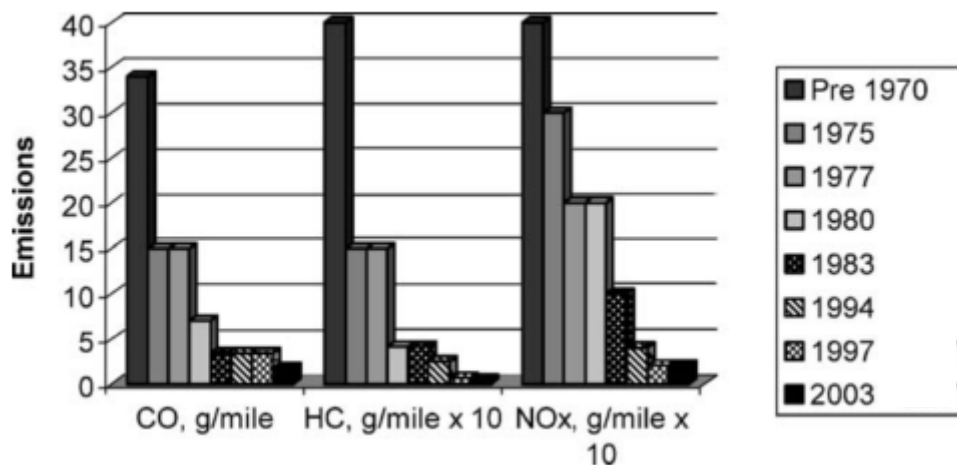
Figure 1.2 The progression of emission limits in the USA over the last 4 decades [2]

Nowadays there are millions of cars equipped with catalytic converter of different capabilities in the world to comply with various local emission control legislations. The best of these converters features an average 90 % reduction in emission of all regulated pollutants compared to 1960's level with a greatly prolonged life time between 100,000 to 120,000 kilometre [4].

1.1.2   The design of catalytic converters for emission control

The major pollutants in the emission from a motor vehicle engine that uses fossil fuel are nitroxide (NO_x), carbon monoxide (CO) and hydrocarbons (HC). The source of these harmful species is due to the use of air as the oxidant in combustion and the inevitable incomplete combustion of fuel in engines no matter how engine modifications are performed [5]. Two precious metal substances were proposed to be the catalyst in the afterburner converter to

accelerate the conversion reactions: platinum (Pt) for oxidative conversion, which was later replaced or co-used with palladium (Pd) due to price concerns and rhodium (Rh) for reductive conversion [6]. The equations describing these conversion reactions are shown from Equation 1-1 to Equation 1-3.

Oxidation

$$Hydrocarbon + O_2 \xrightarrow{Pt/Pd} CO_2 + H_2O$$

<div align="right">Equation 1-1</div>

$$CO + O_2 \xrightarrow{Pt/Pd} CO_2$$

<div align="right">Equation 1-2</div>
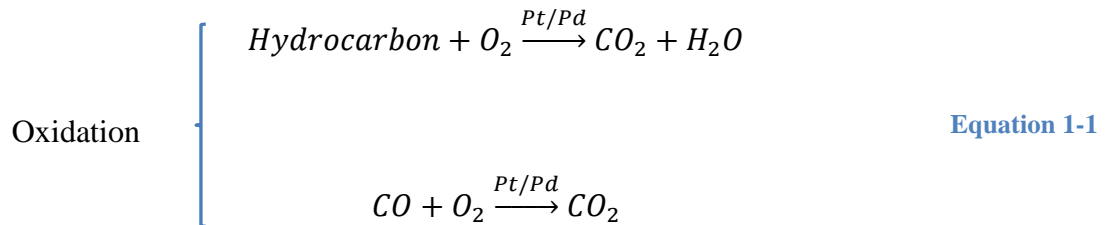
Reduction ⟵

$$NO_x + CO \xrightarrow{Rh} N_2 + CO_2$$
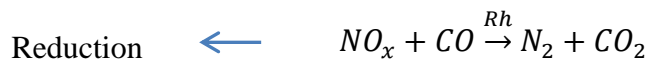
<div align="right">Equation 1-3</div>

The design of catalytic converters to reduce these harmful emissions is shown in Figure 1.3. The chemical reactions occur in the two monoliths which are situated inside the converter. Given the fact that CO is needed for the reduction reaction and more CO and less NO_x are often produced in a fossil fuel run engine, the reduction reaction is designed to take place first to neutralise the NO_x emission. The oxidation reactions then happen in the second monolith to completely remove any residual CO and the unreacted hydrocarbon. The design of a monolith as shown in the lower part of Figure 1.3 is intended to increase the contact area between the exhaust gas and the catalyst so that the conversion reactions can progress more quickly. However, on the other side, the porous structure of the monolith would inevitably decrease its mechanical strength; therefore an expanding mat has to be built around the monolith to prevent it from being damaged during operation. The outermost shell of a catalytic converter is usually a stainless steel housing fixed to hold the components of the converter together to allow modulated installation in vehicles.

Expanding mat
Insulates, seals and provides an unbreakable enclosure for the monolith

Stainless steel housing

Lambda probe
Measures the residual oxygen content in the exhaust gas

Ceramic monolith
Substrate for the catalytic noble metal

A close look on the monolith
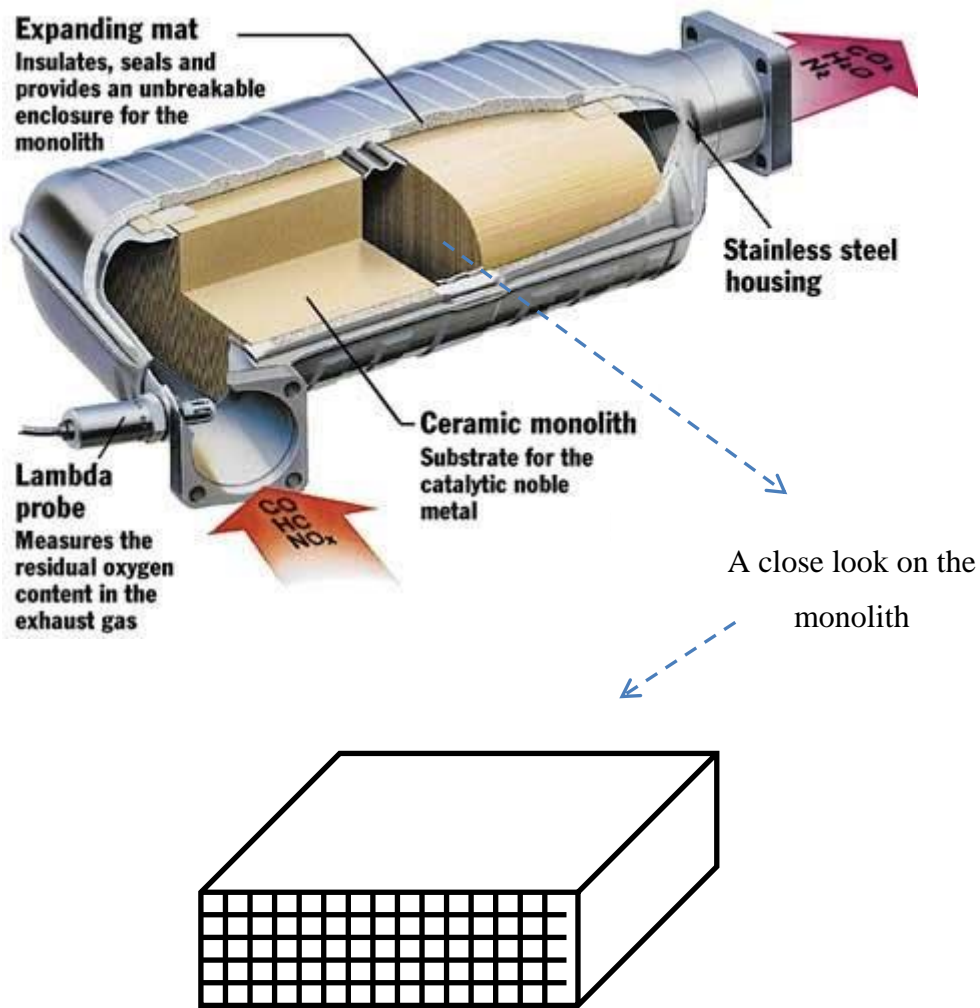
Figure 1.3 Design of a catalytic converter [7]

There are two choices for the material used to build a monolith. The first choice is FeCrAl alloys which consist of mainly iron, coupled with a moderate amount of chromium (20 % to 30 %) and a minor amount of aluminium (4 – 7.5 %). The second choice is a synthetic cordierite which has a chemical formula of $2MgO \times 2Al_2O_3 \times 5SiO_2$.

1.1.3   The use of catalyst layer in catalytic converter

As can be seen in Figure 1.4, there is an extra coating of material on the surface of the interior channels of the monolith.
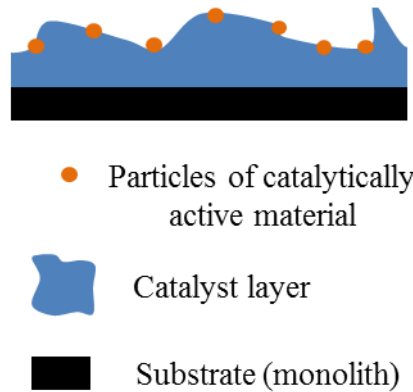
Figure 1.4 Details of the coating on the surface of monolith interior

In this coating, particles of catalytically active material (e.g. Pt, Pd and Rh) are dispersed on a high surface area catalyst layer; the catalyst layer therefore functions as a support for the actual catalyst. The good adhesion property provided by the catalyst layer and a satisfactory strength of itself are both important for the service life of a catalytic converter which often experiences strong vibration during car running.

1.1.4   The manufacturing of catalyst layer for automobile emission control

Materials of the catalyst layer can be made from a variety of materials. Aluminium oxide (also called alumina), titanium dioxide, silicon dioxide (also called silica), or a mixture of silica and alumina can all be used. The reasons that these materials are a good choice are related to their satisfactory refractory properties and ability to form bodies with high surface area to volume ratios.

Manufacturing of a catalyst layer carrying the catalytically active material is performed in two ways conventionally. The first method which is called the precipitation pathway is shown in Figure 1.5. The meaning of precipitation refers to a deposition process of catalytically active material on the catalyst layer.

The diagram showing the second method, an impregnation pathway, is shown in Figure 1.6. The main difference between the two routes is that in the precipitation method, the catalyst layer and the catalytically active material are deposited together in one process; while in the impregnation pathway, the catalyst layer is deposited first followed by a separate introduction

process of the catalytically active material. Both methods involve a calcination step at the end to promote sintering.
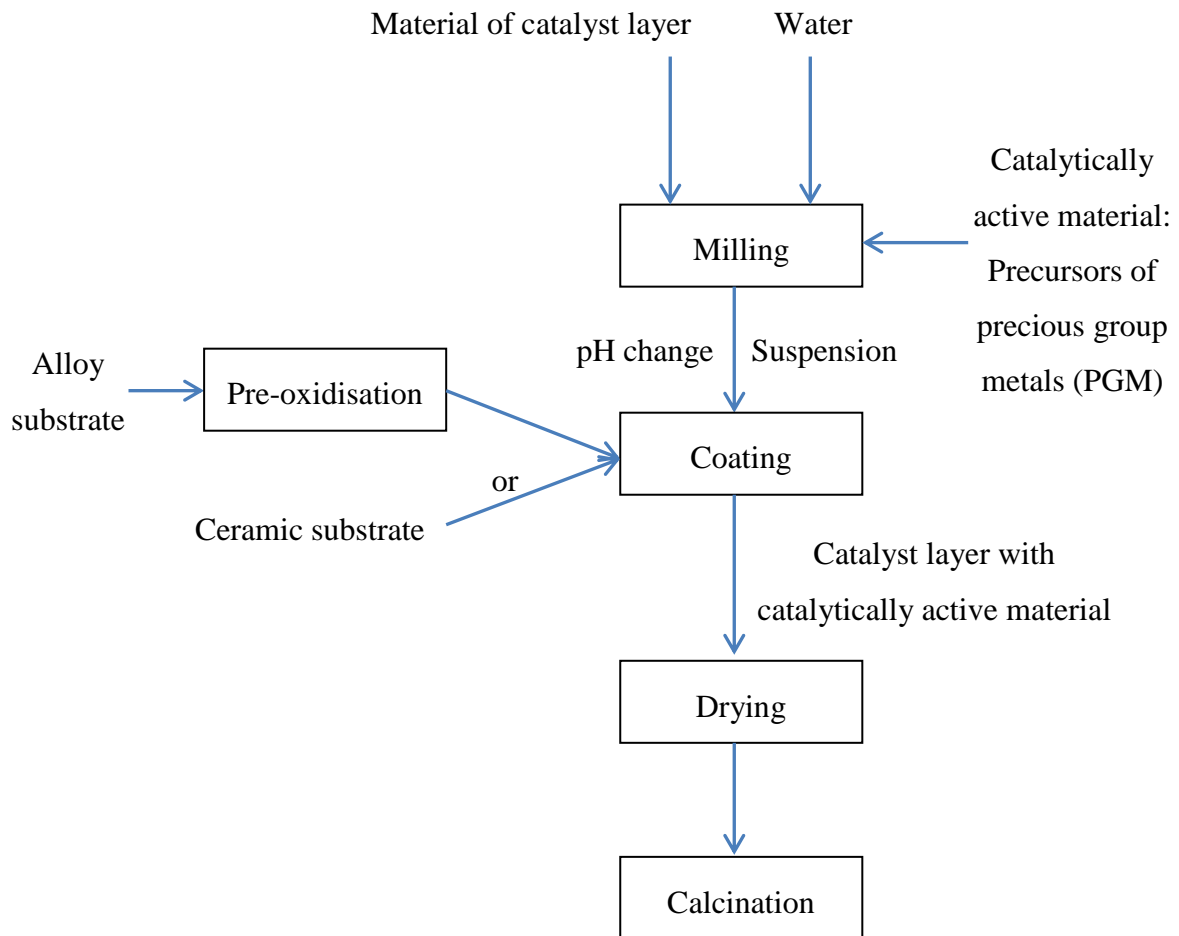
Figure 1.5 The manufacturing process of catalyst layer by precipitation [8]

A suspension is obtained after the milling step, followed by pH change, as shown in Figure 1.5 and Figure 1.6. The suspension would contain particles only for the catalyst layer in the impregnation route and particles for both the catalyst layer and the catalytically active material in the precipitation route. The application of the suspension onto the monolith can be done in two ways. The first method requires the substrate to be manufactured into a monolith first, followed by pouring the suspension through the monolith or sucking the suspension into the monolith. The second method has the order reversed, but is only applicable for FeCrAlloy substrate. The suspension is first of all applied onto the substrate which is then coiled to form a monolith [9].
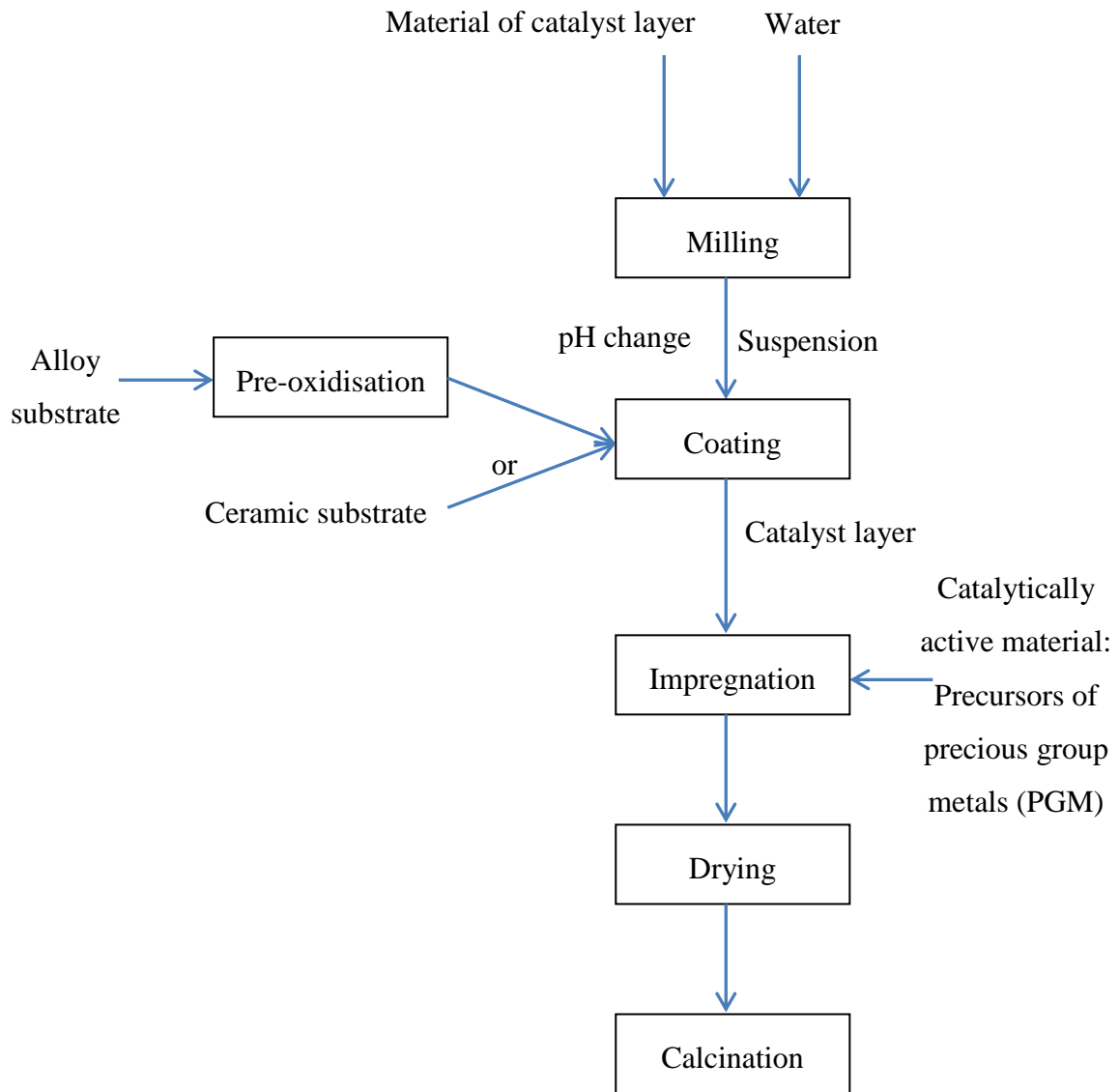
Figure 1.6 The impregnation pathway to prepare catalyst layer [8]

1.2 Granular catalyst supports

1.2.1 The importance of granular catalyst supports in industry

Apart from the catalyst layer, catalyst supports are also available in a variety of other shapes [10] as shown in Figure 1.7 to fulfil different duties required in process industry.
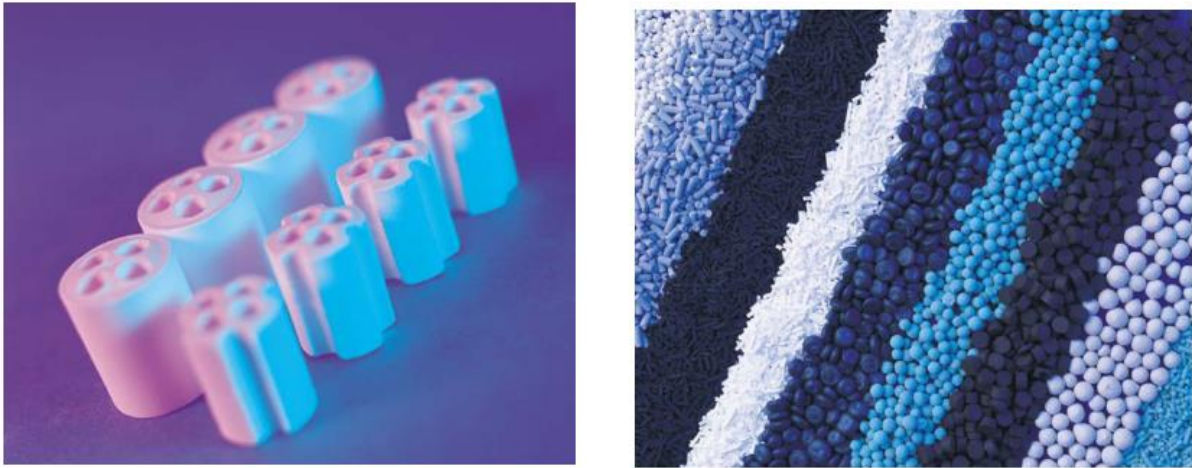
Figure 1.7 Catalyst support in the shape of quadrilobe, extrudate, pellet and granule [Courtesy of Johnson Matthey Plc, [10]]

A very widely applied type of these catalyst supports is the granular catalyst support. Granulated catalyst supports are often used for important processes in chemical engineering industry such as feedstock purification and hydrogenation reactions. Feedstock purification is designed to remove contaminants of sulphur in inlet gas streams since sulphur is often a catalyst poison. Hydrogenation reactions are involved in both production of food products and petrol. Unsaturated fats and fatty acids are exposed to pressurised hydrogen gas in nickel catalysts supported by granular catalyst support. This hydrogenation process is used to increase the melting point of unsaturated compounds for further production of other food products such as margarine and confectionery [11]. Oil refineries apply hydrogenation reaction in cracking process of long-chained hydrocarbons to increase the production of petrol [12].

1.2.2 The manufacturing of granule supported catalyst for industrial applications

The production process of granule supported catalyst can also be done in two pathways, which are precipitation and impregnation. In the precipitation route, soluble metal salts are mixed with base to form a gelatinous material by precipitation. The precipitated material is aged in carefully controlled conditions to allow crystals to be formed. The crystals are then filtered out from the mother liquor, followed by washing to remove any unwanted products which may function as catalyst poison. After drying and calcination, the filtered washed cake turns into finely divided nanometre sized crystallites (usually metal oxide) which are

catalytically active. Due to the small size, these crystallites tend to agglomerate under the influence of Van der Waals forces to form aggregates of micrometre scale, which are termed as primary agglomerates. These primary agglomerates are seldom used as the final form of products. They often have to undergo further size enlargement processes with a carrier material such as granulation to form larger bodies of required size (often millimetre scale), shape, strength and porosity depending on the application employed. The larger entities formed are termed as granules or secondary agglomerates.

In the impregnation route, forming of the carrier material take places first. The forming step is often carried out by wet granulation of the carrier material with binders to produce a high surface area granular catalyst support. The granular catalyst support is then impregnated with a mixed metal salt solution; catalytically active material (usually metal oxide) will then be recovered from the impregnated metal salts after the drying and the calcination process.

1.3 The application requirements of catalyst layer and granular catalyst supports

One of the important physical properties of both catalyst layer and granular catalyst support is the mechanical strength [13]. In the case of a catalyst layer, the catalyst layer needs to have a high enough mechanical strength to withstand the strong vibration in a catalytic converter to ensure durability. In reality, catalyst layer has been found to fail in both cohesive and adhesive mode. A cohesive strength occurs when a catalyst layer fails from within itself while an adhesive failure is the case that a catalyst layer detaches from its substrate. A schematic diagram showing the two types of failure is shown in Figure 1.8.

In the case of granular catalyst supports, since this type of support is often employed in packed bed columns where a pressure condition is required, the mechanical strength of granular catalyst support therefore has a significant influence on the productivity of the column in which it is used. A mechanically weak granular support may fragment under the set pressure in the column; the fragments resulted could then lead to a pressure drop in the column according to Ergun's equation, deviating the process from its desired operating condition. Fragments of granular catalyst support may also be carried away by fluids leaving the column.
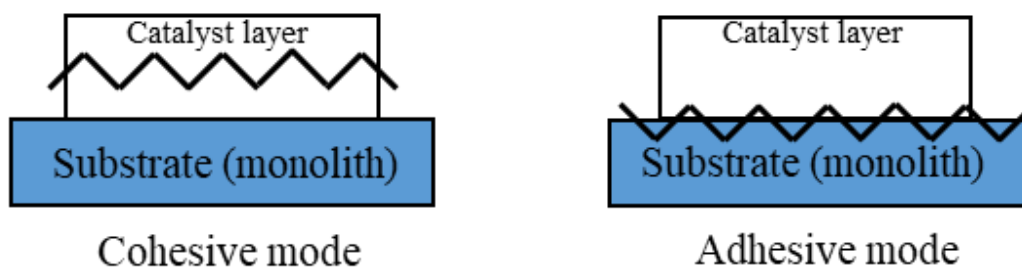
Figure 1.8 Two failure modes catalyst layer

Regarding the breakage of granular catalyst supports, there is an important question concerned with the location of the breakage. As discussed in section 1.2.2, granular catalyst support is formed by agglomeration of primary agglomerates when primary agglomerates are themselves comprised of aggregated nanosized crystallites. It is then uncertain whether the breakage of granular catalyst supports occurs between primary agglomerates or within primary agglomerates.

1.4 The need for research

Although catalyst layer and granular catalyst support have been widely and successfully used in industry for several decades, there is still limited research on their physical properties, in particular the mechanical strength.

Given the significance of mechanical strength of catalyst layer as outlined in section 1.3 and its important applications described in section 1.1, this project was initiated with the aim of developing methods to separately quantify the cohesive and adhesive strength of a catalyst layer. The strength results obtained were then analysed to understand the interactions between particles of catalyst layer during the manufacturing route. The material to prepare the catalyst layer was selected to be γ-alumina (Al_2O_3) which is a common choice to make catalyst layer.

In terms of granular catalyst support, the research was setup to investigate the breakage pattern of granular catalyst support, whether structural failure of granular catalyst supports occurs within primary agglomerates or between primary agglomerates. Boehmite which can

be considered as hydrated γ-alumina (AlOOH) was chosen to study granular catalyst support in this project due to its capability of being converted to γ-alumina in calcination.

1.5   The structure of thesis

The introduction of the thesis presented the industrial applications of catalyst layer and granular catalyst support and the current challenges that are confronted. In this section, the principle of the design of these catalyst supports and the manufacturing process were also discussed.

Following the introduction, a literature review was provided to identify the current knowledge gaps in dealing with the challenges encountered. The literature review mainly looked at the effect of various formulation and process parameters on the quality of both catalyst layer and granular catalyst support and in the meantime the way that such quality is assessed. In terms of the assessment methods, flaws in the current assessment methods were discussed to identify direction of further improvement. Regarding the catalyst layer, it was identified that the strength measurement of catalyst layer suffered from two drawbacks. The current methods either struggled to differentiate between the cohesive and adhesive strength of the catalyst layer or failed to report the strength based on a unit of stress which is less dependent on the testing environment. In respect of the granular catalyst support, it was noticed from the literature review that many publications at the moment did not consider the strength of primary particle when evaluating mechanical failure of granular catalyst support. It is still unclear that whether structural failure of granular catalyst support occurs between primary particles or within primary particles themselves. More details on how these research gaps were identified would be given in the literature review (Chapter 2).

The subsequent chapters were then arranged in a step by step manner to tackle the knowledge gaps identified from the literature review. Chapter 3 first of all introduced the main experimental materials used for this study. The methods adopted to prepare the suspension consisting of particles of catalyst layer was also presented.

Chapter 4 showed a method to separately quantify the cohesive strength was then presented with the strength reported based on unit of stress. The data gained were verified by a number of indirect methods such as disintegration and penetration.

Chapter 5 then expanded the preparatory parameters and evaluated the effect of pH and relative humidity on the cohesive strength of catalyst layer. Explanation for the trend was given mainly based on particle mobility derived from sedimentation study. However, in this chapter, splitting of samples used for the cohesive strength test occurred, which lead to the development of a uniform drying system in the next chapter.

Chapter 6 first of all presented the development work of a uniform drying system which was designed to resolve the sample splitting issue encountered in Chapter 4-5. The uniform drying system was then employed to generate a more comprehensive profile of the cohesive strength of catalyst layer at different pHs and drying rates. Development of explanation for the trend observed was facilitated by rheological study and online monitoring of particle packing process. Following the understanding gained, a correlation between the cohesive strength obtained and interparticle forces as predicted by the DLVO theory was also established.

Chapter 7 entered a different property of the catalyst layer, i.e. the adhesive strength. It first of all described an in-house developed new method which is capable of quantifying the adhesive strength of catalyst layer and reporting the strength based on unit of stress. The method developed was then used to test the adhesive strength of catalyst layer on three different substrates at various pH conditions. One of the substrates was derived from the primary particles selected as the subject of study in the next Chapter.

Chapter 8 looked at granular catalyst support. It began by presenting a method developed in this study to quantify the strength of primary agglomerates of boehmite powder. The strength data gained was verified by a number of indirect methods such as disintegration, deformability, etc. The same powder was then granulated to produce granular catalyst support. The strength of primary agglomerates of boehmite powder and that of granular catalyst support made from it was compared. The comparison allowed the author to have a more accurate assessment about the exact location of structural failure of granular catalyst support.

Chapter 9 applied the same strength quantification methods developed in the previous chapters to investigate the difference between dry-milled and wet-milled γ-particles. Together with the literature, the difference was finally attributed to the presence of hydroxyl groups on the surface γ-particles.

Chapter 2 Literature Review

2.1 Material

The material to prepare catalyst layer in many studies is based on γ-alumina [8, 14-17]; therefore γ-alumina is chosen to be the material discussed in the literature review. γ-alumina is a transitional phase of alumina. Alumina has the full name of alumina oxide which is a chemical compound of aluminium and oxygen with the chemical formula Al_2O_3. The following alumina phase diagram (Figure 2.1) shows the range of temperature where γ-alumina exists.
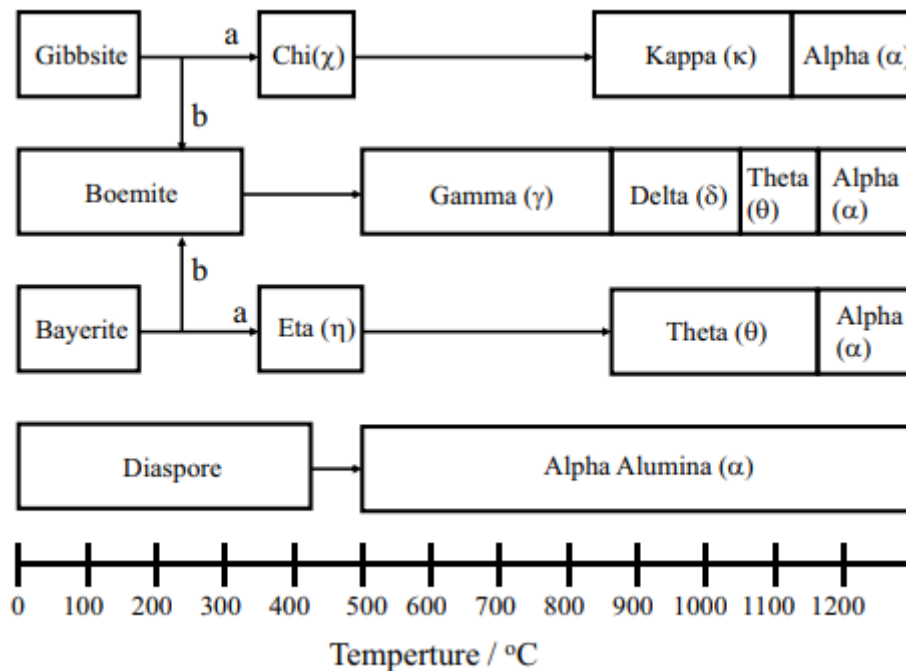
Figure 2.1 Phase diagram of alumina [18]

γ-alumina, being a transitional alumina, finds its applications in ceramics, in particular as an adsorbent and catalyst support material [19-21] because of its characteristic physical properties such as high surface area to volume ratio. It is normally in applications below 900 °C as a higher temperature would cause γ-alumina to undertake phase change into the δ phase. γ-alumina appears a white powder at room temperature, is odourless and has a bulk density of around 800 kg/m^3 [22]. The structure of γ-alumina is revealed by techniques such as NMR [23] and IR [24]. It is often described as a defective cubic spinel type [25]. The crystal lattice

of γ-alumina is shown in Figure 2.2. It could be seen that Al ions occupy both octahedral and tetrahedral positions while oxygen ions are arranged in a close-packed stacking to produce oxygen layers. It should also be noted that there are vacancies on some positions for cations (the aluminium ions). The vacancy of positive ions in the structure can also be deduced from the ratio of anion-cation. As the anion-cation ratio is 4 : 3 for an ideal spinel, therefore cation vacancies have to be made to ensure the balance of positive and negative charge in a unit cell; based on charge neutrality, there are 8 cation vacancies for every 160 ions where 96 of them are oxygen ions and 64 of them are aluminium ions. For each unit cell, there are 32 oxygen ions and 64/3 aluminium ions for stoichiometry balance.
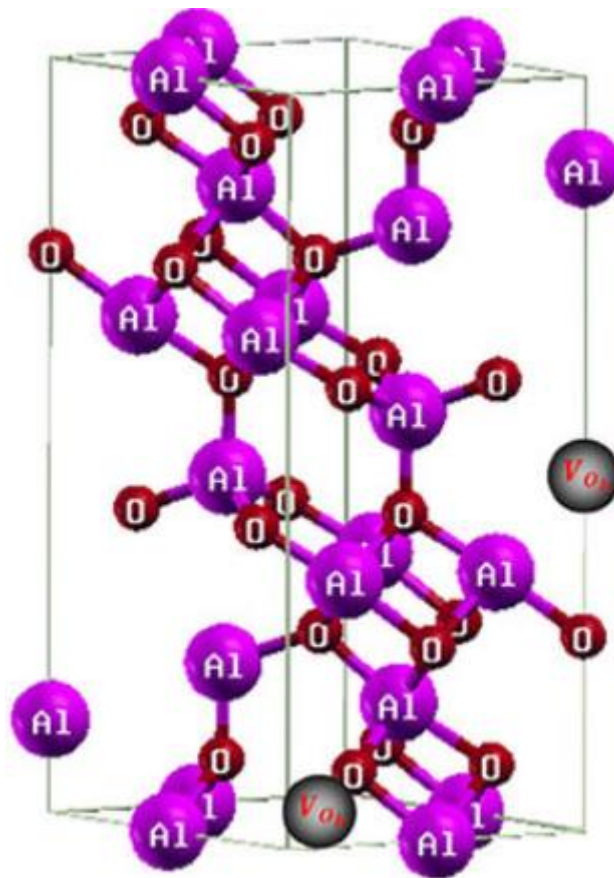
Figure 2.2 Crystal lattice structure of γ-alumina [26]

Boehmite is the phase of alumina that exists at a lower temperature than γ-alumina. It is often used the material to produce granular catalyst support; therefore the properties of boehmite is discussed in the literature review here. Boehmite is in fact an aluminium oxide hydroxide (hydrated alumina) with a chemical formula of γ-AlO(OH)). Given that possibility of phase change, boehmite can be used as a precursor to produce γ-alumina through a calcination

process at temperature staring from about 500 ℃. At room temperature, it appears as a white powder and has a bulk density of 250 kg/m^3 to 640 kg/m^3 depending on the agglomeration status of the powder [27]. Boehmite also represents the main component of many bauxite minerals which are naturally occurring. The crystal structure of boehmite is shown in Figure 2.3. The aluminium and oxygen ions are arranged to produce double layers of octahedron and hydrogen atoms are attached on the outside. In this double layer structure, oxygen ions are in cubic packing. Due to the presence of hydrogen atoms, there is hydrogen bonding from the hydroxyl ions between neighbouring double layer structures.
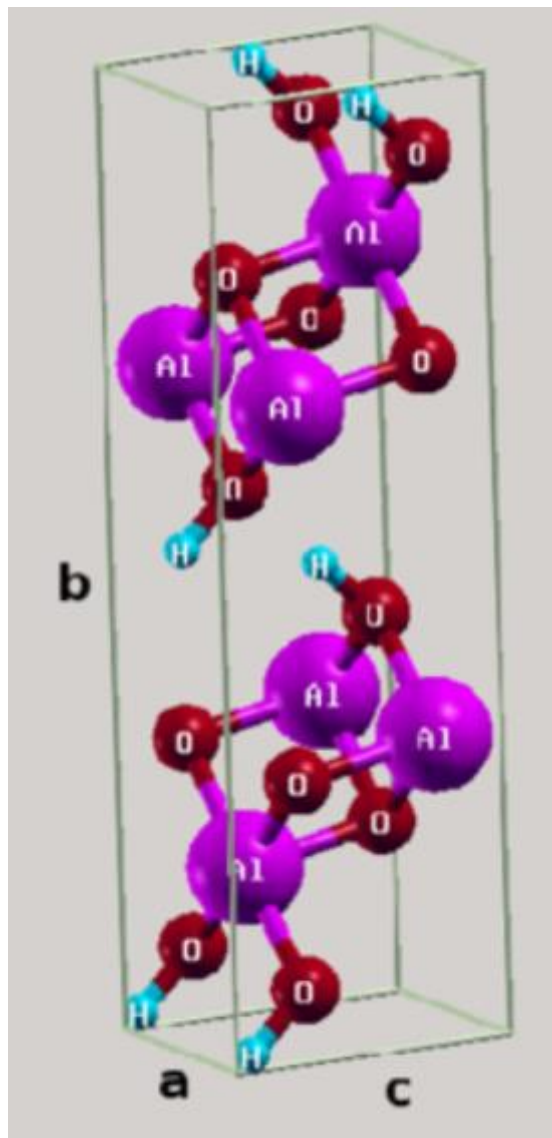
Figure 2.3 Crystal lattice structure of boehmite [28]

2.2   Catalyst layer

2.2.1   Introduction

Due to the extensive use of catalytic converters over the last few decades, a sizable number of studies on catalyst layer are available in the current literature. The aspects that have been looked at mainly consist of the effect of various formulation and process parameters on the quality of catalyst layer (mainly the strength of it). A list of all of these parameters and the quality of the catalyst layer examined in the current literature (summarised from [14 - 43]) are shown in Figure 2.4.

Preparation parameter:

Formulation parameters

Powder characteristics
- Particle shape
- Particle size
- Particle type

Solid content

Preparation parameter:

Process parameters

Milling condition

pH of suspension

Alloy substrate pre-oxidisation

Coating methodology

Drying and calcination

Derived parameters:

Suspension viscosity

Strength of catalyst layer

Figure 2.4 List of formulation and process parameters investigated and quality of the catalyst layer examined in current literature

16

As already stated in Chapter 1, catalyst layer in real applications is found to fail two ways which are the cohesive mode and adhesive mode. The definition of cohesive strength is the strength of bonding between particles in the catalyst layer while adhesive strength is described as the bonding strength between particles in the catalyst layer and the substrate, as can be seen in Figure 1.8.

2.2.2   Quality assessment of catalyst layer – mechanical strength

A range of methods which are currently used in the literature to measure the strength of catalyst layer is presented in Table 2.1. In this review, the type of methods used to quantify the strength of catalyst layer is classified into two groups which are group 1 methods and group 2 methods.

A brief introduction for the methods presented in Table 2.1 is given here. As can be seen in Table 2.1, ultrasonic vibration test is one of the most common methods currently used to evaluate the strength of catalyst layer in literature. This strength test is conducted by exposing a sample of catalyst layer to ultrasound of known magnitude in an ultrasonic bath for a set duration; the mass loss occurred from the sample is then measured and used as an indication for the strength of the catalyst layer. The ultrasound is transferred by a liquid and acts to weaken the bonding between particles of the catalyst layer [29]. A schematic diagram showing the experimental setup for the ultrasonic vibration test is shown in Figure 2.4. In the research conducted by [30], the vibration test was run between 5 to 60 min in a bath filled with petroleum ether.
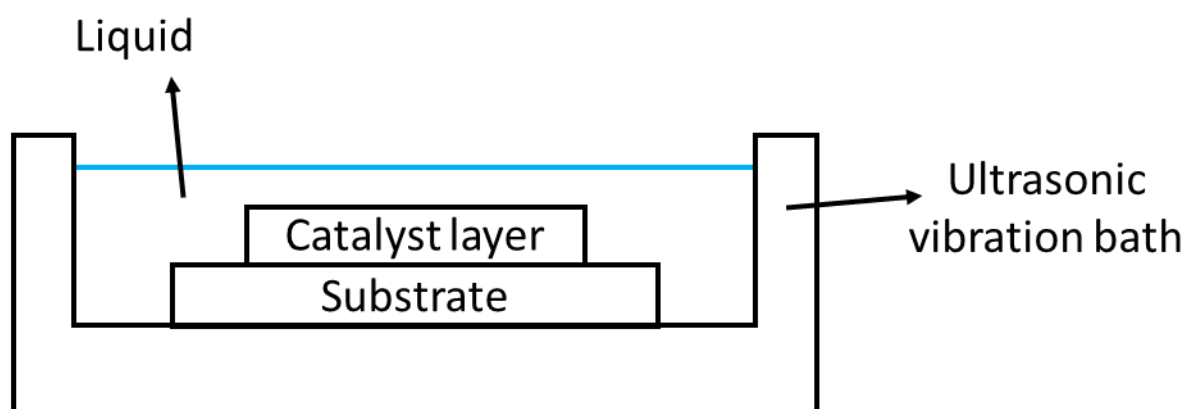
Figure 2.5 Schematic diagram for the experimental setup of ultrasonic vibration test

The second method in group 1 methods is termed as the simulated environment test. It has also gained some popularity in the current literature as a way to test the strength of catalyst layer. The principle of this method is that a high velocity flow of hot air is passed in parallel directions over a catalyst layer sample (as can be seen in Figure 2.6) with the mass loss of the sample after the test being recorded as an indication for the strength of the catalyst layer. The high velocity of the hot air flow acts to detach particles from the catalyst layer. An example of the test can be found in [14] where the temperature of the environment was set to be 800 °C and the free volume velocity of the air was chosen to be 100000 h^{-1}.
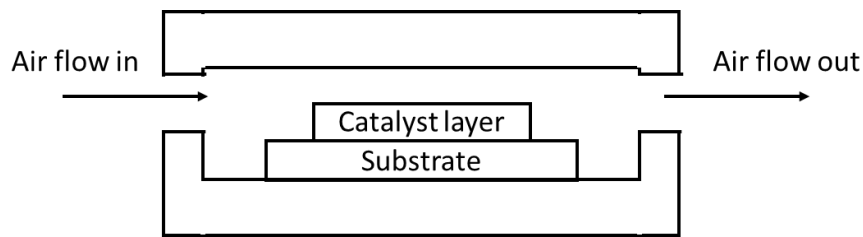
Figure 2.6 Schematic diagram for the experimental setup of simulated environment test

The third and fourth test in group 1 methods are rarely used in the current literature. The drop test conducted in [31] was carried out by dropping catalyst layer sample in a monolith from a 50 cm height on a hard surface with the channel of the monolith facing down; the weight loss arising from the drop was recorded to indicate the strength. The test can be said to work on using the kinetic energy developed in the fall to break the bonding between particles.
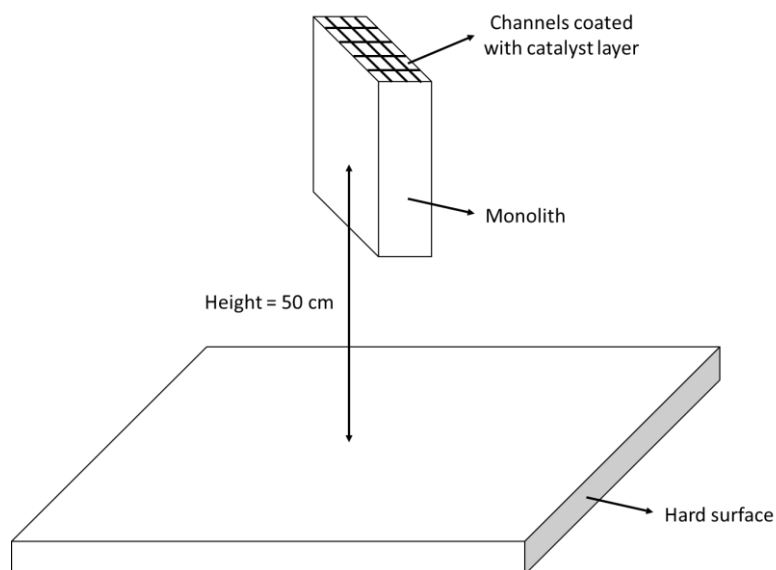
Figure 2.7 Schematic diagram for the experimental setup of drop test

The abrasive test employed in [32] utilised an abrasion tester (Suga, NUS-1). In the tester, the sample was designed to constantly move against an abrasive material which consisted of particles of 12 μm. The abrasive material was also rigidly fixed and set to apply a normal load of 3 N on the sample. The abrasive action was then repeated for 400 cycles at a fixed velocity of 0.04 m/s, equalling to a total distance of 25 m. The following equation (Equation 2-1) was then used to calculate a wear rate which was used as an indicative parameter for the strength of catalyst layer.

$$Wear\ rate = \frac{Weight\ loss}{Density \times Sliding\ distance}$$

<div align="right">**Equation 2-1**</div>

The pull-off method, as seen in Figure 2.8, measures the force that is required to pull off a catalyst layer from a substrate [30].
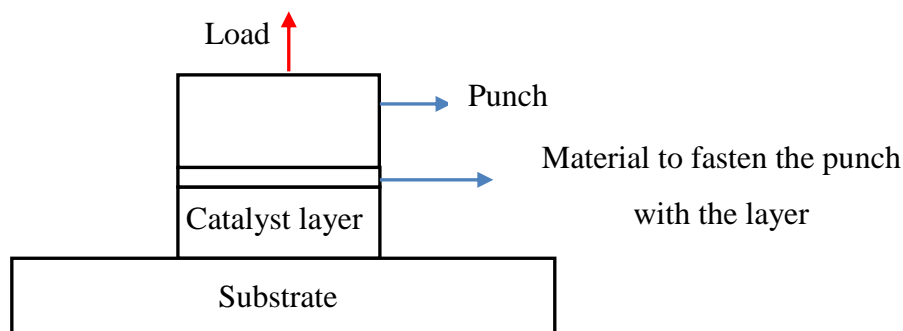
<div align="center">**Figure 2.8 Schematic diagram showing the experimental setup of the pull-off method**</div>

Another version of the pull-off method was designed to measure the work done required to pull off a catalyst layer from a substrate [22]. The work done was calculated by finding the area under a force over displacement curve when the force reached the point that the catalyst layer failed. An example of the force over displacement curve is shown in Figure 2.9. It needs to be noted that this version of the pull-off method began with a compression by the punch on the sample of catalyst layer, followed by decompression and finally pull-off. Therefore a negative stress was present initially due to decompression before the positive stress from the pull-off action was applied.
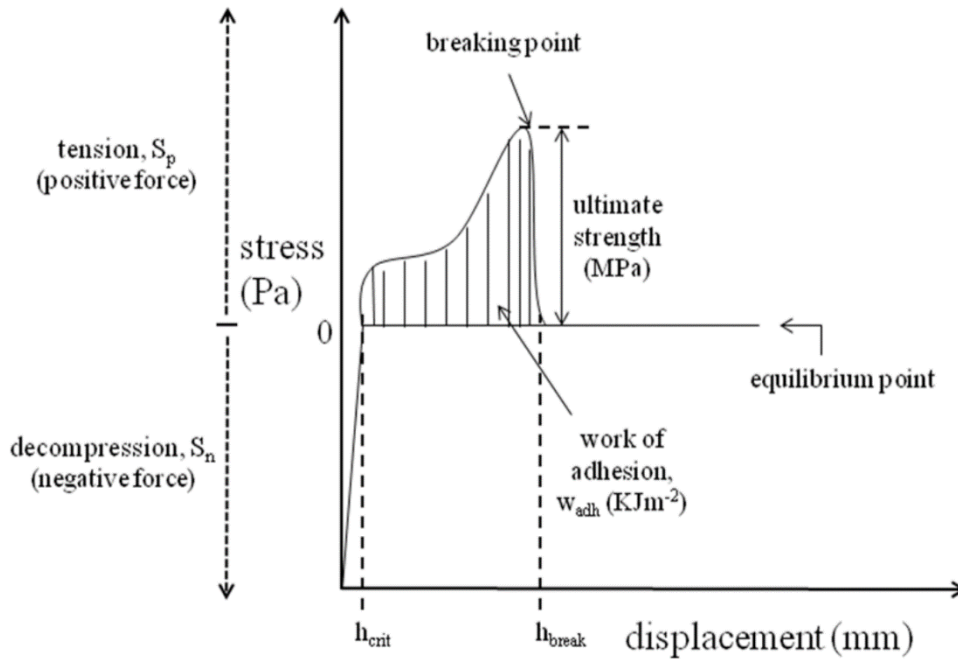
Figure 2.9 Example of calculation of work done in the pull-off method

The experimental setup of the scratch test, employed in [33], can be seen in Figure 2.10. A sample of catalyst layer was scratched with an increasing load by a stylus with a diamond tip. The critical load at which the catalyst layer began to detach from the substrate was recorded as used to indicate the strength of the catalyst layer. The critical point was determined by acoustic emission and confirmed by inspection in a microscope.
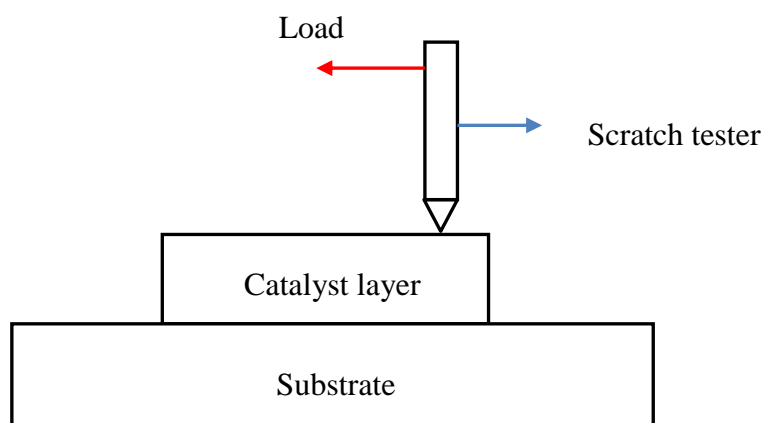
Figure 2.10 Schematic diagram showing the experimental setup of the scratch test

Density measurement in group 2 methods evaluates the strength of catalyst layer based on density measurement of catalyst layer, as employed in [34]. A higher density would correlate with a stronger catalyst layer.

Table 2.1 Summary of existing techniques of measuring coating strength

Publication	Group 1 method				Group 2 method		
	Ultrasonic vibration bath	Simulated environment	Drop test	Abrasive test	Pull-off method	Scratch test	Density
[22]					✓		
[30]	✓	✓			✓		
[31]			✓				
[32]				✓			
[33]						✓	
[34]							✓
[35]	✓						
[36]	✓						
[37]	✓						
[38]	✓	✓					
[39]	✓	✓					
[40]	✓	✓					
Comment	Problem 1: Indirect measurement				Moving to direct measurement		
	Problem 2: No distinction between cohesive and adhesive strength						

Although a good amount of literature (as can be seen in Table 2.1) can be found to carry out strength measurement of catalyst layer, there is still insufficient progress on the way the mechanical strength is measured.

The first problem of using group 1 methods is that even though some strength results are normalised, e.g. percentage of mass loss after test, results obtained from different studies can still not be compared due to the fact that these results are not independent of the testing environment. For example, in the case of using an ultrasonic bath to quantify layer strength by measuring mass loss of the sample, if the configuration of the ultrasonic bath used is different or if the magnitude of the ultrasound applied is different, one can hardly make a reliable comparison in layer strength obtained by different studies. Similar problems exist in the thermal shock test (mass loss measurement after the sample has been exposed to a thermal shock), the drop test (dropping catalyst layer samples from a fixed height, followed by measurement of weight loss) and the abrasive test (mass loss of a layer after being abraded) as well, e.g. the ramping rate of heating and cooling, the angle of drop impact, the grade of abrasive paper etc. As the origin of layer strength is the bonding between particles in the catalyst layer (cohesive) and the bonding between these particles and substrate (adhesive), any indirect measurement of these bonding strengths can be affected by external factors as seen above. This is why the group 1 methods are not good enough.

A second problem for group 1 methods is that the design of the method does not contain a way to control the failure pattern of a catalyst layer. The meaning of this statement is that a catalyst layer sample under test could fail either by the cohesive or the adhesive mode, depending on the weakest point of bonding. Because of this, the cohesive and the adhesive strength of a catalyst layer could not be differentiated. As seen in the introduction, a catalyst layer in operation could fail in both the cohesive and the adhesive mode, suggesting that both the cohesive and the adhesive strength are important for the durability of a catalyst layer; it is essential not to mix the cohesive and the adhesive strength in any strength measurement of a catalyst layer.

Although group 2 methods (as described in Figure 2.8 and Figure 2.10) proposed to measure the strength of catalyst layer are designed to be more related to direct measurement of the bonding strength between particles in order to tackle the first problem mentioned above, it could be seen that they are still unable to differentiate between the cohesive and the adhesive failure as explained below; therefore the second problem still remains. In the case of pull-off test, this can be understood that the pulling load in the pull-off method would simply cause the weakest point across both the cohesive and the adhesive strength to fail, therefore there is no mechanism involved to control the failure pattern in order to differentiate between the two ways of failure. In the scratch test, while the scratch tester is moving across a catalyst layer,

the force it applies could not only cause the catalyst layer to fail from the layer itself but may also lead the catalyst layer to detach from the interface between the layer and the substrate; therefore, the cohesive and the adhesive strength results are again mixed. For the last group 2 method, density measurement could give an overall determination of the strength of catalyst layer while there can be a distribution of density across the thickness of catalyst layer. This would suggest that the cohesive and adhesive strength of the catalyst layer can be considerably different.

From the discussion presented in this section 2.2.2, it could be seen that there is a need for a robust method in the study of strength of catalyst layer, which could produce a more direct and distinct measurement on the strength of bonding between particles within a catalyst layer and between these particles and the substrate, based on scientific fundamental quantities for mechanics such as stress [9].

Having recognised this need, it could be seen that the effect of preparation parameters investigated in the current literature, as discussed in section 2.2.3, would suffer from mixing between results of cohesive and adhesive strength. Therefore it would be unclear to say whether the observed change in the strength of catalyst layer is originated from a change in the cohesive strength or the adhesive strength. This issue would be undesired as catalyst layer is found to fail in both cohesive and adhesive mode in real applications. In fact, understanding of the effect of different preparation parameters on both the cohesive and adhesive strength of catalyst layer individually would be highly necessary for the aim of producing more durable catalyst layer in catalytic converters in future.

2.2.3   Preparation parameters

2.2.3.1   Powder characteristics

The definition of powder characteristics is wide in the current literature. It could cover the shape, type and size of the primary powder.

In the work of Agrafiotis [14], the effect of powder type on the strength of catalyst layer was investigated. The manufacturing process of the catalyst layer was performed with 3 different alumina powders and an alumina sol: a commercial γ-alumina powder, gibbsite ($Al(OH)_3$) which is a more hydrated aluminium hydroxide powder, boehmite ($AlOOH$) which is a less hydrated aluminium hydroxide powder, and an aqueous sol of aluminium nitrate. A sol is

defined as a colloidal suspension which consists of very small solid particles stably suspended in a continuous medium [41]. The two hydrated aluminas and the alumina sol were first converted into γ-alumina by a calcination process. Then the 4 different γ-alumina materials were all made into a suspension individually, followed by milling, coating, drying and calcination all under the same condition. The strength of catalyst layer produced from each suspension was performed using a high velocity air flow parallel to the surface of the sample and the strength of catalyst layer was reported based on mass loss of the monolith during test. The following trend was observed: the strength of the catalyst layer produced from the 3 derived γ-aluminas always showed a higher value than that made from the commercial γ-alumina. This observation in strength was thought to be caused by two factors: the extent of mechanical anchorage between particles of the catalyst layer and the magnitude of attractive force between these particles. When in suspension, the derived γ-alumina powders had larger particle size compared to the commercial one, which resulted in less mechanical anchorage in catalyst layer formed from the derived γ-alumina powders. However, due to the fact that particles of the derived γ-alumina powders contain nanometre scale particles that can exhibit attractive force with other particles in neighbouring particles, the catalyst layer produced from the derived alumina powders was still stronger than that made from the commercial one. But in this work, the reason why the derived alumina powders seem to have these strength determining nanometre particles formed is not provided.

In another research which looked at the effect of powder characteristics [42], the element of particle size in powder characteristics was closely examined. The research used alumina, zirconia, titania and ceria and applied these powders on cordierite honeycombs via suspension deposition. The suspension contained 35 wt% solid content and was ball milled for different amounts of time before the application. The reason that the milling time was varied was to allow different particle size to be reached so that the effect of particle size from different powder types can be evaluated. Following deposition, the catalyst layer samples obtained were then dried and calcined before strength measurement was carried out. The strength of the layer samples was determined by exposing the samples to a stream of fast moving hot air parallel to the samples, simulating the operation conditions in a catalytic converter; the mass loss of the samples was then recorded, a higher mass loss would indicate for a weaker strength. The conclusions arrived were that irrespective of the powder type, a smaller particle size gave rise to a lower weight loss, suggesting a higher strength of the catalyst layer was achieved. To take the conclusion further, it was then reported that the

source of the strength is mainly derived from anchoring and interlocking of particles in the catalyst layer with the substrate but less originated from chemical affinity mechanisms at the interface between the catalyst layer and the substrate.

The effect of particle size in suspension on the strength of catalyst layer was investigated by a few authors. In [14], γ-alumina powder was wet-milled to obtain different particle sizes in a unimodal particle size distribution. Ceramic monoliths were then dip-coated in the suspension. The strength test was performed using a high velocity air flow parallel to the surface of the sample and the strength of catalyst layer was reported based on mass loss of the monolith during test. The finding from this research showed that a smaller particle size would give rise to stronger catalyst layer. The higher adhesive strength (strength between the catalyst layer and the substrate) was a result of the greater extent of interlocking between the γ-alumina particles and the surface irregularities of the substrate. This was because as the particle size was reduced, more particles were able to adsorb onto the surface irregularities of the substrate. The higher cohesive strength (strength within the catalyst layer) was achieved as the small particle size resulted in a tighter packing of the particles, causing the inter-particle force (both of mechanical and interfacial nature) to be stronger. Similar results to this research, i.e. smaller particles can lead to a stronger catalyst layer were also obtained by [43] where a metallic substrate was used in comparison to the ceramic substrate in [14]. In these In addition, in the research by [43], the researcher also stated an important observation in the measurement of strength of catalyst layer, which was conducted by ultrasonic vibration test. The point was as the mass of particles increases by the cubic powder of the size of particles, therefore the presence of large particles in catalyst layer would contribute to a higher weight loss after the vibration test if these particles are removed during the test.

Particle size distribution in suspension is characterised by the spread of the distribution and the number of peaks in the distribution. The strength of catalyst layer in relation to particle size distribution was investigated by [36] who confirmed that a combination of a narrow particle size distribution and fine particles could result in a tighter packing on a ceramic substrate. The reason offered by the researchers was that the small particles of the suspension managed to stick at the interface between the catalyst layer and the substrate to provide a firm resistance to the ultrasonic vibration test conducted. On the contrary, they stated that large particle size and a broad particle size distribution would be detrimental for obtaining strong catalyst layer. However it should also be noted that in some studies, the effect of particle size distribution in suspension is probably misjudged to some extent due to the effect of particle

size in suspension [[22], [40]] as the authors simply attributed the higher strength of catalyst layer to a shift from a unimodal to a bimodal particle size distribution when the particle size in suspension was actually reduced. Therefore, the alleged findings on the effect of particle size distribution in suspension on the strength of catalyst layer may still need to be verified further.

2.2.3.2 Solid content

The formulation to produce a suspension from which the catalyst layer is made usually contains a type of alumina powder and a liquid mixture (e.g. deionised water, acid solution etc.) and the alumina powder is dispersed and suspended in the liquid mixture. Solid content is regarded as the mass percentage of the alumina powder used in the whole formulation.

The effect of solid content on the strength of catalyst layer has been scarcely studied in the current literature. This effect was looked at in [44] where the strength of catalyst layer was assessed by ultrasonic vibration test. The solid content was varied from 10 wt% to 40 wt% and the results revealed that the weight loss of the catalyst layer after the vibration test increased with the increasing solid content from 10 wt% to 30 wt%; however at the solid content of 40 wt%, the weight loss decreased. In order to provide the explanation for the observation, the researchers described that three types of physical particle interaction existed in the system, which are (i) interparticle attraction (ii) hydrodynamic interactions and (iii) particle-particle frictional interactions. When the solid content is from a medium to high level, the first and third interactions were more significant than the second one; while when the solid content was a low level, hydrodynamic interaction would be more dominant.

The effect of solid content on the strength of catalyst layer was also investigated in [43] by a simulated environment test and it was determined that a higher solid content would lead to a higher weight loss. The reasoning behind this observation was stated to be caused by the difference in thermal expansion coefficients between alumina (the material to prepare catalyst layer) and the metallic substrate (made of FeCrAlloy). Although in this paper, a range of solid content was investigated, the optimum solid content was finally decided to be around 35 wt%, as the strongest catalyst layer with a reasonable loading of catalyst layer was achieved at this level of solid content.

The term loading of catalyst layer is defined as the percentage of mass of suspension retained on substrate after coating, drying and calcination. It was mentioned by a few authors studying catalyst layer [36, 43, 45] that a higher solid content in the suspension would lead to a higher loading due to more particles present in each application of the suspension. However, it was also reported that the satisfactory level of solid content was around 40 wt% as an excessively high solid content would lead to a poor distribution of the suspension over the substrate due to the increased suspension viscosity. This finding probably suggested why there has not been many paper specifically looking at the effect of solid content on the strength of catalyst layer; because if there is not a uniform catalyst layer achieved on the substrate or simply the substrate receives limited amount of catalyst layer, it becomes irrelevant to study the strength of such catalyst layer.

2.2.3.3   pH of suspension

The process parameter, pH of suspension, can be altered by adding an acid into the suspension. In [43], γ-particles mixed with $Ce_{0.68}Zr_{0.32}O_2$ was used to prepare catalyst layer on metallic substrate made of FeCrAlloy. The pH of the suspension was adjusted by using either acetic acid or nitric acid of concentration equals to 1.0 M and a range of pH from 3 to 8 was investigated. The strength of catalyst layer in this research was characterised by using an ultrasonic vibration test which was carried out in a water bath at 120 W, 60 Hz and for 1 h. The sample was then dried at 120 ℃ for 3 h. There was not any information regarding the geometry of the testing environment (including the distance between the source of ultrasound and the position of the sample) and the size of the sample. The results revealed that the chemistry nature of the acid added did not have an effect on the strength of catalyst layer. It was also shown that the strength of catalyst layer prepared from suspension adjusted by both the acetic acid and the nitric acid demonstrated a low weight loss (high strength) from pH = 3 to 6; the weight loss started to dramatically increase at pH = 7 onwards. The weight loss between pH = 3 and 6 was kept below 2% while the weight loss at pH = 7 increased to 40%. In terms of the explanation of the results, the researcher attributed the low weight loss from pH = 3 to 6 to be a reason of particle dispersion in the suspension. In this pH range, γ-alumina particles are positively charged as the pH is below the isoelectric point of alumina. The isoelectric point of alumina is described as the point of zero surface charge [46]. γ-

alumina particles in suspension at pH = 3 to 6 therefore offer positive charge based repulsion as stated by [42] cited in [43].

A different result regarding the effect of pH on the strength of catalyst layer was obtained by [22]. In this work, the ultrasonic vibration test was performed in a beaker at 300 W and 60 Hz for 30 min using petroleum ether as the liquid. Information regarding the size of sample and the geometry of the ultrasonic vibration test were again missing. The sample was then dried at 110 ℃ for 2 h. A good strength of catalyst layer was produced for pH = 4, 5 and 6 as these 3 pHs resulted in weight loss of catalyst layer less than 12% after the vibration test while a low strength of the catalyst layer was produced at pH = 7 with the weight loss being about 20 %. It could be noticed that the weight loss at poor strength was only just 10% higher than what was regarded as a good strength when the results in [43] claimed that the weight loss between strong catalyst layer and weak catalyst layer was almost 38%.

Another research which investigated the effect of pH on the strength of catalyst layer was conducted in [34]. The researcher measured the strength of catalyst layer based on density measurement of the layer. In this work, the highest strength of catalyst layer was reported at pH = 1.35. The strength did not change much from pH = 1.35 to pH = 4.2 approximately; at pH = 4.2 approximately onwards, the strength started to decline significantly. In comparison with the results stated in [22, 43], there seems to exist some difference where the pH conditions for good strength was altered.

In a different work by [44], the researchers selected pH = 3.5 to produce their catalyst layer, regarding this pH level as a good condition for preparing strong catalyst layer. The strength of the catalyst layer produced was tested by an ultrasonic vibration test at 33 kHz for 1 h using acetone as the medium. After test, the samples were dried; however the drying condition was not given. At this pH level (pH = 3.5), a significant weight loss was encountered, being at 47.8% and 33.6% for the suspension with a solid content of 30 wt% and 40 wt%, respectively. The good strength in this work was determined at a dramatic 30% weight loss, which was much higher than the level determined for good strength in previous researches [22, 43]. In fact, in [43], a weight loss of around 30 to 40% was regarded as poor strength.

From the above discussion, the huge difference in the determination of the criteria for good strength made it difficult for different researchers to compare their results. Taking this argument further, without a universal method of measuring the strength of catalyst layer

prepared from different pHs, it would be challenging to quantitatively describe the variation of this strength.

2.2.3.4 Viscosity of suspension

Many parameters in formulation and process can affect the viscosity of suspension; therefore in Figure 2.4, viscosity of suspension was regarded as the derived parameter.

In terms of the effect of particle size on viscosity suspension, it was found that a smaller particle size would give rise to a higher suspension viscosity due to a greater contact area per mass for shearing during viscosity measurement [47]. As discussed in section 2.2.3.2, the formulation parameter, solid content, if taken into more profound consideration, can be incorporated into the effect of suspension viscosity because the viscosity of the suspension strongly depends on the solid content as determined by [40, 47]. In these work, it was reported that the higher the solid content the higher the viscosity of the suspension due to the fact that when there were more particles in the suspension, a higher friction force would be experienced during shearing of the suspension. The effect of viscosity suspension on the strength of catalyst layer can therefore be anticipated in previous discussion from the individual effect of particle size and solid content (section 2.2.3.1 and 2.2.3.2) in the literature.

The effect of pH on suspension viscosity was evaluated in [34]. The lowest viscosity was achieved at pH = 3 at different levels of solid content, which was not the pH condition where the strongest catalyst layer was made. The strength of catalyst layer in this study was indicated by density measurement of the layer. In a different study [22], viscosity of the suspension and strength of the catalyst layer were both characterised; the strength of catalyst layer in this work was measured based on weight loss of the sample in an ultrasonic vibration test. The correlation between viscosity of the suspension and strength of the catalyst layer showed that the lowest viscosity was reached at pH = 4 where the strongest catalyst layer was also produced. However the strength of the catalyst layer still remained in a high level at pH = 3 when the viscosity of it increased significantly to a similar level as pH = 7. The strength of catalyst layer at pH = 7 was determined by the researcher to be significantly lower than that at pH = 3, which was not explained for. From the above discussion, it would be essential to carry out further investigation to explain the complexity in the relationship between suspension viscosity and strength of catalyst layer.

2.2.3.5 DLVO theory

The interaction between particles in a suspension is governed by the DLVO theory [48]. The theory describes that an electric double layer (a layer consisting of both positive and negative charge) is formed on the surface of particles suspended in a medium, as shown in Figure 2.11.
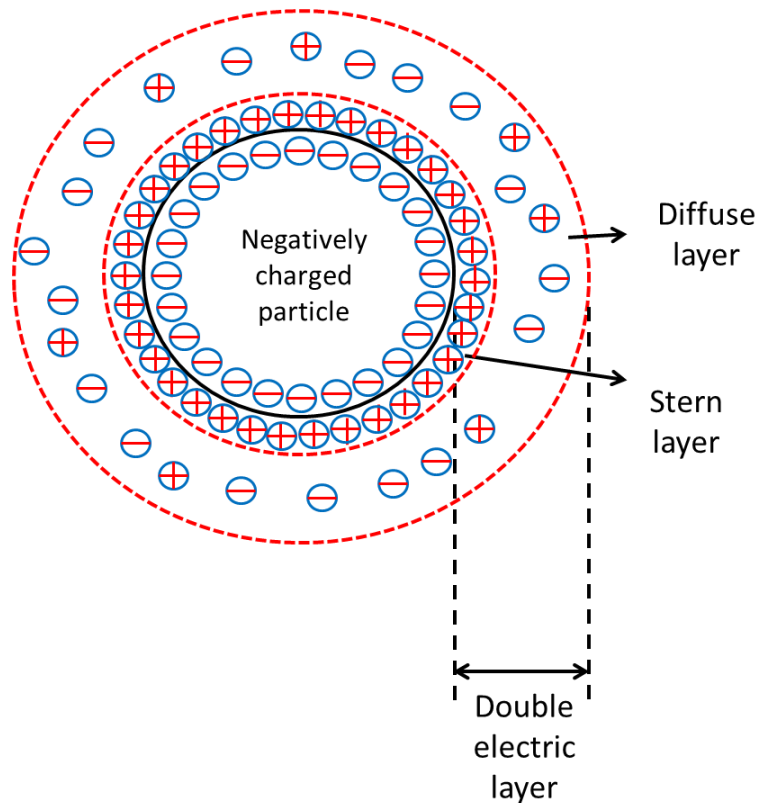
Figure 2.11 Electric double layer on surface charged particle suspended in a suspension

In this electric double layer, there are two sub-layers: a stern layer and a diffuse layer. The stern layer consists of electrostatically firmly bound ions carrying the opposite charge to the surface charge of particles. In the diffuse layer, ions have more mobility than those in the stern layer. In addition, the concentration of ions with the opposite charge to that on particle surface is slightly lowered, while the concentration of ions with the same charge to that on particle surface is slightly increased. The thickness of the dielectric layer, which is related to the concentration of electrolyte present in the suspension, governs the interaction between the particles, as can be seen in Figure 2.12.
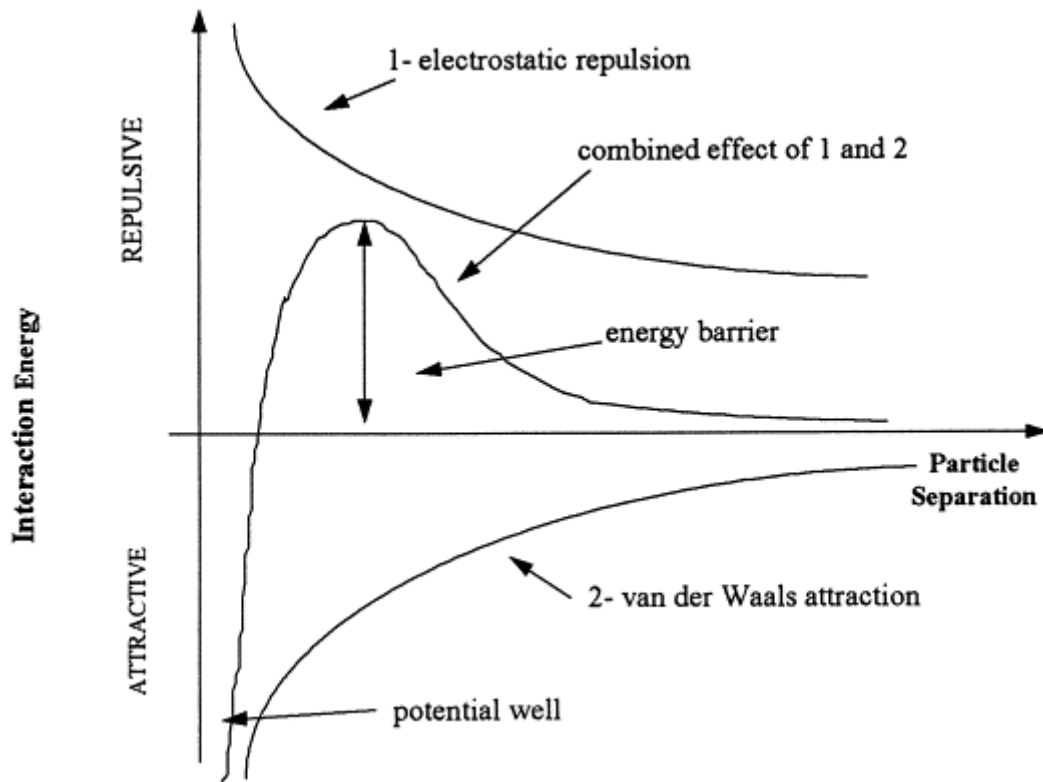
30

Curve 1 stands for the repulsive force between particles, which is caused by the electrostatic effect. Curve 2 represents the attractive force between particles, which is a result of van der Waals attraction. As the distance between particles becomes smaller, both forces start to increase. The competition between these two forces is the key to understand the stability of a suspension. The combined force in this case exhibits an energy barrier which particles in the suspension have to overcome in order to agglomerate as shown in Figure 2.12.

The equations developed in the DLVO theory are presented in Equation 2-2 to Equation 2-6.

$$V_{rep} = 2\pi\varepsilon\varepsilon_0 R\zeta^2 e^{-\kappa D}$$

Equation 2-2

where ε = dielectric constant of water , ε_0 = vacuum permissivity , R = particle radius , ζ = zeta potential, κ = reciprocal of Debye length, D = separation between particles

$$\kappa = \left(\frac{k_B T \varepsilon_0 \varepsilon}{2q^2 N_A I}\right)^{-\frac{1}{2}}$$

where k_B = Boltzmann constant , T = absolute temperature , q = elementary charge , N_A = Avogadro's number, I = ionic strength

$$I = \frac{1}{2}\sum_{i=1}^{n} z_i^2 c_i$$

where z_i = valence of ion of type i, c_i = concentration of ion of type i

$$V_{Van} = -\frac{AR}{12D}$$

where A = Hamaker constant

$$V_{tot} = V_{rep} + V_{Van}$$

where V_{tot} = total potential energy

Equation 2-2 shows the expression to determine the repulsion potential between particles. It involves the use of a number of physical constants which are dielectric constant of water and vacuum permissivity. Zeta potential can be experimentally determined. The expression for K is shown in Equation 2-3 where other physical constants such as Boltzmann constant, elementary charge and Avogadro's number are present. K is termed as the reciprocal of Debye length; therefore the reciprocal of K represents Debye length which is effectively the length of an electric double layer [50]. From Equation 2-3, it could also be seen that the ionic strength is involved in the calculation of the Debye length. The ionic strength can be

computed from Equation 2-4. A higher concentration or a higher valence charge of the ion would contribute to a higher ionic strength. It could be seen that as the ionic strength is proportional to the quadratic power of the valence charge; therefore the ionic strength could be increased more significantly, if a single charge valence ion is replaced by an ion with multiple valance charges.

An increase in the ionic strength, according to Equation 2-3, would result in an increase in K. As K is the reciprocal of Debye length, therefore an increase in the ionic strength actually corresponds to a shorter Debye length, meaning that the effective radius of electrostatic repulsion from the electric double layer on charged particles is reduced. If the zeta potential is kept constant, such changes would give rise to a reduction in the repulsion potential; this suggests that particles in suspension are more likely to agglomerate with each other rather than staying as a stable dispersion. In other words, the relationship between Debye length and repulsion potential is that a shorter Debye length would lead to a lower repulsion potential. This indicates that a narrow electric double layer is not effective in creating strong repulsion potential between particles, there is a greater chance that particles can overcome this repulsion barrier by their thermal motion to agglomerate with each other. On the opposite, a greater overlapping in electric double layer (wider electric double layer) would generate more effective repulsion to repel particles to stay as a stable dispersion.

In terms of the effect of separation between particles on repulsion potential, it can be seen from Equation 2-2 that an increasing separation between particles would cause repulsion potential to behave in an exponential decay manner. On the other hand, particle radius is in a linearly proportional relationship with repulsion potential while zeta potential has a quadratic power on repulsion potential. This means that particles with higher charges are more effective in enhancing repulsion potential than merely increasing the size of particles.

Equation 2-5 is used to determine the attraction potential. The attraction potential is in nature a result of Van der Waals force acting over the separation between particles. After computing the repulsion potential and the attraction potential separately, Equation 2-6 compares the two potentials; in the theory, the attraction potential is regarded as positive while the repulsion potential is taken as negative. The summation of the two potentials gives the net potential between particles.

2.2.3.6　Coating methodology

By far the most widely used coating methodology in preparing catalyst layer is dip-coating as it is easy and economical to apply [43], [51], [30], [37].

The application of suspension by dip-coating is usually performed by immersing a chosen substrate in the suspension followed by withdrawing the substrate and blowing off the excess suspension with an air jet. In the research carried out in [37], a metallic substrate made of FeCrAlloy was dip coated. The substrate was immersed in alumina suspension for 15 s and withdrawn at different speeds ranging from 1.7 cm/min to 7.6 cm/min. The effect of withdrawal speed on loading of catalyst layer was investigated in this paper and the results suggested that a variation in the withdrawal speed in this range did not change loading of catalyst layer greatly. The reason behind the limited influence was that there was a maximum amount of catalyst layer that could be deposited in each dip coating. This was a combined result of particle size, solid content, pH of suspension. Having noticed this observation, in this work, the researchers then decided to increase loading of catalyst layer by performing multiple runs of dip coating and investigated the effect of multi-stage dip-coating on the strength of catalyst layer. From a ultrasonic vibration test conducted in petroleum ether for 30 min (the frequency and power of the vibration test were not given), the results showed that a satisfactory strength for the catalyst layer was still reached after a second round of dip-coating however the third time of dip-coating caused a high weight loss of catalyst layer after the vibration test.

In another paper [52] which described about preparation of alumina based catalyst layer by dip-coating, a dip-coating procedure of the following steps was carried out. A metallic substrate made of 0Cr20Al7Y ferrite stainless steel (meaning that 0 wt% of Cr, 20 wt% of Al, 17 wt% of Y and 63 wt% of Fe) was dip-coated for one time by immersion in an alumina slurry for 1 min following by withdrawal. The withdrawal speed was not given in the paper. The strength of the catalyst layer was measured by ultrasonic vibration test at 120 W and 40 kHz with no time given. The samples obtained achieved approximately 22% weight loss after the vibration test.

It could be seen that occasionally spray coating and electrophoretic deposition were also used in preparing catalyst layer; but they have not gained much attention in research community due to difficulties in applying them on an industrial scale [39].

2.2.3.7 Drying

Drying in the manufacturing process of catalyst layer aims to remove molecules of the suspension medium, e.g. water, ethanol etc. and in the meantime allow particles to pack to give a formed body. The precautions that have to be taken here are not to form cracks during drying.

The effect of some drying conditions has been examined in the literature. As the drying process is concerned with the removal of molecules of the suspension medium, the rate at which these molecules are removed, i.e. the drying rate, can affect the quality of catalyst layer produced. This is because the rate of drying process has an influence on how γ-alumina particles pack together during drying. A few authors have found that a fast drying process is detrimental in obtaining high strength catalyst layer [36] and [53]. This was thought to be due to the high thermal stress developed in a fast drying process, which caused cracks to form in the catalyst layer obtained. A fast drying process (which was carried out from 120 ℃ to 280 ℃ for duration ranging from 5 min to 2 h as seen in literature) was found to only have removed molecules of the suspension medium near the free surface of the suspension, forming a solid layer, which then prevented molecules of the suspension medium in the bulk of the suspension from evaporating. The molecules in the bulk were in fact trapped and remained in the catalyst layer until the end of the drying process. The calcination process that followed involved the use of more intensive heating, which caused these trapped molecules to escape from the bulk of the catalyst layer. This escapement process was found to be associated with a high shrinkage in the volume of the coating, which was regarded as a signal of a high thermal stress. The development of this high thermal stress eventually caused the catalyst layer to crack.

In a different work [37], the effect of post-deposition procedure which included drying and calcination was investigated. The results suggested that there was not a substantial influence of drying temperature on the strength of catalyst layer, provided the drying temperature was kept above 100 ℃. In comparison to [36] and [53], this work seemed to have generated different conclusion regarding the drying rate on the strength of catalyst layer. In the previous two studies, the researchers concluded by stating that a faster drying process would lead to a reduction in the strength of catalyst layer however in [37], this effect seemed not to exist. This could be because in the latter study, the drying temperature used was too high to display any measurable effect of drying rate on the strength of catalyst layer.

2.2.3.8   Calcination

The effect of calcination temperature on the quality of catalyst layer was explored by [36]. This work used two different calcination temperatures (500 ℃ and 900 ℃) to carry out heat treatment of the catalyst layer after drying. Strength characterisation of the catalyst layers prepared was performed by ultrasonic vibration test set at a power of 1000 W and a frequency of 25 kHz. The duration of the tests were kept at 20, 40, 60 and 80 min. The weight loss of the longest test for the sample calcined at 900 ℃ was found at 18.3% while the sample calcined at 500 ℃ was determined at 26.0%. The results showed that a higher calcination temperature would cause the strength of catalyst layer to increase. The reason for this observation was investigated by X-ray diffraction (XRD). The original γ-phase was found to convert into the δ-phase when the temperature was increased to 900 ℃. Although δ-alumina is a more compact structure than γ-alumina, showing a higher strength in its formed body, the porosity of its formed body is lower than that formed by γ-alumina, which is often not acceptable in the catalyst industry.

Another research which looked at the effect of calcination temperature on the strength of catalyst layer was [37]. Uncalcined samples and samples calcined at different temperatures which were 400 ℃, 700 ℃ and 900 ℃ for 10 hours. The ultrasonic test conducted for strength measurement showed that the weight loss for these 3 calcination temperatures were 1.6%, 0.8% and 0.08%, respectively, suggesting that higher calcination temperature would give rise to a higher strength for the catalyst layer.

2.2.3.9   Preoxidisation of alloy substrate

A high calcination temperature can increase the level of pre-oxidisation of the FeCrAlloy substrate to create the so-called alumina whiskers to bind with the catalyst layer, which essentially improved the adhesive strength. The formation of alumina whiskers on FeCrAlloy substrates is observed in a number of publications ([54], [55], [56]) and a general conclusion is that such formation will occur at temperatures above 850 degrees. Alumina whiskers are formed due to the presence of aluminium in FeCrAlloy substrate; the nature of alumina whiskers is oxidised aluminium with the chemical formula of Al_2O_3. The reason that alumina whiskers are preferred is due to the fact that they offer better adherence for the catalyst layer coated on a FeCrAlloy substrate.

2.3   Granular catalyst supports

The extensive use and the importance of granulation process for the preparation of granules have seen numerous papers published on this topic in the literature; however the majority of these studies still focus on granulation of food and pharmaceutical materials, a scarce amount of them has dealt with ceramic material such as boehmite. This part of the literature review has drawn a summary of the existing literature on granulation of boehmite powder (which can be considered as hydrated γ-alumina) or just alumina powder in general since not much literature specifically deals with granulation of boehmite powder.

2.3.1   Introduction

Before the literature review of granular catalyst supports began, it would be important to state the definition of two entities which are primary agglomerates and secondary agglomerates or granules. A description of these two entities has been briefly given in section 1.2.

Finely divided nanometre sized crystallites of boehmite, due to the small size, tend to agglomerate under the influence of Van der Waals forces to form aggregates of micrometre scale, which are termed as primary agglomerates. These primary agglomerates often have to undergo further size enlargement processes such as granulation to form larger bodies (often millimetre scale). The larger entities formed are termed as granules or secondary agglomerates.

2.3.2   Preparation of granular catalyst supports

One research used α-alumina as the powder, polyvinyl alcohol as the binder and a high shear mixer as the granulation equipment [57]. Increase in either liquid solid ratio (a ratio between the amount of liquid added during granulation and the amount of powder being granulated, abbreviated as L/S or binder amount was found to increase the size of the granules obtained. This was because both of these two parameters would lead to the same effect during the granulation process, i.e. more binder was made available on the surface of powder for further growth of granules to take place. This statement was also expressed by [58] where the growth mechanism involved was studied using alumina powder (the phase of which of was not specified) and found to consist of three stages as can be seen below (Figure 2.13).

No significant change in size	Moderate increase in size	Significant increase in size
1st regime: A balance between attrition of loosely formed agglomerates to release more fine particles and agglomeration of fine particles	2nd regime: Layering of fine particles onto agglomerates from the 1st regime; Densification of these agglomerates; Transport of binder from the core of growing agglomerates to the surface to allow more growth	3rd regime: Coalescence between agglomerates to form large granules as the end product

Figure 2.13 Growth mechanism in granulation of alumina powder

The effect of calcination temperature on the strength of α-alumina granules was investigated by [57]. A higher calcination temperature, which promoted more solid bridges to be formed between the granules by sintering, lowered the granule porosity; but increased the granule strength. SEM was used to visualise the solid bridges formed between the α-alumina granules under higher calcination temperature, which was seen as a more dense packing of the α-alumina particles.

2.3.3 Characterisation of granular catalyst support

Although γ-alumina granules have been successful produced as catalyst support for industrial processes and the effect of different formulation and process parameters on the manufacturing process has been studied to a certain extent, there is a variable that is often omitted by a lot of authors ([59], [60], [57]), i.e. the existence of primary agglomerates. Boehmite powder or alumina power in micrometer scale, usually used as the starting material for granulation process, are in fact already agglomerates of even smaller nanosized particles. These agglomerates, which can be called primary agglomerates, can be a result of the sol-gel preparation procedure and influence the granulation process to affect the quality of granules produced at the end. At the moment, when evaluating the strength of γ-alumina granules, the

strength of these primary agglomerates has seldom been taken into consideration. Table 2.2 shows summary of the methods currently used to assess strength of γ-alumina granules. After appreciating how these tests are performed, it is not difficult to note that none of them has shown any consideration of the effect of the strength of boehmite primary agglomerates on the strength of γ-granules which are produced from boehmite primary agglomerates.

Attrition test can be performed by tumbling granules in a drum or tube, followed by measuring the mass loss of the granules. An impact test is usually performed by using an air flow to carry granules to hit a target, followed again by the measurement of the mass loss of the granule. A bulk compression test first of all involves compression of a group of granules (predetermined mass) in a circular die to a certain force and fitting algorithm (as shown in Equation 2-7) is then used to calculate the yield strength of the granules from the stress over strain behaviour during compression. A crushing test is conducted by using a punch travelling at a pre-set speed to crush a single granule; the force at which the granule fails is noted. The equation to calculate granule strength based on this method is shown in Equation 2-8.

$$lnP = ln\left(\frac{\tau}{\alpha}\right) + \alpha\varepsilon_n + ln(1 - e^{-\alpha\varepsilon_n})$$

where P is the applied pressure, τ is the average granule strength, α is a friction related constant, ε_n is the natural strain

<div align="right">**Equation 2-7**</div>

$$\sigma = \frac{4F}{\pi D^2}$$

where σ is the granule strength, F is the force at which failure of granules is detected, D is the diameter of granule

<div align="right">**Equation 2-8**</div>

As the strength of boehmite primary agglomerates has not been taken into consideration when examining the strength of γ-alumina granules in the current literature, whether the failure of these granules occurs at the bonding between boehmite primary agglomerates or within these primary agglomerates still remains unknown. A knowledge of this difference

will allow researchers to better understand the failure of γ-alumina granules and their structural properties.

Table 2.2 Assessment method of alumina granule strength

Attrition test	Impact test	Bulk compression test	Crushing test
[57]	[10]	[57]	[61]
[62]		[62]	[60]
		[63]	[60]
			[62]

2.4 Measurement of bonding between particles

It can be seen in the previous discussion in the literature that the strength of catalyst layer is highly related to bonding between particles in the catalyst layer. One of the ways to evaluate bonding between particles, although not in the catalyst industry, is by measuring the tensile strength of a tablet created from the particles of interest. This method is widely adopted in the pharmaceutical industry where granules consisting of drug particles and excipient particles or just the primary particles are compressed to make a tablet ([64] and [65]). During measurement of the tensile strength of a tablet, the following stress development in the tablet can be anticipated.

As the piston goes down, the tablet is being compressed. At the top part of the tablet where it is initially in contact with the piston, a compression zone is formed. The compressive stress in the zone increases as the piston moves down further. The highest concentration of compressive stress is reached at the tip of the compression zone where the compressive stress starts to act as tensile stress to open the tablet along its diameter. In this way, the tensile stress is a measure of bonding between particles along the central plane. The force applied by the piston that causes the tablet to develop tensile failure would be used with the dimension of the tablet to work out the tensile strength of it according to Equation 2-9.

$$Tensile\ strengh\ of\ tablet = \frac{2 \times Force}{\pi \times Diameter \times Thickness}$$
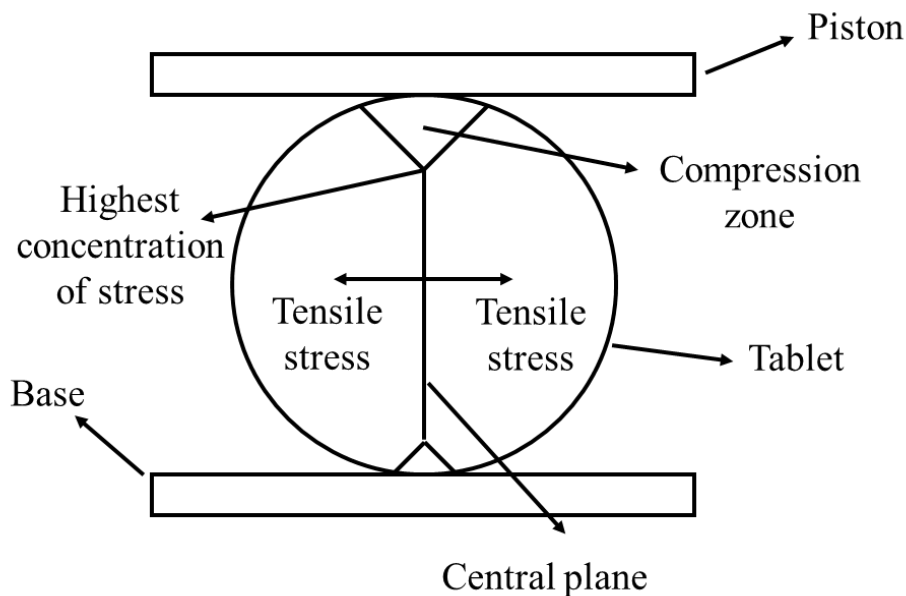
Figure 2.14 Development of stress during measurement of tensile strength

2.5 Summary of knowledge gaps in the current literature

As mentioned in the introduction, the majority of literature in the field of catalyst study still focuses on the chemical properties of catalyst, i.e. how fast and/or selective the conversion reactions happen; there have not been enough publications which have looked at the physical properties of catalyst supports which have allowed the excellent chemistry of catalyst to be realised.

From the relative limited research work on physical properties of catalyst support, two forms or shapes have been paid particular attention in the above literature review, which are catalyst layer and granular catalyst support.

In terms of the catalyst layer, amongst the work which has focussed on a parametric study in this subject, it has been critically spotted that the strength of catalyst layer, suffers from a poorly developed measurement method. The majority of the current methods are either incapable of differentiating between the cohesive and adhesive strength of the catalyst layer or fail to report the strength on unit which is independent of the testing environment. These

41

disadvantages create difficulties for the research community to answer two questions: (1) which failure mode is more critical in determining the life time of catalytic converters (2) how the results from one author can be compared with those in other publications.

As for granular catalyst support, the preparation procedure of primary alumina powder, the subsequent granulation process and the characterisation of granular strength have been discussed in details. The discussion revealed that many authors ignore the existence of the pre-agglomerated status of alumina powder when evaluating granular strength. The pre-agglomerated status of alumina powder, which will be referred as primary agglomeration in this thesis, can be a result of the commonly used sol gel powder preparation procedure. Whether structural failure of granular catalyst support occurs between primary agglomerates or within primary agglomerates which are used to form the granular catalyst support still remains unknown to the ceramic community.

2.6 Research Aims

Having recognised the current challenges in the literature for the characterisation of the strength of a catalyst layer, the current thesis aims to develop a scientific method that is capable of separately quantifying the cohesive and adhesive strength of a catalyst layer and reporting the final result based on the unit of stress. The use of a stress unit would therefore allow different researchers to compare the strength result of their sample; the separate quantification of the strength of the catalyst layer would enable us to better understand the limiting factor in the life of catalytic converters.

With regards to the granular catalyst support, the thesis aims to quantify the strength of primary agglomerates and granular catalyst support (also known as secondary agglomerates) and then determines whether the failure of granular catalyst support is a result of the failure within primary agglomerates or between primary agglomerates.

Chapter 3 Experimental materials and methods

3.1 Introduction

In this chapter, the materials and the general methods which are used in this PhD work are presented. More detailed experimental methods which are specific to the individual chapter are shown in the relevant chapters.

3.2 Experimental materials

The experimental material used to study catalyst layer is the γ-alumina powder (SCFa140; ex-Sasol). The SEM images of it are shown in Figure 3.1.
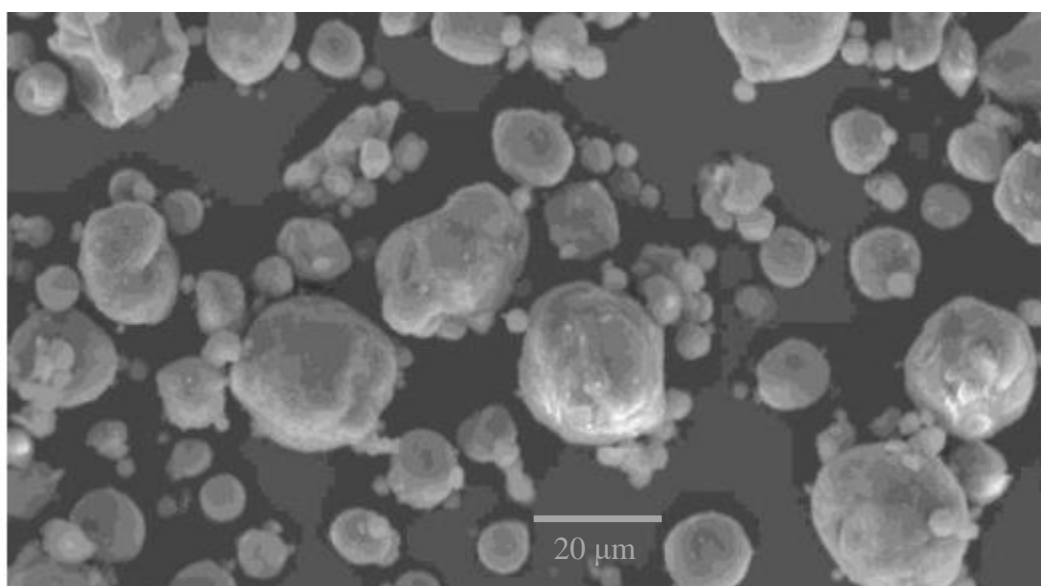
Figure 3.1 SEM images of γ-alumina powder (SCFa140)

The experimental materials used to study granular catalyst supports are both boehmite powder which are referred in the study as Versal 250 and Versal 700, respectively. The supplier of the boehmite is UOP. The SEM images of the powder are shown in Figure 3.2 and Figure 3.3.
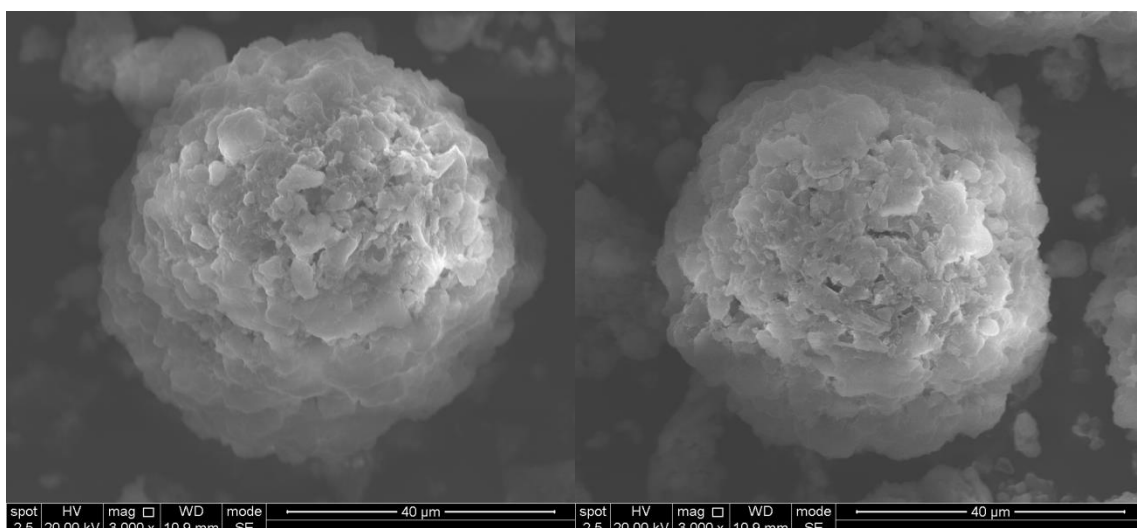
Figure 3.2 SEM images of Versal 250 boehmite powder
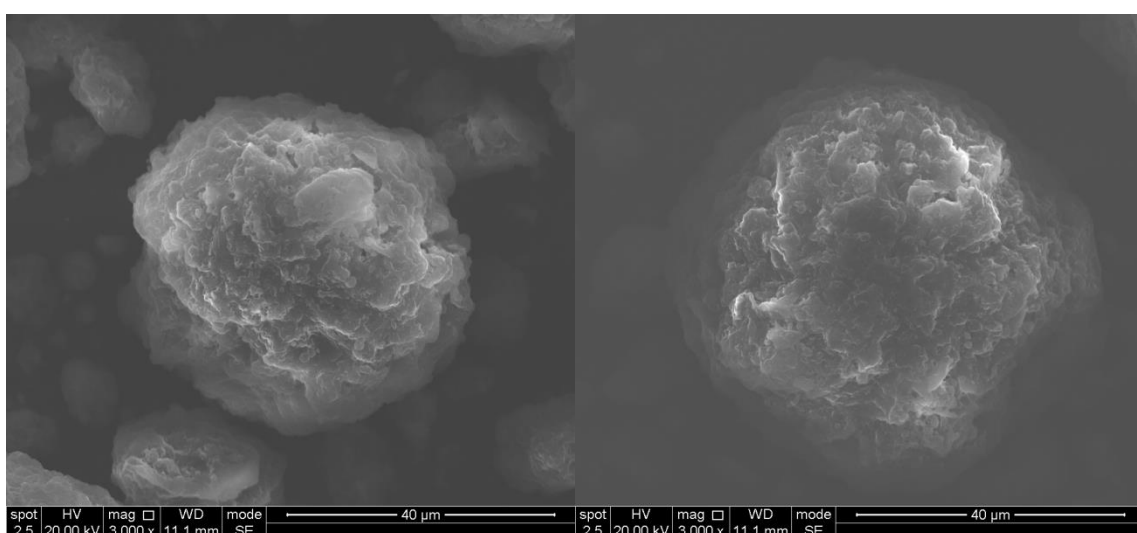
Figure 3.3 SEM images of Versal 700 boehmite powder

3.3 Preparation of suspension

The γ-alumina powder used to catalyst layer study was pre-mixed with deionised water to obtain a suspension containing 40 wt% solid. This suspension was then wet-milled to reduce the size of γ-alumina particles down to a level of just a few micron. The milling conditions to fulfil this task are presented in Table 3.1.

Table 3.1 Milling conditions for preparing γ-alumina suspension

Mass of powder (g)	Mass of liquid (g)	Milling media	Milling time (min)	Milling speed (rpm)	Percentage of volume occupied by beads
200	300	1 mm yttrium stabilised zirconia beads	4	3950	70 % (corresponding to an approximate volume of 70 ml)

A mill (M250/100, Eiger) was chosen for this grinding task due to its ability to achieve particle size reduction to near sub-micron level in a much shorter time than the conventional stirred bead mill which cannot operate at high milling speed. It is equipped with a pre-dispersion screw to transport the feed from the funnel into the grinding chamber where a high energy agitator is situated to accelerate the grinding media. The impact events generated in the grinding chamber ensure that a desired particle size of a few micron can be achieved.

The criterion of this milling process was to reduce the size of the original γ-alumina particles down to between 1 and 20 micron (volume based particle size distribution: $d_{10} \approx 2 \, \mu m, d_{50} \approx 8 \, \mu m, d_{90} \approx 18 \, \mu m$) as measured by laser diffraction (Malvern Mastersizer-3000). This small size of alumina particles was found to be necessary for a strong catalyst layer to be made (otherwise the catalyst layer would simply just be a loose compaction of powder instead of a formed body). The reason for this increase in strength with a reduction in particle size is fairly intuitive that a smaller particle size can give rise to an increased surface area per unit volume of particles, which would lead to more inter-particle bonding per unit volume of particles and finally resulted in the formation of a stronger catalyst layer or other formed bodies. Apart from the small particle size, the fact that the milling procedure was carried out in the presence of water was also found to be important to obtain catalyst layer with satisfactory strength (as examined in Chapter 9).

3.4 Measurement of isoelectric point (IEP) of γ-alumina

The definition of isoelectric point (IEP) is the pH at which a particle has a zero surface charge. Surface charge is determined by zeta potential measurement. The measurement principle of zeta potential is based on an electrokinetic phenomenon. A suspension of particles with known viscosity is first of all subject to an electric field of known strength. This electric field acts across the suspension to mobilise particles. Particle motion depends on the nature and the magnitude of their charge. Positively charged particles will move to the electrode with negative charge and vice versa. The velocity of particle motion is proportional to the magnitude of their charge. The velocity of particle motion can be determined from laser scattering. An incident laser beam with a known frequency is introduced to radiate through the suspension. Due to movement of particles, the laser beam experiences scattering which causes a change in the wave frequency. The shift in the frequency as a result of particle motion is then used to determine velocity of particle movement. Velocity of particle motion is then calculated from Equation 3-1.

$$\Delta v = \frac{2Vn\sin\left(\frac{\theta}{2}\right)}{\lambda}$$

where Δv = amount of shift in light frequency, n = refractive index, θ = scattering angle, V = velocity of particle motion, λ = wavelength of laser,

Equation 3-2 could then be used to determine electrophoretic mobility of particles at a particular strength of electric field.

$$U = \frac{V}{E}$$

where U = electrophoretic mobility of particles, E = strength of electric field

Equation 3-3 is then finally used to determine the zeta potential of particles.

$$\zeta = \frac{4\pi\eta U}{\varepsilon}$$

Equation 3-3

where ζ = zeta potential, η = viscosity of suspension, ε = dielectric constant of conductive medium

It could be seen from the above equations that zeta potential is dependent on a number of parameters. Material properties of the sample such as particle size and particle shape could affect the scattering angle and the velocity of particle motion as well and as a result influence zeta potential. For this reason, it can be expected that it is more accurate to present zeta potential as a range rather than a single value.

Based on a range of literature, the isoelectric point of alumina particles of different phases can be seen in Table 3.2

Table 3.2 IEP values of γ-alumina from literature

Literature	Isoelectric point
[22]	7 (gamma)
[46]	7.5 (alpha)
[66]	9.1 (alpha)
[67]	7.5 (alpha)

From the values in Table 3.2, it could be said that the IEP of γ-alumina particles is in the range between pH = 7 to pH = 9.

Chapter 4 Development of the Cohesive Strength Method (Tablet Method)

4.1 Introduction

It had been discussed in Chapter 1 that catalyst layer in service fails in both the cohesive and the adhesive mode; it was then pointed that in the current literature there is no method to separately measure the cohesive and the adhesive strength which are both important. Therefore, in this chapter, a method to separately measure the cohesive strength of catalyst layer was developed. The method is also referred as the tablet method. A number of indirect methods to verify the strength data gained from the tablet method were also presented.

4.2 Development of the method

4.2.1 Principle of the measurement

The cohesive strength of a γ-alumina catalyst layer was measured using a tablet method. The tensile strength of a tablet upon compression is a direct measurement of the inter-particle bonding. Therefore, if the tablet is made from the same material as the catalyst layer, then the cohesive strength of the catalyst layer can simply be determined from crushing this tablet.

4.2.2 Experimental method

4.2.2.1 Tablet preparation

The difference between the conventional way of producing tablets which is by powder or granule compression and the current method of making tablets is that the current method is a "wet" approach, producing tablets by drying a suspension. As the suspension is flowable, there is a need to make a tablet die in which the suspension can then be dried. It was decided to make the tablet die from cutting a tube because this is probably the easiest way to obtain a die of cylindrical shape with consistent dimensions and in good quantities as measurements need to be repeated.

After a number of trials with different pipes such as silicone pipe and plastic pipe, nylon pipe was finally selected to make the tablet dies. This is because nylon pipe is hard and tough enough to withstand the cutting force from a pipe cutter without deformation to allow a smooth and straight finish. To further help with the cut finish, a steel rod was pushed through the pipe to minimise deformation resulted from the cutting force. This height was chosen to be 10 mm to keep a roughly one to one ratio between the height of the tablet die to its diameter. The diagrams showing the above description are presented in Figure 4.1.
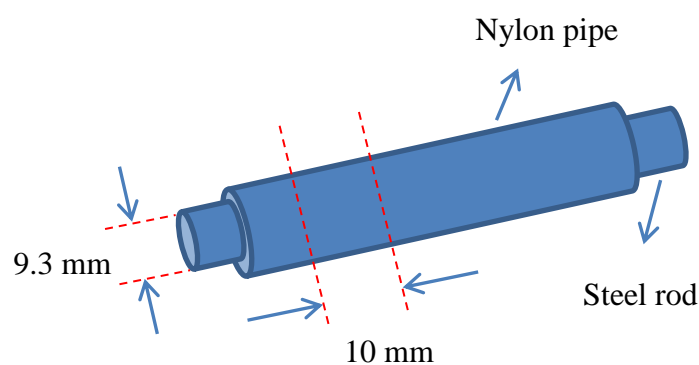

Figure 4.1 Cutting of nylon pipe to make tablet dies

After the tablet dies were made, each of them was fixed onto a microscope glass slide on one side using a two-component epoxy glue. The technique for applying the glue needs to be noted as it can interfere with the quality of the tablets produced.

The tablet die was first placed on the glass slide. Due to the straight and smooth cut finish, the tablet die can rest in good alignment with the glass slide. The glue was then applied outside of the tablet die at the bottom of the die (as seen in Figure 4.2). The two-component epoxy glue had an approximately 5-minnute-long working time. During this time, the liquid glue could be easily applied to cover the entire circumference of the bottom of the tablet die.

The pH of the suspension was selected as one of the experimental parameters because as shown in the literature (section 2.2.3.3) it would be desired to obtain separate measurement of cohesive strength of the catalyst layer based on stress. A Jenway 3510 pH meter was then used to measure the pH of the suspension. A 10 M HCl solution was employed to change the pH to the acidic range. A 10 M NaOH solution was used to change the pH to the basic range. The amount of acid or base that was added to the suspension in order to change the pH to the

required value was recorded to ensure that the added solution does not change the specified solid percentage greatly.
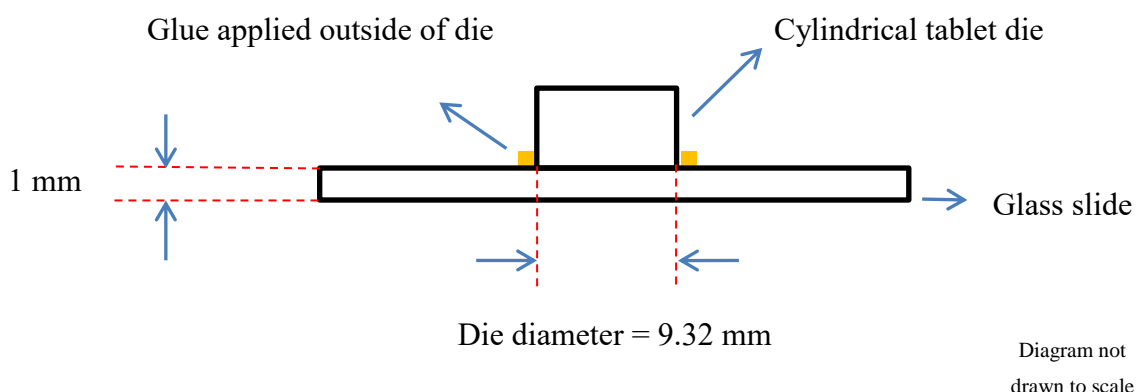

Figure 4.2 Gluing of the tablet die onto a glass slide

For 50.0 g of suspension that was produced at the milling conditions stated in section 3, the amount of acid or base needed for the various pH changes is shown in Table 4.1. The pH of a freshly prepared suspension using the stated milling conditions was around 5.5 roughly. The acid or based added to the suspension was properly mixed with the suspension.

Table 4.1 Amount of acid (10 M HCl) and base (10 M NaOH) added for the required pH changes

	Mass of acid = 0.1 g	pH = 5.5 for a freshly wet milled suspension	Mass of base = 0.1 g	Mass of base = 0.4 g	Mass of base = 0.5 g
pH	4		6	8	10
New solid percentage	39.92%		39.92%	39.68%	39.60%

According to Table 4.1, it can be seen that the added amounts of acid and base did not change the desired solid percentage significantly.

The suspension milled as described in Chapter 3 was used to fill the die using either a plastic pipette or a medical syringe. The choice of the addition tool was dependent on the flowability of the suspension. In turn, the flowability of the suspension was dependent on the pH of the suspension. The pH of the suspension was one of the experimental parameters to be

investigated for the cohesive strength of catalyst layer. For suspension with low pH, plastic pipettes were used as the suspension was quite flowable. However for suspension with high pH, medical syringes were used to allow the transfer of the highly viscous suspension without involving air bubbles. In both cases, the mass of the suspension added as about 0.8 g as shown in Figure 4.3.
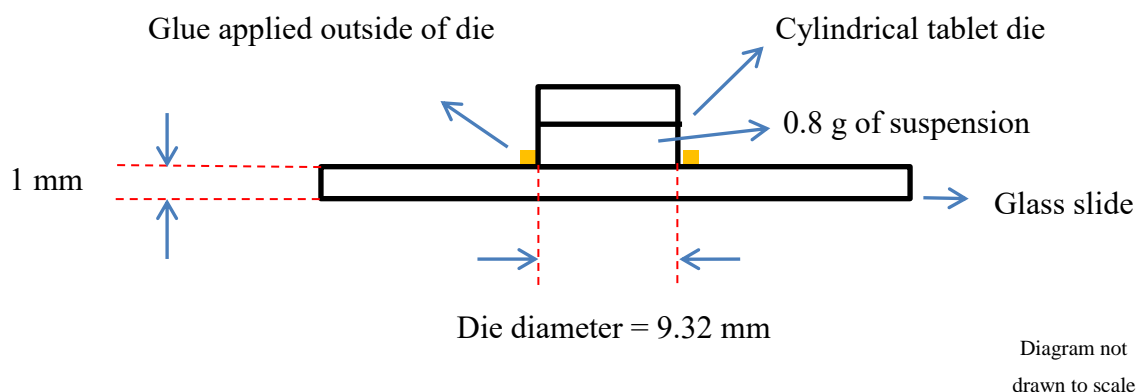

Figure 4.3 Addition of suspension into a glass slide

The drying took place a fixed relative humidity and temperature condition by using an environment chamber (Series KMF, Binder GmbH). After the suspension was completely dried, the tablets needed to be removed from the dies. A surgical knife was used to cut the glue at the interface between the tablet die and the glass slide. Due to the sharpness of the surgical knife, the glue could be cut without the need of applying great force; therefore the tablet samples in the die could be left intact. A glass rod with its head covered with some cotton wool was then used to gently push the tablets out of the dies.

4.2.2.2   Testing the strength of the tablet

As already stated earlier in the chapter, the tensile strength is a direct measurement of the strength of inter-particle bonding between particles; therefore this measurement can directly give the cohesive strength of the catalyst layer. The experimental setup for measuring the tensile strength of tablets is described in Figure 4.4. This measurement was done using a material testing equipment (Zwick/Roell Z 0.5, Germany).
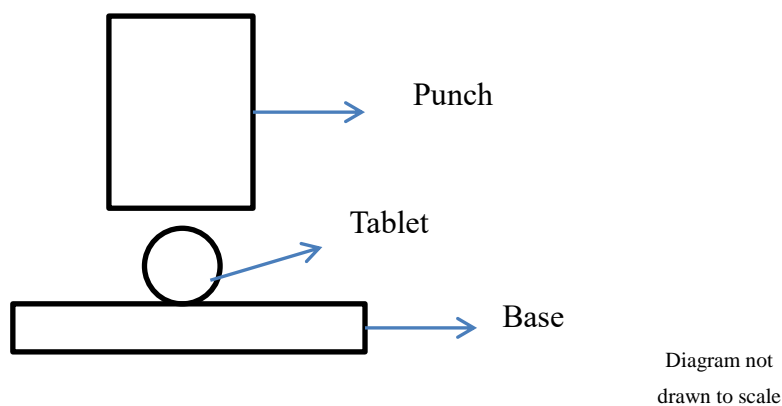
Punch

Tablet

Base

Diagram not
drawn to scale

Figure 4.4 Experimental setup for testing the tensile strength of tablets

A tablet sample was vertically placed on a base. A punch was set to move down to compress the tablet to tensile failure. The rate at which the punch moved down was controlled to be 5 mm/min. The diameter and the thickness of the tablet were measured. The force being applied by the punch that caused the breakage of the tablet was recorded. The Brazilian equation (Equation 4-1) was used to calculate the tensile strength of the tablet

$$Cohesive\ strength = Tensile\ strength = \frac{2 \times Breakage\ force}{Tablet\ diameter \times Tablet\ thickness \times \pi}$$

Equation 4-1

4.3 Results and discussion

The following results were obtained for the cohesive strength of a catalyst layer as measured by the tablet method. For each point, 8 measurements were carried out.

It can be seen that the cohesive strength peaked at pH = 4 and gradually decreased as the pH was increased to higher values. This is the first set of results regarding catalyst layer reported in the unit of stress. In order to verify that the novel method developed here was giving a true comparison in the cohesive strength, other supporting measurements (disintegration section 4.4 and penetration section 4.5) were employed to prove the cohesive strength obtained here.
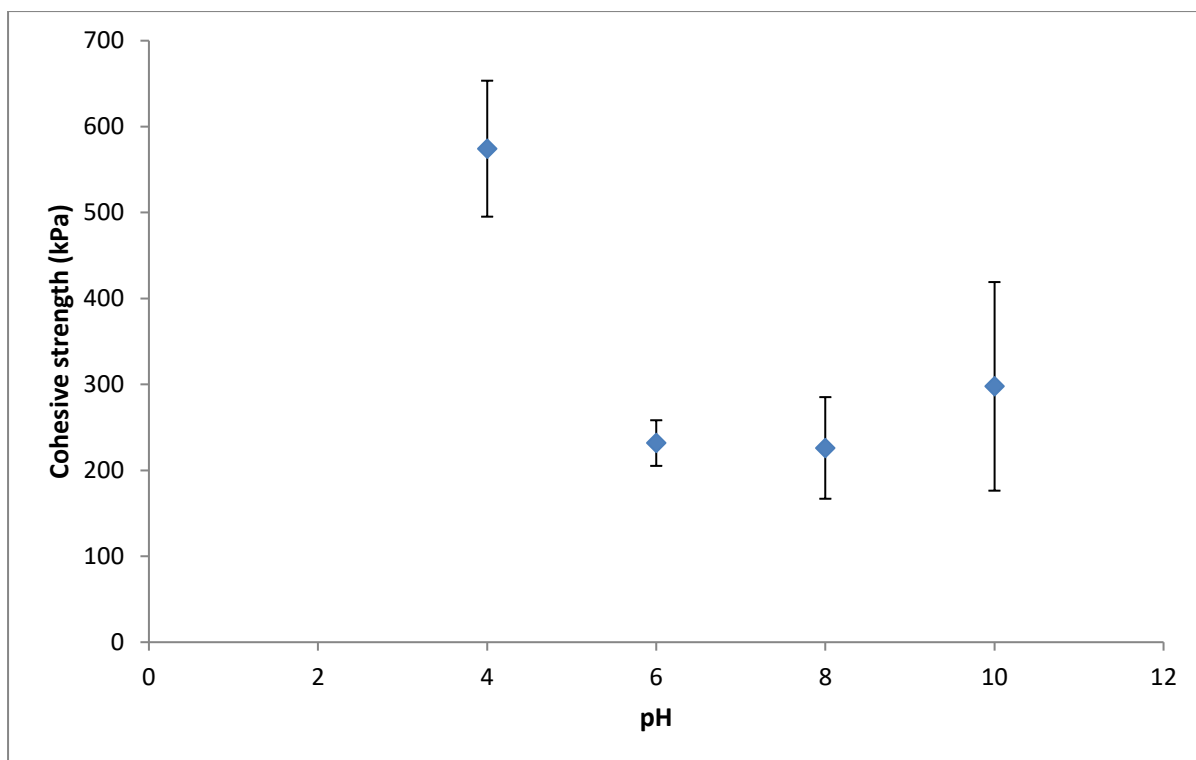
Figure 4.5 Cohesive strength of catalyst layer as measured by the tablet method

4.4   Indirect method 1 of strength measurement – disintegration of tablet

4.4.1   The idea behind the measurement

The cohesive strength of tablet formed by γ-alumina particles is related to the way that these particles pack. If a more porous structure is formed, the strength of the body would be expected to be low and vice versa. Another property of a more porous structure is that it is more vulnerable to water penetration due to its larger internal pore space. This susceptibility to water penetration usually leads to a faster disintegration process of the structure. Therefore quantifying the disintegration process of the tablets can serve as an indirect method to determine the cohesive strength of the tablet. If a similar trend in the cohesive strength is observed with this method, then the cohesive strength measurement from the novel tablet method proposed here can be supported.

Given that γ-alumina is a material capable of conducting electricity when in its aqueous form, therefore one way of quantifying the disintegration process is by measuring conductivity.

4.4.2 Experimental method

A Jenway 4520 conductivity meter was used to measure the conductivity. The tablets tested were produced according to the procedure described in section 4.2.2. The following experimental setup was used for this measurement.

For each experiment, 250 ml of deionised water of 20 °C was used. A magnetic stirrer was placed in the centre of the beaker used. The 4th power which represents an agitation speed of 300 rpm, was selected on the motor (Kika Werke RT 10 Power). The tablet was placed in a basket and immersed in the water.

The temperature and conductivity combined probe was inserted against a mark to make sure that it would always be placed in the same position. It was important to check that the temperature was not changing significantly during the measurement. The reason for this was that as the measurement of conductivity here was done with time, an increase in temperature which can accelerate the motion of ions may cause the conductivity to rise greatly in a short time.

The value of conductivity of the deionised water before the tablet was loaded was measured as the background conductivity. The value of conductivity when the entire tablet disintegrated was regarded as the maximum conductivity. The following equation (Equation 4-2) was used to normalise the data of tablets made at different pHs in order to have a comparison [68].

$$Percentage\ disintegrated = \frac{Conductivity - minimum\ conductivity}{Maximum\ conductivity - minimum\ conductivity}$$

<div align="right">

Equation 4-2

</div>

4.4.3 Results and discussion

The conductivity profiles of the disintegration of the tablet made at different pHs are shown below.
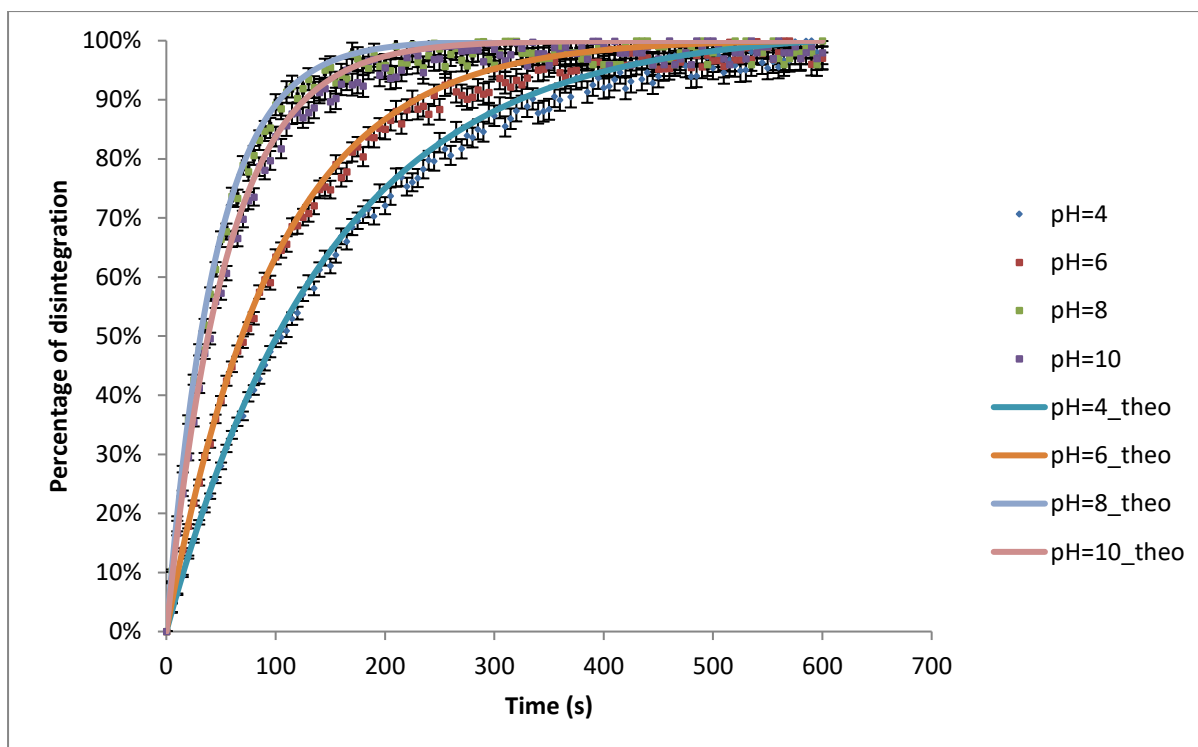
Figure 4.6 The conductivity profile of the disintegration of the tablet made at pH = 4, 6, 8 and 10

The results in Figure 4.6 indicated that tablets produced at pH = 8 and 10 had a low cohesive strength, as suggested by their fast disintegration process; tablets produced at pH = 6 still had a relatively higher cohesive strength compared to these two pH values, as shown by its relatively slow disintegration process; and the tablets made at pH = 4 had the highest cohesive strength owing to its slowest disintegration. The hypothetical explanation behind the concurrent trend in the cohesive strength and the disintegration profile was that a low strength tablet sample would have more pores inside it, making the sample more vulnerable for water penetration to initiate disintegration.

A theoretical relationship was also determined for each disintegration curve. It could be seen that the disintegration curve presented an increasing trend approaching the 100% point asymptotically, therefore Equation 4-3 was used to fit for the experimental data to determine the time constant.

$$Percentage\ of\ disintegration = -e^{-\frac{t}{T}} + 1$$

Equation 4-3

where t = time, T = time constant

55

Least square regression was used to obtain the time constant for each disintegration curve which is shown in Table 4.2. It could be seen that a slower disintegration corresponds to a larger time constant.

Table 4.2 Determination of time constant

pH	4	6	8	10
Time constant (s)	151	98	46	54

4.5 Indirect method 2 of strength measurement - penetration into tablet

4.5.1 The idea behind the measurement

A similar explanation can be stated here for the idea behind this the penetration measurement. A more porous tablet which would have a lower tensile strength would be more susceptible to penetration of a liquid. Using this concept, the cohesive strength measured by the newly developed tablet method can be verified.

4.5.2 Experimental method

The following experimental setup (Figure 4.7) was employed to carry out the penetration experiment. The principle of the measurement is based on the use of a high speed camera to capture the penetration process of the liquid and the penetration time can be calculated from the number of frames taken for the penetration process to complete.

The high speed camera employed was the Photron Fastcam 1024 PCI manufactured by Itronx Imaging Technologies. A framerate of 3000 was selected. The liquid used was water coloured with a red dye (erythrosine B, acid red 51, Sigma–Aldrich) for better visualisation. The liquid was dispensed from an electronic pipette (Eppendorf Xplorer) which was secured at the same position for each penetration test. The tablet sample was placed vertically underneath the electronic pipette over a distance of 1 cm. The short distance was tested to be

sufficient for the droplet to form at the tip of the pipette without contacting the tablet sample and impact the tablet without developing too much kinetic energy.
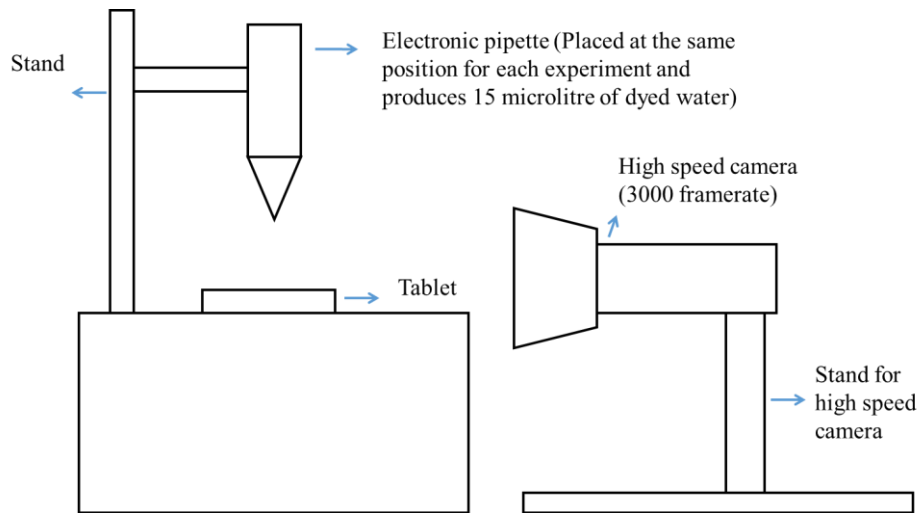

Figure 4.7 The experimental setup for performing the liquid penetration test on γ-alumina tablets
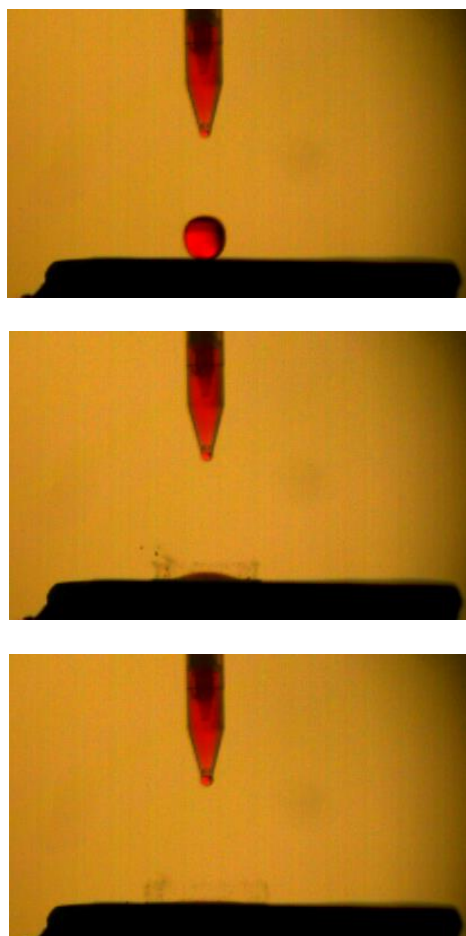

Figure 4.8 A series of images captured by the high speed camera, showing an example of the penetration process (top: droplet landing; middle droplet penetrating: bottom: penetration complete)

An example of the pictures taken from the high speed camera is shown in Figure 4.8. The top image shows that the droplet has just landed on the tablet; the middle image shows that the droplet is penetrating into the tablet; the bottom images shows that the penetration process is completed.

4.5.3   Results and discussion

The following results (Figure 4.9) were obtained from the penetration experiment. It could be seen from Figure 4.9 that tablets prepared at pH = 4 had the longest penetration time while tablets made at pH = 8 showed the shortest penetration time. The trend of penetration time was in close agreement with the cohesive strength presented in Figure 4.5, indicating that more porous tablets demonstrated a lower cohesive strength. This finding suggested that the cohesive strength as measured by the tablet method developed was valid and the method can be applied to a wider range of preparatory parameters.
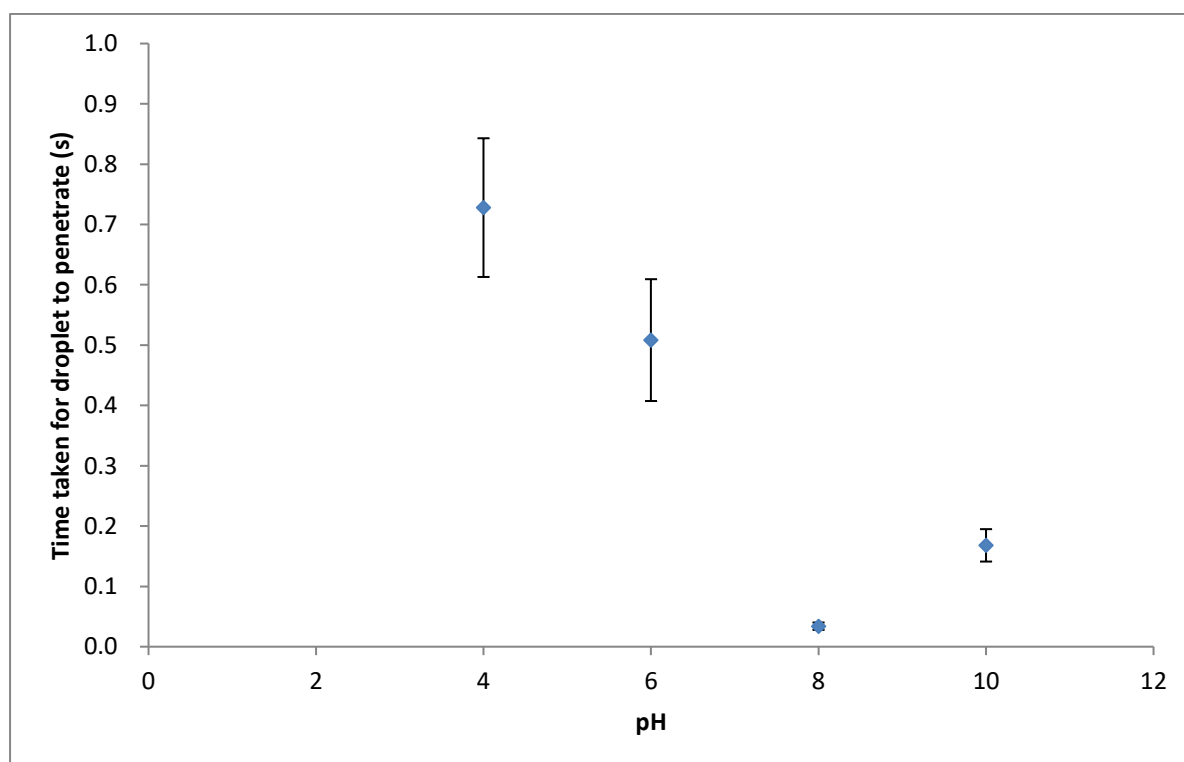

Figure 4.9 Penetration time for tablets made at different pHs

4.6 Combination of methods

After the determination of the cohesive strength of catalyst layer by the above both direct and indirect methods, it was decided to prepare more comprehensive graphs (Figure 4.10 and Figure 4.11) combining the results from these methods. It could be seen that both the time constant and the penetration time displayed similar trends to the cohesive strength profile.
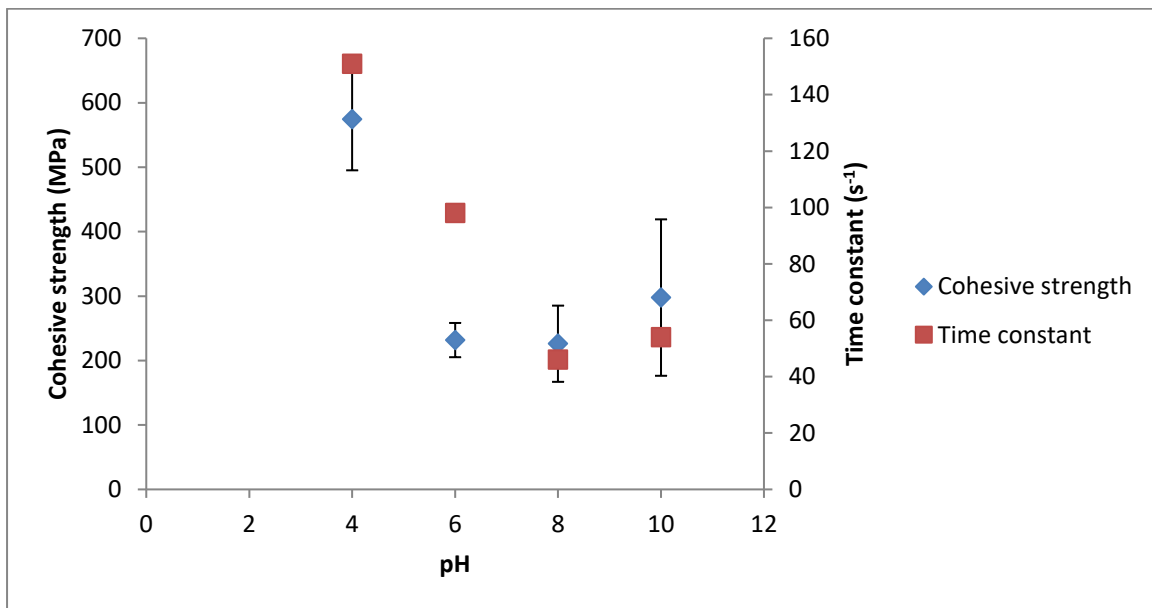

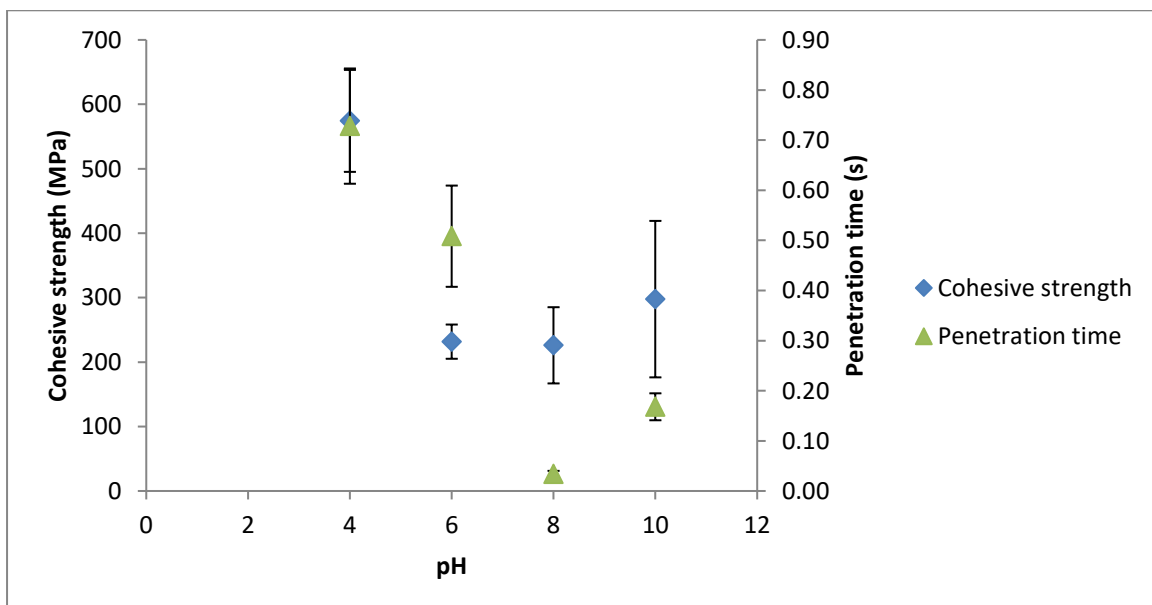**Figure 4.10 Cohesive strength and time constant at different pHs**

Figure 4.11 Cohesive strength and penetration time at different pHs

4.7 Conclusion

A novel method to separately quantify the cohesive strength of catalyst layer made of γ-alumina and report the strength on unit of stress has been invented. The method works by turning γ-alumina suspension into a tablet whose tensile strength can be easily calculated by the Brazilian equation. The cohesive strength of the catalyst layer which is in fact the bonding strength between particles of the layer is deemed to be equal to the tensile strength of the tablet made of the same particles, as the tensile strength of the tablet is a measure of the inter-particle bonding strength at the central plane of the tablet.

The tablet method was supported by results from two other methods which indirectly quantified the strength of tablet: the disintegration method and the penetration method. The disintegration method showed that tablets with a lower tensile strength (catalyst layer with a lower cohesive strength) had a much shorter disintegration time and vice versa. The penetration method demonstrated that tablets with a lower tensile strength were also found to exhibit shorter penetration time and vice versa.

The verification of the novel tablet method by the other two methods suggested that the cohesive strength results obtained by the tablet method are valid and the method can be applied to understand the effect of a wider range of preparatory parameters.

Chapter 5 The effect of relative humidity and calcination on the cohesive strength of catalyst layer

5.1 Introduction

Since the tablet method developed in Chapter 4 was shown to be valid, Chapter 5 aimed to apply this method under a calcination condition and relative humidity to understand the behaviour of cohesive strength of catalyst layer.

5.2 Drying conditions

The relative humidity during drying of the suspension was chosen to be examined as stated in the literature that this factor was not consider at present. Three different sets of drying condition (as shown in Table 5.1) were selected to investigate the effect of relative humidity on the cohesive strength. The seven different pH conditions described above were all dried under these three drying conditions to obtain a full profile of the cohesive strength. The drying was performed in an environment chamber (Series KMF, Binder GmbH).

Table 5.1 Drying condition of the suspension

Set	1	2	3
Temperature (˚C)	25	25	25
Relative humidity (%RH)	20	40	60

5.3 Calcining the tablet

Calcination is a requirement in the manufacturing process of the γ-alumina catalyst layer. The effect of calcination was investigated in this chapter. The temperature used for the calcination process [conducted in a furnace (Carbolite)] was 500 ℃ and the duration of calcination was 2 hours.

5.4 Results and discussion

5.4.1 The effect of calcination

The effect of calcination temperature was tested in this chapter. The tablets were prepared at a wider pH range. The addition of acid (HCl) and base (NaOH) to adjust the pH can be seen in the following table. The tablets tested were dried at 25 ℃ and 40 %RH (the same drying condition carried out in Chapter 4 where calcination was not conducted) in order for the results from different calcination temperatures to be comparable. The same suspension prepared in Chapter 3 was used here.

Table 5.2 Amount of acid (10 M HCl) and base (10 M NaOH) added for the required pH changes

	Acid (HCl)			Base (NaOH)			
pH	2	4	6	8	10	12	14
Mass of acid (g)	1.0	0.1	N/A	N/A	N/A	N/A	N/A
Mass of base (g)	N/A	N/A	0.1	0.4	0.5	1.7	3.6
New solid percentage	39.22%	39.92%	39.92%	39.68%	39.60%	38.68%	37.31%

A quick calculation, assuming both the acid and the base could completely dissociate, returned with a suspension pH more aggressive than the currently measured values. This suggested that the assumption of complete dissociation may be wrong. As the starting pH of the γ-alumina slurry was around 5, meaning that there was already a quantity of H^+ ions in the suspension, a certain degree of inhibition on the dissociation of the acid can be expected and therefore the assumption of complete dissociation may not be true. This would indicate that more HCl would be needed to shift the pH to the lower pH values required. As for the basic side, an extra amount of NaOH would be needed initially to neutralise the existing H^+ ions in the suspension before the pH can be lifted to even higher values.

The cohesive strength of tablets obtained in chapter 4 (where no calcination was used) and in this chapter (where calcination was performed at 500 ℃ for 2 hours) is presented below in Figure 5.1. A number of 8 measurements was performed for each point. It could be seen that the tablets after calcination are higher than those before calcination. This suggested that there was a sintering process that occurred between γ-alumina particles during calcination, which improved the cohesive strength of catalyst layer.
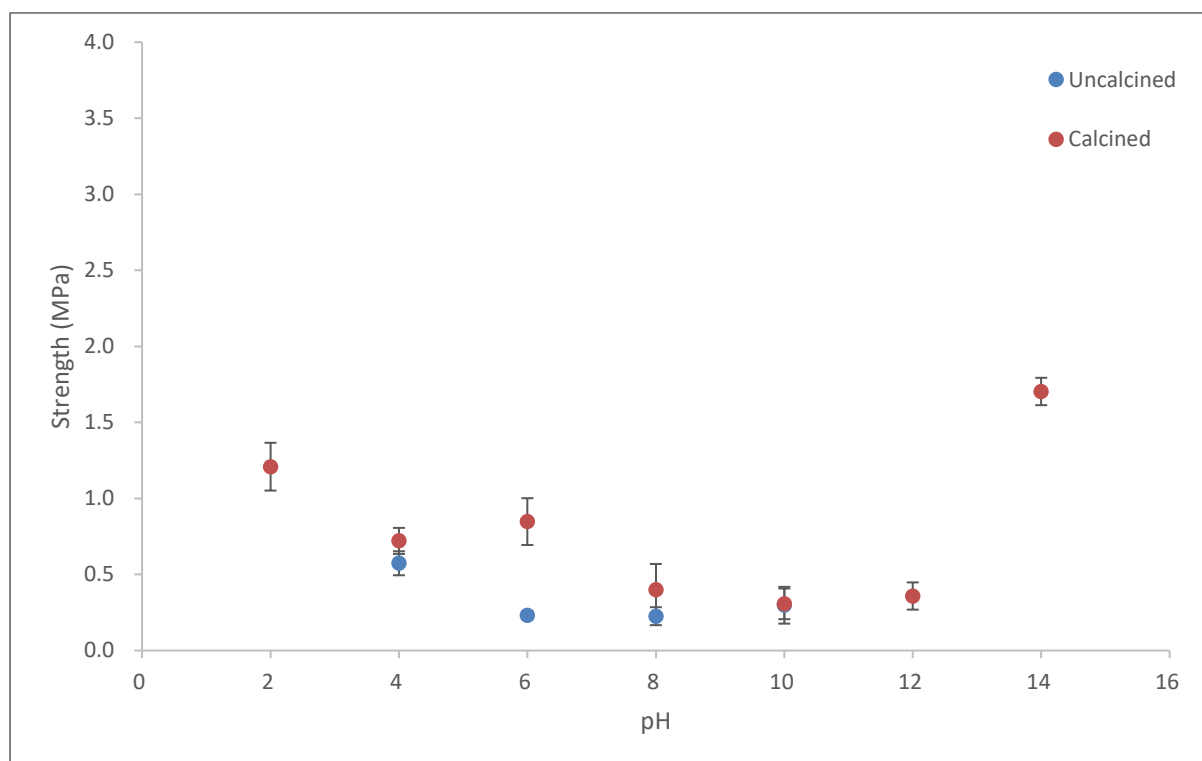

Figure 5.1 The effect of calcination on the cohesive strength of catalyst layer

5.4.2 The effect of relative humidity

The cohesive strength of catalyst layer at the three different drying conditions: 20, 40 and 60 % RH and at different pHs are shown in Figure 5.2, Figure 5.4 and Figure 5.5. A number of 8 measurements was performed for each point. Before the effect of relative humidity is discussed, it is necessary to explain the variation of the cohesive strength of the catalyst layer at different pHs.

The trend of the cohesive strength of the catalyst layer at different pHs can be divided into 2 regimes based on the isoelectric point of γ-alumina. The isoelectric point (IEP) of a material is defined as the pH which makes the surface charge of the material zero and the IEP of γ-

alumina is from 7 to 9 as seen in Chapter 3. On the acidic side of the isoelectric point, the cohesive strength exhibited a zig-zag behaviour, showing a medium strength at pH = 2, reaching the minimum of the whole figure at pH = 4 and recovering again to an even higher strength at pH = 6. In the range of isoelectric point, the cohesive strength was found to be at a low value. On the basic side of the isoelectric point, when the pH was still close to the isoelectric point, the cohesive strength was maintained around the same level as that shown at the isoelectric point. As the pH started to move away from the isoelectric point pH, the cohesive increased and reached the maximum point of this curve at pH = 14.
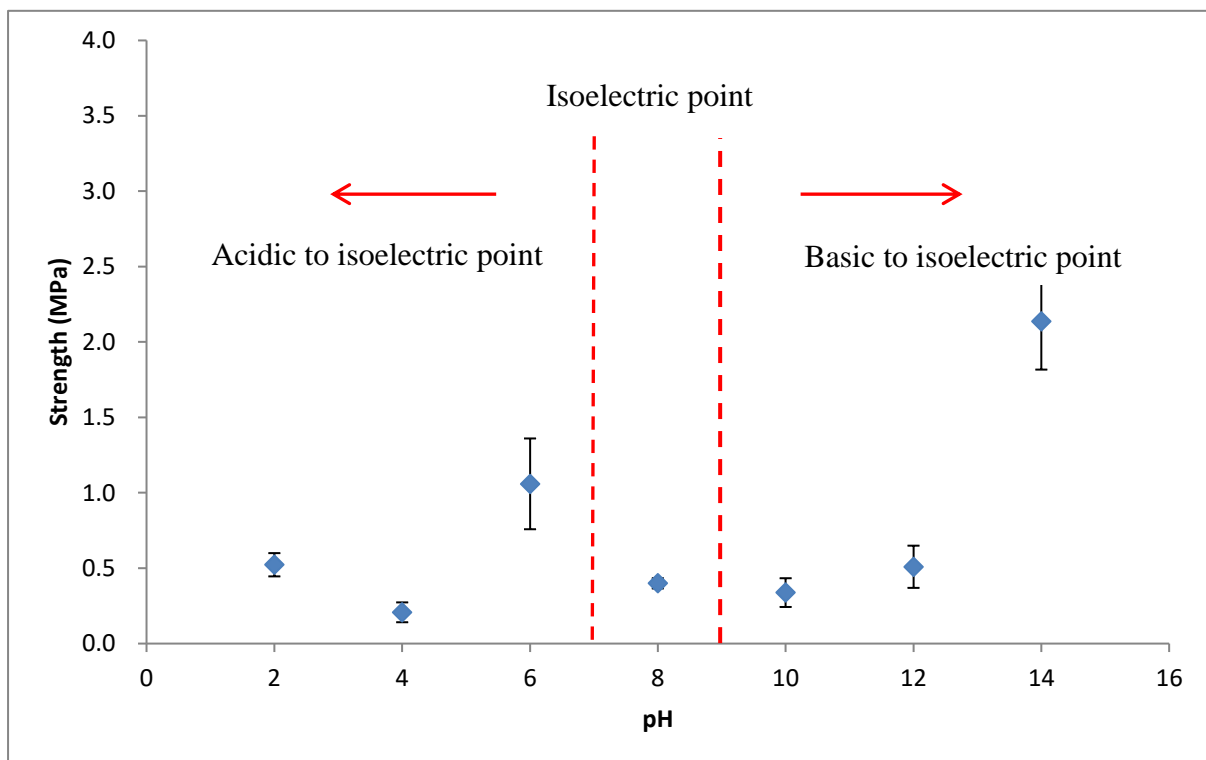
Figure 5.2 The effect of pH on the cohesive strength of catalyst layer dried at 20 %RH

The explanation for the strength trend observed is given here. At pH=8 which is very close to the isoelectric point, due to the lack of surface charge, strong van der Waals attraction dominated between γ-alumina particles. This suggests that there was very little mobility of individual γ-alumina particles during the drying process and as a result of this, the γ-alumina particles were not able to adjust themselves to form a tight packing, leaving a low tensile strength of the tablets and therefore indicating a low cohesive strength of the catalyst layer at this condition (as seen in Figure 5.3). This situation did not change greatly as the pH was increased from 8 to 10, indicating that this increment in pH was simply not sufficient to

introduce enough surface charge on γ-alumina particles to enhance their mobility in suspension for them to travel to more favourable sites to form a strong tablet which is expected consist of more closely-packed γ-alumina particles.

The situation started to change as the pH was increased from 10 to 12 and showed a significant difference when the pH was shifted from 12 to 14. The current argument for the change is as follows. The increased concentration of OH^- in the suspension medium led to an increased surface charge on γ-alumina particles, causing the particles to separate from each other due to electrostatic repulsion. This separation of γ-alumina particles granted them extra mobility in the suspension and therefore they were able to travel more freely in the suspension. The free movement of γ-alumina particles allowed them to closely pack with other γ-alumina particles during drying, giving rise to a high cohesive strength formed (as seen in Figure 5.3). As the research progressed, it was noticed that a flocculated status existed between γ-alumina particles at high pHs, which would be explained in more details in Chapter 6.

High mobility   Drying   Tighter packing

Low mobility   Drying   Loose packing
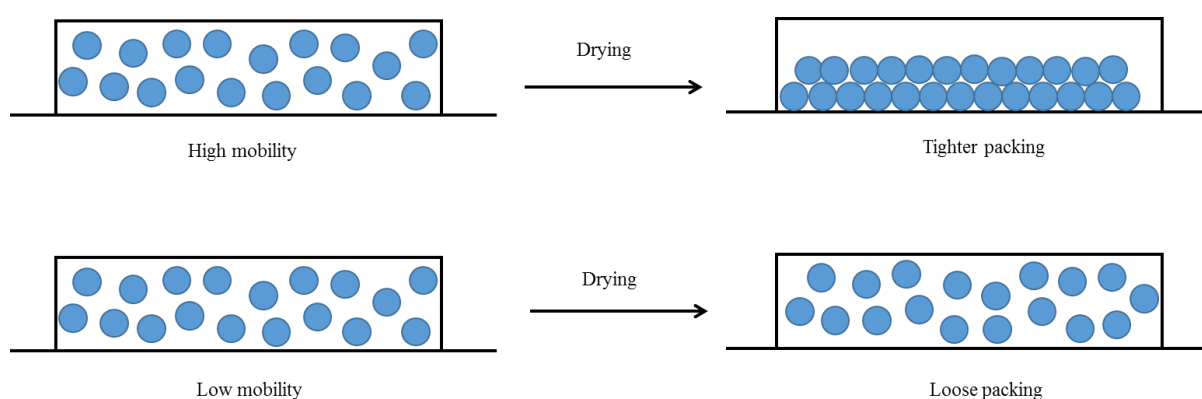
Figure 5.3 The effect of particle mobility on drying

Following the above explanation, a deviation from the isoelectric point would then cause an increase in the cohesive strength of the catalyst layer. Based on this trend, the strength behaviour at pH = 2 and 6 was in close agreement and the same explanation as above (for the strength behaviour from pH = 8 to pH = 14) can be applied. However the strength at pH = 4 did not agree with this trend; it showed a decrease in strength from pH = 6. In fact, during the manufacturing process of tablets at pH = 4, after drying, the tablets were found to separate into two parts: one upper thin tablet with a shiny top surface and one lower thick tablet.

In this chapter, the lower tablet was used for the cohesive strength test. The process happened during the drying process was proposed to be that γ-alumina particles, especially the small ones managed to were carried by water to the top of the tablet die and agglomerated to become a formed body there. The existence of this process can be verified by the shiny top surface formed on all tablet samples produced at pH = 2 and 4. Therefore the current measurement of cohesive strength at pH = 4 using the tablet method probably cannot represent the true cohesive strength at this condition. More details about this tablet splitting issue and the solution to avoid it would be given in Chapter 6.

The cohesive strength of the catalyst layer at 40 and 60 %RH as measured by the tablet method was also determined as seen in Figure 5.4 and Figure 5.5. In both cases, at pH = 8, the cohesive strength was at a very low level, due to the effect of neutral surface charge as explained earlier in this section. Similar strength was again found at pH = 10 as the increased OH^- concentration was not sufficient enough to cause any significant change in the mobility of γ-alumina particles. As the pH was moved from 10 to 14, the cohesive strength was also found to start to increase dramatically, as a result of the additional amount of OH^- ions into the suspension to further enhance the mobility of γ-alumina particles. For the acidic side of the isoelectric point, the cohesive strength at pH = 2 and 6 was again higher than that close to the isoelectric point due to the increased surface charge by the introduction of H^+ ions. A change in this trend occurred for the cohesive strength at pH = 4 (at 60 %RH) that the strength at this pH increased with the relative humidity applied upon drying. This change will be explained in more details later in this section.
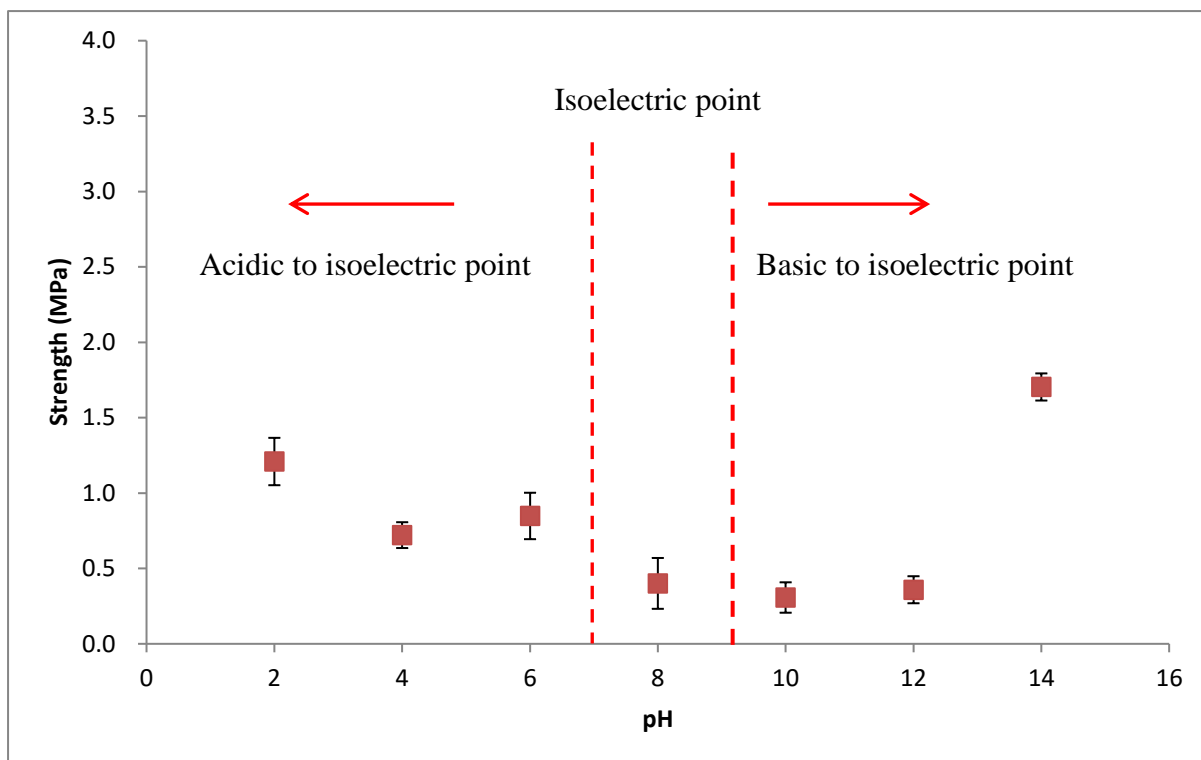
Figure 5.4 The effect of pH on the cohesive strength of catalyst layer dried at 40 %RH
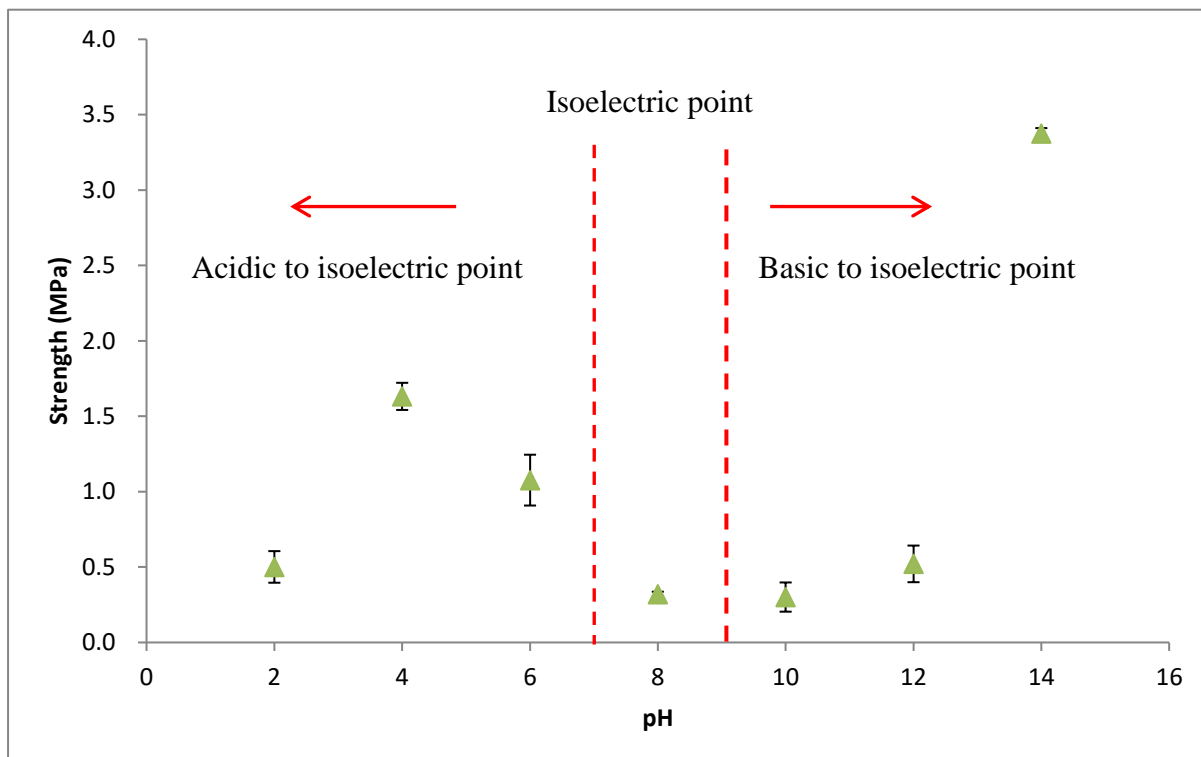
Figure 5.5 The effect of pH on the cohesive strength of catalyst layer dried at 60 %RH

It is worth noting that the presence of Na^+ in catalyst layer may post a threat as Na^+ can act as a catalyst poison in real catalyst system, Due to this concern, a more suitable choice of base (e.g. NH_3) for pH adjustment was then used in the subsequent chapters to give a more genuine representation of the cohesive strength.

The effect of relative humidity during drying on the cohesive strength of catalyst layer is shown in Figure 5.6. One very obvious observation is that when the pH was close to the isoelectric point (pH = 6, 8 and 10 and 12), a change in the relative humidity for drying did not affect the cohesive strength greatly, meaning that the effect of particle surface charge was still dominating. When the pH was increased further in the basic side, a slow drying process (high relative humidity upon drying) led to an increase in the cohesive strength. This effect was made clearer when the pH was raised to 14. The cohesive strength obtained by drying at 20 and 40 %RH was still quite close to each other as shown by the error bar; the cohesive strength resulted from drying at 60 %RH was however significantly higher than the other two. The explanation for these observations was related to the drying rate of the drying process. A slower drying process allowed the particles to have more time to find a favourable packing site to generate a more closely packed structure; however a fast drying process may not give sufficient time for most particles to pack in a close pattern. A similar situation occurred for the tablets (the lower part of the tablets after splitting) prepared at pH = 4 at the 3 drying conditions. The relationship between cohesive strength and relative humidity upon drying at pH = 2 still awaits further investigation. More explanation were provided following the discussion of DLVO in Chapter 6.
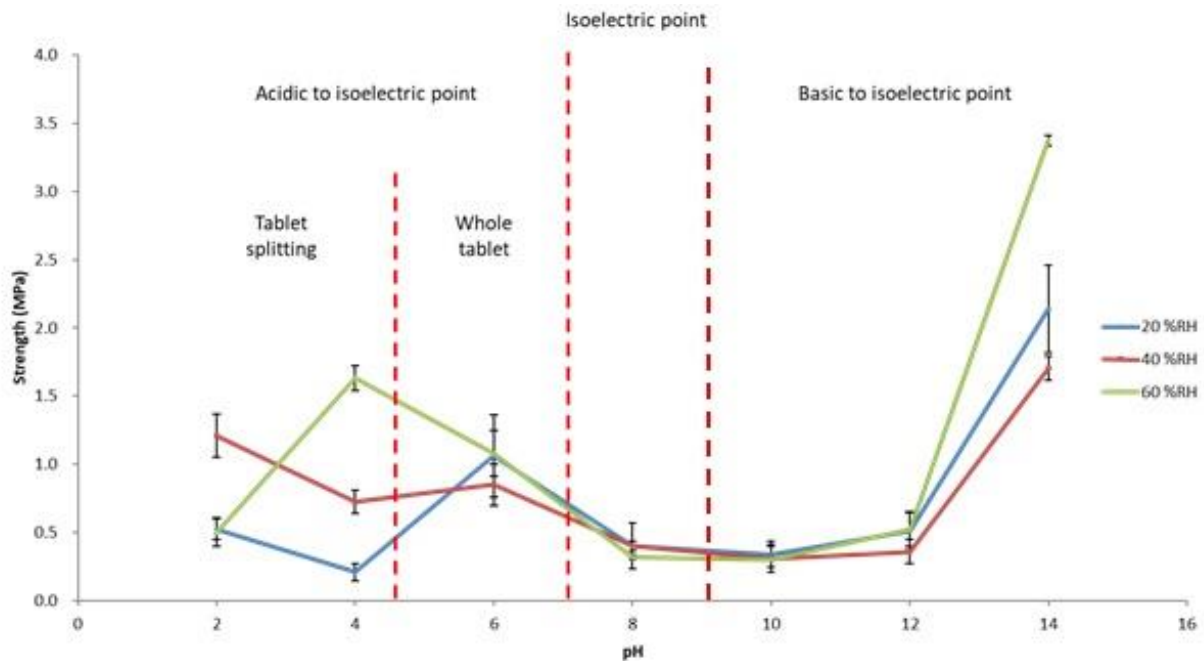
Figure 5.6 The effect of relative humidity on the cohesive strength of catalyst layer

5.5 Sedimentation of suspension

5.5.1 The idea behind measurement

The reason for a sedimentation measurement of the suspension was mainly to support the cohesive strength study conducted and described above. The sedimentation study described here can give a representation of the particle rearrangement process. In addition, the findings from the sedimentation study are more relevant to the cohesive strength obtained at 60 %RH given that the drying rate at that high relative humidity is very slow.

5.5.2 Experimental method

After the suspensions were prepared and had their pH adjusted, the suspensions were then sealed in a glass beaker and placed in a stable horizontal bench unattended for 24 hours. The height of the suspension at the start of this experiment and that of the unsedimented layer were both measured (as shown in Figure 5.7).
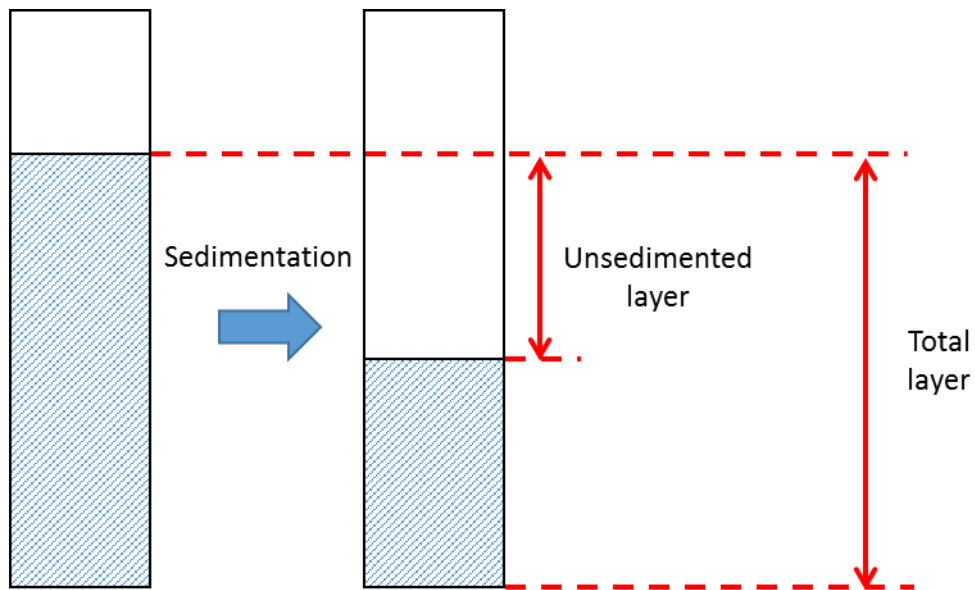
Figure 5.7 Setup of sedimentation experiment

The results were input into the following equation to calculate the extent of sedimentation.

$$Extent\ of\ sedimentation = \frac{Height\ of\ unsedimented\ layer}{Height\ of\ original\ suspension}$$

Equation 5-1

From the above definition, it can be seen that a high extent of sedimentation number would indicate a high level of sedimentation and the vice versa.

5.5.3 Results and discussion

The extent of sedimentation was measured and presented in Figure 5.8.
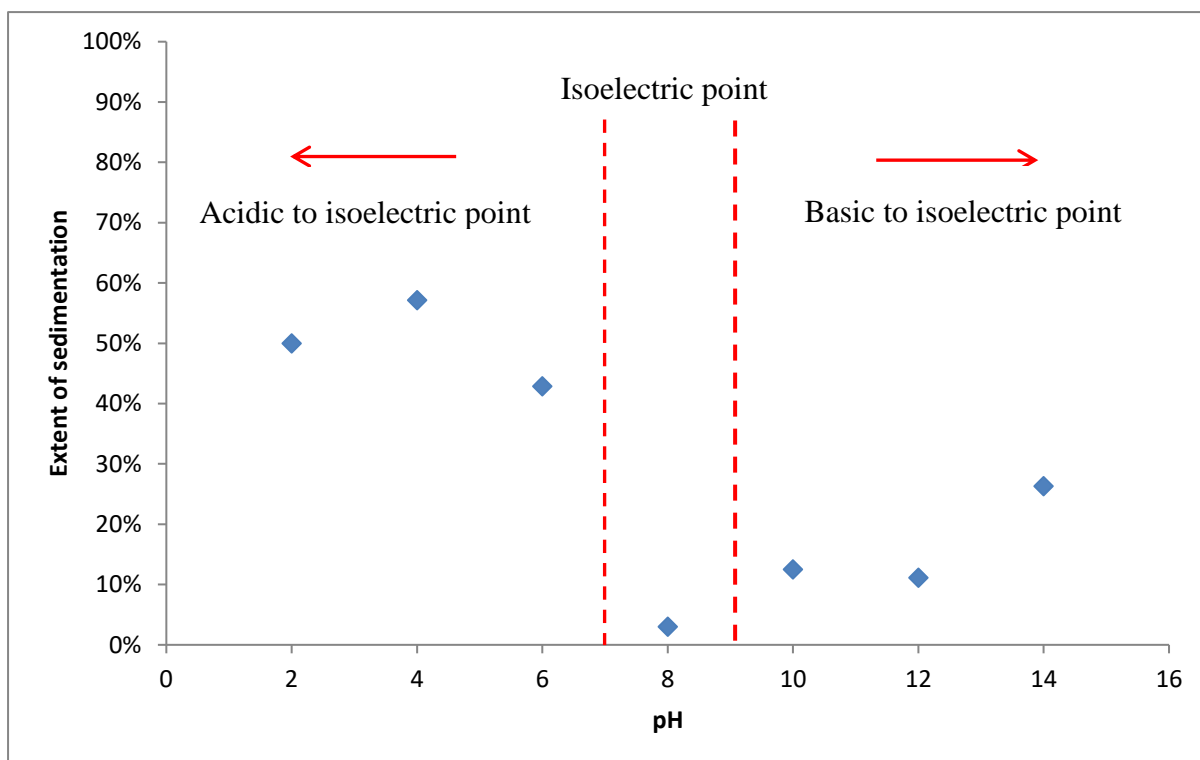
Figure 5.8 Extent of sedimentation for the suspension

It can be seen from Figure 5.8 that the extent of sedimentation results should be divided into two regimes which are the acidic regime to the isoelectric point and the basic regime to the isoelectric point. Very close to the isoelectric point which is at pH = 8, the lowest extent of sedimentation was found. This result agreed with the hypothesis made earlier in the explanation for the cohesive strength that particles at pH = 8 experienced limited rearrangement during drying to form a tablet, leaving the cohesive strength consistently at a low level.

As the pH moved to the basic side of the isoelectric point, the extent of sedimentation started to increase. A level-off was held between pH = 10 and 12 while a more obvious decrease was noted at pH = 14. The increase in the extent of sedimentation can be attributed to the greater repulsive force between particles which encouraged more particles to move relatively freely to pack during sedimentation. The slight change in the extent of sedimentation from pH = 8 to pH = 12 was in close agreement with their cohesive strength behaviour, demonstrating a better fit for the sedimentation study to represent the packing process of particles during drying.

The higher extent of sedimentation was located in the acidic regime to the isoelectric point. The explanation for the increase in sedimentation as the pH moved down from the isoelectric point to pH = 6 is the increased repulsive force as more positive charge was added to the surface of particles during the pH transition, giving particles more free movement to pack during sedimentation. The behaviour at pH = 2 and 4, due to the issue of tablet splitting, cannot be linked with the cohesive strength results at the moment. Further modification for the cohesive strength method developed was necessary to first of all resolve the splitting issue.

The above discussion can also be seen in Figure 5.9 where the extent of sedimentation was plotted with the cohesive strength. One point to be noted is that although the repulsive force between γ-alumina particles only existed when the suspension was wet, the eventual sedimentation of the particles after rearrangement by repulsive force is assisted by gravity force.
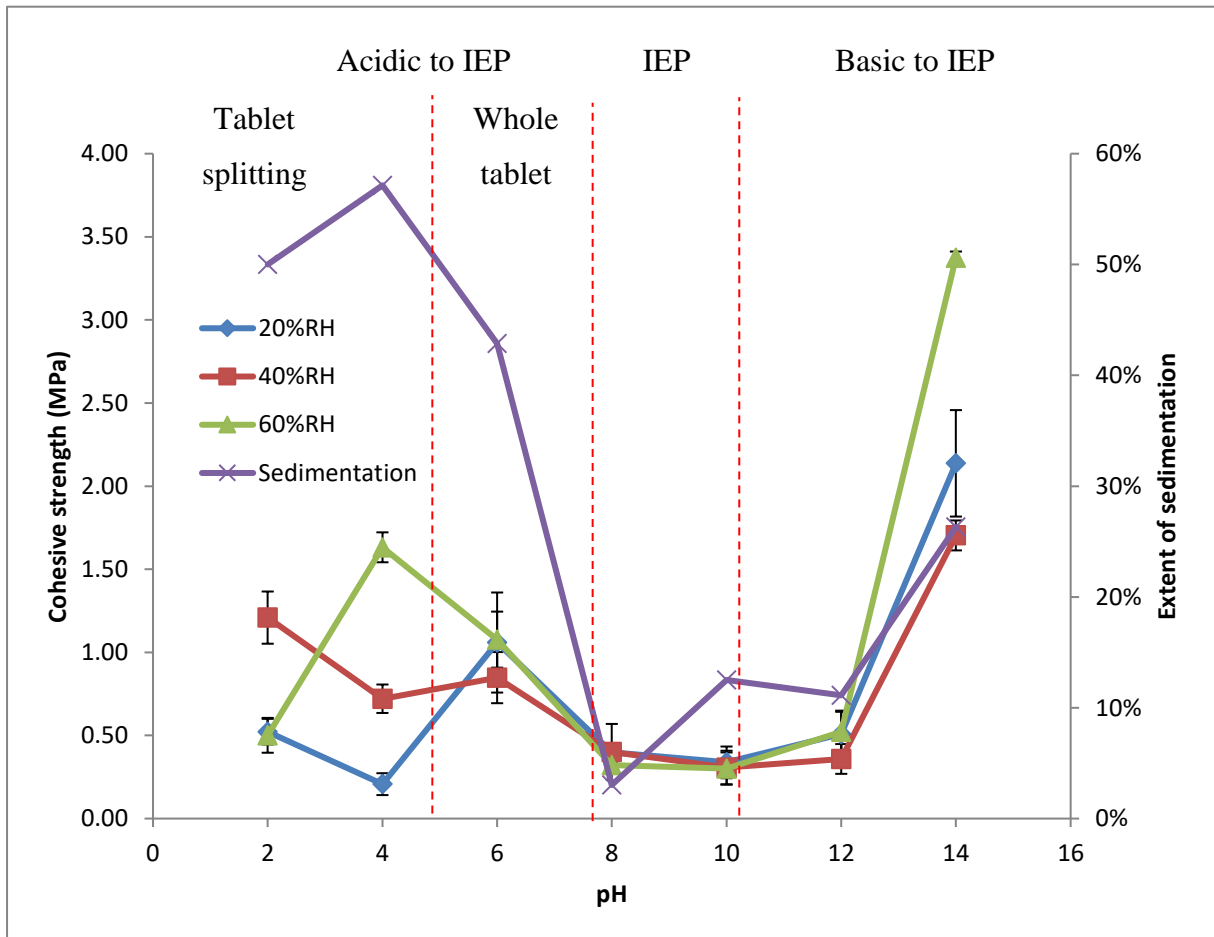
Figure 5.9 Correlation between extent of sedimentation and cohesive strength

5.6 Structure of tablet

5.6.1 idea behind the measurement

The porosity of the tablets produced at pH = 8 and pH = 14 (60 %RH relative humidity) was compared. The reason why these two pHs were selected was because according to the cohesive strength measurement described earlier in this chapter, these two pHs seemed to produce catalyst layers with highly distinctive strength profiles. The structural information obtained can be used to understand the difference observed in the strength measurement from the tablet method between the tablets produced at these two conditions.

5.6.2 Experimental method

This measurement was carried out using X-ray. An X-ray machine (Scanco μ CT35) was employed to scan part of the tablets produced. The reason that a part of the tablet was scanned was because the original tablets were too big to fit into the smallest sample holder of the X-ray machine for the highest resolution to be used. The scanning was performed slice by slice of the samples placed in the holder. The smallest slice distance (3.5 micron) which would give the highest resolution in the X-ray images was selected for the measurement.
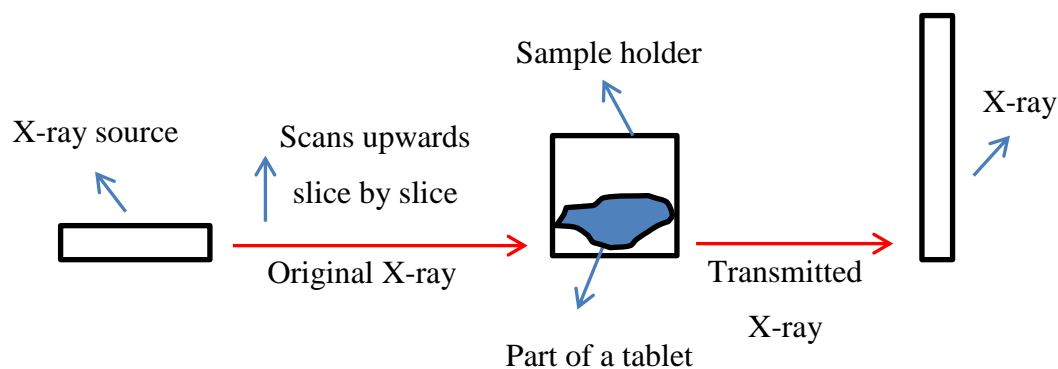
Figure 5.10 X-ray scanning of the primary agglomerates to obtain porosity data

5.6.3 Results and discussion

The X-ray tomography images of part of a tablet produced at pH = 8 and 14 are shown in Figure 5.11. The images were randomly selected from the targeted positions of the sample;

therefore they would give a good insight into the structural difference in tablets produced at these two pH conditions.
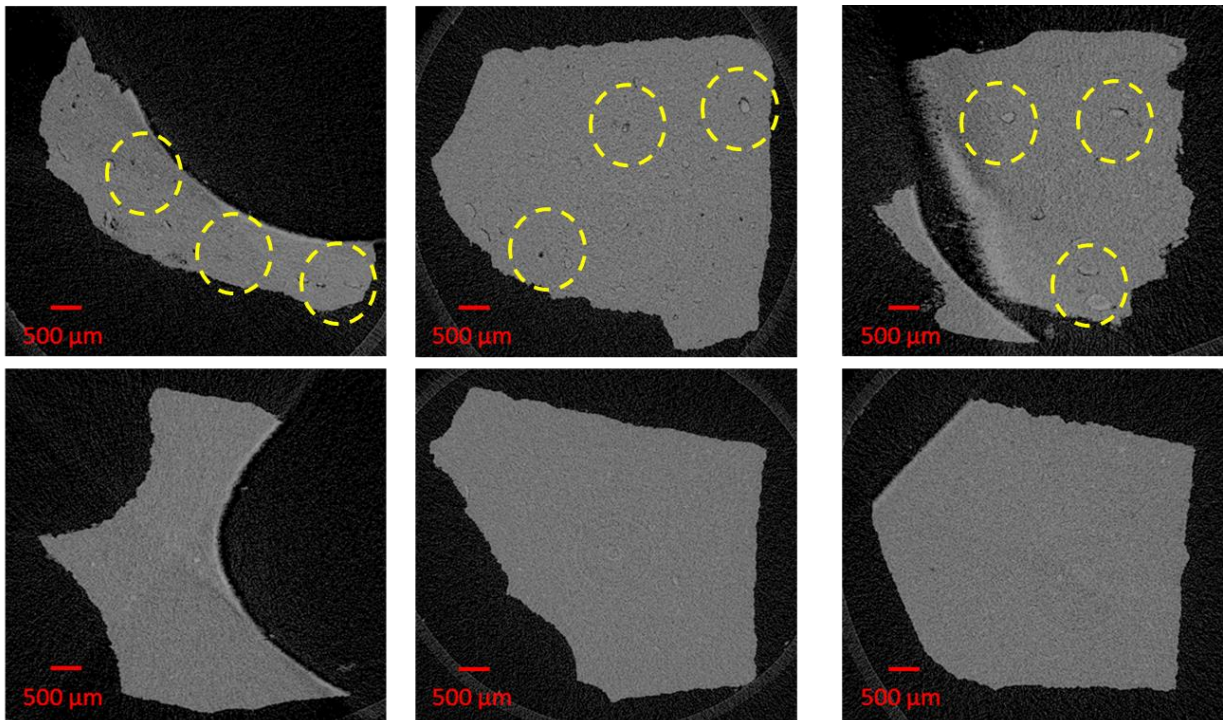
Figure 5.11 X-ray scan of tablets made at pH = 8 (upper) and 14 (lower)

A comparison between the upper (pH = 8) and the lower (pH = 14) showed that pH = 14 generated a more compact structure than pH = 8 at all of the three positions where the scans were presented [Tablets produced at pH = 8 showed more structural defects inside them than those made at pH = 14]. Recalling the cohesive strength measurement earlier that the cohesive strength at pH = 14 was higher than those at pH = 8 as described in this chapter, these images therefore could serve as a good support for the strength trend observed before.

5.7 Conclusion

In conclusion, the tablet method developed in Chapter 4 has been applied to understand the effect of calcination and relative humidity. Calcination was noticed to increase the cohesive strength due to the process of sintering. A higher relative humidity during drying was also found to improve the cohesive strength as a slower drying process allowed more time for particles to develop tight packing.

The variation of cohesive strength with regards to pH was also explained based on the understanding of particle mobility. The general trend observed was that at pHs close to the isoelectric point, the cohesive strength was found to be low due to the low mobility of γ-alumina particles to pack during drying. An increased cohesive strength was seen when the pH moved away from the isoelectric point, meaning that the γ-alumina particles gained more mobility to pack during drying. The argument regarding particle mobility was also demonstrated in the sedimentation measurement of the suspension. At pHs close to the isoelectric point, the extent of sedimentation was very low, corresponding to a poor particle rearrangement process during drying while at pHs away from the isoelectric point, the extent of sedimentation improved, suggesting better particle mobility to adjust themselves to pack during drying.

The samples made at 60 %RH for pH = 8 and 14 were also chosen for X-tomography analysis due to their distinct cohesive strength. The analysis confirmed the explanation regarding particle mobility as the tablets created at pH = 8 were found to have many structural defects which acted as weak points in the structure than those at pH = 14 which showed a more uniform tight packing.

The splitting of tablets at pH = 4 and 2 limited the author to obtain a comprehensive profile of cohesive strength with regards to pH as only the bottom part of the tablets were tested in the current setting. A modification to the existing experiment setting was necessary to ensure intact and whole tablets would be formed after the suspension was dried. Another point for modification is the elimination of Na^+ in the suspension. A different base would be chosen for the adjustment of pH to the basic side to remove the concern of catalyst poison.

Chapter 6 Structure control of γ-alumina tablet

6.1   Introduction

It was mentioned in Chapter 5 and tablet splitting occurred at certain pH conditions during drying of the suspension. The reason behind splitting was first of all chosen for investigation in this chapter. The knowledge gained was then applied to design a system that could avoid splitting.

6.2   Experimental method

A scanning electron microscope (SEM) was employed to investigate the reason behind the splitting of tablet. The model of the SEM used was Jeol (USA). The γ-alumina tablet samples were subject to gold coating before being viewed under the SEM. The coating equipment used was EMScope (model SC 500). The sputter coater worked at a low vacuum of a pressure around 0.06 Tr. The coating chamber was filled with Argon gas. An electric field was generated by a current of 15 mA.

6.2.1   Results and discussion

The SEM images of the tablets are presented in Figure 6.1 and Figure 6.2. The tablets used were from pH= 2 and 4 dried at 60 %RH in Chapter 5. It could be seen that the majority of particles in the top part of the tablet were small particles while most of them in the bottom fragment are large particles. This is suggesting that during the drying process, migration of particles has occurred. The small particles moved to the top of the tablet while the large particles stayed in the bottom of the tablet. A schematic diagram showing the migration process which lead to the splitting of tablet samples can be seen in Figure 6.3.

Top		
Bottom		
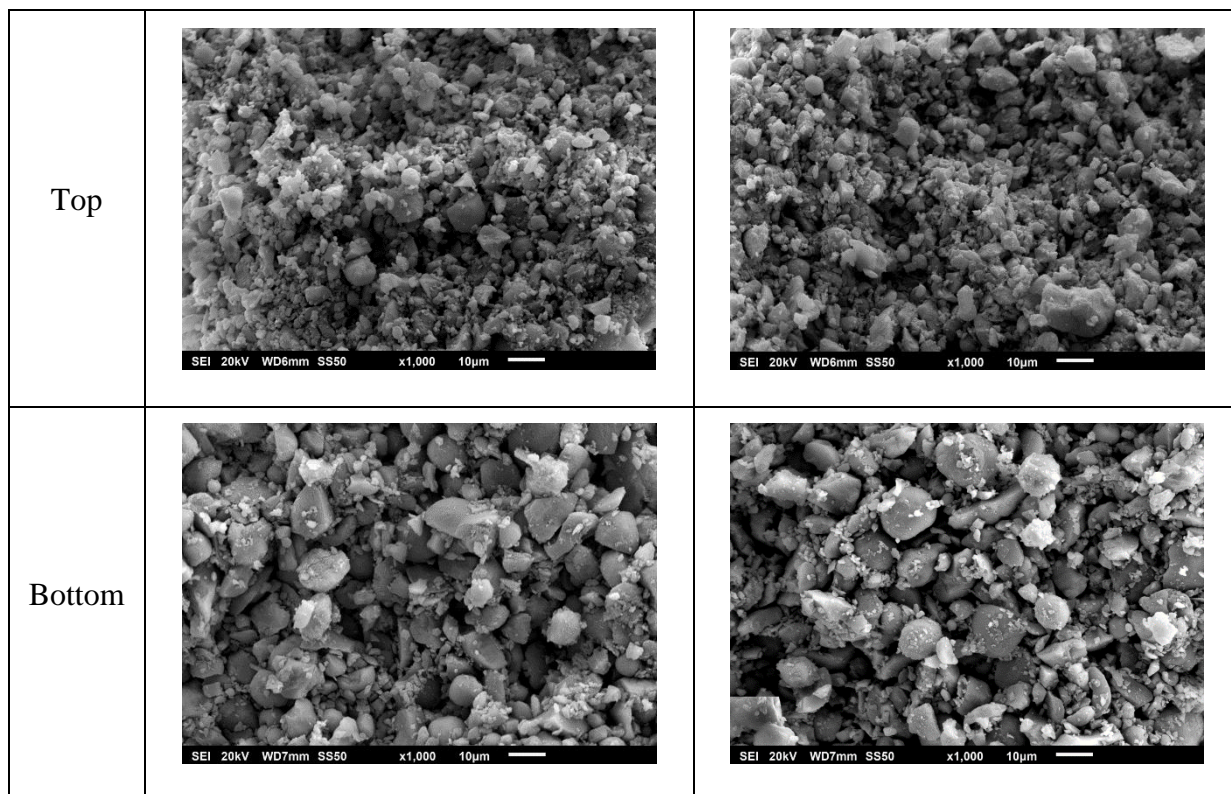
Figure 6.1 Images of γ-alumina tablets made at pH = 2

Top		
Bottom		
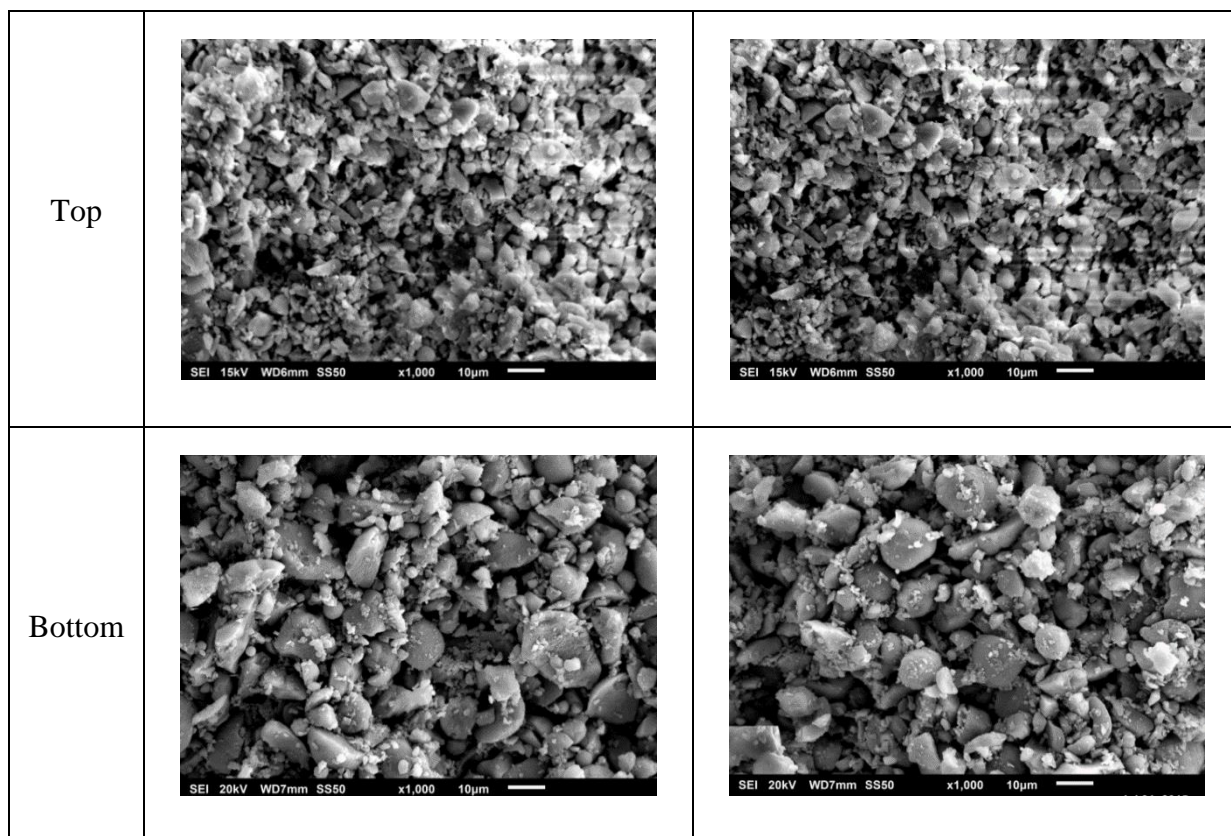
Figure 6.2 Images of γ-alumina tablets made at pH = 4
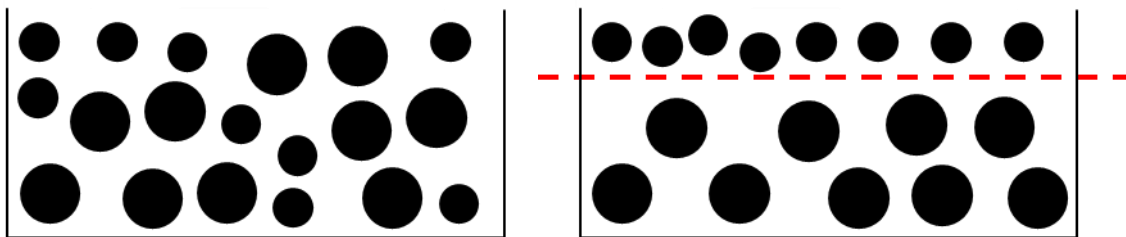
Figure 6.3 Schematic diagram showing splitting of tablets by migration of particles

6.3 Development of uniform drying method

6.3.1 Idea behind method

It could be seen from the previous discussion that tablet splitting was mainly caused by migration of γ-alumina particles during drying. In addition, it can be further noticed that the direction of migration is towards the drying front and smaller particles are able to travel more towards the drying front than bigger particles. In this regard, a uniform drying system was thought to be able to reduce this segregation effect and result in an intact (whole, non-splitting) tablet.

6.3.2 Experimental method

The experimental setup shown in Figure 6.4 was employed to produce tablets from the γ-alumina suspension under a uniform drying system. A quantity of 0.6 g of the suspension was added into a tablet die made of filter paper. The use of filter paper die was thought to be able to create a uniform drying environment for the γ-alumina suspension and therefore solve the problem of tablet splitting at certain preparation conditions. The drying was performed at 40% RH in the environment chamber (Series KMF, Binder GmbH), followed by calcination at 500 ℃ for 2 hours in a furnace (Carbolite).

One of the difficulties that had been overcome during the development of the method was the grade of filter paper. The grade of the filter paper needs to be small enough to prevent any solid particles from passing through and also large enough to create enough drying rates at all drying fronts for the uniform drying to be effective. The second concern is based on the fact that one drying front (the top surface) is made of air; therefore it may present a higher drying

rate compared with the two drying fronts (the side and the bottom surface) for the uniform system to be invalid.

γ-alumina
suspension
mass = 0.6 g

Glue applied around the
circumference of the tablet die

Filter paper

Filter paper

Tablet diameter = 9.3 mm
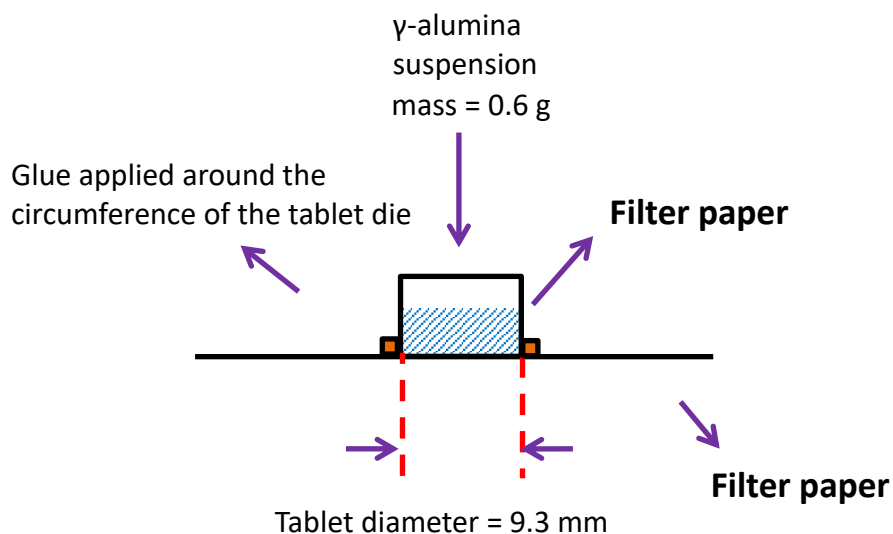
Figure 6.4 Experimental setup of producing tablet sample under uniform drying system

Three types of filter paper were tried which had a grade of 40 μm, 5-8 μm and 1 μm. In order to test the effect of pore size of the filter paper, suspensions with different particle size were needed as well. The milling procedure outlined in Chapter 3 was followed with a variation in milling time to create different particle sizes. Three different particle sizes were generated as a result as shown in Table 6.1.

Table 6.1 Particle size distribution of the three suspensions used to test the grade of filter paper

Suspension 1	$d_{90} = 9.37\ \mu m, d_{50} = 3.76\ \mu m, d_{10} = 1.41\ \mu m$
Suspension 2	$d_{90} = 4.11\ \mu m, d_{50} = 2.04\ \mu m, d_{10} = 0.78\ \mu m$
Suspension 3	$d_{90} = 3.10\ \mu m, d_{50} = 1.50\ \mu m, d_{10} = 0.57\ \mu m$

The pH adjustment was performed with 10 M HCl and 96 wt% NH_3; the use of NH_3 could avoid the presence of Na^+ in the suspension, which could potentially act as a catalyst poison in real catalytic system. The pH range tested was from pH = 2 to pH = 10 in an increment of 1.

The cohesive strength results of tablets made from suspension 1 from Table 6.1 using filter paper of grade 40 μm is shown in Figure 6.5.
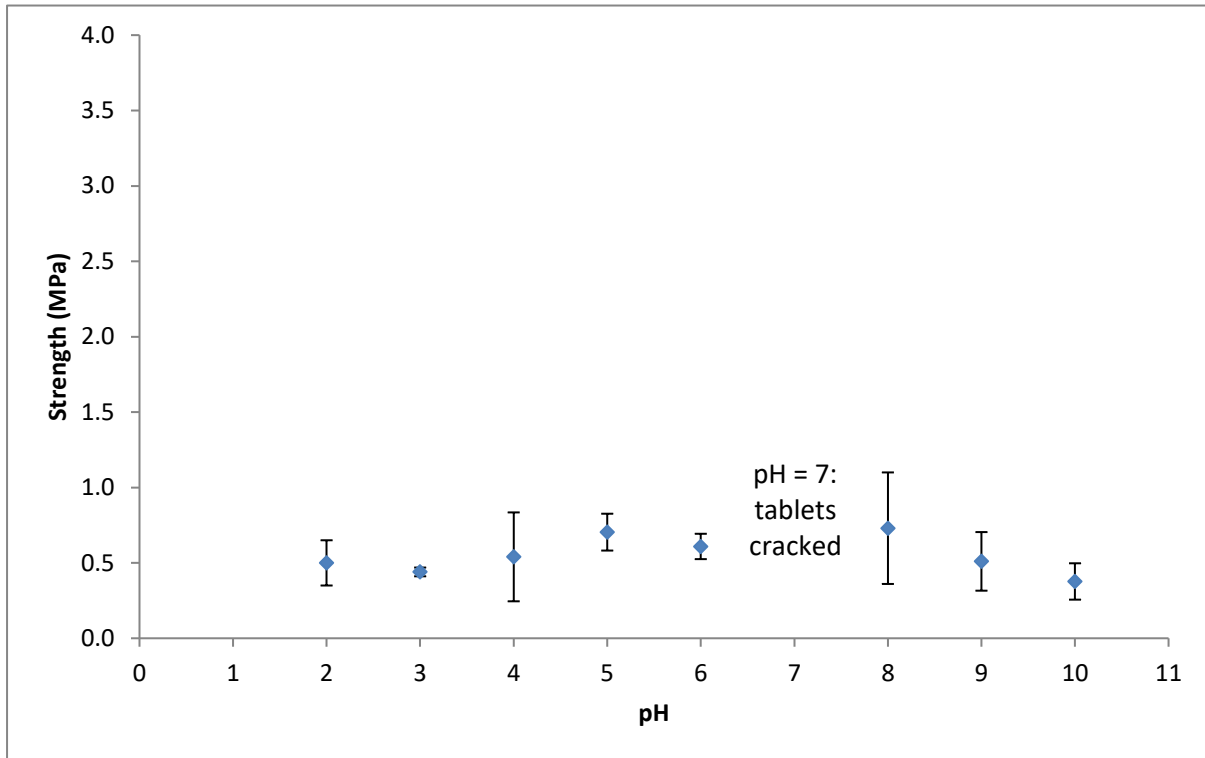
Figure 6.5 The cohesive strength versus pH for tablets made from suspension 1 using filter paper with a grade of 40 μm

It could be seen from Figure 6.5 that the cohesive strength did not vary with pH greatly; it was almost a flat trend from the lowest pH tested to the highest pH of the range. This suggested that the grade of the filter paper used was probably too coarse that the filter paper did not manage to prevent small particles of the suspension from leaving the system. A much smaller pore size would be necessary to carry out tablet preparation.

The cohesive strength results for the same suspension (suspension 1) from Table 6.1 are presented in Figure 6.6; in this figure, the tablets were made using filter paper of a grade of 5-8 μm. It could be seen from Figure 6.6 that given the variation in the cohesive strength versus pH for suspension 1, the filter paper with grade 5-8 μm was sufficient to retain the small particles of this suspension in the system during drying; in addition, intact tablets were created, suggesting that the pore size was also sufficient for a uniform drying environment to be developed.

The same filter paper (pore size = 5-8 μm) was then used to create tablets using suspension 3 which had the smallest particle size. The cohesive strength results as shown in Figure 6.7 were obtained.
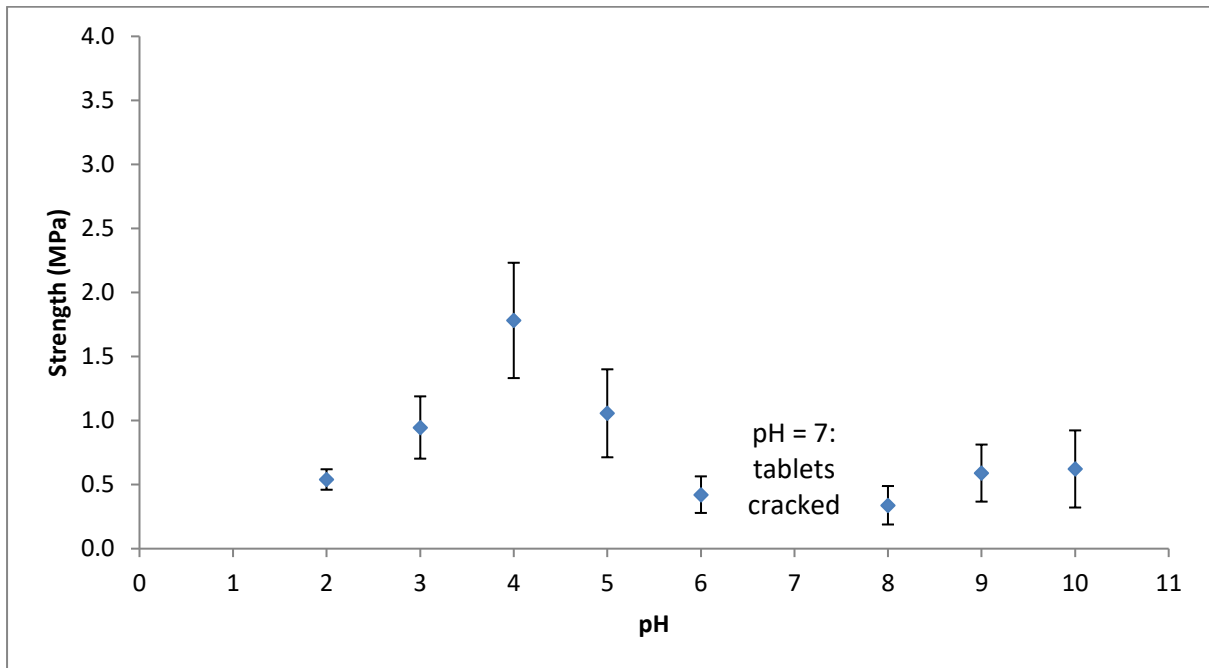
Figure 6.6 The cohesive strength versus pH for tablets made from suspension 1 using filter paper with a grade of 5-8 μm
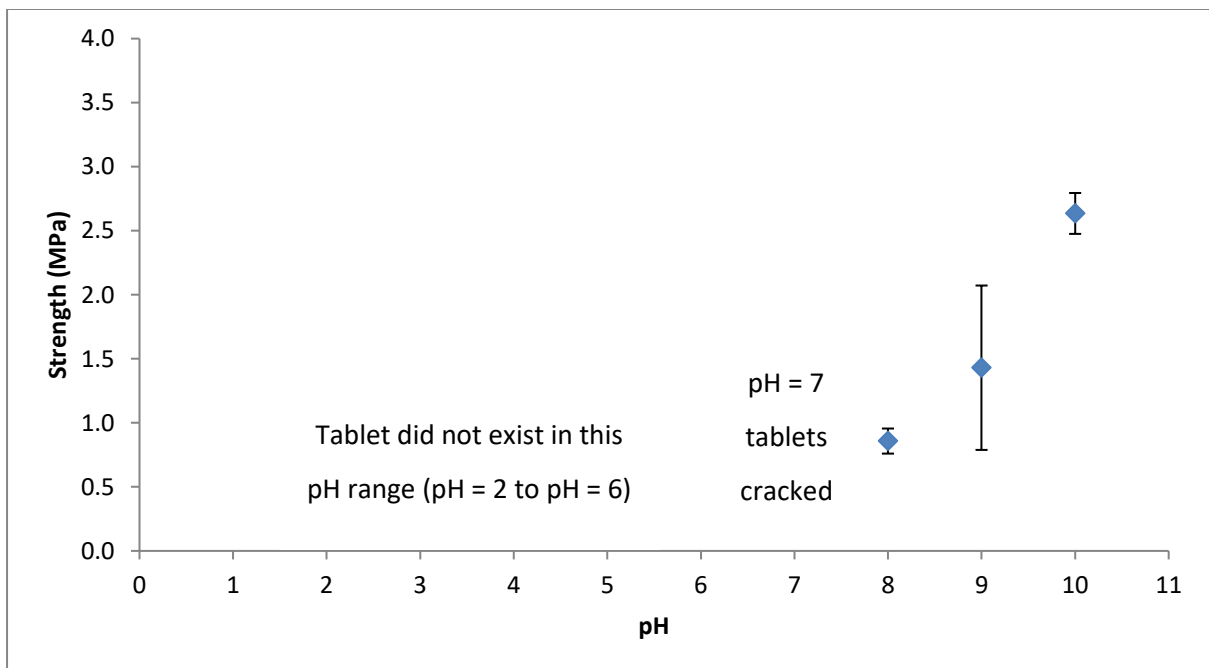
Figure 6.7 The cohesive strength versus pH for tablets made from suspension 3 using filter paper with a grade of 5-8 μm

It can be seen from Figure 6.7 that the filter paper with pore size (5-8 μm) was probably insufficient for the suspension with the smallest particle size, given that most particles escaped from the system at the low pH conditions.

Filter paper with the grade of pore size being 1 μm was then tested for suspension 3 which has the smallest particle size. The results can be seen in section 6.4. Although there were many cracks developed during drying at low pHs which would need further explanation, tablets were successfully formed at all pH conditions, indicating that the pore size was small enough to retain all particles and no splitting was observed, meaning that uniform drying was secured. Therefore the cohesive strength profile for suspension 3 prepared using the filter paper with pore size being 1 μm would be presented later in this chapter as part of the study of the effect of particle size.

6.4   Results and discussion

The cohesive strength for the three suspensions in Table 6.1 tested using the selected filter paper (pore size being 1 μm) is presented in Figure 6.8.
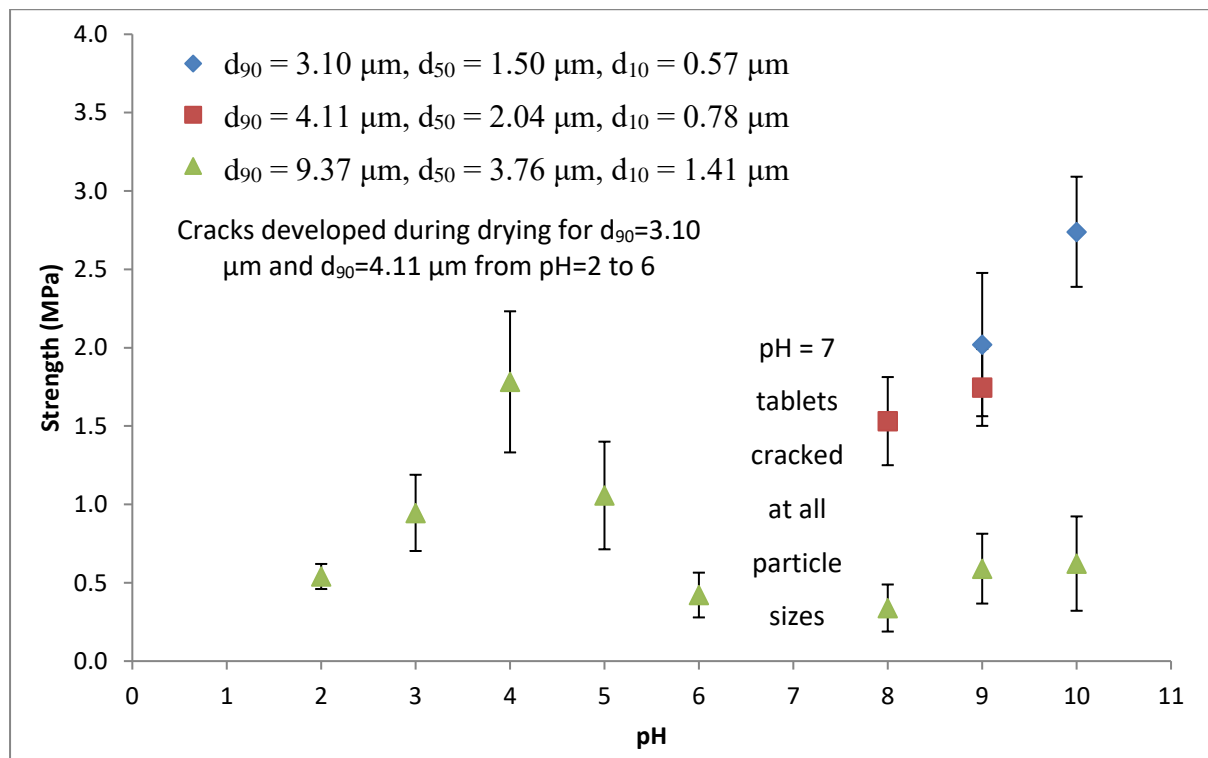
Figure 6.8 The cohesive strength profile versus pH for suspensions with different particle size

It should be first of all stated that using the uniform drying system (facilitated by the filter paper system), no tablet splitting occurred for the low pH conditions (e.g. pH = 2, pH = 4) which experienced tablet splitting in the earlier study (Chapter 5). SEM images were taken for the top and bottom of the tablets made under the uniform drying system as shown in Figure 6.9. In terms of the effect of particle size on the cohesive strength, the formulation with the largest particle size (d_{90}=9.37 μm, d_{50}=3.76 μm, d_{10}=1.41 μm) resulted in tablets with no cracks in the whole pH range except pH=7. In contrast, the formulations consisting of smaller particles did not generate crack free tablets at any pHs except from pH=8 to 10; the tablets formed in the low pHs developed radial cracks during drying of the suspension despite the uniform drying environment employed (images shown in Table 6.5 and Table 6.6). Further explanation on why radial cracks developed at these conditions will be given in section 6.9.

The effect of pH can also be identified from Figure 6.8. For the formulation (d_{90} = 9.37 μm and d_{50} = 3.76 μm, d_{10} = 1.41 μm) which had a whole series of crack-free tablets formed except at pH=7, the highest cohesive strength was obtained at pH=4; as the pH deviated from pH=4 in the range of pH=2 to 6, the cohesive strength was found to decrease. From pH=8 onwards, all of the three formulations demonstrated an increasing cohesive strength as the pH was increased. At pH=7, tablets were never able to be formed without cracks even using the most favourable particle size distribution. This is because pH=7 is extremely close to the isoelectric point (IEP) of γ-alumina; when this condition is reached, a zero surface charge condition is triggered for the γ-alumina particles, eliminating their capability to move during drying of the suspension to develop good packing. This finding does not disapprove the results shown for pH = 8 in the previous two chapters (Chapter 4 and 5) as both pH = 7 and 8 were very close to the isoelectric point of γ-alumina. The fact that cracks were observed for tablets prepared at pH = 7 and no crack was recorded for tablets prepared at pH = 8 can be explained as pH = 7 is probably closer to the IEP of γ-alumina than pH = 8.

		Non-uniform drying	Uniform drying
Top	pH = 2		
	pH = 4		
Bottom	pH = 2		
	pH = 4		
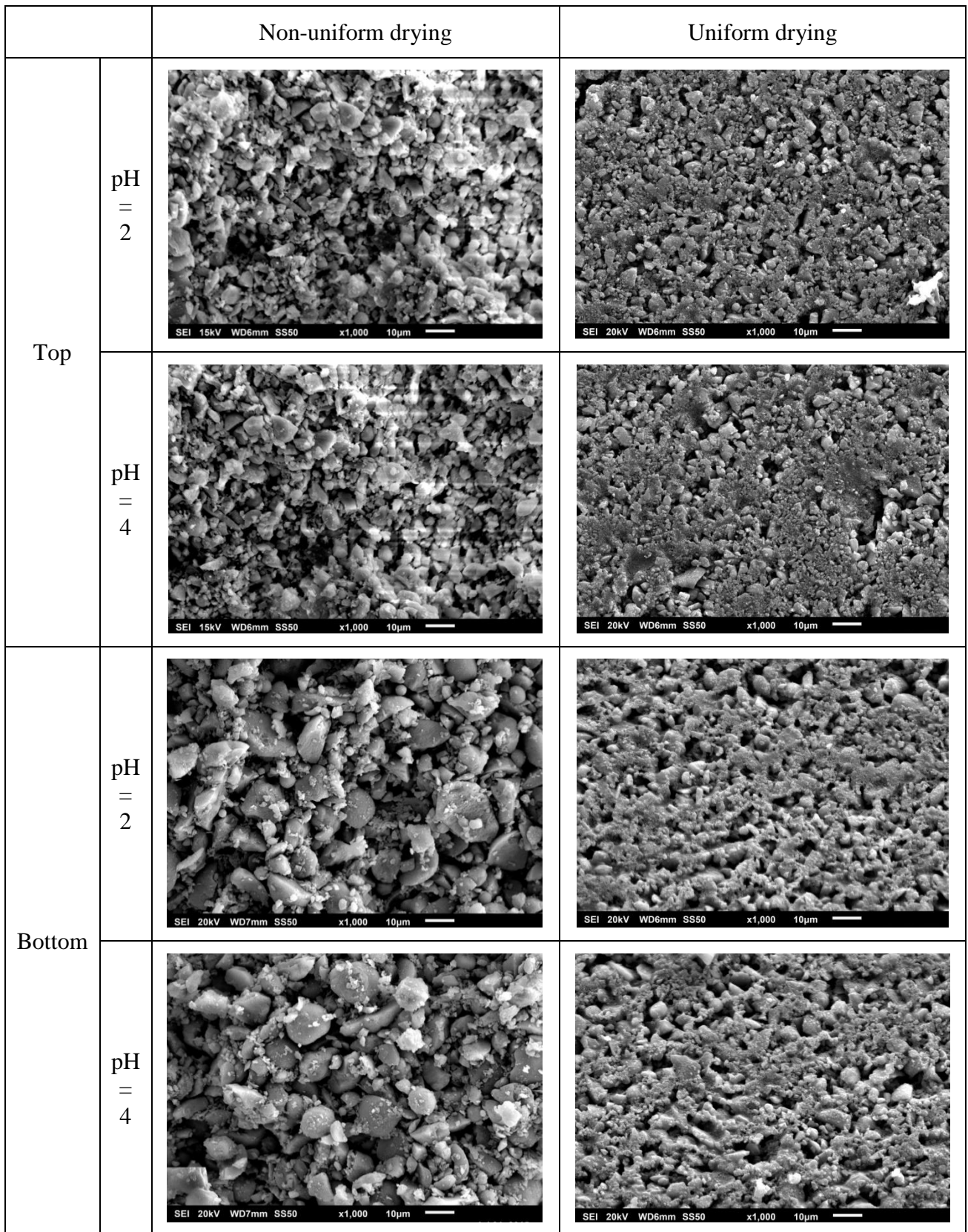
Figure 6.9 Images comparing the top and bottom of γ-tablets from the non-uniform drying and the uniform drying

6.5　Viscosity of suspension

6.5.1　Idea behind the measurement

Viscosity of the suspension which could influence the particle rearrangement process was deemed as a much simpler and easy approach to relate to the cohesive strength.

6.5.2　Experimental method

The viscosity of the γ-alumina suspension was measured using a rheometer (Malvern Kinexus) at 25 ± 0.1 ℃. The geometry used was parallel serrated plates with a gap size of 0.6 mm. The choice of serrated plates was to prevent particle sedimentation during viscosity measurement. The use of a gap size of 0.6 mm which was more than 20 times greater than the largest particle present in the suspension was designed to minimise particle blockage during the viscosity measurement. A cooler was used to maintain the temperature. The shear rate applied was from 1 s^{-1} to 1000 s^{-1}.

6.5.3　Results and discussion

The viscosity result for the suspension 1 (in Table 6.1) is presented in Figure 6.10. It is useful to test this suspension as this was the only suspension that produced crack-free tablets in most pH conditions.

The behaviour of the viscosity of the suspension at various pHs should be viewed differently in 3 regimes according to the isoelectric point of alumina. At pH lower than the isoelectric point, the viscosity showed an interesting trend. The viscosity decreased as the pH increased from 2 to 4 but increased as the pH moved towards the isoelectric point. The viscosity reached the maximum value at the pH closest to the isoelectric point. At pH higher than the isoelectric point, the viscosity was found to decrease continuously as the pH moved above from the isoelectric point.
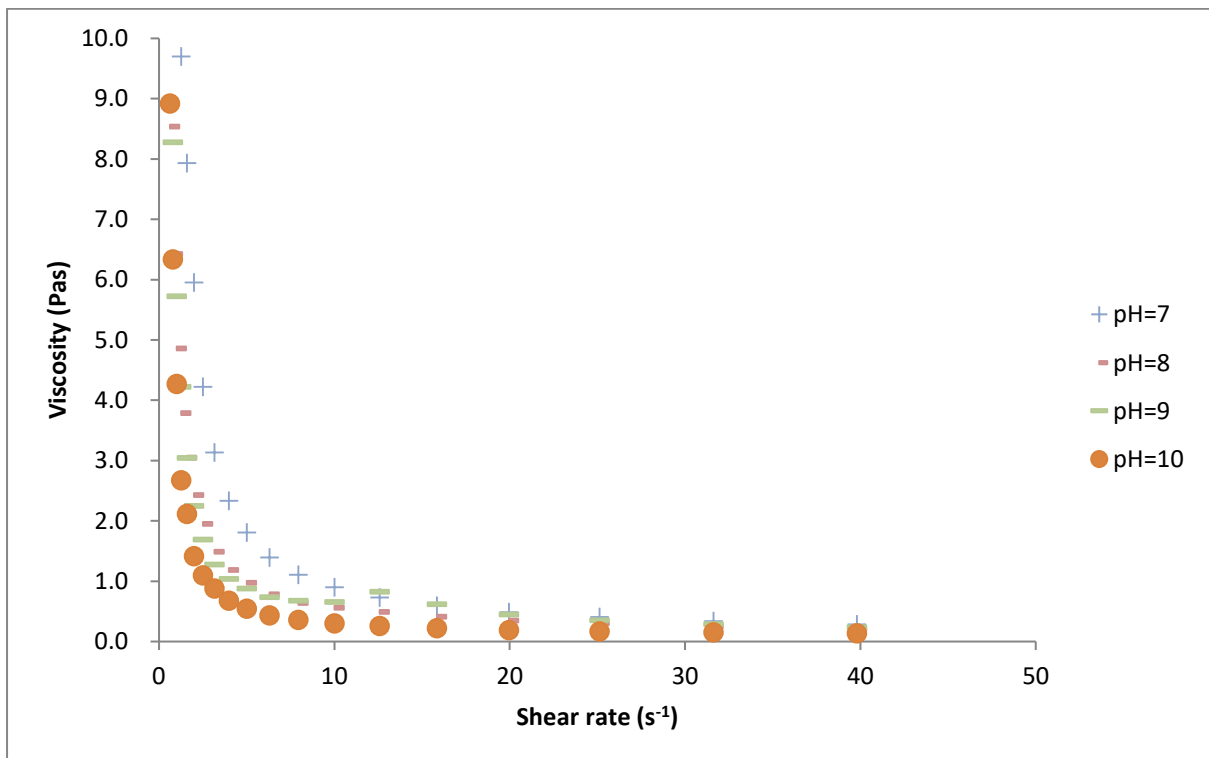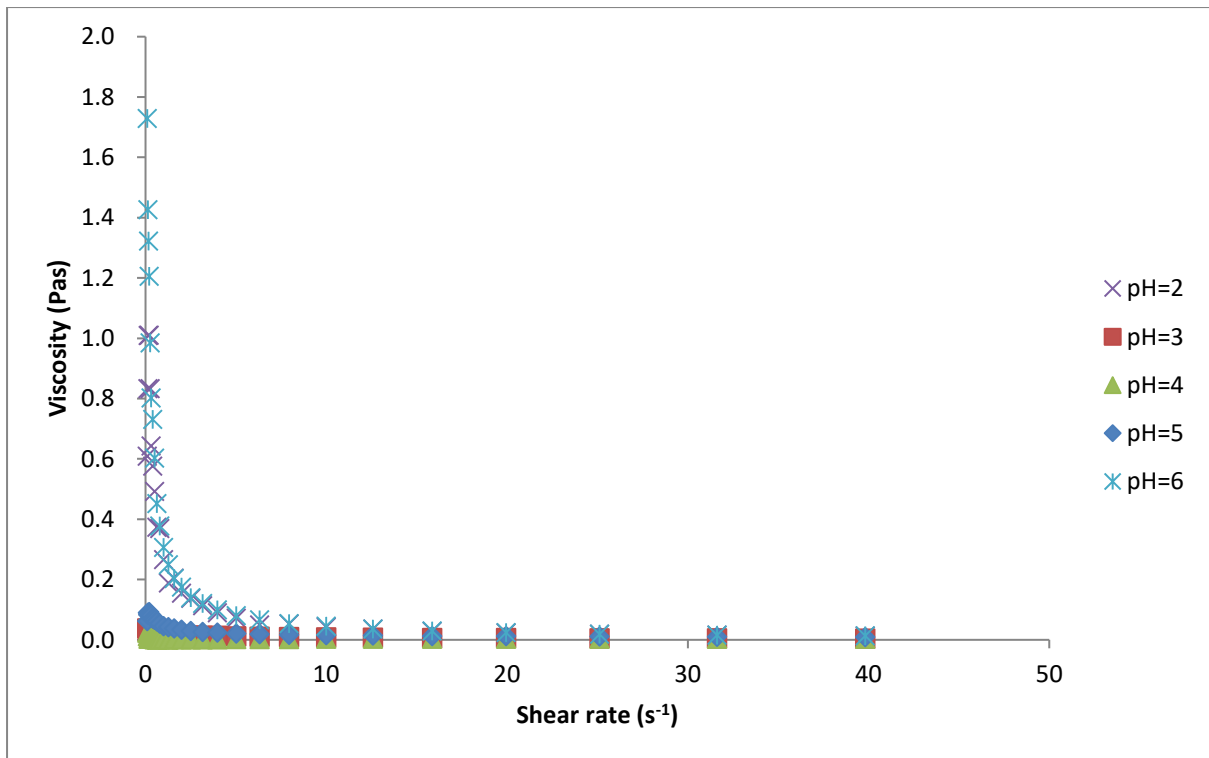
Figure 6.10 Viscosity versus shear rate for suspension 1 at different pHs (pH = 2 to 6 in the upper figure and pH = 7 to 10 in the lower figure)

The viscosity profile of the γ-alumina suspension at different pHs can be quantitatively characterised according to Equation 6-1.

$$\mu = k\dot{\gamma}^{n-1}$$

$$\text{or } \sigma = k\dot{\gamma}^{n}$$

where σ = shear stress, μ = shear viscosity, k = proportionality constant, $\dot{\gamma}$ = shear rate, n = power constant

The fitting parameter n describes flow behaviour, i.e. if n > 1, the flow behaviour is shear thickening while if n < 1, the flow behaviour is shear thinning. The fitting parameter k denotes flow consistency. For a viscosity profile with the same n, a larger k value would move the whole curve up without altering the shape of the curve. One example of the fittings is shown in Figure 6.11. As can be seen, the goodness of fitting is satisfactory.
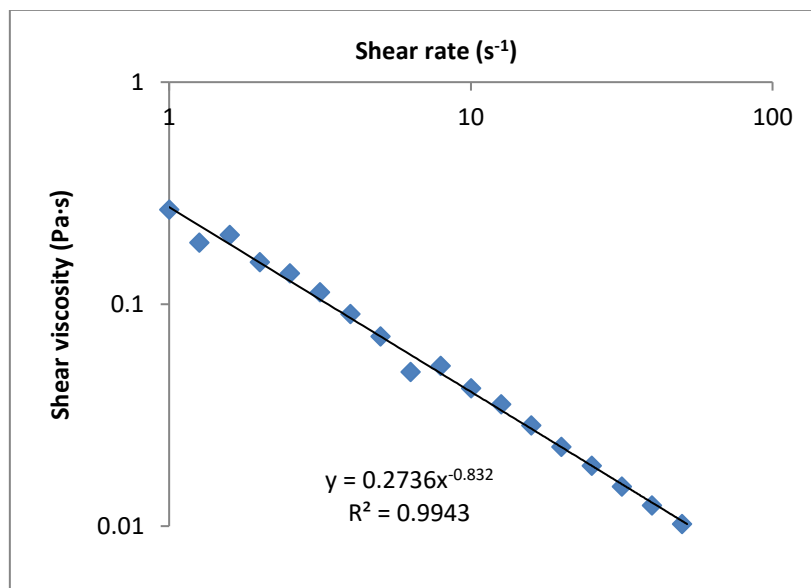
Figure 6.11 Fitting of viscosity data for pH = 2

The two fitting parameters obtained are plotted versus pH as shown in Figure 6.12.
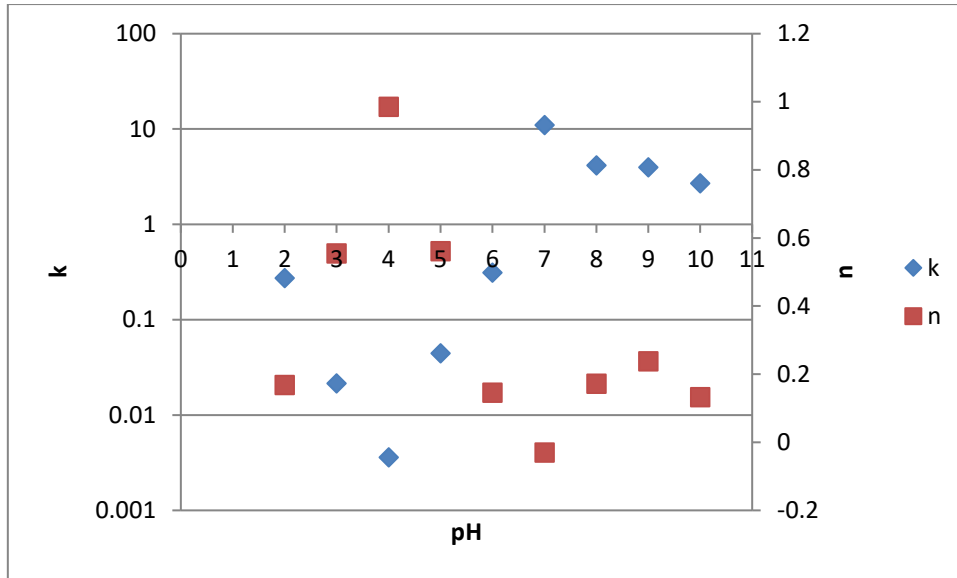
Figure 6.12 Fitting parameters of viscosity data versus pH

It is relatively easy to start the explanation of the viscosity data at the isoelectric point. Since the definition of the isoelectric point is that the surface charge of particles is neutral, it is not difficult to anticipate that at the isoelectric point there is no electrostatic resistance to separate the γ-alumina particles, leaving the van der Waals attraction dominate the system. This strong attraction between γ-alumina particles caused by the van der Waals forces aggregated the alumina particles and therefore significantly increased the viscosity of the suspension.

As the pH was increased further from the isoelectric point, negative charge was regarded to start appearing on the surface of alumina particles. The net negative surface charge causes some electrostatic repulsion between γ-alumina particles, making the suspension to flow relative easily; but it still needs to be noted that the γ-alumina particles at this pH still remains in a flocculated status [69]. The flocculated status can be more confirmed in section 6.6.

When it comes to pHs lower than the isoelectric point, the viscosity behaviour becomes more complex. Moving away from the isoelectric point to lower pH, a net positive charge starts to be built up on the surface of γ-alumina particles. The formation of this net surface charge generates the electrostatic repulsive force between γ-alumina particles again, leading to a reduction in viscosity as the pH was decreased from 7 to 4. However, this decreasing trend in viscosity was not observed as the pH was reduced from 4 to 2. This further reduction in pH has in fact resulted in an increase in the suspension viscosity, which was thought be caused by a complex competition between attractive and repulsive force acting between γ-alumina

particles. This relationship would be quantitatively demonstrated later in this chapter (as seen in section 6.7).

6.6 Online monitoring of suspension drying and PIV

6.6.1 Idea behind the measurement

The information gained from the viscosity measurement was not sufficient to explain the tendency in the cohesive strength, especially when it comes to the use of different drying conditions (as can be seen in Figure 5.6 where the effect of relative humidity on the cohesive strength was demonstrated), because it is not possible to alter the relative humidity in the geometry of the viscosity measurement. An on-line monitoring experiment was then performed to obtain real time particle packing information during drying under different drying conditions to further understand the effect of drying conditions.

6.6.2 Experimental method

The experimental setup for on-line monitoring of the particle packing process of γ-alumina suspension is shown in Figure 6.13. Although the on-line monitoring was performed on a model system rather than the actual filter paper drying system used to produce the tablets, information gained regarding particle packing process is still thought to be useful in understanding the different cohesive strengths obtained.
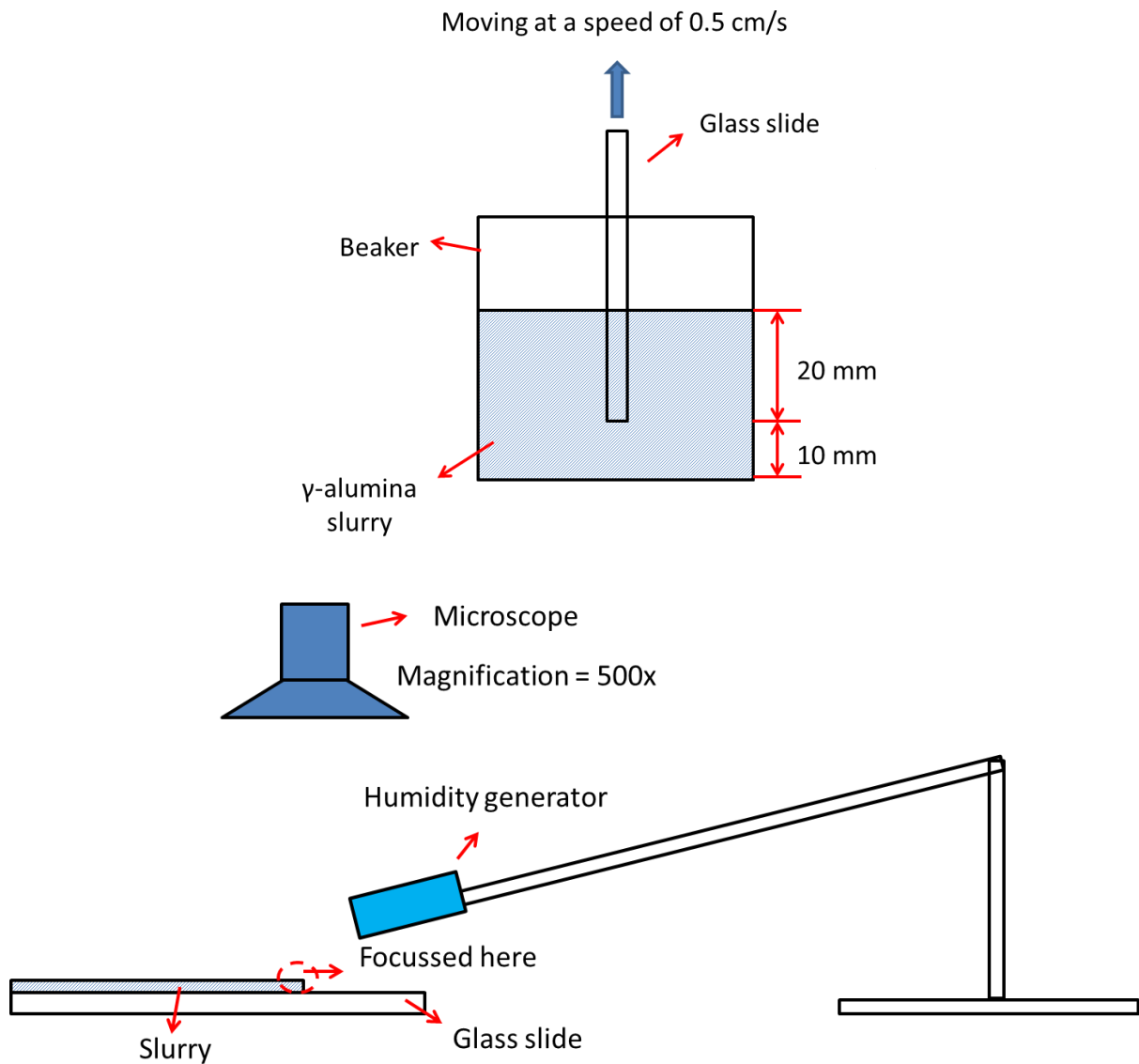
Figure 6.13 Experimental setup for on-line monitoring of particle packing during drying of γ-alumina suspension

The sample for online monitoring was prepared by dip-coating a glass slide in a reservoir of γ-alumina suspension with known height. The withdrawal speed was set to be roughly 0.5 cm/s to ensure a uniform coating. The online monitoring was carried out under a microscope (Keyence VHX-5000) at a magnification of 500x. The area of view was chosen to be next to the free edge of the wet coated layer. A humidity generator (GenRH-A) was used to provide the same drying condition (40 %RH) implemented in preparation of the tablets in section 6.3.

In order to gain quantitative information from the online monitoring experiment, the packing velocity of γ-alumina particles was determined. The packing velocity was obtained from the particle imaging velocimetry technique (PIV). The online particle motion recorded by the microscope (at a frame rate of 15 per second and a resolution of 1600×1200) was processed using the plug-in tool PIV Lab 1.32 in Matlab to calculate the packing velocity of particles. The software works by tracking the movement of particles over known pixels in each frame to return the velocity of particles. An example of particle motion determined by the PIV technique is shown in Figure 6.14. The magnitude and vector of the vectors (shown as green arrows) indicates the direction and the speed at which the particles are travelling, respectively. The particle identified in the red box was found to exhibit physical movement during the drying process, as can be seen from its relative position with reference to the grid from image 1 to 3. This movement was detected by the PIV technique and vectors assigned to indicate its magnitude and direction. From image 3 to 4 where the particle was found to be physically stagnant, the PIV algorithm did not generate any vector for this particle but was still sensitive to its surrounding where motion took place.
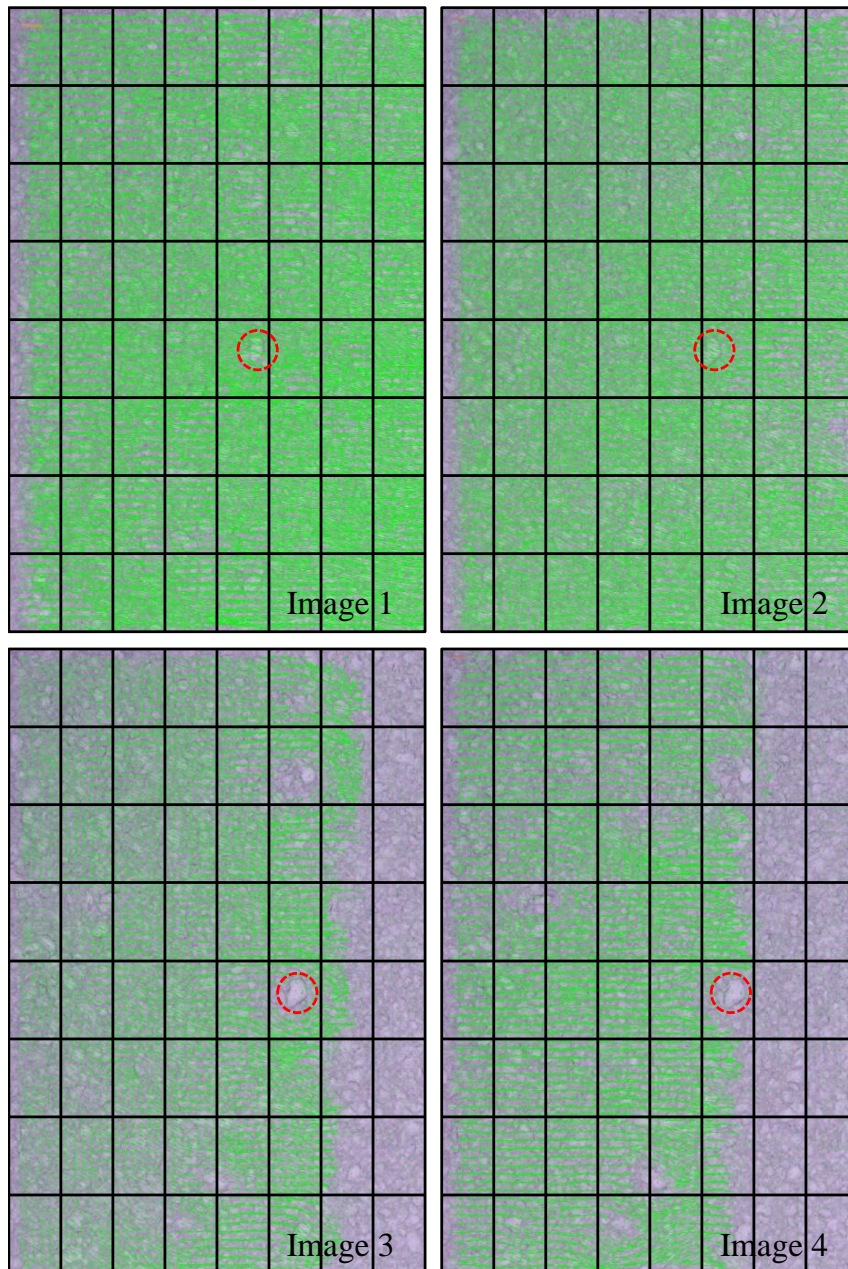
Figure 6.14 Example of particle motion determined by the PIV technique

6.6.3 Results and discussion

Particle packing velocity determined by the PIV technique from the online monitored suspension drying is reported in Figure 6.15. Suspension 1 in Table 6.1 was used in this case.
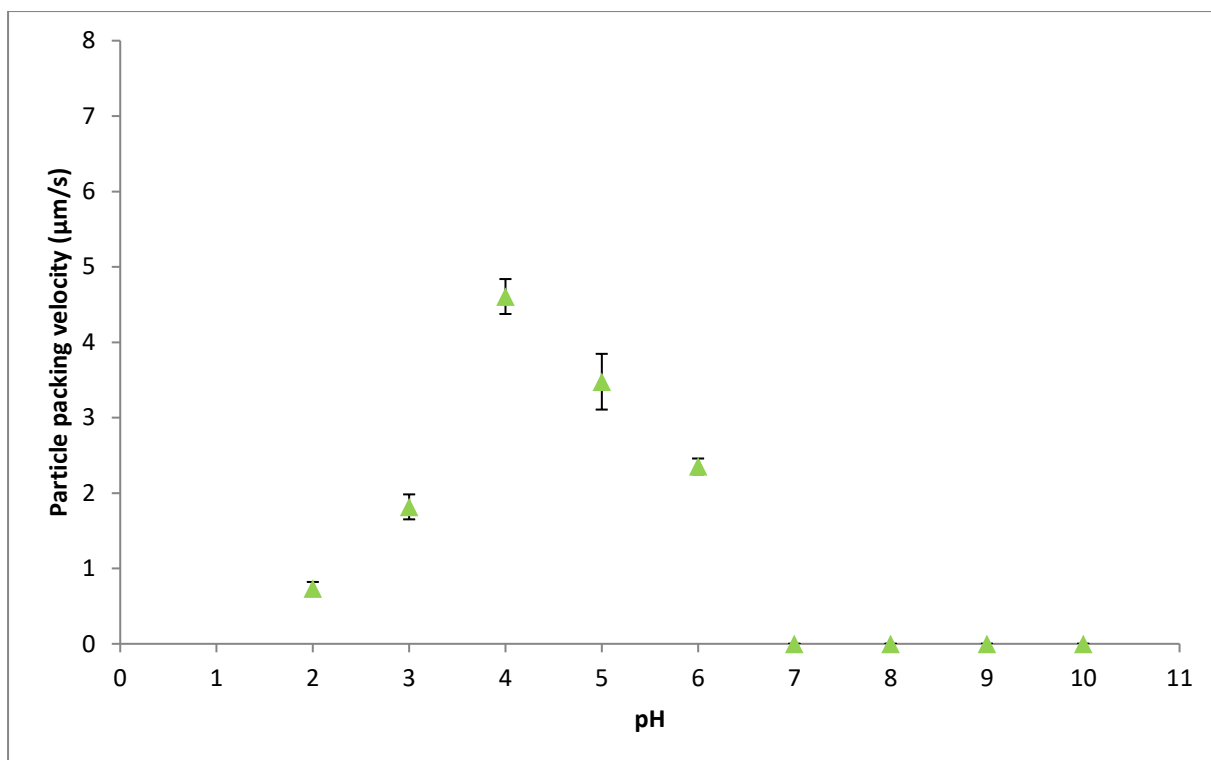
Figure 6.15 PIV measurement of particle packing velocity

It can be seen that at pH = 7, the particle mobility was zero because of the zero surface charge at the IEP. The fact that γ-alumina particles were stagnant indicated that they did not exhibit any motion during drying of the suspension to form favourable packing, leaving cracks to develop in all tablets produced at pH = 7 regardless of particle size (as seen in Figure 6.8).

In contrast, γ-alumina particles at pH = 4 showed the highest particle mobility, suggesting that γ-alumina particles at this condition had the highest chance to rearrange themselves to develop tight packing during drying. The tighter packing led to high cohesive strength as shown in Figure 6.8. The reducing cohesive strength as pH moved from pH = 4 (until pH = 7) was also in agreement with the probability that γ-alumina particles could arrange themselves to construct compact packing as indicated by the particle packing velocity in Figure 6.15.

When the pH was increased above the pH = 7, the particle mobility was not found to improve as opposed to the particle behaviour on the acidic side of the isoelectric point although the viscosity did show an decreasing trend in this pH transition as shown in Figure 6.10. This was because γ-alumina particles in this pH range remain in a flocculated status [69] and the viscosity measured in Figure 6.10 was in fact apparent viscosity. In more details, the flocculated status of γ-alumina particles kept the particles still during PIV measurement;

however the increasing negative surface charge on the particles as the pH moved from 7 to 10 still contributed to facilitate the movement of particles under direct external force application during viscosity measurement. The development of surface charging on γ-alumina particles would be more discussed in section 6.7.

6.7 Charging behaviour on γ-alumina particles

6.7.1 Idea behind the development

It was shown in Figure 6.15 that the mobility of particles at pHs at IEP and higher than the IEP was almost zero, although the viscosity and the cohesive strength did show a decreasing (Figure 6.10) and increasing (Figure 6.8) trend in this pH transition, respectively. Therefore it would be useful to build theoretical work regarding fundamental inter-particle interactions to understand the real reason behind the complex relationship between particle mobility, viscosity and cohesive strength.

6.7.2 Explanation of charging behaviour of γ-alumina particles

The charging behaviour on the surface of γ-alumina particles can be described in two steps. The first step is ionisation of surface groups. A schematic diagram showing the ionisation process can be seen in Figure 6.16. Ionisation of surface hydroxyl groups by H^+ will take place when the pH of the γ-alumina suspension is adjusted to be lower than the isoelectric point; surface OH groups will be ionised by OH^- when the pH is increased above the isoelectric point. No ionisation will occur when the pH is at the isoelectric point.

The ionisation of γ-alumina particles in the suspension gives rise to surface charge for these particles on which an electric double layer (initially introduced by DLVO theory [48]) is then created. The structure of the electric double layer on γ-alumina particles is depicted in Figure 6.17.

Acidic to IEP

Basic to IEP
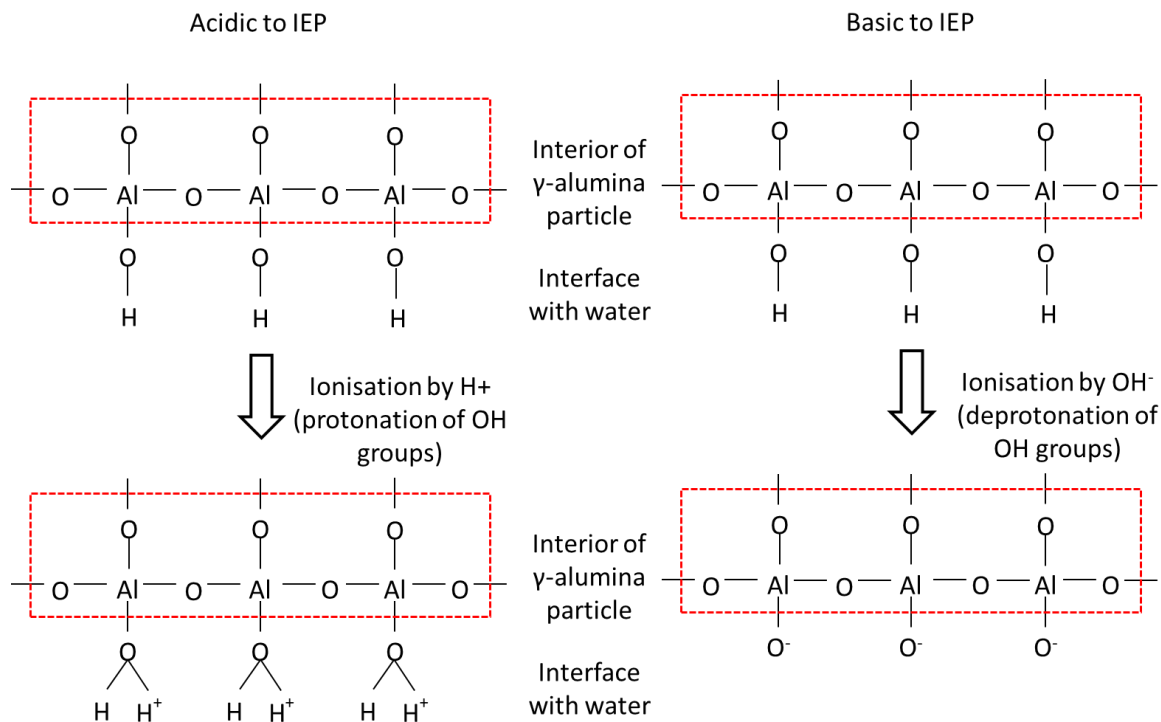
Figure 6.16 Ionisation of OH groups on the surface of hydrated γ-alumina particles

The electric double layer can be divided into two parts which are the Stern layer and the diffuse layer. The Stern layer contains purely counterions (ions with the opposite charge to the surface charge of γ-alumina particles) firmly attached onto the surface of γ-alumina particles. The diffuse layer is comprised of a distribution of counterions and coions (ions with the same charge to the surface charge of γ-alumina particles) interchangeable with the bulk of the suspension due to thermal motion ions. Charge neutrality is maintained for each individual particle within its electrical double layer.

When two charged γ-alumina particles approach each other, the double electric layer on their surface starts to repel, whereas the Van der Waals force between the particles acts to attract them. The result is a balance of the two forces, governing the mobility and packing of γ-alumina particles. The equations to calculate potential energy for electrostatic repulsion and Van der Waals attraction for two spherical particles with their particle radius much greater than the separation between them are shown from Equation 2-2 to Equation 2-6 [70].
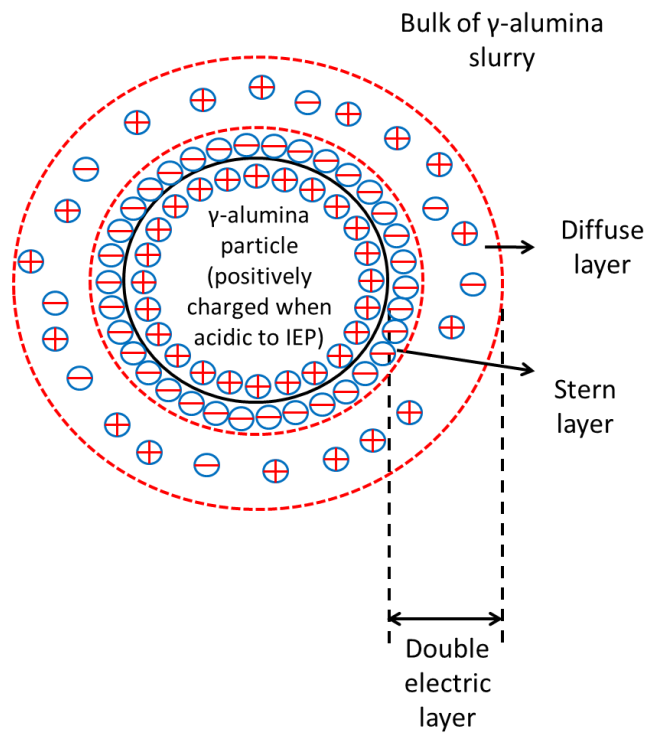
Figure 6.17 Schematic diagram of electric double layer on γ-alumina particle when pH is acidic to the IEP
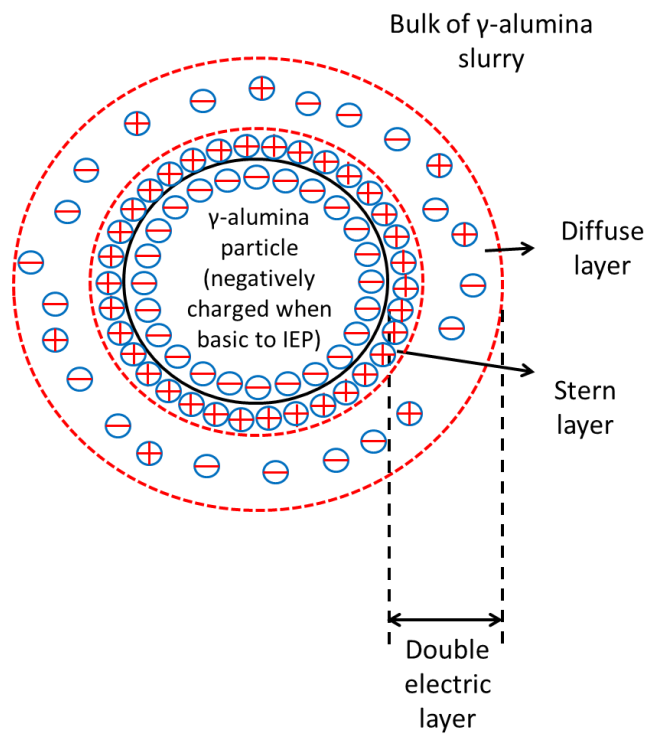
Figure 6.18 Schematic diagram of electric double layer on γ-alumina particle when pH is basic to the IEP

The d_{50} of suspension 1 in Table 6.1 (d_{90}=9.37 μm, d_{50}=3.76 μm, d_{10}=1.41 μm) was used for R. The zeta potential value was taken from Novak and König [46]. The ionic strength can be calculated from the fact that both HCl and NH_3 are monovalent electrolytes and their concentration can be worked from the pH value. The input data collected for the DLVO theory in the experiments are shown in Table 6.2.

Table 6.2 Input parameters for the DLVO theory

pH	Zeta potential (mV)	I (mol/m^3)
2	65	10
3	61	1
4	59	0.1
5	42	0.01
6	16	0.001
7	0	0.0001
8	-8	0.001
9	-25	0.01
10	-31	0.1

Constants	
R (m)	1.88×10^{-6}
A (J)	1.6029×10^{-20}
ε_0 (A^{2}s^{4}kg^{-1}m^{-3})	8.854×10^{-12}
ε	80.4
k_B (m^{2}kgs^{-2}K^{-1})	1.38×10^{-23}
T (K)	293
q (C)	1.602×10^{-19}
N_A	$6.022\times10^{+23}$

The predicted potential curves using the DLVO theory were generated as presented in Figure 6.19 and the peak potential plotted in Figure 6.20. As can be seen from Figure 6.19, the DLVO theory predicted that the highest and consistently high repulsive potential was achieved at pH=4, indicating that γ-alumina particles at this condition are well separated from each other and able to adjust themselves in any orientation to form good packing throughout the drying process. Experimentally, the well-maintained separation contributed to the high particle packing velocity as measured in Figure 6.15, which then aided to achieve a compact structure to give rise to a high cohesive strength as determined in Figure 6.8.

When pH was reduced further from pH=4, as predicted by the DLVO theory, although the peak in repulsive potential is maintained, the particles could start to be much closer to each other before they experience the high repulsion as indicated by the significantly lowered repulsion with increasing separation. The closer distance allowed between γ-alumina particles

increased the chance that these particles can overcome the repulsion barrier and leave the particulate system in attraction dominated, eliminating the capability of γ-alumina particles to pack during drying; as a result, the particle packing velocity was reduced and the cohesive strength resulted was also lowered as experimentally determined.
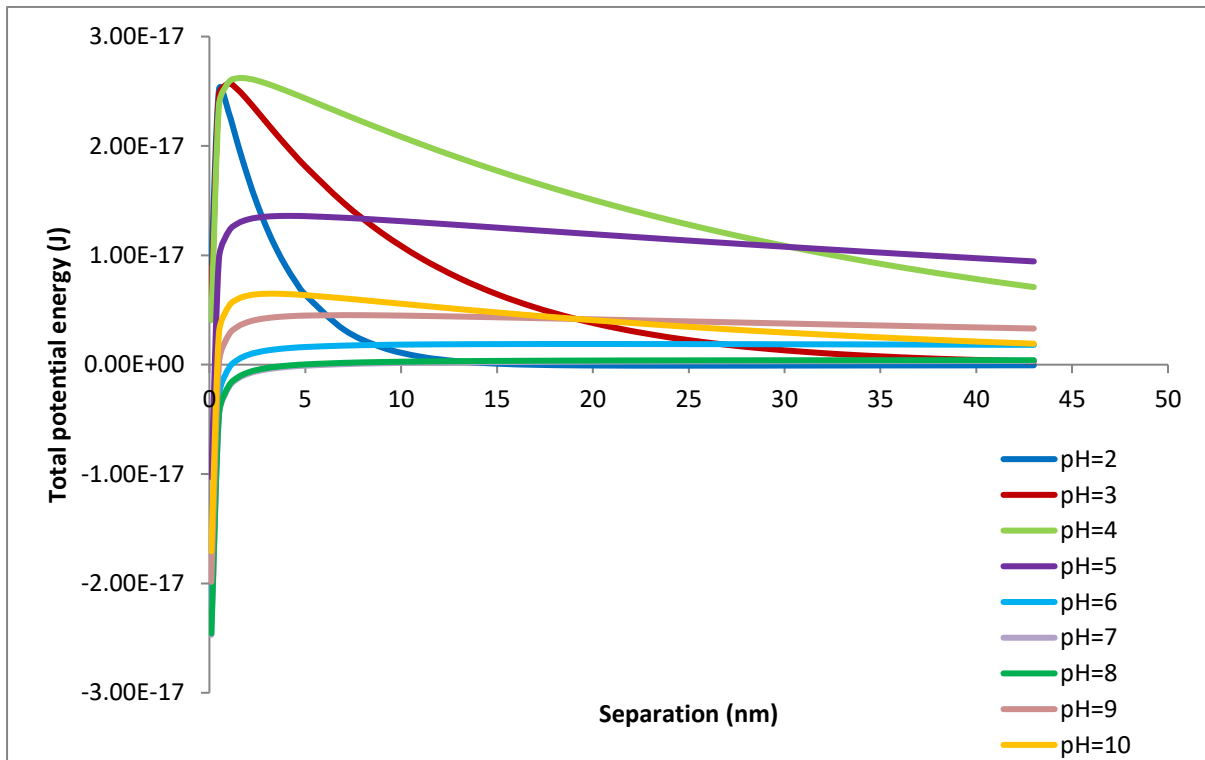
Figure 6.19 Potential curves predicted by the DLVO theory
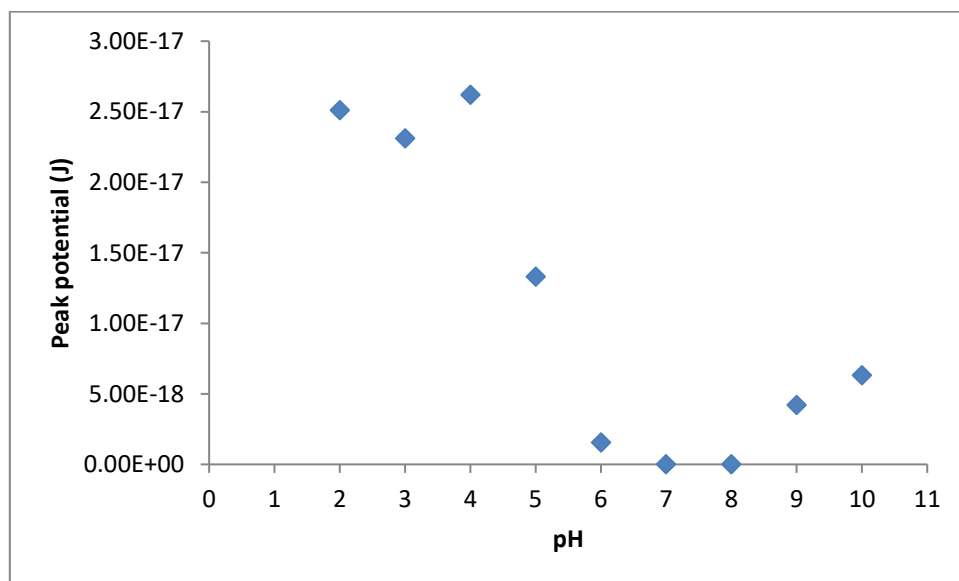
Figure 6.20 Peak potential versus pH

When pH was increased from pH=4 before reaching pH = 7, the repulsion barrier was gradually being removed as shown by the theory. The gradual removal of this repulsion barrier meant that more γ-alumina particles can overcome the electrostatic repulsion force between them and become dominated by the Van der Waals attraction, disabling γ-alumina particles to develop favourable packing during drying. Experimentally, such packing behaviour of particles was confirmed by the reduced particle packing velocity and the low cohesive strength as pH was increased from pH = 4 to pH = 5 and pH = 6.

As pH is increased above the isoelectric point from pH = 8 to pH = 10, the repulsion barrier is slowly being built as shown by the DLVO theory; however, the magnitude of it is not strong enough to prevent the majority of γ-alumina particles to separate from each other and develop good packing during drying, as can be demonstrated from the zero particle packing velocity experimentally determined at these pH values. The lower mobility from pH = 8 to 10 is highly related to the formation of a flocculated structure [69], as previously explained in section 0 and 6.6. Such claim can also be more supported when the crack pattern of tablets was reviewed in section 6.9.

Another way of looking at the variation of potential energy with pH was by the salt concentration. An increase in the salt concentration would normally shorten the range of repulsive effects therefore promoting the effect of Van der Waals attraction. From pH = 2 to pH = 4, a decrease in salt concentration was found to encourage the repulsive effects; however when the pH was further increased from pH = 5 onwards into the isoelectric region, the further lowered concentrations of salt were not sufficient provide enough ionisation on the surface of γ-alumina particles, changing the balance to Van der Waals force dominated. After the pH was raised above the isoelectric region, the increased ionisation on the surface of γ-alumina particles was found to help the repulsive effects increase.

6.8 Effect of drying using a uniform drying system

6.8.1 Idea behind the measurement

Given the effect of drying rate on the cohesive strength investigated in Figure 5.6 which still experienced tablet splitting, it was deemed as necessary to perform uniform drying under different drying conditions to see the effect of drying rate from the uniform drying system.

6.8.2   Experimental method

The tablets produced were guided by the procedure outlined in section 6.3.2. Three different drying conditions were employed as seen in the Table 6.3.

Table 6.3 Drying condition implemented in the uniform drying

Drying condition 1	Drying condition 2	Drying condition 3
25 ℃ 40 %RH	25 ℃ 80 %RH	Hot air stream (air velocity 3.5 m/s, air temperature = 45 ℃)

Drying condition 1 was already implemented in section 6.3.2 with the results showing in section 6.4. Drying condition 2 would be performed in an environment chamber (Series KMF, Binder GmbH). Drying conditioning 3 would be carried out under a hot air stream with the properties of the air as shown in Table 6.3, as measured by a probe (TSL VelociCalc). The hot air was applied above the filter paper dies as shown in Figure 6.21.
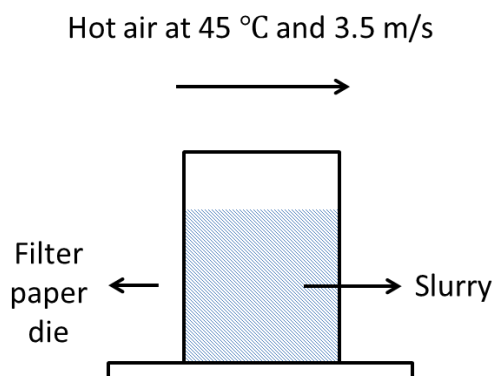
Figure 6.21 Hot air drying the suspension

All drying conditions employed suspension 1 in Table 6.1 as it was the one which produced crack free tablets in the low pH conditions.

Online monitoring was also performed for the two additional drying conditions (drying condition 2 and 3). The experimental setup utilised has been slightly modified from that in Figure 6.13. The modified experimental setup is shown in Figure 6.22 and Figure 6.23.

In both cases the main experimental setup was still the same as that stated in section 6.6.2. A humidity generator (GenRH-A) was used to provide the high humidity condition implemented in drying. Hot air was provided by a hairdryer. Both the temperature and the air velocity were measured by a probe (TSL VelociCalc). The same air velocity and temperature used for drying of tablet samples (as shown in Table 6.3) was applied for the online monitoring experiments.
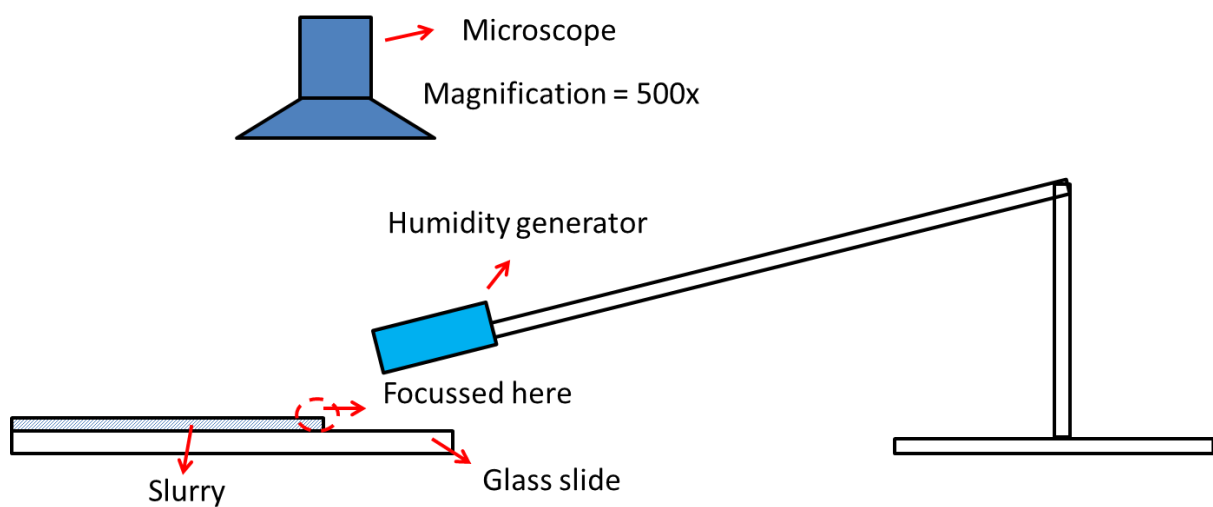
Figure 6.22 Experimental setup for online monitoring drying condition 2
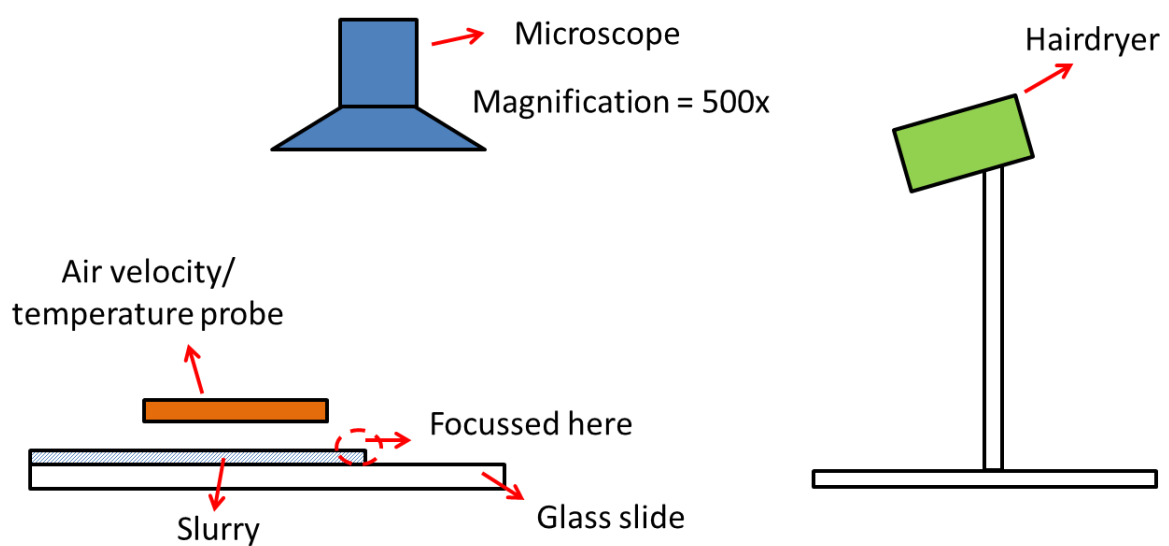
Figure 6.23 Experimental setup for online monitoring drying condition 3

The PIV technique (as seen in section 6.6.2) was again used to quantify the particle packing velocity from the online monitored suspension drying process.

6.8.3 Results and discussion

The effect of drying condition on the cohesive strength can be seen in Figure 6.24. The slower drying rate from the high relative humidity condition managed to improve the cohesive strength. This can be understood from the argument that a slower drying rate provided more time for γ-alumina particles to pack. This argument is supported from the measurement of particle packing velocity as shown in Figure 6.25. At all pH tested, the particle packing velocity was found to be higher for room temperature drying than for drying at 80 %RH.
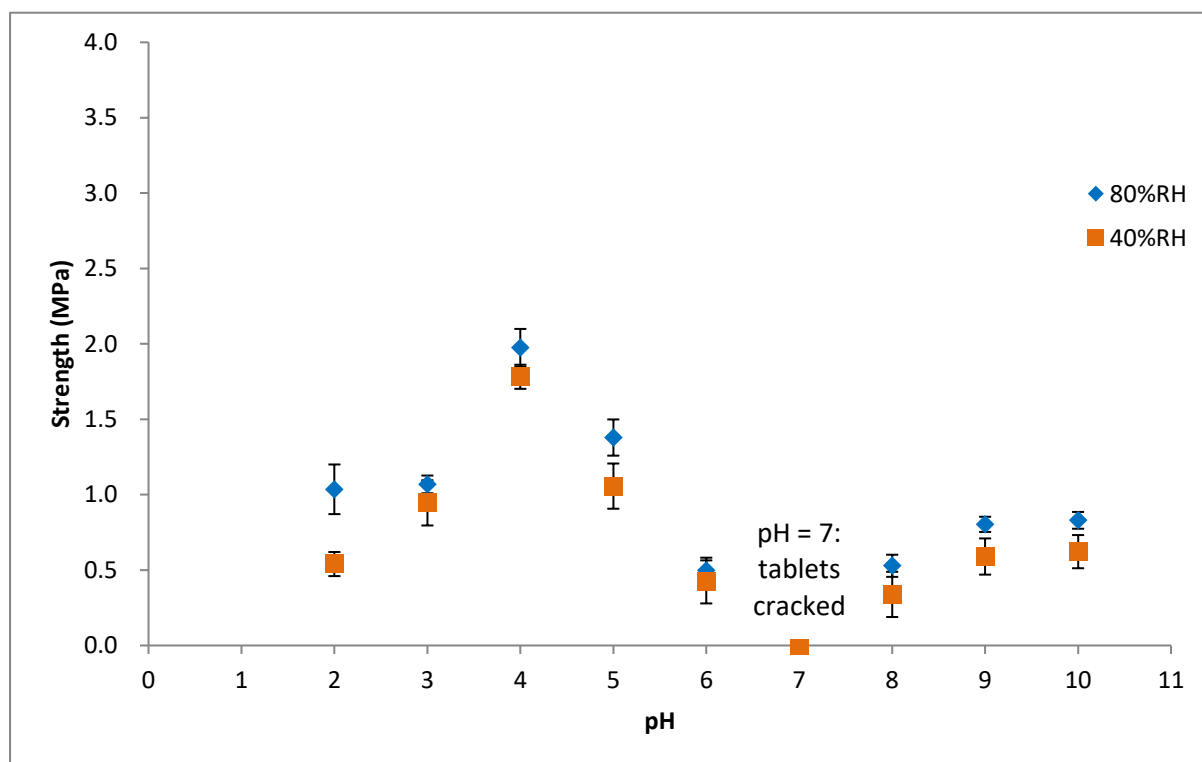
Figure 6.24 The effect of drying condition on the cohesive strength
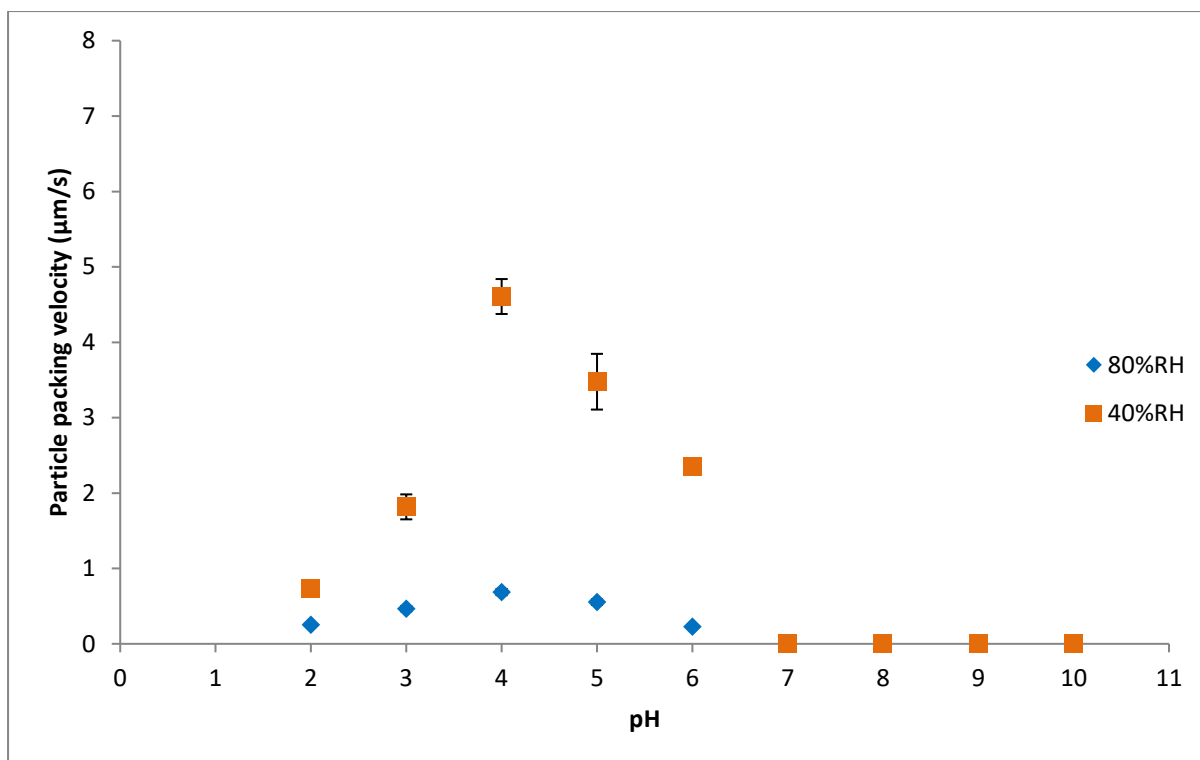
Figure 6.25 The effect of drying condition on particle packing velocity

For the drying condition under the stream of hot air, tablets were not able to be formed due to the γ-alumina suspension sticking on the side of filter paper die from which the hot air was coming, as schematically demonstrated below.
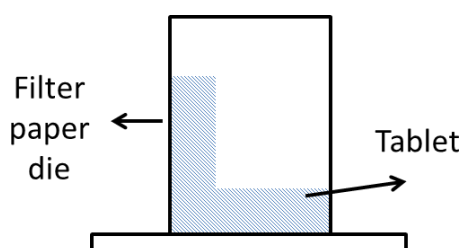
Figure 6.26 Schematic representation of the tablet samples dried under the hot air condition

The very fast drying imposed by the hot air left γ-alumina particles with no time to pack but instead they stuck to the side of filter paper die. Particle packing behaviour under the hot air drying condition was also online monitored. It was found that while the particles near to the dried edge were approaching the edge to pack, the particles remaining in the suspension were heavily influenced by the stream of hot air as can be seen in Figure 6.27 which consists of three images taken in continuous time. Vectors on the right side of the images which show particle motion towards the dried edge were found to exhibit uniform directions towards the

dried edge; while vectors on the left side of the images were noted to have random directions. This would that there would be a reduced degree of packing in the catalyst layer formed under such drying conditions. From the perspective of a force analysis, it could be said that at the edge of drying, drag force exerted by water on particles dominates while in the centre of drying, air flow induced drag force is more significant.

The observation made here can have implications for industrial manufacturing of catalytic converters in which the catalyst layer is produced by drying washcoat with a fast moving hot air on a conveying belt. It can be anticipated that in industrial manufacturing the strength of the catalyst layer would suffer a reduction in the cohesive strength as implied by the disturbing effect on particle packing from a fast moving hot air stream.
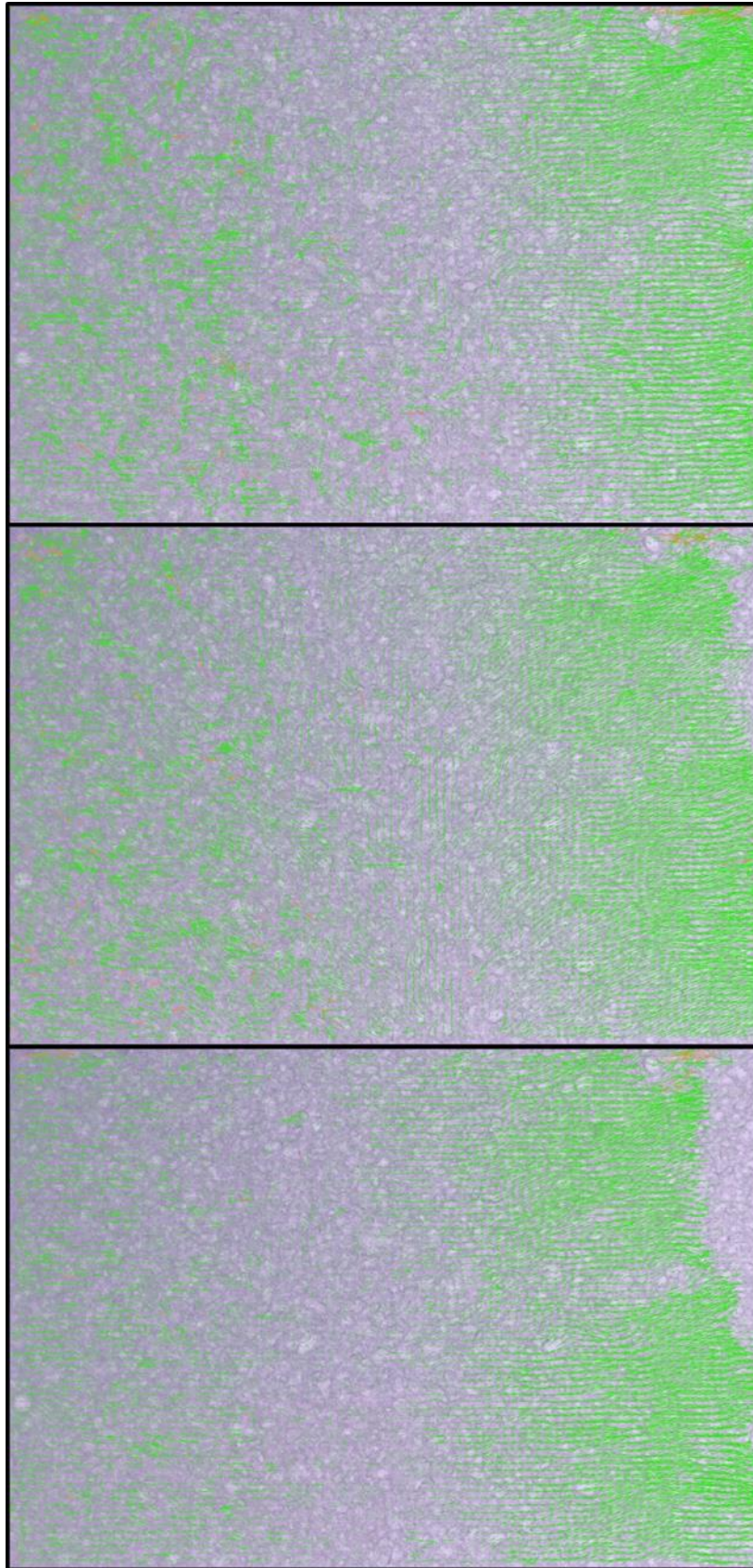
Figure 6.27 Movement of γ-alumina particles under hot air (from top to bottom in time)

6.9 Cracking pattern

The cracking pattern of the tablets prepared at 40 %RH drying using the three different formulations in Table 6.1 can be seen from Table 6.4 to Table 6.6. Four samples were included for each experimental condition.

It can be observed from the tabulated images that tablets exhibited radial cracks at pHs lower than the isoelectric point while the cracks shown at pH = 7 were more of a random character. It should also be noticed that tablets formed between pH=2 to pH=6 were all in close contact with the filter paper dies while those formed between pH=8 to pH=10 were separate from the dies, confirming the particle packing velocity pattern determined in Figure 6.15. γ-alumina particles in the acidic pHs to the isoelectric point are generally more mobile compared than those in the pHs basic to the isoelectric point; therefore γ-alumina particles between pH=2 to pH=6 are more easily influenced by drag force during drying and tend to move in the same direction as water. On the opposite, γ-alumina particles in the high pH conditions form a flocculated structure, disabling their capability to travel to the side of the die wall. In addition, between pH=8 to pH=10, tablets formed from smaller particles showed more shrinkage compared with those formed from larger particles. This could be explained from a tighter packing provided by small particles.

The development of radial cracks in pH=2 to 6 in the formulations containing many small particles is schematically shown in Figure 6.28 which shows a top view of the tablet. As small particles are able to travel to the side of filter paper die during drying, the area closer to the side would be more compacted compared to the centre. Given this understanding, for formulations that contain a large proportion of small particles, the less uniform packing in the radial direction of the tablets would cause cracks to first of all appear in the edge of the tablets and propagate in the radial direction towards the centre of the die.
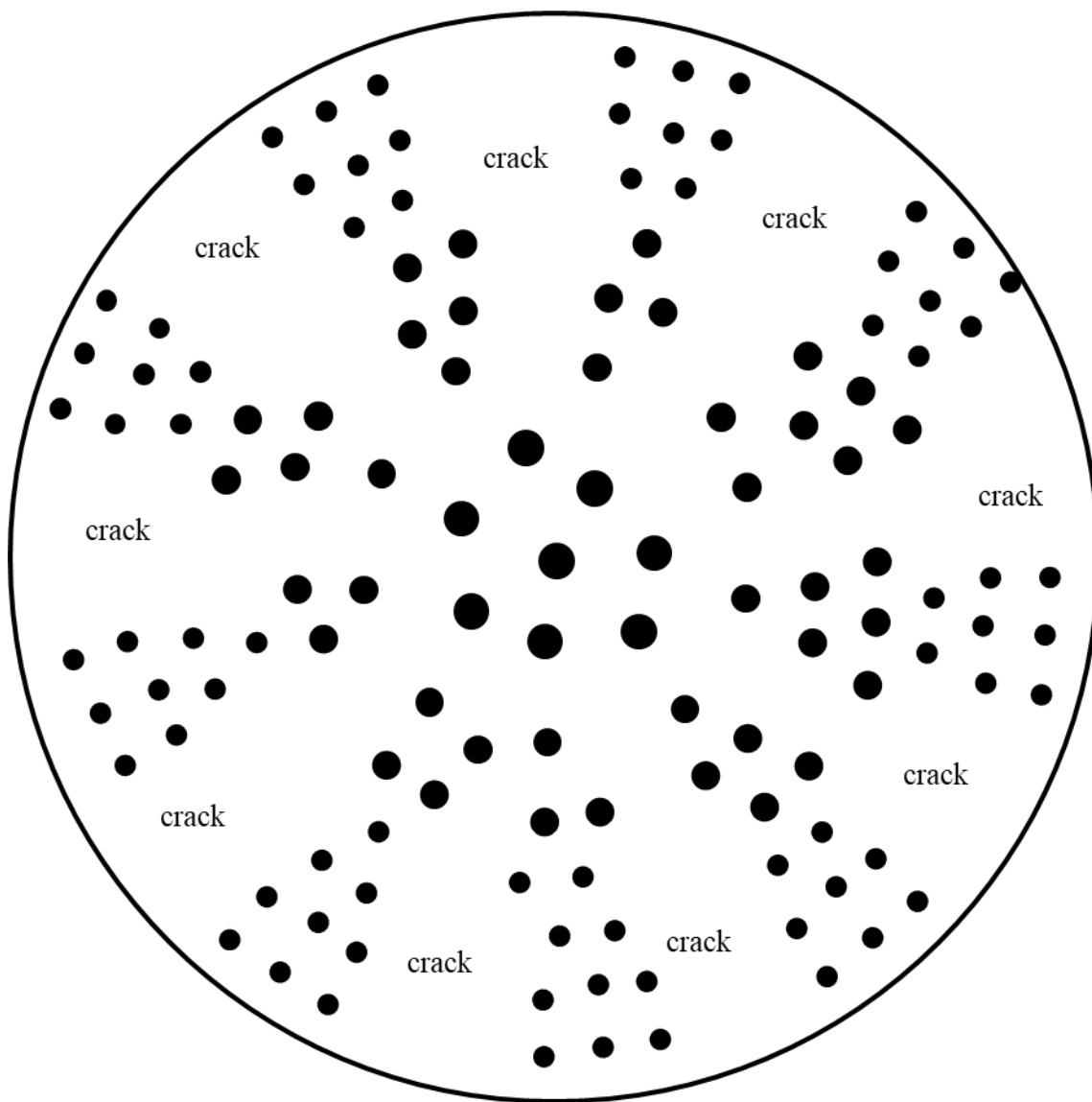
Figure 6.28 Schematic diagram showing the development of radial cracks in catalyst tablets made with dominating small particles at low pHs

Table 6.4 Cracking pattern for the formulation (suspension 1 in Table 6.1)

pH=2				
pH=3				
pH=4				
pH=5				
pH=6				
pH=7				
pH=8				
pH=9				
pH=10				

108
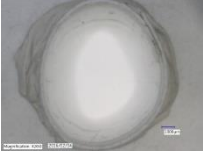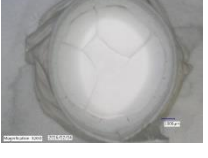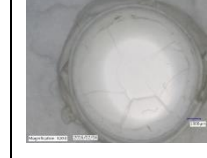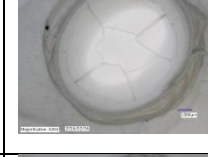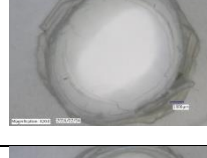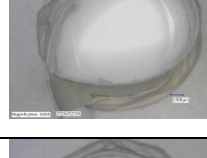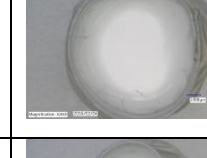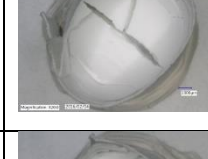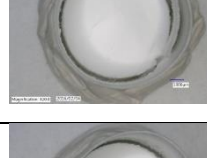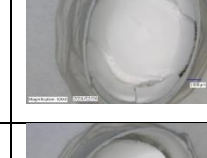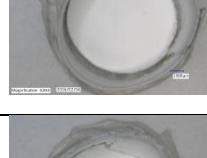
Table 6.5 Cracking pattern for the formulation (suspension 2 in Table 6.1)

pH=2				
pH=3				
pH=4				
pH=5				
pH=6				
pH=7				
pH=8				
pH=9				
pH=10				

109
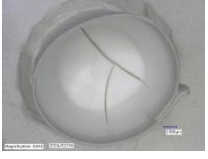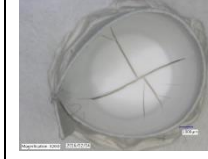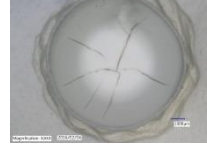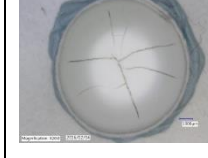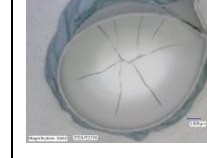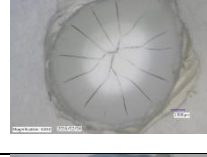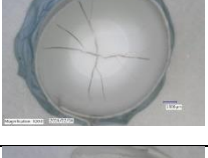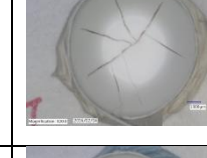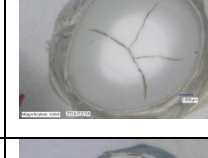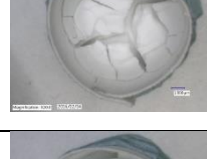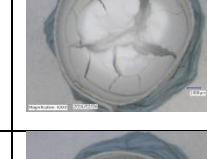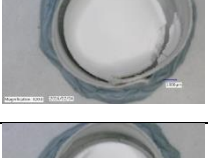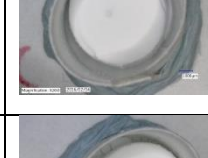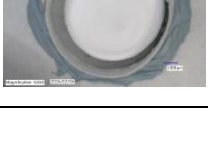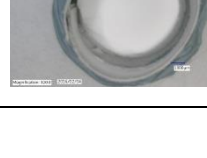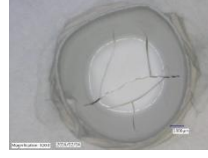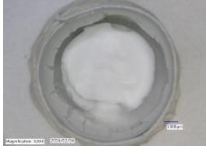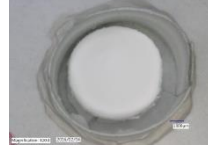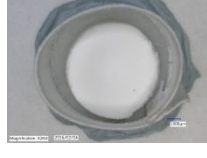
Table 6.6 Cracking pattern for the formulation (suspension 3 in Table 6.1)

Give the stable crack propagation of the tablets, it was decided to also investigate the fraction energy at different pHs. The fracture energy can be determined by calculating the area under the curve of force versus displacement. One example of such curves is shown in Figure 6.29.
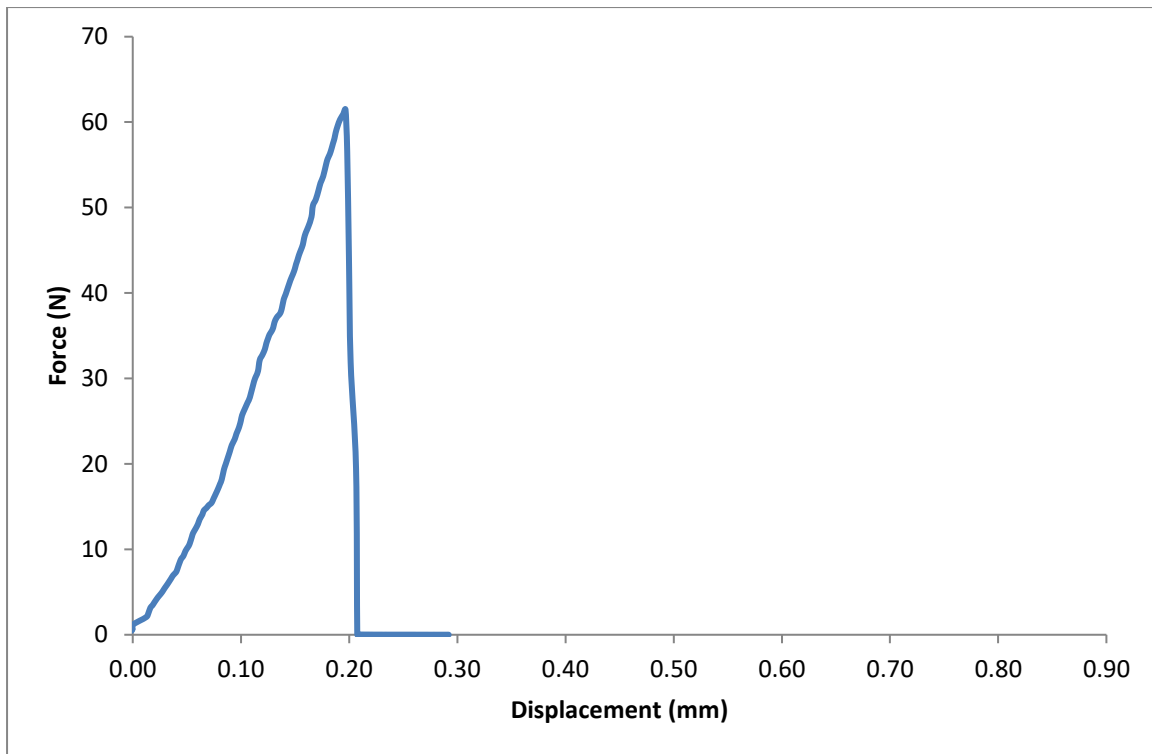
Figure 6.29 Example of force versus displacement

The fracture energy at different pHs from suspension 1 is shown in Figure 6.30. As could be seen that, a similar trend with regards to pH is obtained.
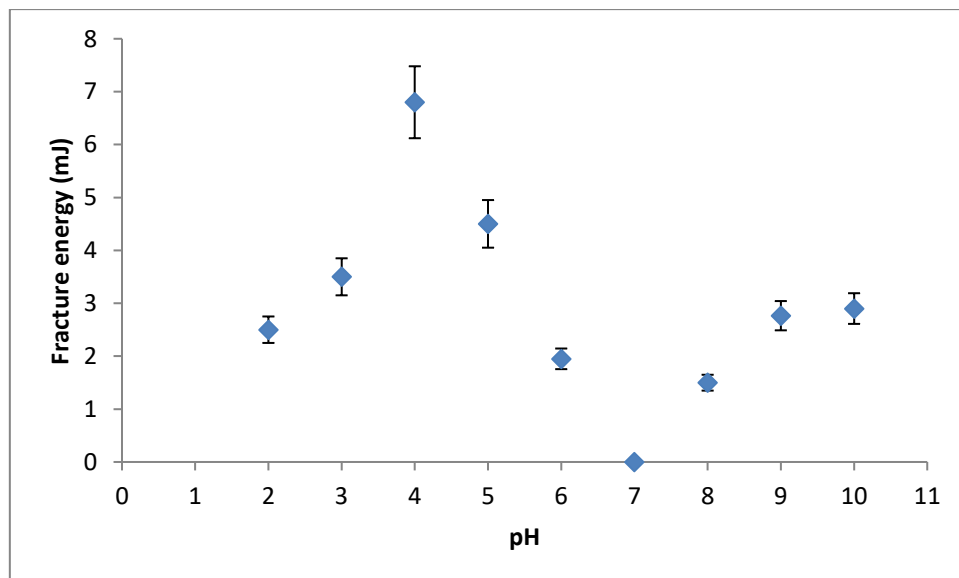
Figure 6.30 Fracture energy of suspension 1 at different pHs

111

6.10 Effect of particle size distribution

6.10.1 Idea behind the measurement

As described in section 6.4 that it would be necessary to have both small and large particles present in order to prevent tablets from cracking during drying, therefore this section was specifically designed to investigate to see the effect of particle size distribution on the cohesive strength.

6.10.2 Experimental method

The procedure outlined in section 6.3.2 was followed to produce tablets. The suspension used was guided by the preparation steps in Chapter 3 with a variation in the milling time. The properties of the suspension finally obtained are presented in the tablet below.

Table 6.7 Properties of suspension to be mixed for produce bimodal distribution

Suspension 4	$d_{90} = 11.0\ \mu m, d_{50} = 4.3\ \mu m$
Suspension 5	$d_{90} = 4.0\ \mu m, d_{50} = 2.1\ \mu m$

The two individual suspensions in Table 6.7 were then mixed at 1 to 1 ratio to obtain a mixed suspension with bimodal particle size distribution.

6.10.3 Results and discussion

The cohesive strength profile for the mixed suspension is presented in Figure 6.31. The cohesive strength of the mixed suspension and suspension 1 in Table 6.1 was compared. The reason that suspension 1 was chosen was because it had a similar characteristic particle size compared with the mixed suspension. The d_{90} and d_{50} values of the mixed suspension were deemed to be a weighted averaged of the two original suspensions, therefore being 7.5 μm and 3.2 μm, respectively; these two characteristic particle sizes were not too much different from that of suspension 1 in Table 6.1, which had its d_{90} and d_{50} values as 9.37 μm and 3.76 μm.
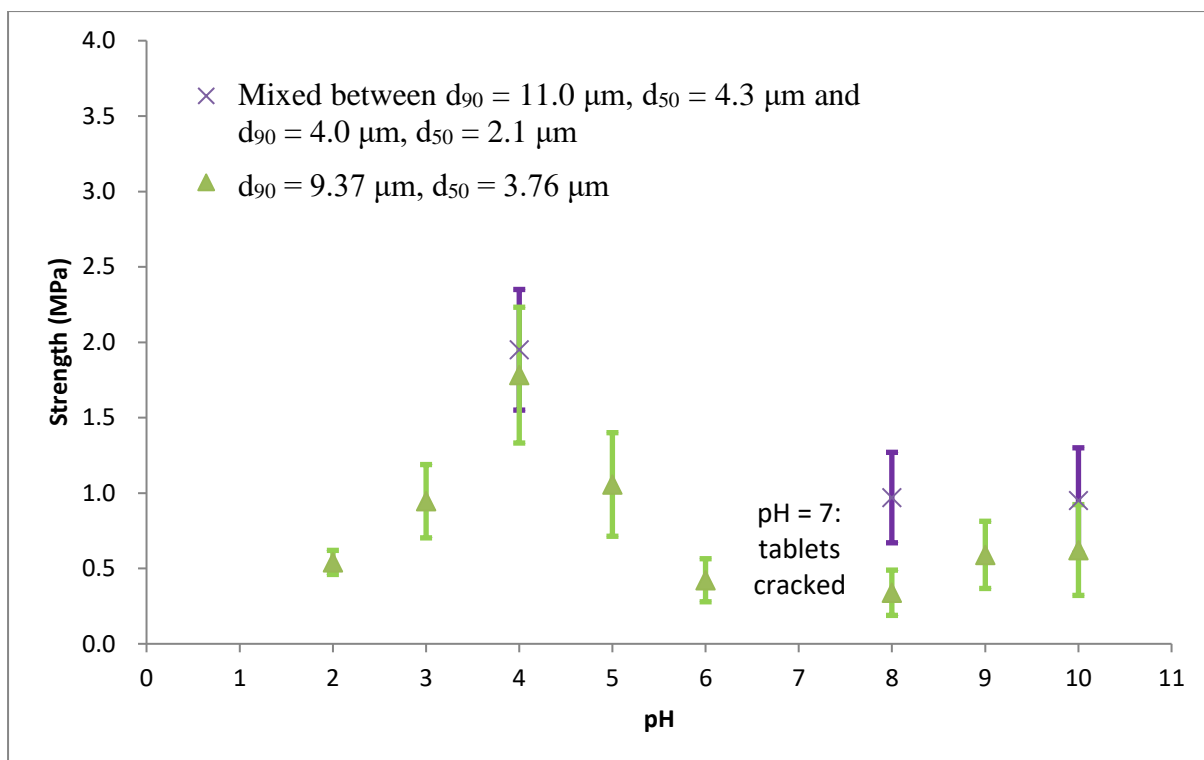
Figure 6.31 Cohesive strength profile for a mixed suspension and an original suspension

It was therefore interesting to compare the cohesive strength obtained from the mixed suspension and suspension 1 given the different particle size distribution and similar characteristic particle size. It can be noted from Figure 6.31 that at the three pHs tested (pH = 4, 8 and 10), the mixed suspension all demonstrated a higher cohesive strength than suspension 1, indicating that a bimodal particle size distribution could further improve the cohesive strength of catalyst layer due to tighter particle packing.

6.11 Effect of calcination temperature

6.11.1 Idea behind the measurement

As an interest to give a comprehensive understanding of the effect of the process parameters on the cohesive strength, the effect of calcination temperature was studied.

6.11.2 Experimental method

The procedure outlined in section 6.3.2 was followed to produce tablets. Suspension 1 due to its capability of producing crack-free tablets in the low pH conditions was chosen to be used. Two calcination temperatures were tested which were 500 degrees and 700 degrees. The calcination time was kept at 2 hours for both temperatures.

6.11.3 Results and discussion

The cohesive strength for the effect of calcination temperature is reported in Figure 6.32.
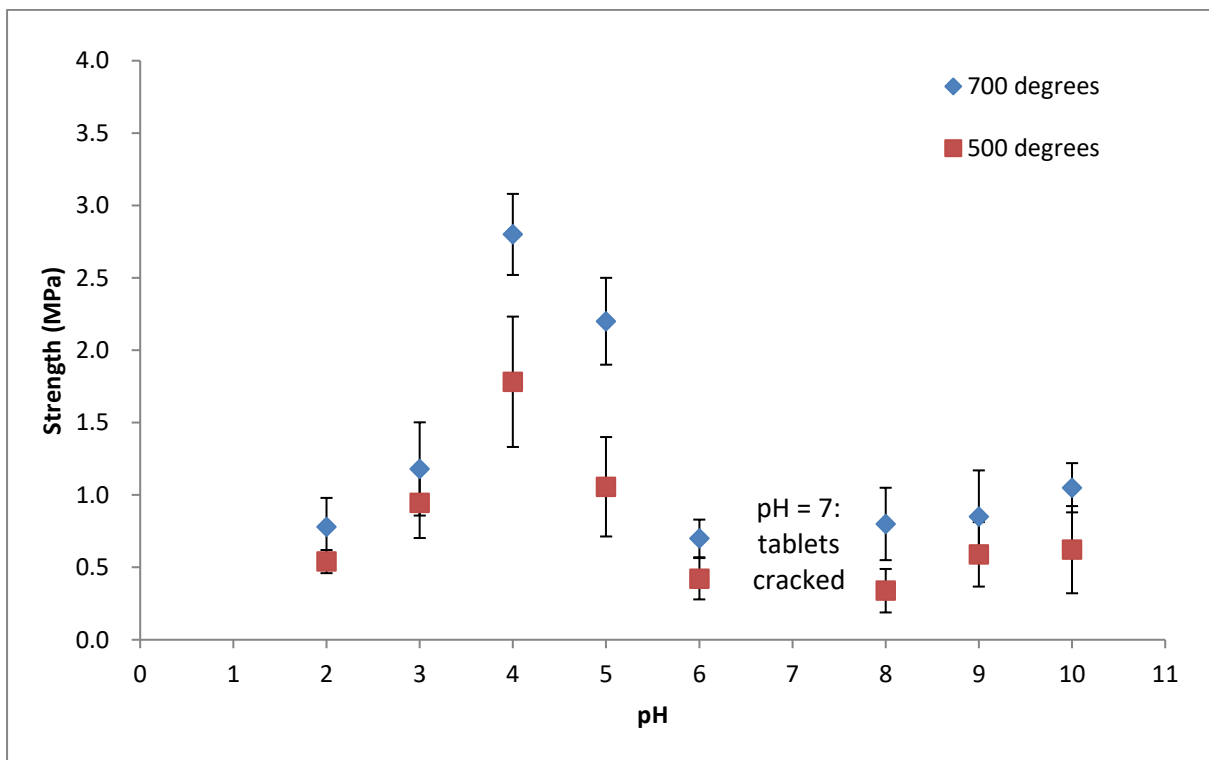
Figure 6.32 Cohesive strength for the effect of calcination temperature

It can be noticed from Figure 6.32 that a higher calcination temperature resulted in a higher cohesive strength. This could be understood as at a higher calcination temperature, the γ-alumina particles experienced a sintering process to result in a more compacted structure in the tablets.

6.12 Conclusion

In this chapter, a uniform drying system has been created to resolve the tablet splitting issue as identified in chapter 5. The reason behind tablet splitting was first of all investigated and found to be a segregation process of particles. During drying of the suspension, small particles were found to move the top of the tablet while large particles stayed at the bottom, causing tablets produced in this way to split into a top and a bottom fragment. A uniform drying system facilitated by the use of filter paper (with the correct grade) helped overcome this problem.

The development of the uniform drying system then allowed the author to quantify the cohesive strength of catalyst layer at a more comprehensive range of pHs. The trend observed in the pH was correlated with the viscosity measurement and the particle packing velocity study from the online monitoring experiments. The correlation was also theoretically explained by the DLVO theory, showing that at conditions with high cohesive strength, particles were consistently able to move freely during drying to develop a more favourable packing. The effect of drying condition on the cohesive strength was then also measured by implementing the uniform drying system. Online monitoring experiments were employed to understand the reason behind the improved cohesive strength resulted at slower drying rates and the allegedly reduced cohesive strength obtained from fast drying.

Suspension with different particles were tested and found that a good combination of small and large particles were necessary to obtain crack-free tablets at low pH conditions. Apart from elimination of cracks, suspension with more bimodal particle size distribution was also found to increase the cohesive strength due to tighter particle packing. For conditions which did yield tablet cracking, the cracking pattern was studied and explanation for the formation of cracks was given based on particle motion during drying.

The effect of calcination temperature was also studied and a higher calcination temperature was found to result in a higher cohesive strength. This could be understood as the sintering process of γ-alumina particles gave rise to a more compacted structure for the formed body, leading to an increased cohesive strength.

Chapter 7 The novel method of measuring the adhesive strength of catalyst layer

7.1 Idea behind the measurement

As detailed in the literature review, there is currently a lack of methods that are capable of producing a separate measurement of the adhesive strength of the catalyst layer with the unit of stress. For this reason, a unique adhesive strength tester was developed for this project.

7.2 Experimental method

7.2.1 Preparing the substrate

Unlike the measurement of the cohesive strength where no substrate was needed, to be able to determine the adhesive strength of the catalyst layer, the layer sample needed to be prepared on a substrate. In order to make the results of this measurement more applicable in real applications, instead of a model material, the actual substrate used in the industry to manufacture catalytic converters was employed in this project to produce samples for adhesive strength test.

Three different substrates were used for the adhesive strength experiment, which were metal, ceramics and alumina. The metallic substrate used was FeCrAlloy discs of 1 mm thick. These discs had a composition of 22 wt% Cr, 5 wt% Al and 73 wt% Fe. They were pre--oxidised in a furnace (Carbolite) at 900 ˚C for 2 hours before the catalyst layer was applied. The reason of using a thick metallic substrate was that a thin metallic substrate was found to bend after pre-oxidisation, leaving it difficult to find a flat surface for the adhesive strength test to be performed.

The ceramic substrate was made of cordierite and prepared by cutting of a cordierite monolith. The cordierite monolith was cut into rectangular blocks of the same dimension. The wall of the monolith left from the cutting was carefully removed by sand paper.

The alumina substrate used was tablets prepared by direct compression of boehmite powder followed by calcination. Two types of boehmite powder were used which are Versal 250 and Versal 700. The compression took place in a tablet die with an internal diameter of 30 mm.

Two compression forces were used which were 5 kN and 10 kN. For each tablet, 2 g of powder was placed in the die. The equipment employed was Instron model 3367; the punch was set to move down a speed of 1 mm/min to allow enough time for air to escape during compression. Following the direct compression of boehmite powder, all of the tablets made were calcined at 500 ˚C for 2 hours in a furnace (Carbolite)

7.2.2 Preparation of the suspension

Suspension preparation followed the same procedure as outlined in Chapter 3. Suspension 1 in Table 6.1 was chosen to be used as it produced crack free tablets in low pH conditions; therefore if the adhesive strength in all pHs interested can also be tested, then a comprehensive strength profile for the catalyst layer can be obtained.

7.2.3 Coating the substrate

Depending on the flowability of the suspension at different pHs, suspension can be initially applied on the substrate by either a plastic pipette or a medical syringe, similar to that in section 4.2.2.1. For this part of the experiment, the amount of suspension transferred was not controlled as long as there was enough suspension to be spread over the desired area (16 mm by 10 mm) with a wet height of around 200 micron (therefore roughly 10 ml). To ensure that each layer sample produced would have roughly the same desired height, another purpose built apparatus was employed. Figure 7.1 is presented to show this experimental technique which works based on a similar idea to an automatic film applicator. Two pieces of substrate were utilised to balance the height of the substrate on which the suspension was applied so that the height controller can actually set the height of the suspension passed under the gate to a desired value.

As an uncontrolled amount of suspension was applied on the substrate, although the height of the suspension was set, the area over which the suspension spread was still not regulated. To remove the excessive amount of suspension, a trimming process was then undertaken. This trimming process was performed when the suspension became a semi-fluid after drying for approximately 15 minutes. A shape surgical knife was carefully used to cut through the catalyst layer vertically around the pre-determined coating area (16 mm by 10 mm). The

excessive amount of suspension can then be removed without interfering with the catalyst layer in the desired area.

Manually slide through the gate
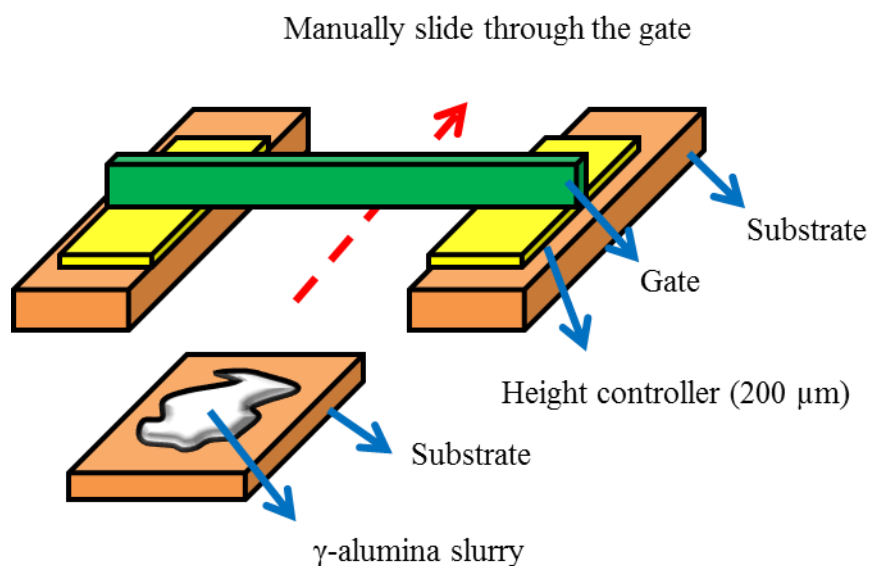
Figure 7.1 Controlling the height of the suspension

The change of the pH was carried out in the same procedure as described in section 6.3.2. The range of pH tested was from 2 to 10 at an interval of 1. The acid used was a 36 wt% HCl solution and the base used was a 96 wt% NH_3 solution. The drying process was performed at 25 ℃ and 40%RH using an environment chamber (Series KMF, Binder GmbH). After the catalyst layer which now had the pre-determined size was fully dried, the same calcination process as described in section 5.3 (500 ℃ for 2 hours) was conducted.

7.2.4 Mounting the coated substrate

Layer samples which were fully dried and calcined were ready for the adhesive strength test. The Sheffield in-house developed adhesive strength tester was used for this measurement. The following figure (Figure 7.2) gives an idea of how the layer sample was oriented before the test. The calcined coated layer was mounted onto a vertical support on a micrometre stage. The position of the catalyst layer can be controlled by the micrometre stage underneath.
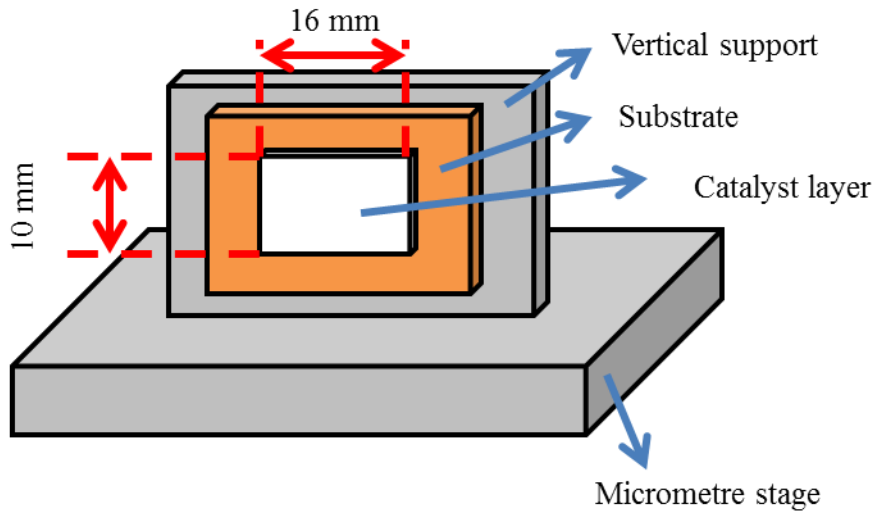
Figure 7.2 Loading of the layer sample onto the adhesive strength tester

After the layer sample was mounted, the base can be installed onto the Zwick Roell material testing equipment (A622057). The specially designed scraper of the adhesive strength tester was then connected via an adaptor to the crosshead of the Zwick Roell machine. A close look of the scraper is provided as follows (Figure 7.3). The angle of the scraper was designed to help the layer removed to leave. The small size of the actual scraping area was found to be useful after a number of trials. The full reason for this small size will be explained in section 7.2.6. The scraper was also designed to be replaceable due to the abrasive nature of the substrate for the current test.
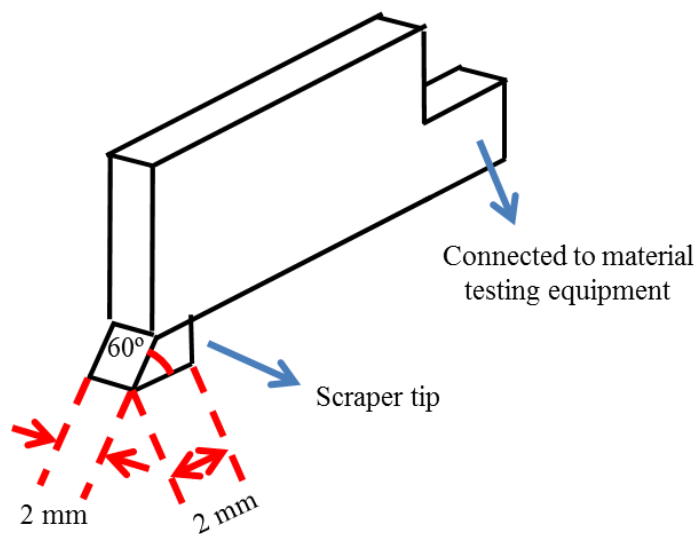
Figure 7.3 A close look of the specially designed scraper

7.2.5　Determining the friction force

The scraper can travel in the vertical direction and the base can move in the horizontal direction. Using these functions, before the start of the test, the scraper can be positioned slightly above the substrate in the vertical direction as shown in Figure 7.4.
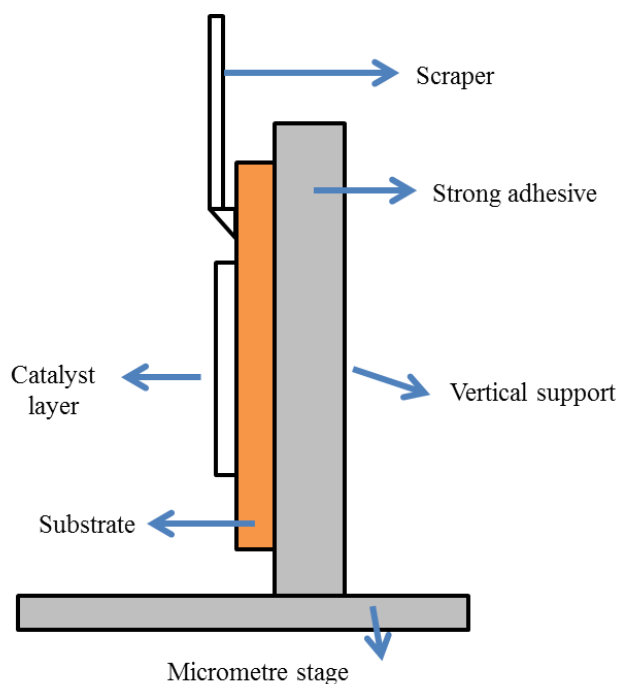
Figure 7.4 Positioning the scraper prior to the adhesive strength test for friction determination

The reason for positioning the scraper in a position away from the catalyst layer prior to the test was that the friction between the scraper and the substrate can be determined first. The magnitude of this friction force is important for two reasons: if the friction is too high, the test result may simply be overwhelmed by the friction force, leaving the low adhesive strength very difficult to be extracted; if the friction is too low, the contact between the scraper and the substrate is simply not sufficient for the scraper to remove the catalyst layer from the interface for the adhesive strength to be detected. Instead, the scraper might cut through the layer in the middle, which does not give the adhesive strength that is originally interested.

7.2.6   Testing the adhesive strength

The true adhesive strength test can now be performed. The scraper was programmed to travel vertically downwards at a speed of 5 mm/min. For the recording of the force signal, a pre-load of 0.01 N was used; the experiment was called to stop when the first peak in force started to drop. The drop from a local maximum of force was an indication that a small area of the catalyst layer failed because of the scraping. This stop condition was used for all adhesive strength tests in order to have consistent experimental conditions. A video camera was used to record the whole adhesive strength test to correlate the real-time force signal with what happened on the catalyst layer.

The use of a small size of the scraper (as mentioned in section 7.2.4) was a key to the successful measurement of the adhesive strength. A previous design of the scraper which had a large scraping area was attempted earlier in this project. For this design, it was inevitable that during the adhesive test, the contact area between the scraper and the substrate was continuously increasing as the test continued. As a result, the friction continued to rise as well, leaving the actual adhesive strength difficult to be found. For this reason, a small scraper size was preferred so that the friction force can be maintained as a constant in the adhesive test and on a low magnitude for the true adhesive strength to be accurately detected. An example result from the adhesive strength is shown in Figure 7.5.
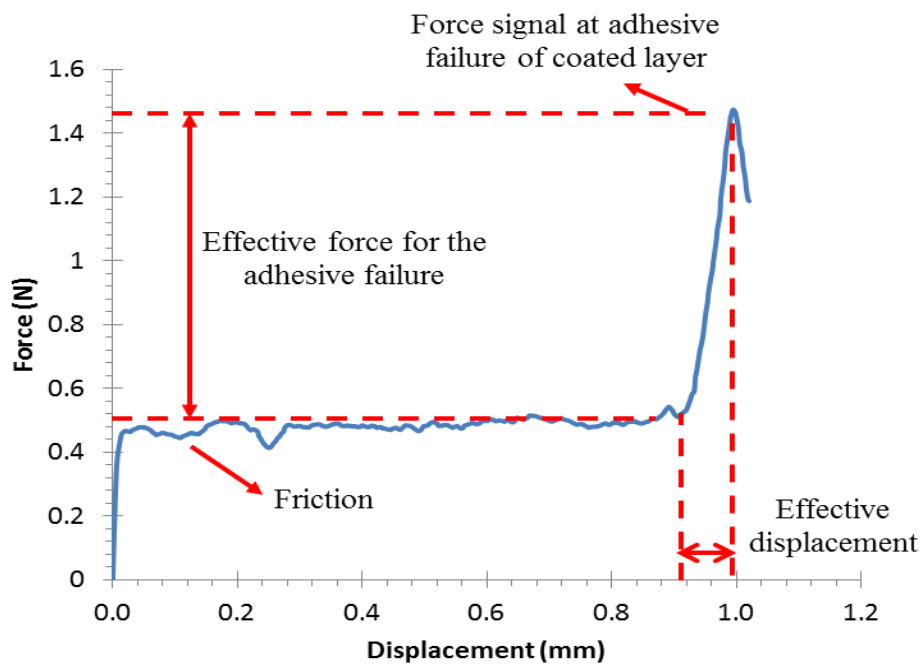
Figure 7.5 Example of how the adhesive strength was obtained

The difference between the almost horizontal force signal which was regarded as friction and the force signal when the catalyst layer was removed was taken as the effective for the adhesive failure. The distance that was travelled between the point when the force signal started to rise and the point of the peak force was regarded as the effective displacement. Given that the width of the scraper is 2 mm, the adhesive strength can be calculated by the following equation.

$$Adhesive\ strength = \frac{Effective\ force}{Effectuve\ displacement \times Scraper\ width}$$

<div align="right">Equation 7-1</div>

7.3 Results and discussion

7.3.1 Cordierite and metallic substrate

The effect of pH on the adhesive strength of the catalyst layer on both the ceramic and metallic substrates is shown in Figure 7.6.
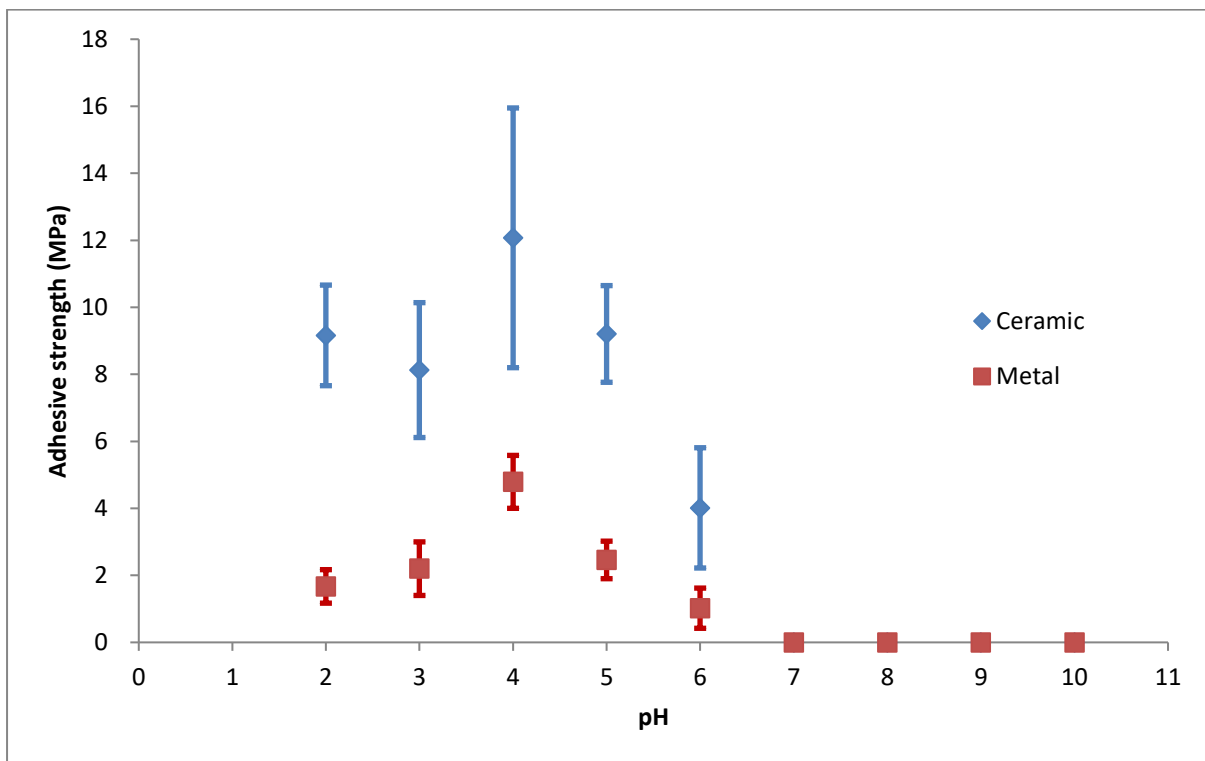
Figure 7.6 The effect of pH on the adhesive strength of catalyst layer on both metallic and cordierite substrate

In general, all of the cordierite samples demonstrated a higher adhesive strength for the catalyst layer than the FeCrAlloy samples. This trend was owing to the high surface roughness provided by cordierite substrate, which can be found with more details in section 7.3.2.

As the pH was reduced from the isoelectric point, the adhesive strength was found to peak at pH = 4 and maintain a relatively high strength. The explanation for the trend regarding the effect of pH is similar to that for the cohesive strength. The increased adhesive strength at pH = 4 was resulted from the tight packing of γ-alumina particles due to extra particle mobility. The high particle mobility was a result of the well-maintained inter-particle separation, as shown by the DLVO theory (section 6.7). The variation of the adhesive strength from pH = 4 to other pH conditions in the pHs lower than 7 can also be argued from the inter-particle interaction as quantitatively demonstrated by the DLVO theory (section 6.7). The better and consistent separation of particles when they were wet, the more likely they were able to travel to the interface between the substrate and the catalyst layer to form a compact structure, giving rise to a high adhesive strength.

At pH = 7 and above, the force required to detach the catalyst layer from the substrate was regarded as 0. This was because at these 4 pH conditions, the catalyst layer simply did not adhere onto the substrate. Similar sample shrinkage behaviour was also observed when preparing tablet samples in this pH range. As can be seen from Table 6.4 to Table 6.6, tablet samples produced at pH = 7 and above exhibited shrinkage behaviour during drying from the die wall. These common observations supported the claim made earlier in section 6.7.2 that γ-alumina particles in this pH range formed a flocculated structure. This structure contributed to the shrinkage behaviour of γ-alumina particles in both the cracking pattern study (section 6.9) and the detachment of the catalyst layer seen in Figure 7.6 at the high pHs.

7.3.2   Surface roughness profile of metallic and cordierite substrate

As it was shown in Figure 7.6 that the adhesive strength on the cordierite substrate was consistently greater than that on the metallic substrate, it would be necessary to investigate the surface roughness profile of the two substrates.

7.3.2.1 Experimental method

A non-invasive surface roughness testing method was employed. The equipment used was a digital microscope (Keyence VHX-5000). The surface profile of both the metallic and the ceramic substrate was visualised under the microscope with the surface profile data exported to a spreadsheet later for further analysis.

7.3.2.2 Results and discussion

An example of the surface roughness profile for both the substrates can be seen in Figure 7.8 and Figure 7.8. The surface roughness profile was then taken for further analysis to calculate important surface roughness parameters. In this study, R_a and R_z values were chosen due to the fact that they are capable of quantitatively explaining the different surface roughness profile of the two substrates investigated here. The following procedure of the analysis was applied.

A centreline was first of all drawn for all surface roughness profiles. The centreline was determined as the arithmetic mean of all of the height data of the profile. The centrelines for the two profiles presented are shown in Figure 7.9 and Figure 7.10.
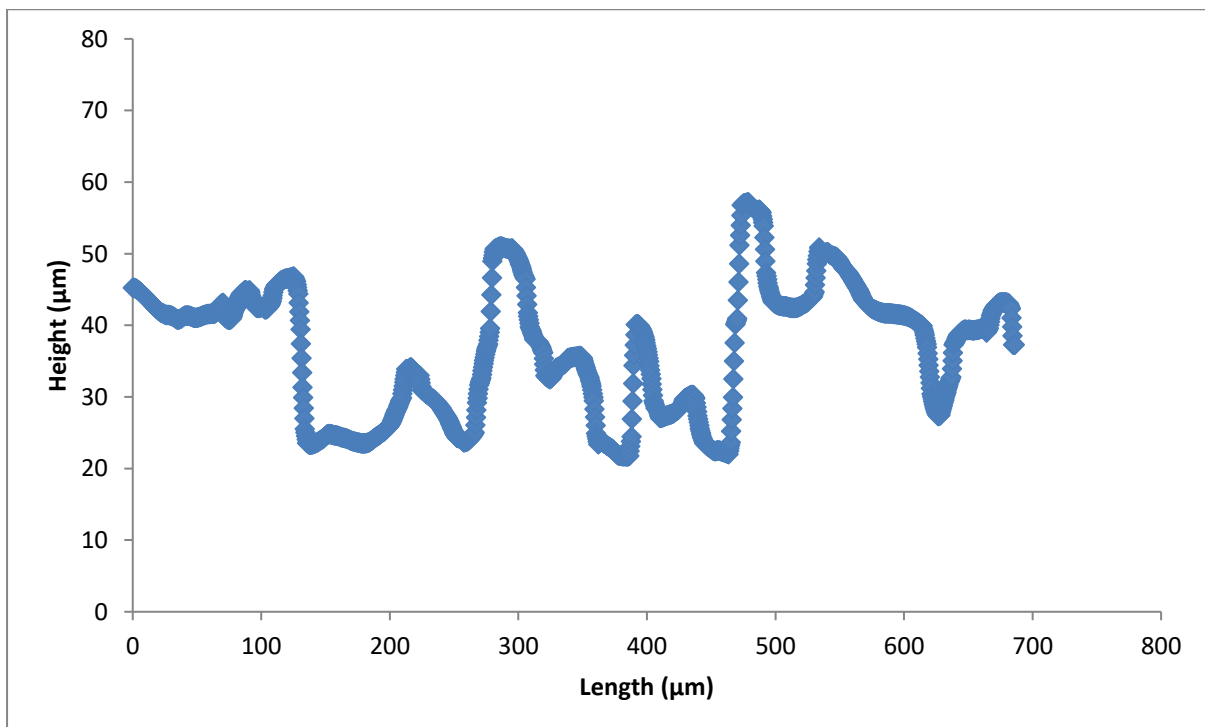
Figure 7.7 Example of surface roughness profile of ceramic substrate taken from the digital microscope
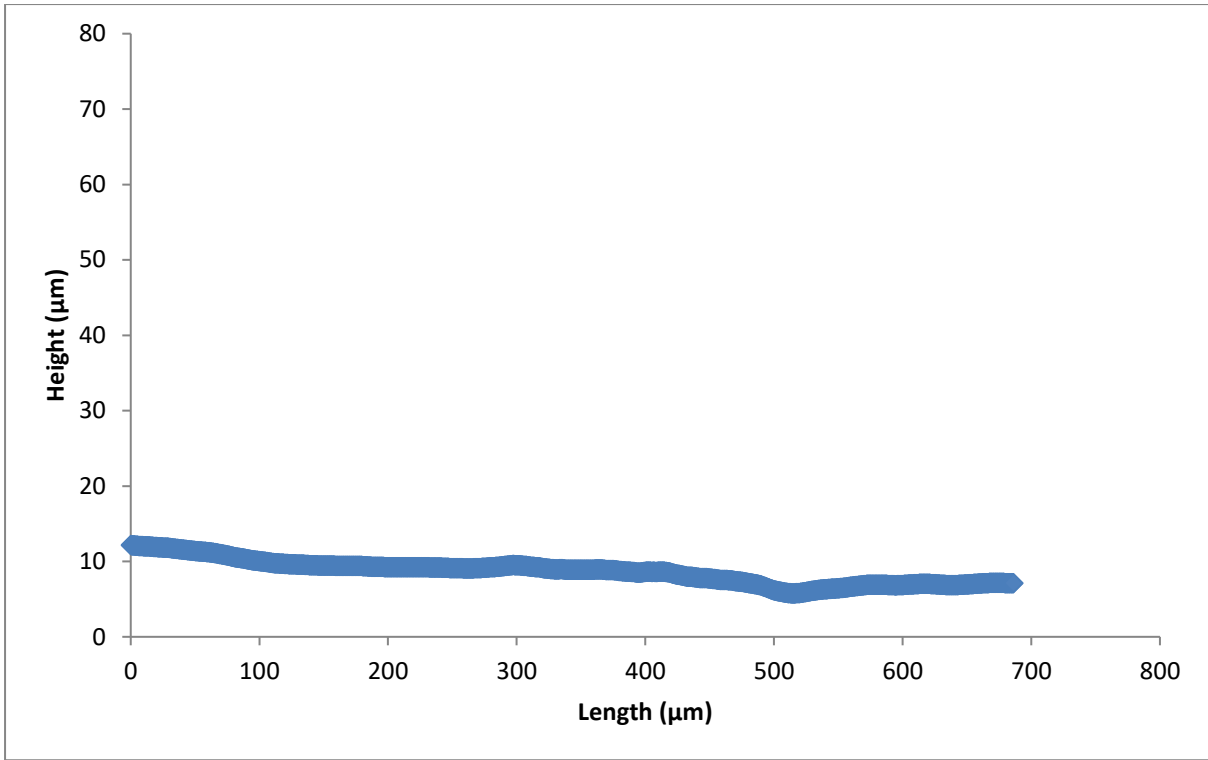
Figure 7.8 Example of surface roughness profile of metallic substrate taken from the digital microscope
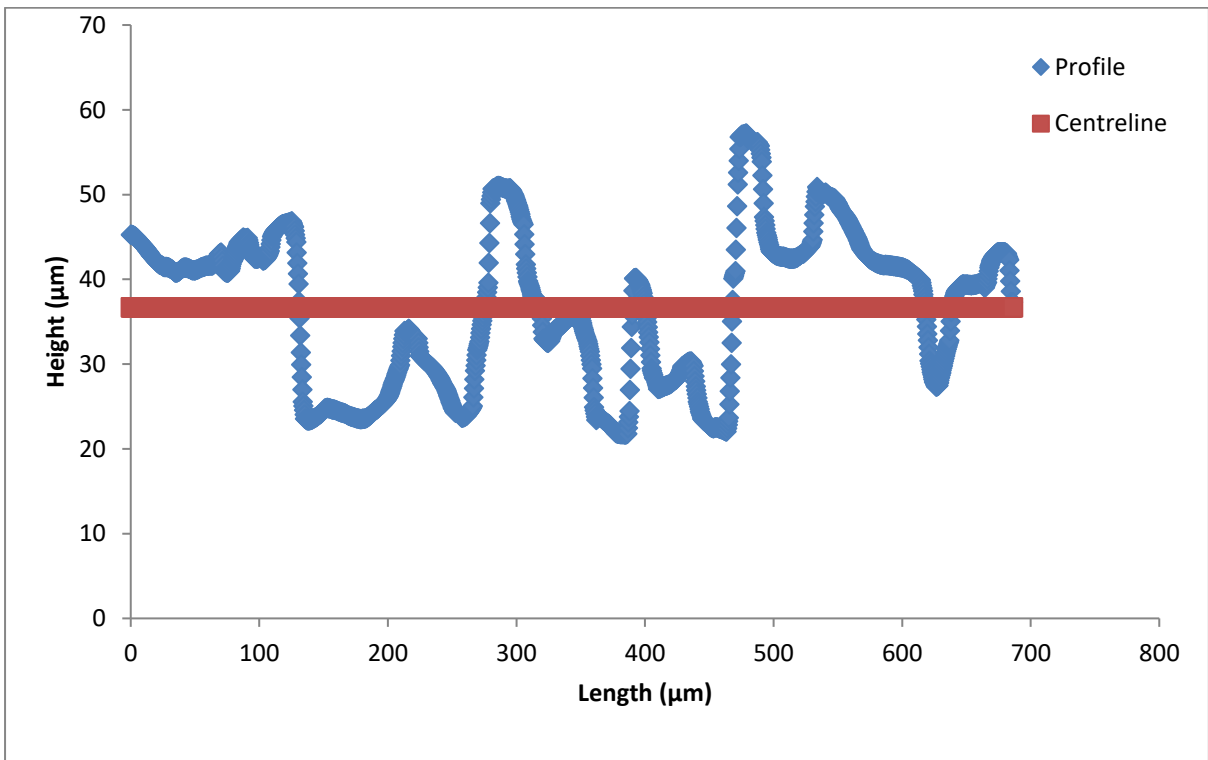
Figure 7.9 Determination of centreline of the profile for ceramic substrate
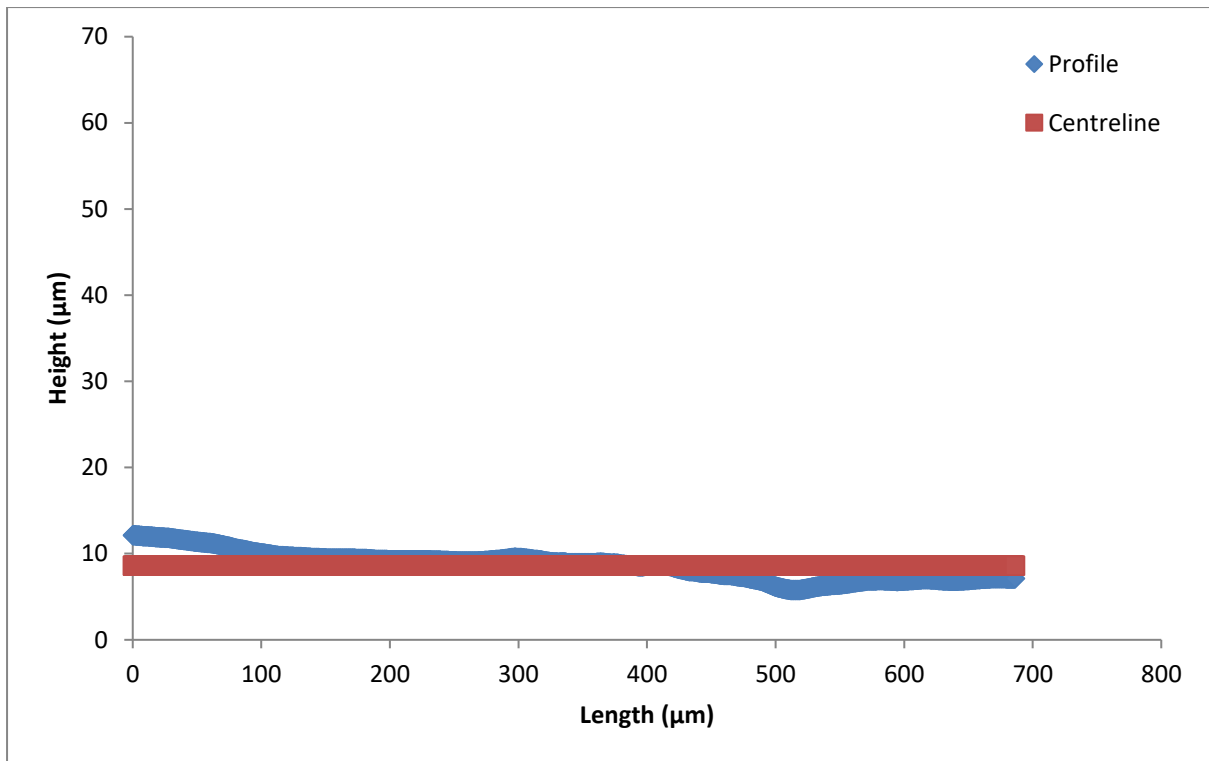
Figure 7.10 Determination of centreline of the profile for metallic substrate

Following the determination of the centreline, deviation between every point on the profile and the centreline was calculated. The absolute value of the deviation was then taken. The arithmetic mean of the absolute values was finally determined as the R_a value [71].

$$R_a = \frac{1}{n}\sum_i^n |y_i - \bar{y}|$$

Equation 7-2

where R_a is the surface roughness parameter for arithmetic mean deviation, n is the number of data points, i is the ith data point, yi is the ith height, $\bar{y}$ is the centreline height

For the R_z value to be computed, the whole surface roughness profile was first of all evenly divided into 5 segments. The following figures (Figure 7.12) were obtained after the division.

126
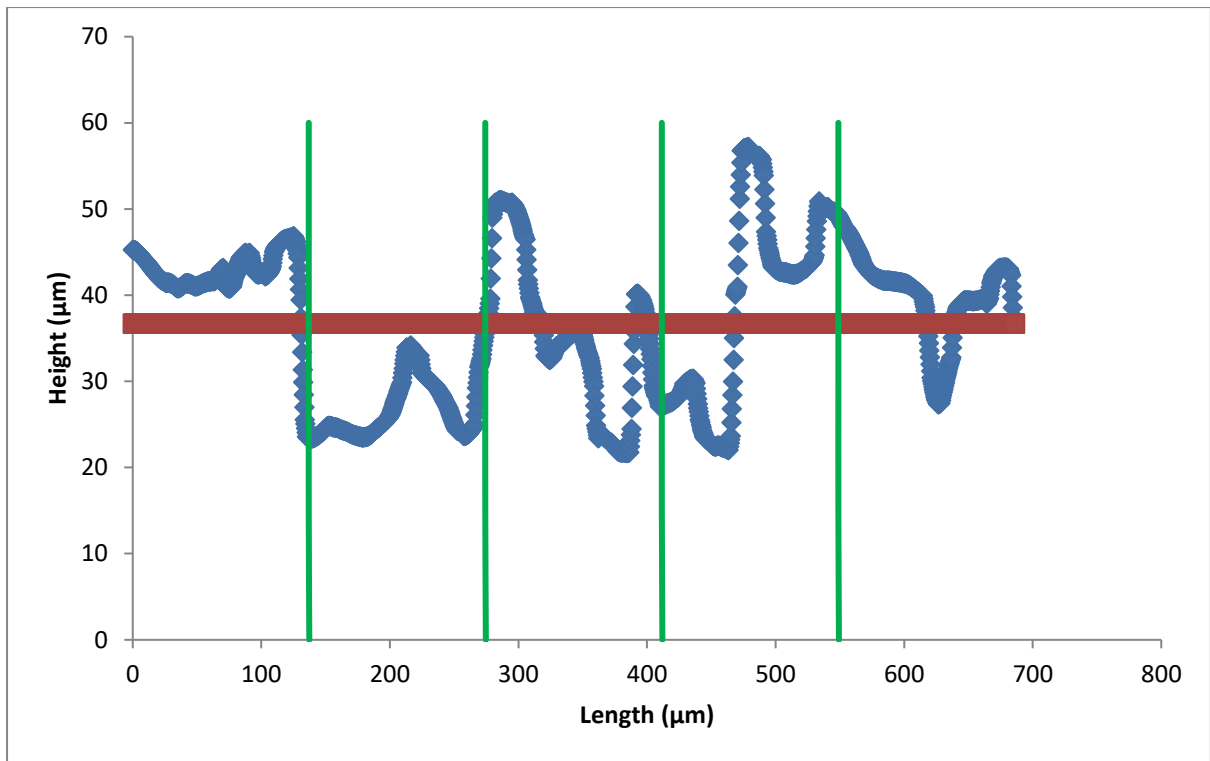
Figure 7.11 Division of the surface roughness profiles for ceramic substrate
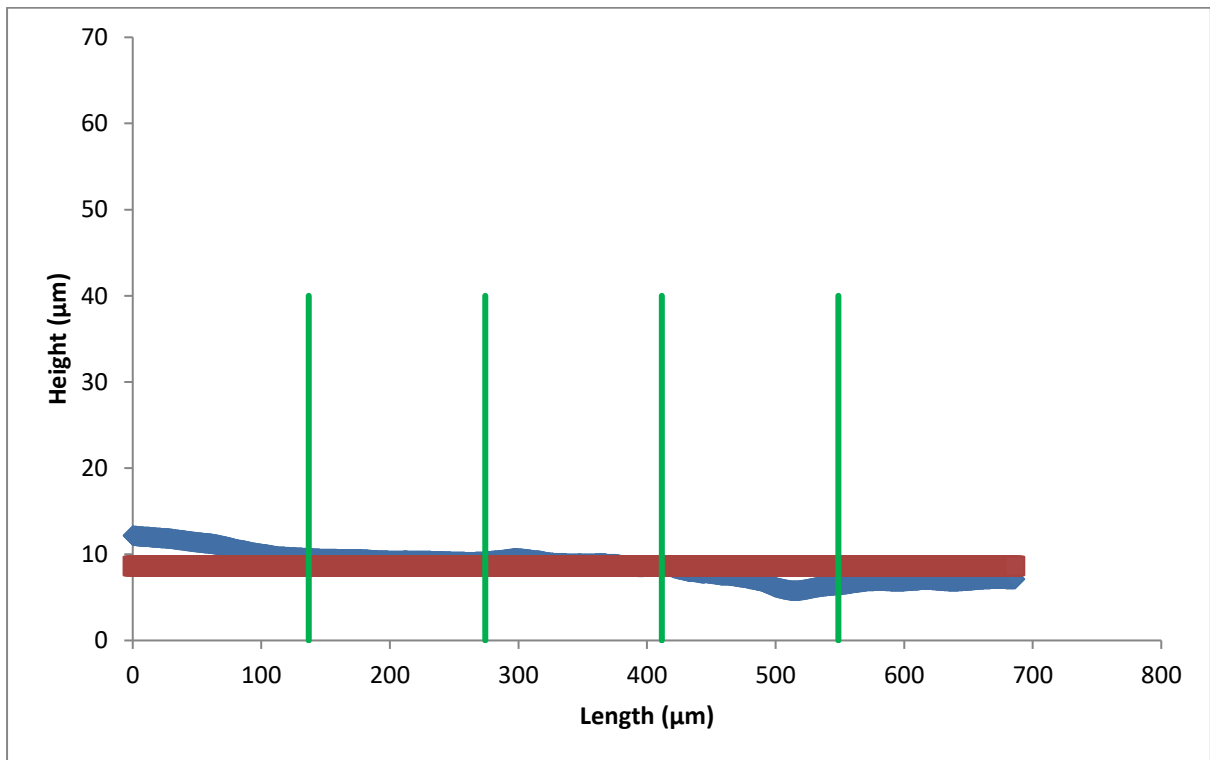
Figure 7.12 Division of the surface roughness profiles for metallic substrate

Following the division, the largest positive deviation (peak) and the largest negative deviation (trough) was identified in each division. The difference between the peak and the trough in each division was then determined. The R_z value was finally obtained as the average of this difference in the 5 divisions [71].

$$R_z = \frac{1}{5}\sum_{i}^{5}\left(x_{peak,i} - x_{trough,i}\right)$$

<div align="right">**Equation 7-3**</div>

where R_z is the surface roughness parameter for average distance between peak and trough, i is the ith segment, x_{peak} and x_{trough} are the deviation for the peak and the trough in the segment considered, respectively.

Following the analysis, a comparison between the Ra and Rz values for the cordierite and the metallic substrate is obtained and shown in Figure 7.13.
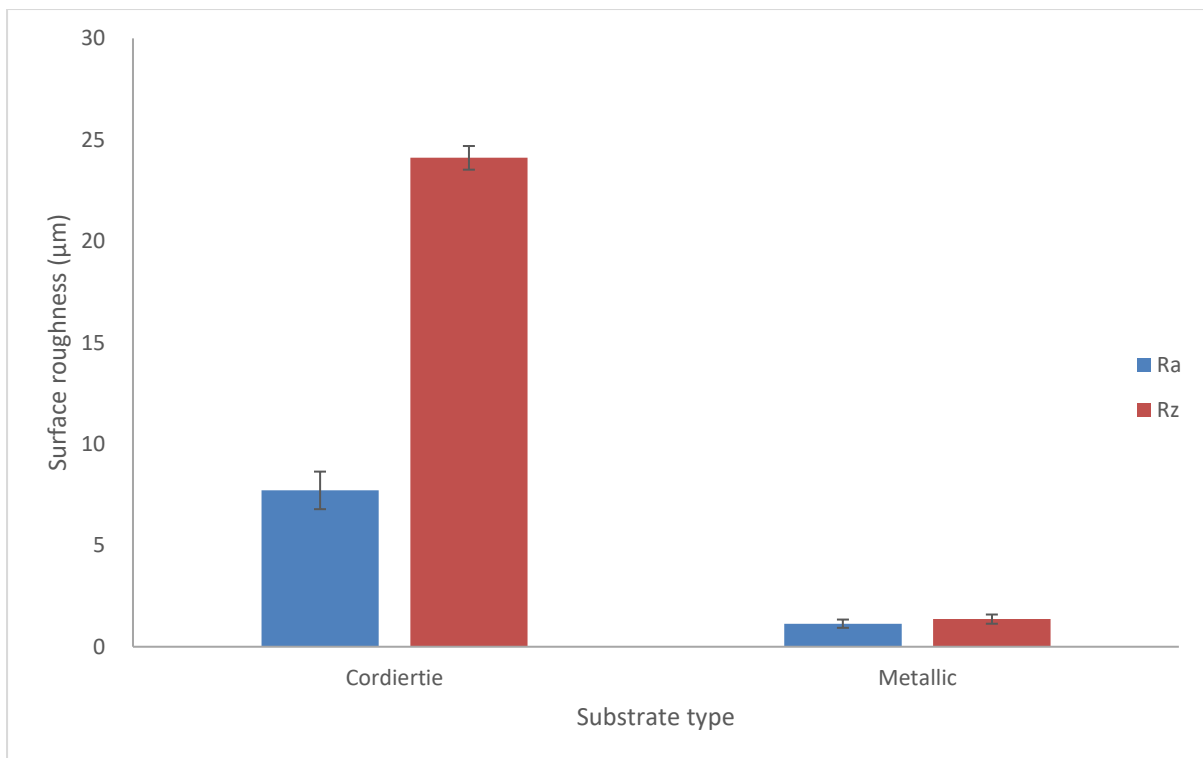
Figure 7.13 A comparison in surface roughness between the cordierite and the metallic substrate

It can be seen from Figure 7.13 that both the arithmetic deviation and the average peak to trough deviation of the cordierite substrate is greater than those of the metallic substrate. In addition, the R_z value of the cordierite substrate is much higher than its R_a value. The above discussion means that the surface profile of the cordierite substrate was featured by a continuous rough surface with random large peaks and troughs. On the opposite, given that the R_a and the R_z value of the metallic substrate is quite close to each other and both being low, the metallic substrate has a relatively smooth surface with regular but small surface roughness.

In addition, it can be noticed that the surface roughness of the cordierite substrate is much greater compared with the particle size of the suspension (suspension 1 in Table 6.1) used to coat it while that of the metallic substrate is closer to the particle size of the suspension. This suggests that many γ-alumina particles were able to attach on the surface roughness of the cordierite substrate to create a strong interface between the catalyst layer and the substrate while fewer particles were able to do so on the metallic substrate. This would explain for the large difference obtained in the adhesive strength between these two types of substrate, as seen in Figure 7.6.

7.3.3 Alumina substrate

Using the alumina tablet substrates prepared in 7.2.1, the effect of compression force on the adhesive strength was determined, as can be seen in Figure 7.14. The γ-alumina suspension was only adjusted to pH=4 to produce catalyst layer on the alumina substrates; as at this pH, the strongest catalyst layer was produced using the metallic and cordierite substrate and the cohesive strength of the layer also reached a peak (Figure 6.8).

The same methods to determine the surface roughness of metallic and cordierite substrate was used to quantify the surface roughness of alumina substrates. The results are shown in Figure 7.15 and Figure 7.16.
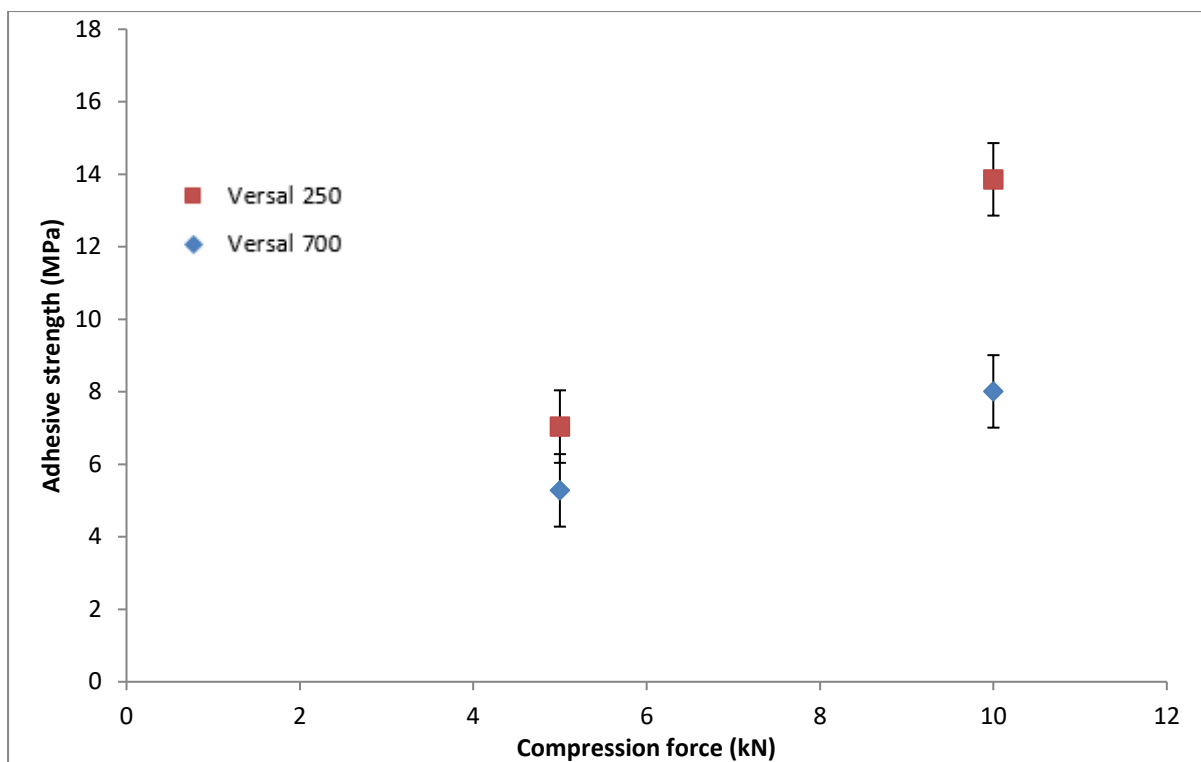
Figure 7.14 The effect of compression force on the adhesive strength on alumina tablets compressed at different forces and calcined at 500 ºC
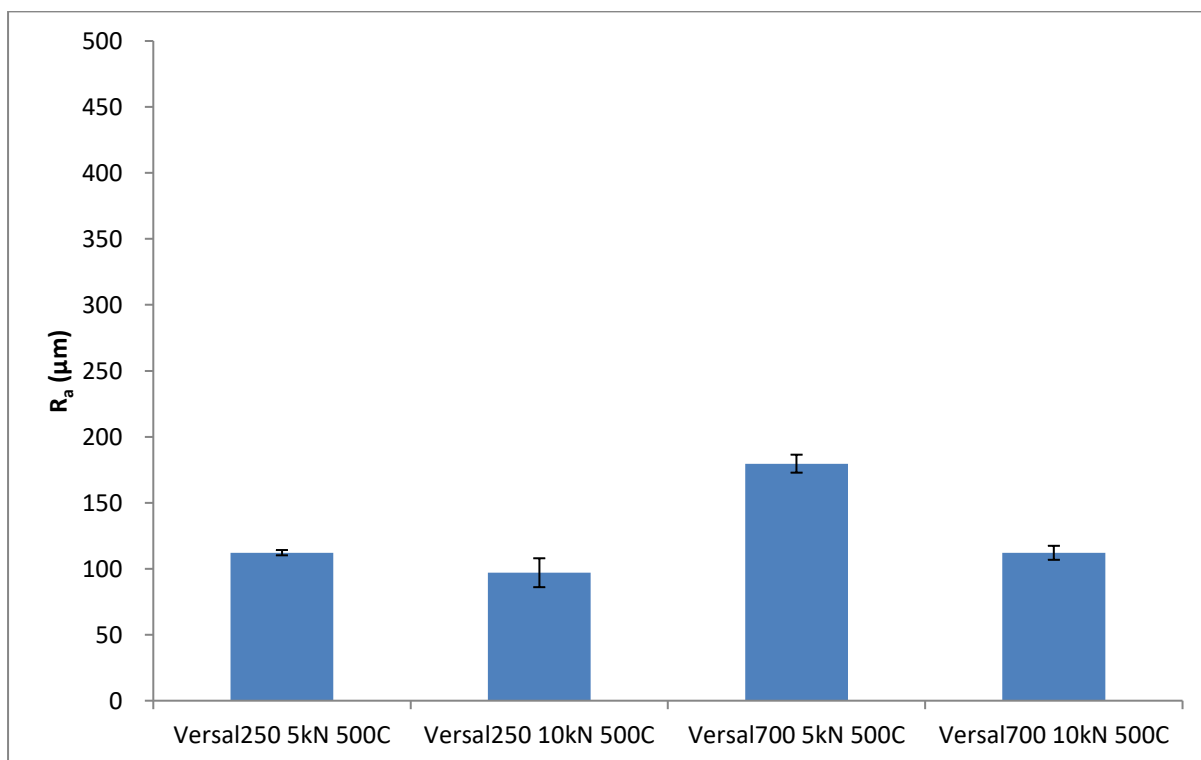
Figure 7.15 Surface roughness by R_a of different alumina substrates
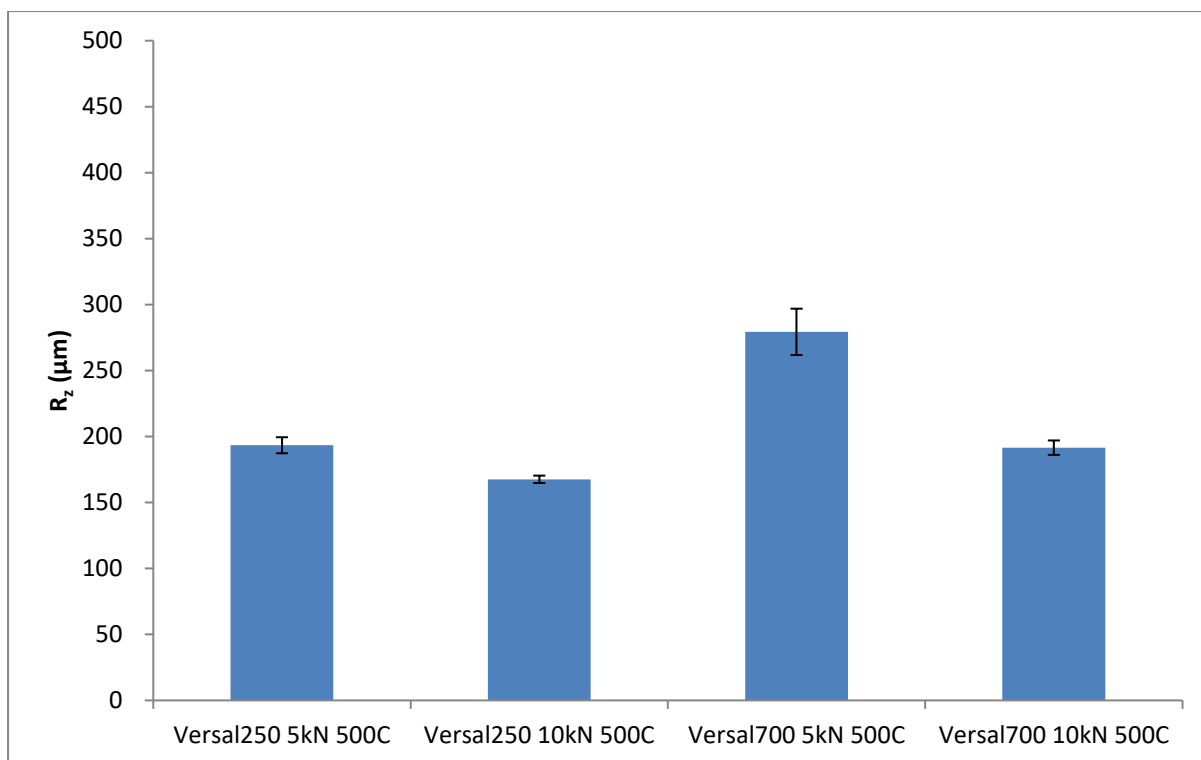
Figure 7.16 Surface roughness by R$_z$ of different alumina substrates

From Figure 7.14, it could be seen that the higher compression force led to a higher adhesive strength of the catalyst for both types of alumina substrates. The porosity of the alumina substrate was measured to understand the effect of compression force on the adhesive strength.

Both types of alumina powder (Versal 250 and 700) were first of all compressed by an excessively high stress to achieve minimal porosity. This high stress was delivered by using a 49 kN compression force acting in a die with a 30 mm internal diameter. An Instron machine (model 3360) was employed for this task and the punch was set at a rate of 1 mm/min to make the tablets. The low speed of compression allows an easy removal of air during compression. The density of these highly compressed tablets can be taken as the true particle density. The following equation (Equation 7-4) was used to compute porosity of other tablets made for adhesive strength test.

$$Porosity = 1 - \frac{Tablet\ density}{True\ particle\ density}$$

<div align="right">**Equation 7-4**</div>
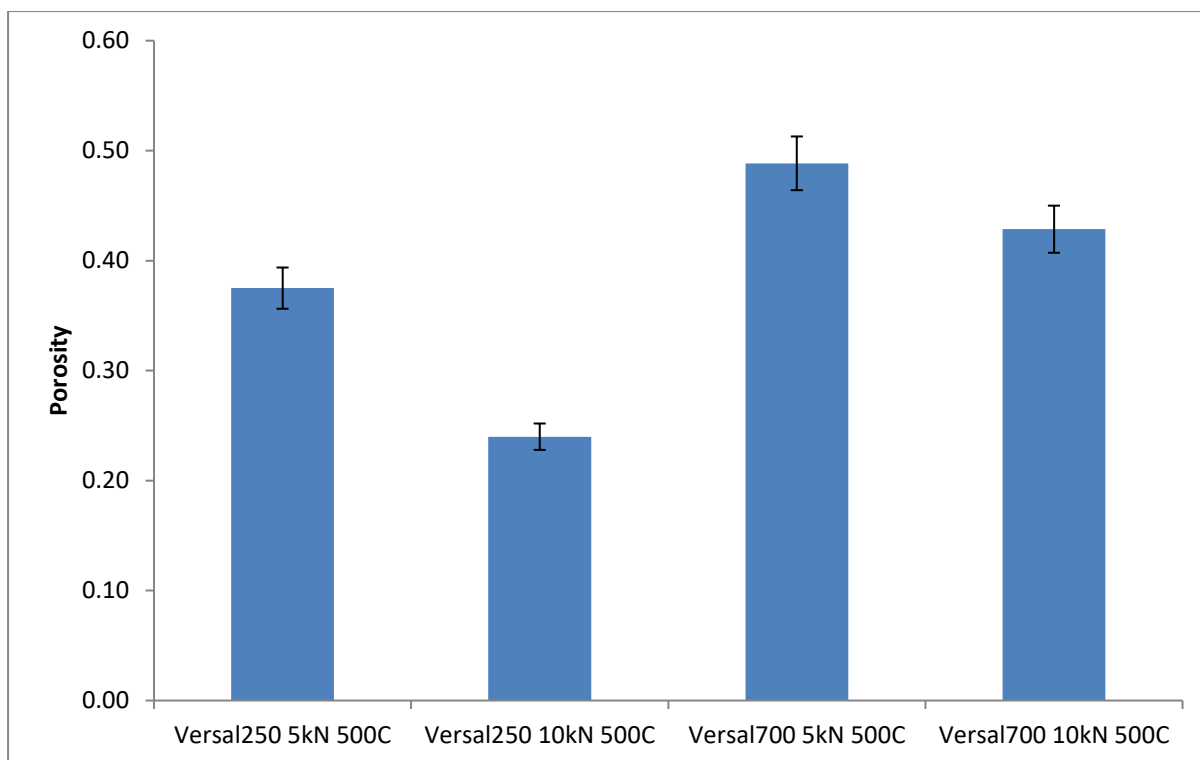
Figure 7.17 Porosity determination of different alumina tablets

It could be seen in Figure 7.17, the higher compression was seen to decrease substrate porosity in both cases, leaving more small sized particles in the γ-alumina suspension to stay on the interface between the catalyst layer and the substrate. The increased proportion of small sized particles at the interface resulted in a stronger pack of the catalyst layer at the interface, giving rise to an increased adhesive strength. The factor of surface roughness however did not show great influence on the adhesive strength in this case. This could be explained as follows. The surface roughness of alumina substrates prepared at four different preparation conditions were characterised by R_a and R_z values as shown in Figure 7.15 and Figure 7.16. The four different preparation conditions were Versal 250 powder compressed at 5 kN and 10 kN followed by calcination and Versal 700 powder compressed at 5 kN and 10 kN followed by calcination. It could be seen that both R_a and R_z for all of the four preparation conditions displayed very high surface roughness compared with those from ceramic and metallic substrate in Figure 7.13. The R_a and R_z values for all of the four preparation conditions were found to be much higher than the particle size in the γ-alumina suspension, suggesting that there would be a good packing of γ-alumina particles on these surfaces. The consistently high surface roughness at all of the four substrate preparation conditions

therefore made the adhesives strength less sensitive to the surface roughness of substrate but more related to the porosity of substrates.

The same message about the relative effect of surface roughness and porosity on adhesive strength could also been on powder types. It would be revealed in Chapter 8 that the strength of primary agglomerates of Versal 700 is higher than that of Versal 250. This could explain for the difference in tablet porosity observed in Figure 7.17 where porosity of tablets made from Versal 250 was always lower than that of Versal 700 at the same compression force and calcination conditions. The lower porosity of Versal 250 substrates allowed more small sized particles in the γ-alumina suspension to pack at the interface between the catalyst layer and the substrate to give rise to a stronger adhesive strength; however the consistently high surface roughness for both Versal 250 and 700 substrates made the adhesives strength less dependent on the surface roughness of substrate

7.4   Conclusion

In conclusion, in this chapter, an adhesive strength measurement technique has been developed. The technique was capable of measuring the adhesive strength of catalyst layer separately and reporting the result based on unit of stress. The adhesive strength was measured on three different types of substrate. For metallic and cordierite substrate, it was found that the adhesive strength of catalyst layer showed a similar trend compared with the cohesive strength in general. The adhesive strength peaked at pH = 4 and from pH = 7 onwards, adhesive strength dropped to zero. The high mobility of γ-alumina particles was determined to the reason for the high adhesive strength at pH = 4. The zero adhesive strength at pH = 7 and onwards was because the catalyst layer detached itself from the substrate. This finding was in close agreement with the cracking pattern determined in section 6.9. The reason behind the detachment was thought to be formation of more structured material at those high pHs. Between metallic and cordierite substrate, it was found that the adhesive strength on cordierite substrate was higher than that on the metallic substrate due to the fact that the cordierite substrate had higher roughness than the metallic substrate. The higher roughness of the cordierite substrate was deemed to allow more γ-alumina particles to adsorb onto the interface to contribute to a higher adhesive strength.

As for the substrate made of alumina powder, the effect of compression force was investigated. pH = 4 was employed for all of the experiments due to the previous knowledge that high adhesive strength could be produced at this condition. A higher compression force was found to lead to a higher adhesive strength. This was because more small γ-alumina particles were allowed to stay on the interface due to a more compacted alumina powder bed. The same knowledge could also be applied to the comparison between Versal 250 and Versal 700 powder from the perspective of strength of primary agglomerates.

Chapter 8 Determination of strength of primary agglomerates

8.1   Idea behind the measurement

The strength of primary agglomerate of the two boehmite powders (trade name: Versal 250 and Versal 700) was measured. The significance of this measurement was to allow future work to correlate the strength of boehmite primary agglomerate with that of boehmite granules (also known as secondary agglomerate). This area as outlined in the literature review (section 2.5) is currently still less known in the field.

8.2   Experimental method

The as-received boehmite powders (which contained primary agglomerates with a range of sizes) were first of all sieved using (Retsch test sieves) to obtain primary agglomerates above 300 micron for the ease of experimental handing. An amplitude of 1 g/mm for a duration of 3 min was used. The measurement of the strength of primary agglomerate was then conducted using the experimental setup (Figure 8.1). The same material testing equipment (Zwick Roell A622057) was employed. The punch was set to move down at a rate of 1 mm/min and a preload of 0.1 N was used. To avoid the effect of moisture on primary agglomerate, each primary agglomerate tested was pre-heated on a hot plate at 120 °C for 1 hour. A thick piece of glass and a strong compression support were used to minimise the deformation of the apparatus in order to obtain the most accurate result on strength. The highlight of the experimental setup employed here was that there was a microscope camera (Dino-Lite Edge AM4115ZTL) looking through the glass from the bottom to observe the compression of the primary agglomerate being tested. The correct size of each individual primary agglomerate examined can be accurately measured by this microscope camera. For the size seen by the microscope camera to be related to the strength calculated (Equation 8-1), spherical primary agglomerates were selected. The process of compression can be recorded for further study.
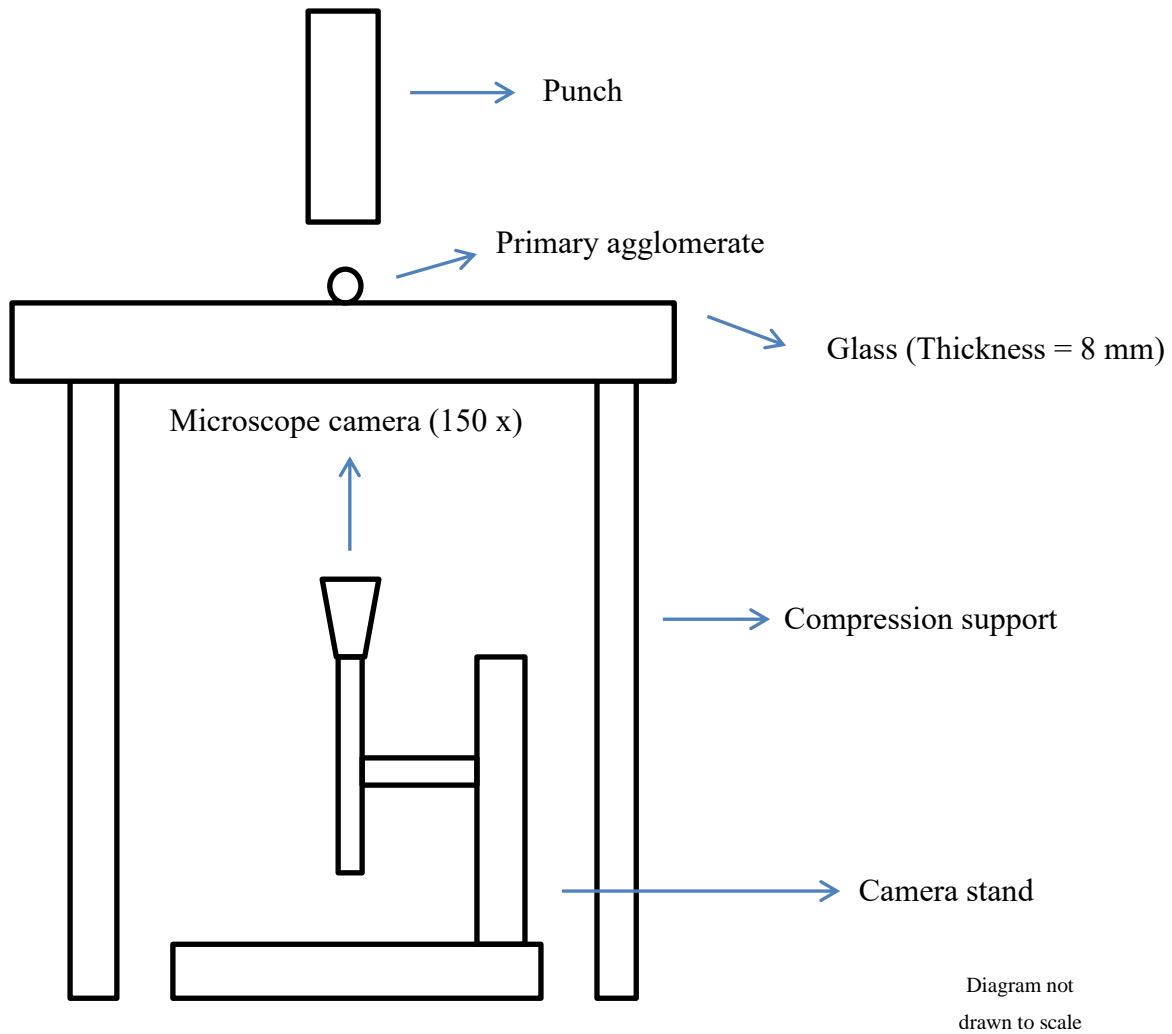
Figure 8.1 Experimental setup to determine the strength of primary agglomerate

The force that caused the primary agglomerate to fail was recorded. The area responsible for the breakage was derived from the diameter of the primary agglomerate which was measured by the microscope camera. The strength of the primary agglomerate was finally calculated using the following equation (Equation 8-1).

$$Strength\ of\ primary\ agglomerate = \frac{Breakage\ force}{Area\ responsible\ for\ breakage}$$

$$= \frac{4 \times Breakage\ force}{\pi \times Diameter\ of\ primary\ agglomerate^2}$$

<div style="text-align: right;">Equation 8-1</div>

8.3   Results and discussion

An example of the force signals received when compressing the primary agglomerates from the two boehmite powders is shown in Figure 8.2. A number of 20 measurements was run for each type of boehmite powder.
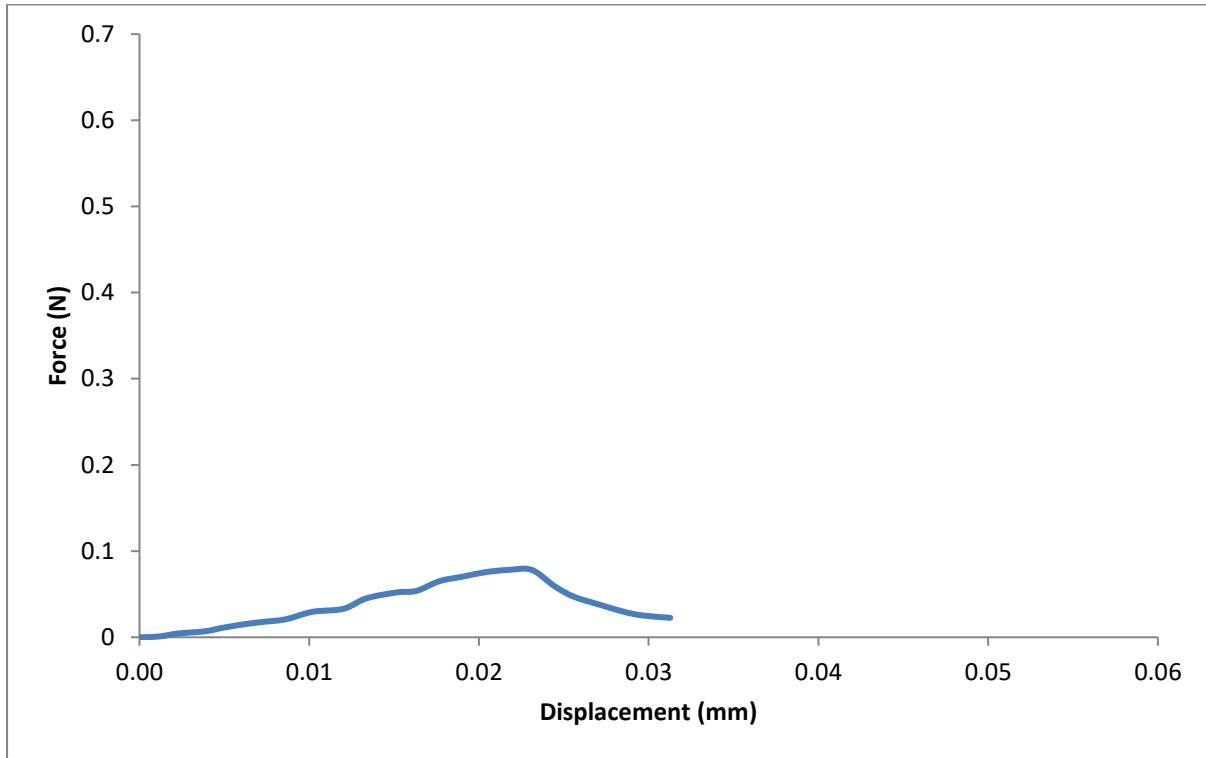
Figure 8.2 Strength measurement of Versal 250 primary agglomerate

The image taken by the upward facing camera for the primary agglomerate tested is presented in Figure 8.3.

100 μm
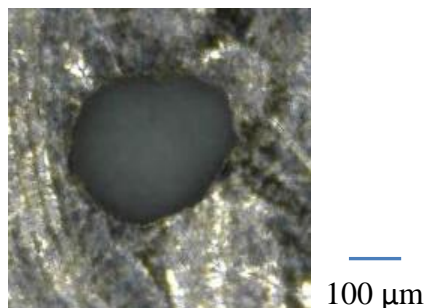
Figure 8.3 Image of primary agglomerates (Versal 250) tested

An example measurement of Versal 700 powder is presented with more shown in Figure 8.4.
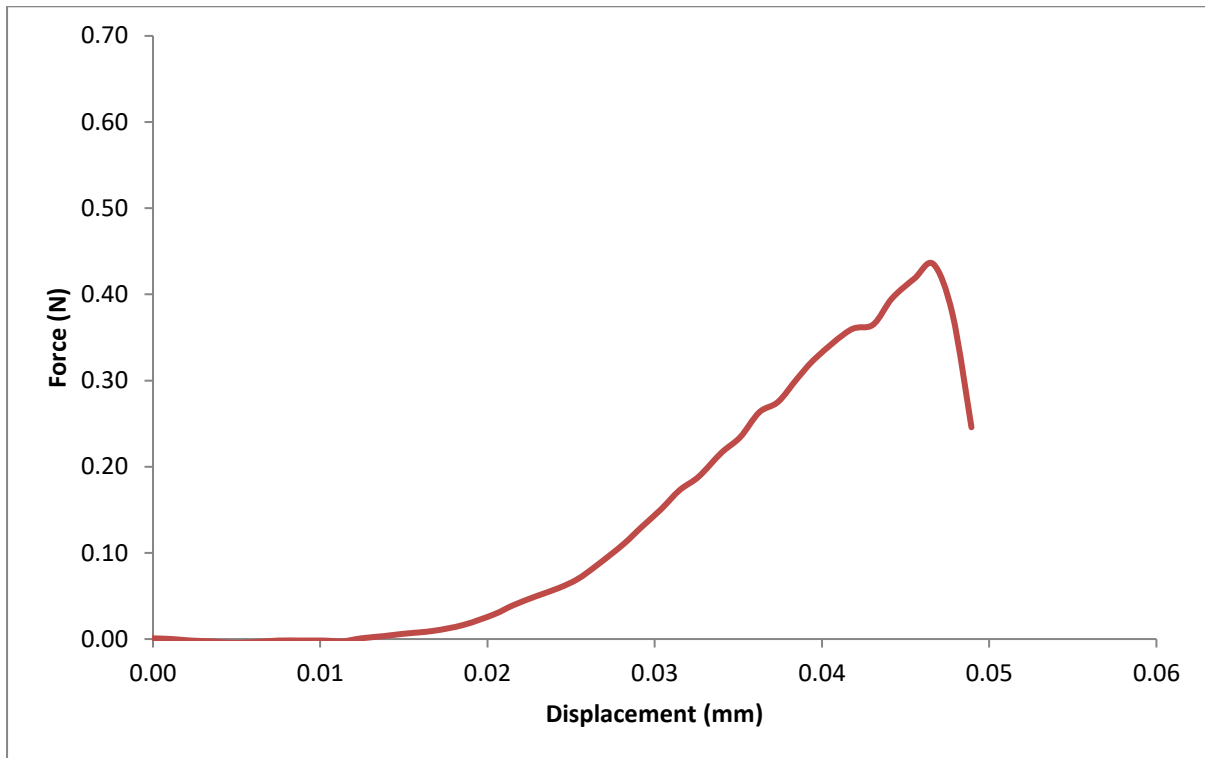
Figure 8.4 Strength measurement of Versal 700 primary agglomerate

The image taken by the upward facing camera for the primary agglomerate tested is presented in Figure 8.5.

100 μm
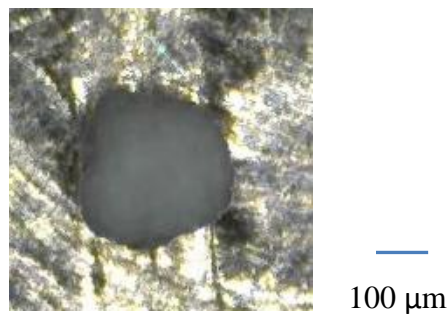
Figure 8.5 Image of primary agglomerates (Versal 700) tested

The comparison of strength of the two types of primary agglomerates can be then made as follows (Figure 8.6). The strength of the primary agglomerates was calculated using Equation 8-1.
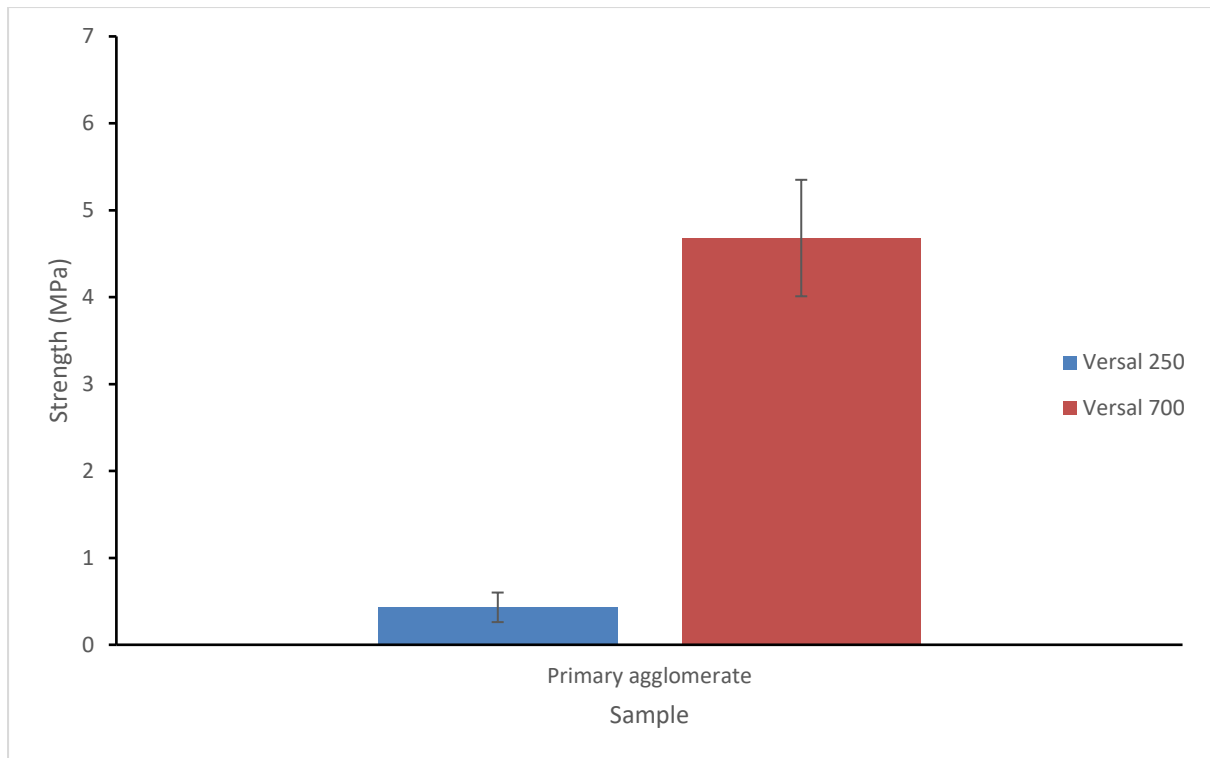
Figure 8.6 Strength of primary agglomerate of the two boehmite powders

The primary agglomerates of Versal 250 were found to be much stronger than Versal 700. Two other sets of results which can both support this result in an indirect manner are presented in section 8.4 and 8.6.

8.4 Disintegration of boehmite primary agglomerate

8.4.1 Idea behind the measurement

The disintegration profile of boehmite primary agglomerate was measured and used as a supportive measurement to the strength of primary agglomerate determined above.

8.4.2 Experimental method

The measurement was performed on a Malvern Mastersizer-S. The original boehmite powder which contained primary agglomerates of a range of sizes was used and fed into the laser zone using deionised water as the dispersion medium. The particle size distribution obtained

is volume based as laser diffraction is the principle of measurement of Mastersizer. Both types of boehmite powder were continuously tested in the Mastersizer and the size distribution measured over time was obtained. The impeller speed was kept at 3000 rpm and the diameter of the impeller was 2 cm. Measurement was taken every 30 s during the circulation.

8.4.3   Results and discussion

The results obtained are shown below in Figure 8.7 (Versal 250) and Figure 8.8 (Versal 700). The results suggested that as the boehmite powder was being circulated for longer time, the Versal 250 powder began to disintegrate while the Versal 700 powder kept its structure. The disintegration process of Versal 250 occurred more at higher agglomerate size and resulted in production of fines as can be seen in Figure 8.7 where the particle size distribution was gradually shifted to the left with an increase in percentage of small particles and decrease in percentage of large primary agglomerates as the test progressed. On the opposite, the particle size distribution of Versal 700 primary agglomerates did not shown any change during the whole circulation time, indicating that primary agglomerates of Versal 700 did not experience any disintegration process during the test. This result could serve as a positive support to the strength measurement in section 8.3 where the strength of Versal 250 primary agglomerate was found to be lower than of Versal 700 primary agglomerate.
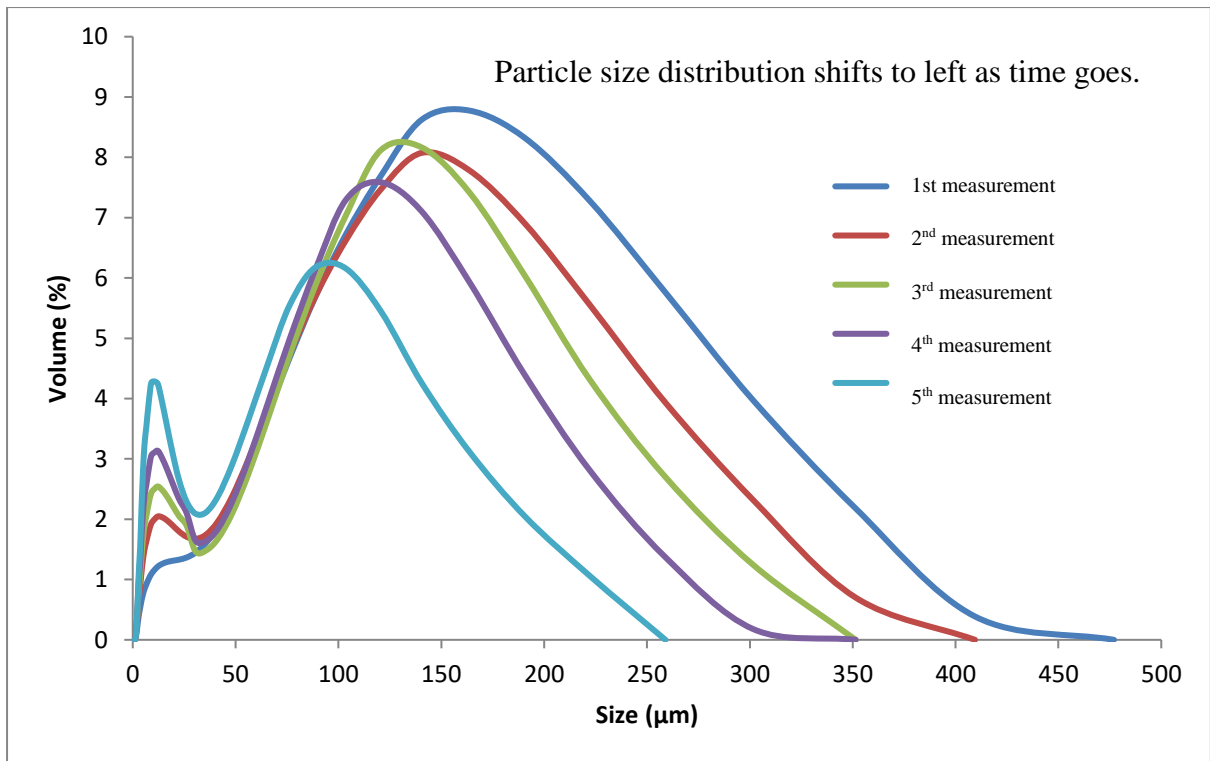
Figure 8.7 Volume based particle size distribution of primary agglomerates (Versal 250) with time
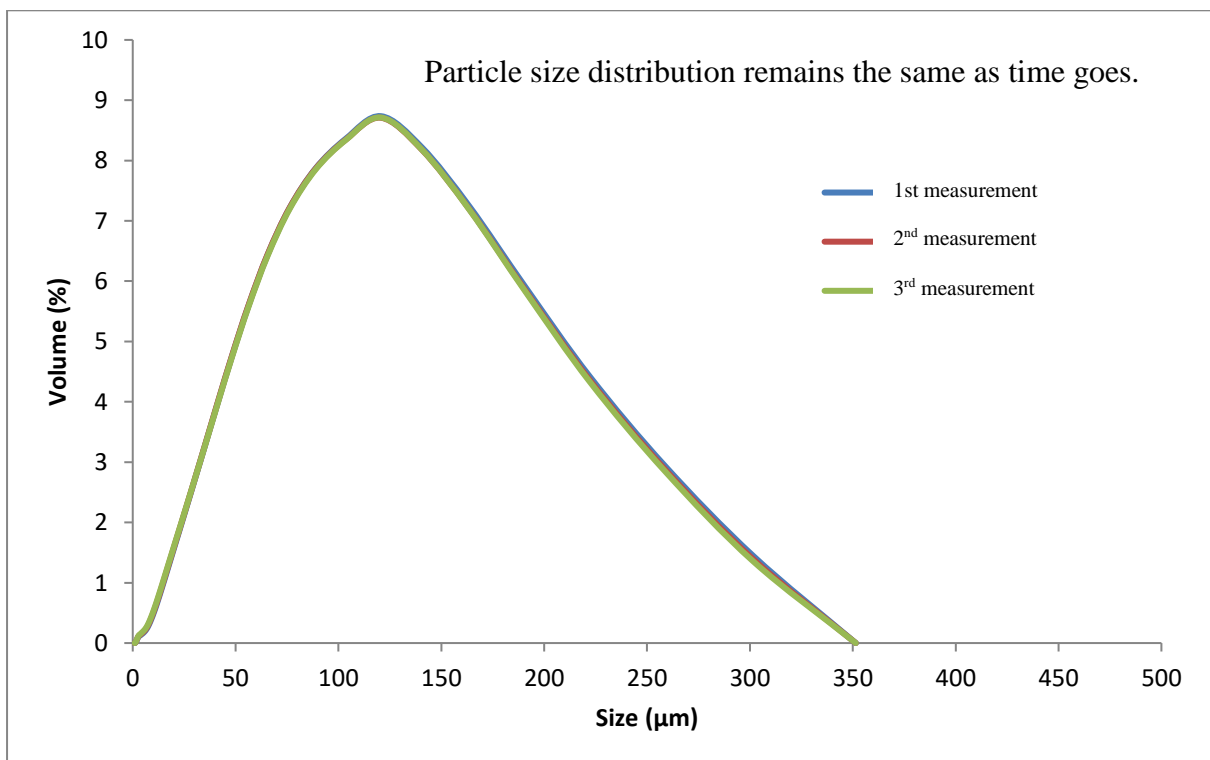
Figure 8.8 Volume based particle size distribution of primary agglomerates (Versal 700) with time

141

8.5   Deformation of boehmite primary agglomerate

8.5.1   Idea behind the measurement

Material deformability can be used to indirectly indicate its strength. The deformability of boehmite primary agglomerates would be tested here to indirectly support the strength measurement conducted in section 8.3.

8.5.2   Experimental method

Both Versal 250 and 700 powder which contained primary agglomerates of a range of sizes were made into tablets by direct compression. The compression took place in a 12 mm tablet die using a material testing equipment (Instron; model number 3367). The compression force reached 10 kN with the punch speed set at 1 mm/min. The use of a slow punch speed was designed to allow air to escape during the compression. In each compression experiment, 1 g of the original boehmite primary agglomerates was prepared. The tablets made were subject to tensile test using a material testing equipment (Zwick/Roell Z 0.5, Germany). The punch was set to move down at a speed of a 5 mm/min. The force that broke the tablet was recorded. The follow equation was used to calculate the tensile strength.

$$Tensile\ strength = \frac{2 \times Breakage\ force}{Tablet\ diameter \times Tablet\ thickness \times \pi}$$

<div align="right">**Equation 8-2**</div>

8.5.3   Results and discussion

The tensile strength of tablets made from both Versal 250 and 700 boehmite primary agglomerates is presented in Figure 8.9.
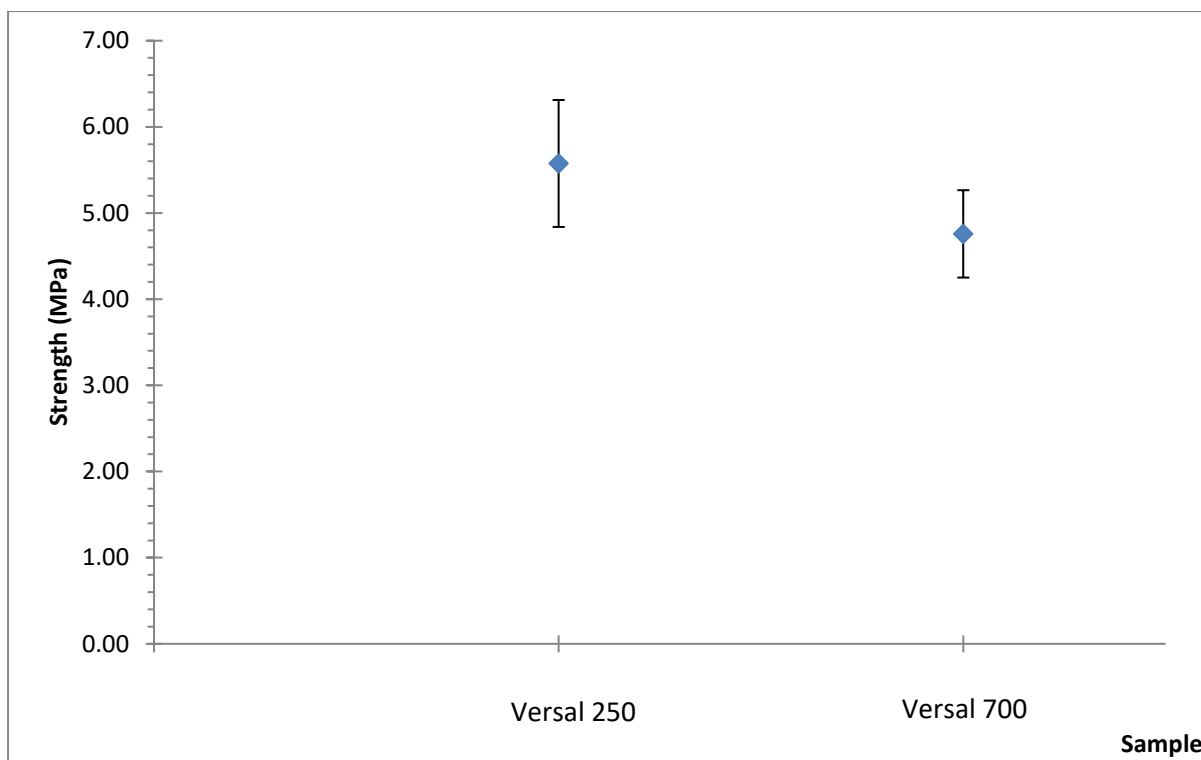
Figure 8.9 Tensile strength of tablets produced by compressing boehmite powder

It could be seen from Figure 8.9 that the tensile strength of tablets made from Versal 250 was stronger than those made from Versal 700. This indicated that during direct compression, primary agglomerates of Versal 250 powder was capable of a greater extent of deformation compared with those of Versal 700 powder, suggesting that particles of Versal 250 primary agglomerates are weaker than those of Versal 700 powder. Such finding supported the strength measurement conducted in section 8.3.

8.6 Internal structure of boehmite primary agglomerate

8.6.1 Idea behind the measurement

An insight into the inside of primary agglomerates of the two boehmite primary agglomerates can allow the structure of these primary agglomerates to be compared. This comparison can be used to understand the difference in the strength measurement in section 8.3 between the two types of boehmite primary agglomerates.

8.6.2 Experimental method

This measurement was carried out by X-ray scanning. The same procedure as in section 5.6.2 was employed. The primary agglomerates scanned were selected from the as-received boehmite powder by sieving using the same sieving procedure in 8.2, therefore the primary agglomerates scanned here were on the same size class as the ones tested in section 8.3.

8.6.3 Results and discussion

The X-ray images obtained are shown in Figure 8.10.

Note: This part is the sample holder.

200 µm
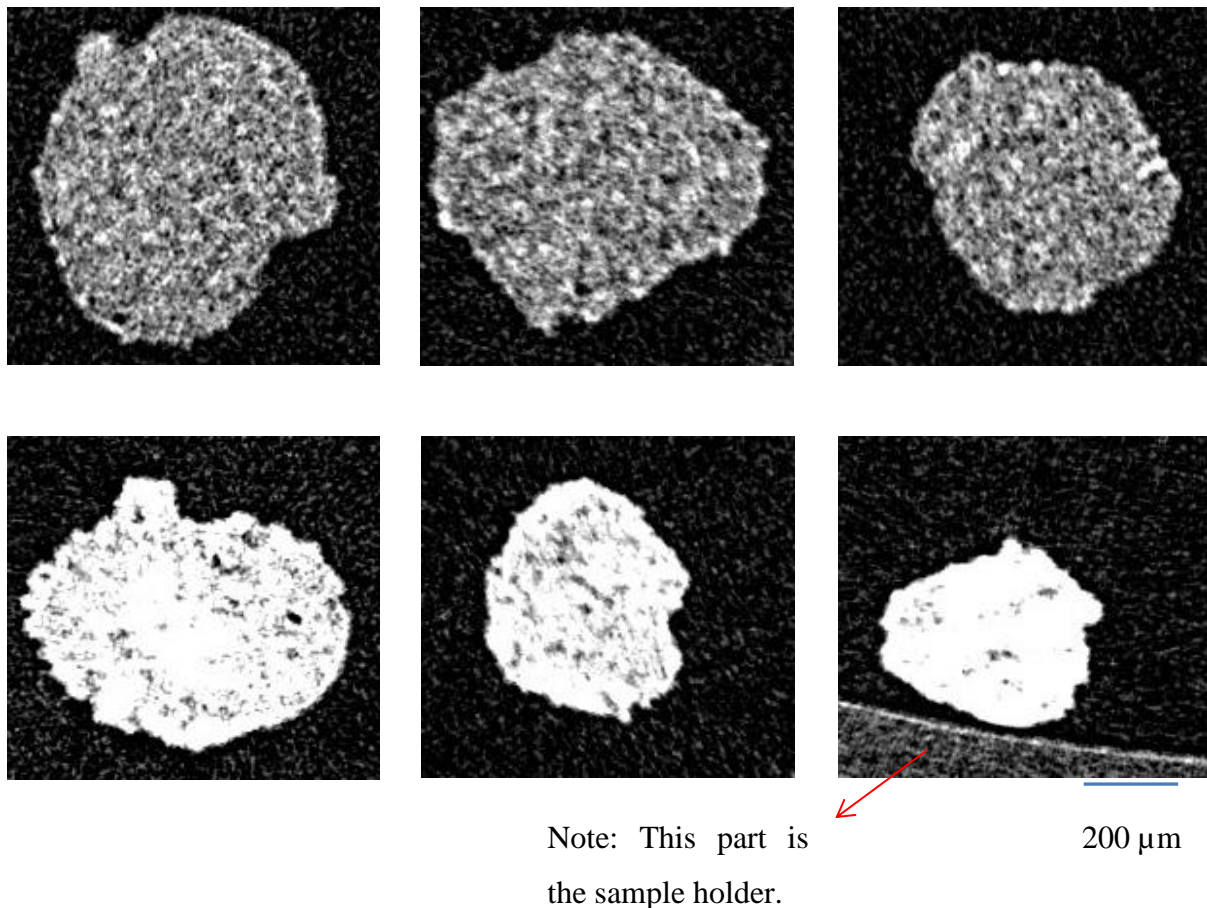
Figure 8.10 X-ray scan of Versal 250 (upper) and 700 (lower) boehmite primary agglomerates

A random selection of the scans of the two boehmite samples was chosen. The X-ray scan of the two boehmite primary agglomerates suggested that Versal 250 primary agglomerates contain more pores than Versal 700 primary agglomerates due to the greater amount of black

144

space (which represents void in X-ray images) in the Versal 250 samples than the Versal 700 ones. In addition, the solid structure of Versal 250 primary agglomerates is less dense than that of Versal 700, reflected by the darker colour of Versal 250 than Versal 700. Given the understanding that a more porous structure would normally be mechanically weaker, the X-ray tomography results also supported the direct strength measurement in section 8.3.

8.7 Comparison between strength of primary agglomerate and second agglomerate

It was identified in Chapter 2 that boehmite powder was already agglomerates. These agglomerates which are referred as primary agglomerates in this thesis are made of nanometre sized bohemite crystals. Primary agglomerates are further granulated to produce boehmite granules (known as secondary agglomerates) which can be used as granular catalyst support. It was identified in the literature review that whether the failure of secondary agglomerate occurs between primary agglomerates or within primary agglomerates is still unknown.

8.7.1 Experimental method

The experimental procedure to produce boehmite secondary agglomerates from the two boehmite powders is described here. The granulator used was manufactured by Eirich and had a volume of 1.5 L. Water was used as the binder and the liquid solid ratio was chosen to be 1.27. Water was sprayed into the granulator at a pressure of 1 bar. During spraying, the impeller speed was set at 3000 rpm. After the spraying was finished, the impeller speed was reduced to 1500 rpm. The granulation time (the growth stage) was allowed for 9 min. The strength of boehmite secondary agglomerates produced was tested using a material testing equipment (Zwick/Roell Z 0.5, Germany) and calculated by Equation 2-8. The size of secondary agglomerates selected for testing was between 1.18 and 1.7 mm.

8.7.2 Results and discussion

The comparison in strength between primary agglomerates and secondary agglomerates is shown in Figure 8.11. It can be seen in Figure 8.11 that the strength of primary agglomerates of Versal 250 is similar to the strength of its secondary agglomerates however the strength of primary agglomerates of Versal 700 is much higher than of the corresponding secondary agglomerates. This suggested that structural failure of granular catalyst supports made of Versal 250 might occur both between primary agglomerates and within primary agglomerates; however structural failure of granular catalyst supports made of Versal 700 is mainly due to the detachment between primary agglomerates. This finding suggested that structural failure of granular catalyst supports does not break between the constituent powders that are used to form them; it could also occur from the constituent powders themselves. Such claim was not mentioned in the current literature as suggested in the literature review (section 2.5).
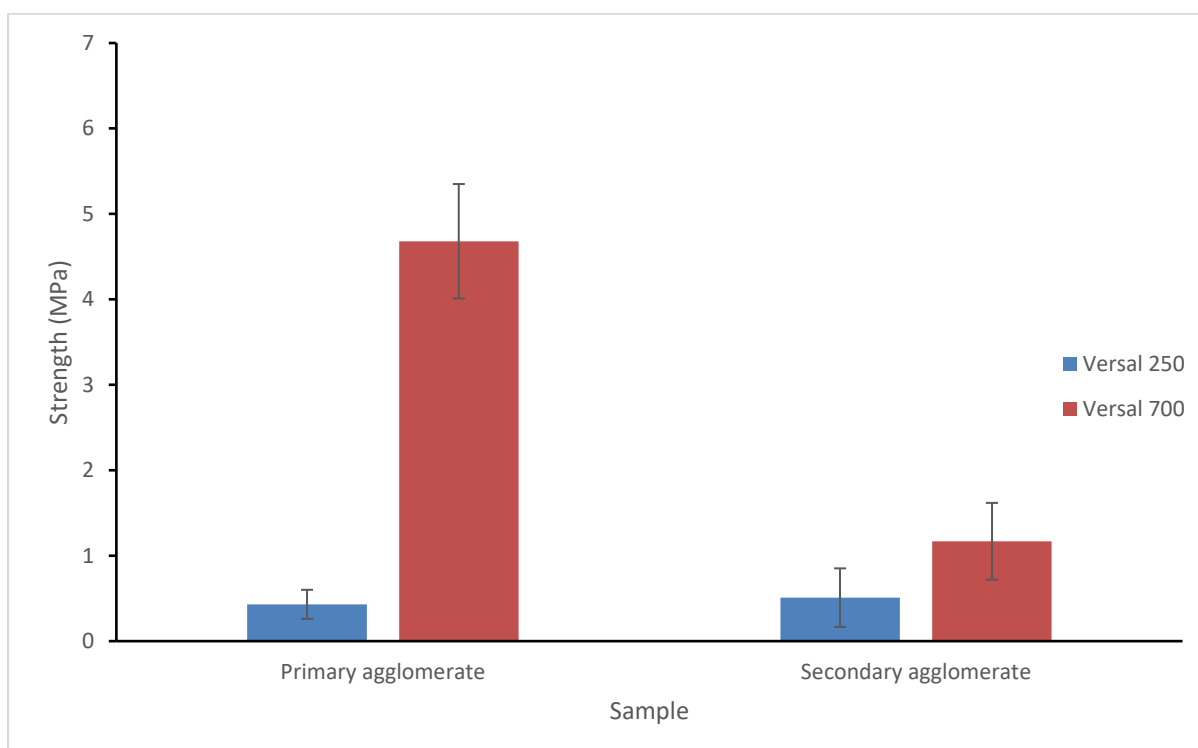
Figure 8.11 Comparison in strength between primary agglomerates and secondary agglomerates

8.8 Conclusion

In conclusion, this chapter presented a new method of directly quantifying the strength of primary agglomerates. The strength results were then verified by a number of methods which

indirectly tested the same strength. The strength data gained were compared with the strength of secondary agglomerates formed from the primary agglomerates. The comparison revealed that for Versal 250, the strength of primary agglomerates was similar to that of the corresponding secondary agglomerates; however for Versal 700, the strength of primary agglomerates was much higher than that of the corresponding secondary agglomerates. This suggested that structural failure of granular catalyst supports can also occur from the failure of the powder itself that is used to produce these supports.

Chapter 9 The difference between tablets produced from wet-milled and dry-milled γ-powder alumina

9.1   Idea behind the development

The purpose behind this section was to see if there would be any difference in strength between tablets from wet-milled and dry-milled γ-alumina, hence the difference in cohesive strength of catalyst layer produced from these types of γ-alumina.

9.2   Experimental method

The dry-milling of γ-alumina powder was performed using a jet mill. The particle size distribution of the dry-milled powder was d_{90} = 15.49 μm and d_{50} = 10.42 μm. The manufacturing of tablets from dry-milled γ-alumina powder was performed using the same procedure as outlined in 4.2.2 but using more concentrated acid and base solution. The concentration of acid and base was varied to see their effect on the strength of tablets produced. NaOH solution of 3M and 6 M, deionised water (which can be considered as zero concentration) and HCl solution of 3 M, 6 M and 10 M were used. The reason that more concentrated acid and base solutions were used can be described as follows. When dry-milled γ-alumina particles were made into a suspension and the pH of the suspension was adjusted, tablets formed from this suspension did not have any measurable strength. Therefore it was decided to mix dry-milled γ-alumina with a much higher concentration of H^+ and OH^- in order to make the strength measurement more practical. The same solid percentage of 40 wt% as in all previous chapters about catalyst layer was employed. In each experiment, 200 g of dry-milled γ-alumina powder was mixed with 300 g acid or basic solution.

9.3   Results and discussion

The cohesive strength of catalyst layer as determined by the tablet method using dry milled γ-alumina is shown in Figure 9.1.
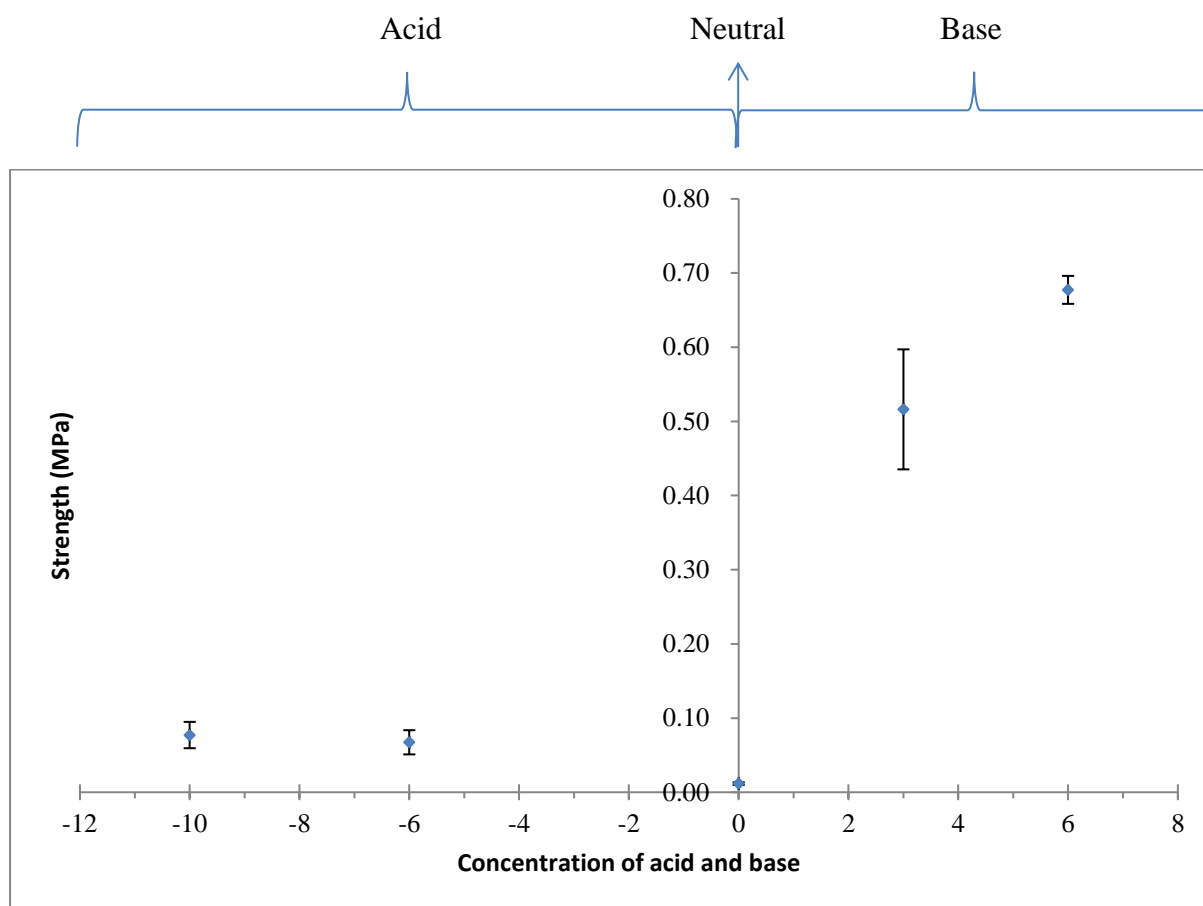
Figure 9.1 The cohesive strength of catalyst layer made from dry milled γ-alumina powder (positive sign stands for concentration of NaOH and negative sign stands for concentration of HCl) as tested by the tablet method

One obvious point to be noted on Figure 9.1 is that dry milled powder mixed with base produced much stronger tablets than that with acid and the higher the base concentration, the higher the cohesive strength. In addition, although an increase in the concentration of acid did increase the strength of tablets, the magnitude of increase was far lower than that observed with the base.

The other observation from Figure 9.1 was that the cohesive strength as measured by tablets produced from dry-milled γ-alumina powder was lower than that produced from wet-milled γ-alumina powder in general. The highest strength (around 0.68 MPa) obtained from the dry-milled powder is regarded as a low value for catalyst layer produced from wet-milled powder.

In terms of the cohesive strength results obtained by using HCl, the reason behind the finding can be attributed to the fact there is a lack of surface hydroxyl groups on dry-milled γ-alumina particles. Similar arguments were also proposed in [72]. The author suggested that a

149

surface reaction forming an aluminium monohydrate layer occurs during wet milling. A washing treatment to remove this hydrated layer was then used by this author and a reduction in the strength of compacted powder was noticed. Combining the results in [72] and the results in this thesis indicated that the presence of surface hydroxyl group on γ-alumina particles is the key to give rise to the cohesive strength for acidic conditions. The role played by hydroxyl group on the surface of γ-alumina particles in these conditions was quantitatively demonstrated in section 6.7 from a surface charging point of view. Similar argument can be used for the basic side of the cohesive strength. Due to the shortage of surface hydroxyl group, there should not be a large change in the cohesive strength. The current large increase in the cohesive strength obtained was therefore a result of the formation of water glass when a high amount of NaOH was used.

9.4 Online monitoring of drying of dry-milled γ-alumina suspension

9.4.1 Idea behind the measurement

In order to further understand the difference between γ-alumina suspension prepared between wet-milling and dry-milling, the online monitoring technique developed in section 6.6 was employed.

9.4.2 Experimental method

The dry-milled powder as presented in section 9.2 was mixed with deionised water to make suspension. The suspension had a solid content of 40%. The same procedure for online monitoring experiments and the following PIV determination as outlined in section 6.6.2 was applied for the suspension.

9.4.3 Results and discussion

The PIV results from the online monitoring experiments are presented below.
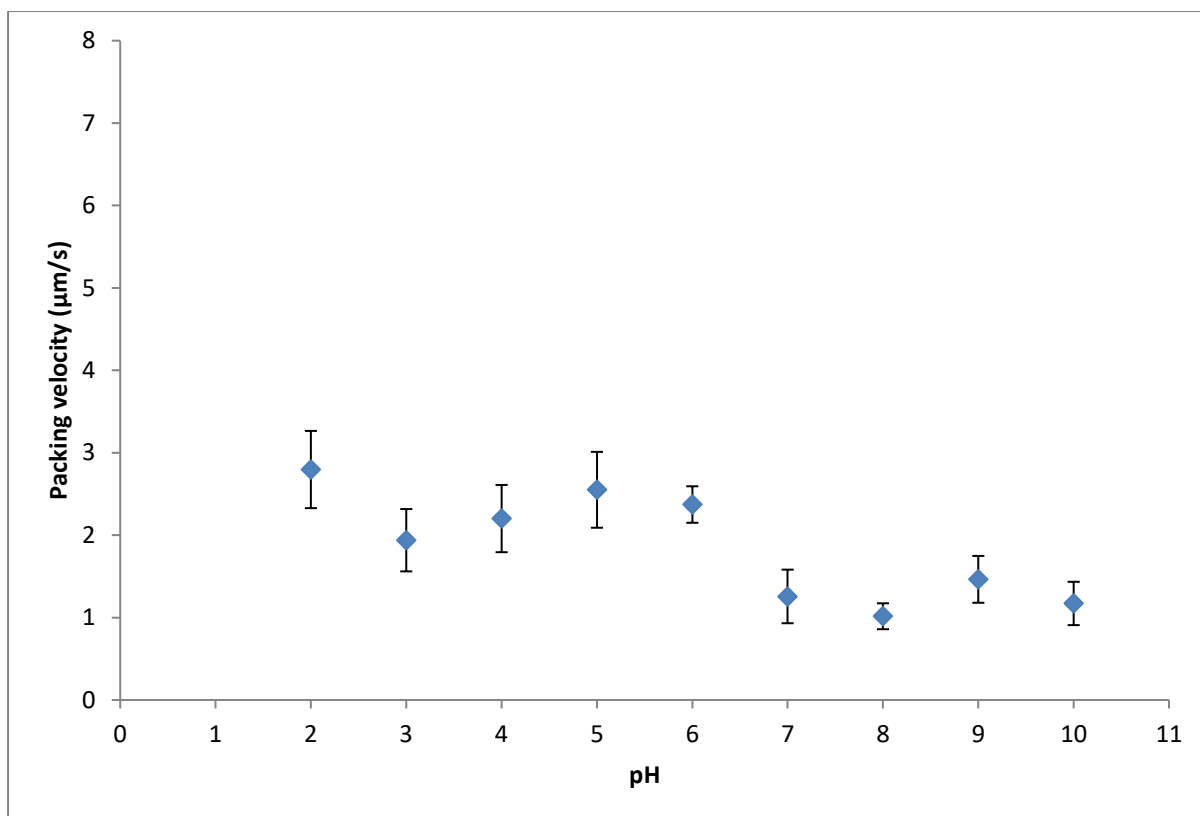
Figure 9.2 PIV results for suspension with dry-milled γ-alumina particles

As can be seen in Figure 9.2, dry-milled γ-alumina particles showed two distinct regions of particle packing velocity. From pH = 7 (inclusive) onwards, the particle packing velocity was reduced in general. Such finding is in close agreement with what was determined for wet-milled γ-alumina particles as shown in Figure 6.15. This further suggested that at pHs higher than the isoelectric point, γ-alumina particles tend to form a flocculated structure. The formation of the flocculated status would act to immobilise the γ-alumina particles as discussed in Chapter 6. Wet-milled γ-alumina particles were found to be completely stagnant at pHs higher than the isoelectric point; dry-milled γ-alumina particles were noted to have a reduced speed due to insufficient surface hydroxyl groups on them to encourage the formation of flocculated structure.

At pHs lower than the isoelectric point, movement of dry-milled γ-alumina particles was recorded. The interesting point to notice was that there was not any effect on the particle packing velocity for these particles as the pH was varied. This implied that dry-milled γ-alumina probably lacked surface hydroxyl groups because the presence of hydroxyl group was the key to the differing packing velocity of γ-alumina particles at different pHs as

discussed in section 6.7. The lack of surface hydroxyl groups on dry-milled γ-alumina particles was also argued in section 9.3 where the cohesive strength of catalyst layer made from dry-milled γ-alumina particles was measured.

9.5   Conclusion

In conclusion, the cohesive strength of catalyst layer made using dry-milled γ-alumina particles was measured in this chapter. The cohesive strength was found to be much lower than that of wet-milled γ-alumina particles. For the low cohesive strength at pHs lower than the isoelectric point, the reason was found to be a lack of hydroxyl group on the surface of dry-milled γ-alumina particles. PIV measurement demonstrated that dry-milled γ-alumina responded with zero effect on their mobility at varying pH conditions. Such argument found support in the literature as shown in [72]. With regards to the results for pHs higher than the isoelectric point, it was determined that the formation of flocculation of γ-alumina played an important role. The formation of flocculation partially immobilised γ-alumina particles as found in the PIV results. An increasing concentration of NaOH contributed to the increase in the cohesive strength due to a possible formation of water glass.

Chapter 10 Conclusions and future work

10.1 Revisit of research aims

Recalling the research aims identified from the literature, the research began with two purposes. The first task was to quantify the cohesive and adhesive strength of catalyst layer separately and report the strength based on unit of stress. The second task was to answer whether structural failure of granular catalyst support occurs within primary agglomerates or between primary agglomerates.

10.2 Cohesive strength of catalyst layer

To answer the research aims, a quantitative method to measure the cohesive strength of catalyst layer based on stress was developed. In this method, catalyst layer (produced by drying of a suspension consisting of wet-milled γ-alumina particles) was cast into a tablet shape by the use of a tablet die; the tensile strength of the tablet could then be regarded as the cohesive strength of the catalyst layer as they both measure the bonding strength between particles of the body. Disintegration test, penetration test and X-ray tomography were then employed to verify the cohesive strength results obtained. It was shown that these indirect methods generated results that supported the strength data gained.

The cohesive strength was found to vary to with pH and at low pH conditions and the tablets produced were noticed to split into a top and a bottom fragment. The reason behind the splitting was determined to a segregation process in which large particles sedimented to the bottom of the tablet die while small particles floated to the top of the die. In order to overcome this problem and obtain a more comprehensive profile of the cohesive strength versus pH, a uniform drying system was proposed. The uniform drying system was facilitated by using filter paper as the material to make tablet dies.

The cohesive strength for wet-milled γ-alumina particles was then successfully determined for a range of pH from 2 to 10 using HCl and NH_3 to adjust the pH. The use of NH_3 eliminated the possibility of water glass formation at high pHs as experienced in the early stage of the current research. The cohesive strength was correlated with viscosity of the suspension, extent of sedimentation of the suspension, particle packing velocity of γ-alumina

particles and charging behaviour of the wet-milled γ-alumina particles as predicted by the DLVO theory. These correlations suggested that at pHs lower than the isoelectric point (point of zero surface charge on the particles), a high electrostatic repulsion between γ-alumina particles when they are wet would lead to a high cohesive strength because of higher chance of particle rearrangement to form tight packing during drying. The high electrostatic repulsion can be directly demonstrated by a high particle packing velocity and indirectly shown by a low suspension viscosity and a low extent of sedimentation. For pHs at the isoelectric point or very close to it, tablets with random cracks were always obtained. This was a result of limited particle rearrangement during drying so that a loose packing with potential to develop random cracks was obtained. In terms of pHs higher than the isoelectric point, it was argued that γ-alumina particles tend to form flocculation. The formation of flocculation between γ-alumina particles was found to immobilise the particles during drying as demonstrated by measurement of particle velocity and suspension viscosity. However, with an increasing pH (or more OH⁻ groups), the cohesive strength was still found to improve probably due to an increasing level of charging.

The effect of particle size on the cohesive strength was also determined using the uniform drying system developed. It was found that a bimodal particle size distribution would improve the cohesive strength due to tighter packing. Crack formation would also be minimised if a sufficient amount of large particles are present. The use of small sized particles only would lead to formation of radial cracks on the tablets during drying at pHs lower than the isoelectric point. Such tablet cracking pattern was explained from the influence of drag force exerted by water on γ-alumina particles during drying.

The effect of drying rate on the cohesive strength was investigated using both the uniform drying system and the online monitoring technique developed. Same drying conditions were applied in both the uniform drying and the online monitoring experiments. The results suggested that a slower drying would lead to a higher cohesive strength. The reason behind the trend was found to be related to particle motion as the viscosity of the suspension and the extent of sedimentation hardly changed at different drying rates. The online monitoring experiments revealed that at a slower drying rate, the particle packing velocity of γ-alumina particles was also reduced. This suggested that the particulate system in the suspension was allowed for a longer time frame for favourable particle rearrangement to occur; the result of this prolonged timeframe for favourable particle rearrangement was an improvement on the cohesive strength. The opposite trend was also noticed. When a γ-alumina suspension was

exposed to a fast moving hot air stream, the γ-alumina particles were noticed to develop random packing under the online monitoring apparatus. It was anticipated that such packing could lead to a reduction in the cohesive strength.

An investigation was also performed on the difference between dry-milled γ-alumina particles and wet-milled γ-alumina particles. The findings suggested that the cohesive strength derived from dry-milled γ-alumina particles was much lower than that of wet-milled ones. The reason behind it was determined to a lack of surface hydroxyl groups on dry-milled γ-alumina particles. The explanation given also gained support in the literature where a surface reaction forming an aluminium monohydrate layer was proposed during wet-milling [72].

10.3 Adhesive strength of catalyst layer

A quantitative method to measure the adhesive strength of catalyst layer was also developed in the thesis to answer for the first research aim. The method works by detaching the catalyst layer by the use of a scraper. The adhesive strength was measured at different pHs and on three different substrates.

For both the metallic (FeCrAlloy discs) and cordierite substrate, the effect of pH on the adhesive strength was found to be similar to that of cohesive strength. At pH = 4, the adhesive strength peaked while a further increase in the pH to and above the isoelectric point resulted in the catalyst layer to completely detach itself from the substrate. The peak adhesive strength at pH = 4 was thought to be of similar reasons regarding good particle motion at this condition. The good particle mobility allowed more γ-alumina particles to pack closely at the interface between the catalyst layer and the substrate, leading to an increase in the adhesive strength. The detachment of catalyst layer at high pH conditions was found to be similar to the tablets shrinkage behaviour observed in the cohesive strength study. It shall be recalled that the tablets in the cohesive strength study at pHs higher than the isoelectric point were found to shrink and detach from the tablet wall.

Between the metallic and the cordierite substrate, the adhesive strength on the cordierite substrate was shown to be higher than that on the metallic one. The surface roughness profile of both types of substrate was quantified using surface roughness parameters R_a and R_z. The parameter indicates that the cordierite substrate was much rougher than the metallic one,

allowing more γ-alumina particles to adsorb on the surface roughness. The more γ-alumina particles adsorbed on the surface roughness would then give rise to a tighter packing at the interface between the substrate and the catalyst layer, leading to an increase in the adhesive strength.

The third type of substrate was chosen to be alumina powder bed. The powder bed was prepared by direct compression of boehmite powder of two different types followed by calcination. The effect of compression force was determined. It was found that a higher compression force would lead to a higher adhesive strength due to the fact that more small sized γ-alumina particles were allowed to pack at the interface as a result of the reduced bed porosity. As for the difference between the powder type, it was found that the boehmite powder with a higher particle strength always resulted in a lower adhesive strength; this could be understood as the weaker particle strength allowed for more mechanical deformation during direct compression, leave more small sized particles to pack at the interface between the substrate and the catalyst layer.

10.4 Granular catalyst support

To answer for the second research aim, a method to directly quantify the strength of primary agglomerate was developed. Strength data gained from this direct method were verified by a number of indirect methods such as disintegration, deformability and X-ray tomography. The same two types of boehmite powder (Versal 250 and Versal 700) that were used in the adhesive strength study were employed here. The strength measurement suggested that primary agglomerates of Versal 250 were weaker than that of Versal 700. Granulation of the two powders was then performed to produce actual granular catalyst support (also knowns as secondary agglomerates). The strength of granular catalyst support was then compared with that of primary agglomerates. It was found that the strength of primary agglomerates of Versal 250 was similar to that of granular catalyst support produced from this powder however the strength of primary agglomerates of Versal 700 was much higher than its corresponding granular catalyst support. This finding suggested that structural failure of granular catalyst support made of Versal 250 could occur both with the primary agglomerates and between the primary agglomerates while similar failure for granular catalyst support made of Versal 700 is more likely to occur between primary agglomerates. The implication

of the finding for a wider granulation community is that for granules formed from powder which is pre-agglomerated, the strength of primary agglomerates cannot be ignored when considering the strength of granules.

10.5 Highlights of the research

The highlight of the research lied mainly on the development of the two methods to quantify the cohesive and the adhesive strength of the catalyst layer. As identified in the literature review, most publications that are concerned with the strength of catalyst layer suffered from two weaknesses. They either tested the strength of catalyst layer by using a method which cannot differentiate between the cohesive strength and the adhesive strength or failed to report the strength based on the unit of stress. Most publications report strength based on mass loss of the catalyst layer after being placed in an ultrasonic bath or a thermal shock reactor; it was argued that such measurement is prone to the testing environment, e.g. a different setting in the ultrasonic bath may alter the mass loss data although the actual strength of the catalyst layer may be the same. The scientific understanding developed from using these methods to test the strength of catalyst layer at different conditions then added more scientific value to the methods developed.

10.6 Future work

10.6.1 Further work on methodology

Based on the development work reached in this thesis, the future work of the thesis was planned to further advance the cohesive and the adhesive strength method. The following suggestion was first of all made as can be seen in the Figure 10.1. In this method, the scraper is allowed to both cut through the catalyst layer within the layer itself and at the interface between the catalyst layer and the substrate. In this way, both the cohesive and the adhesive strength can be obtained in a single experimental setup.
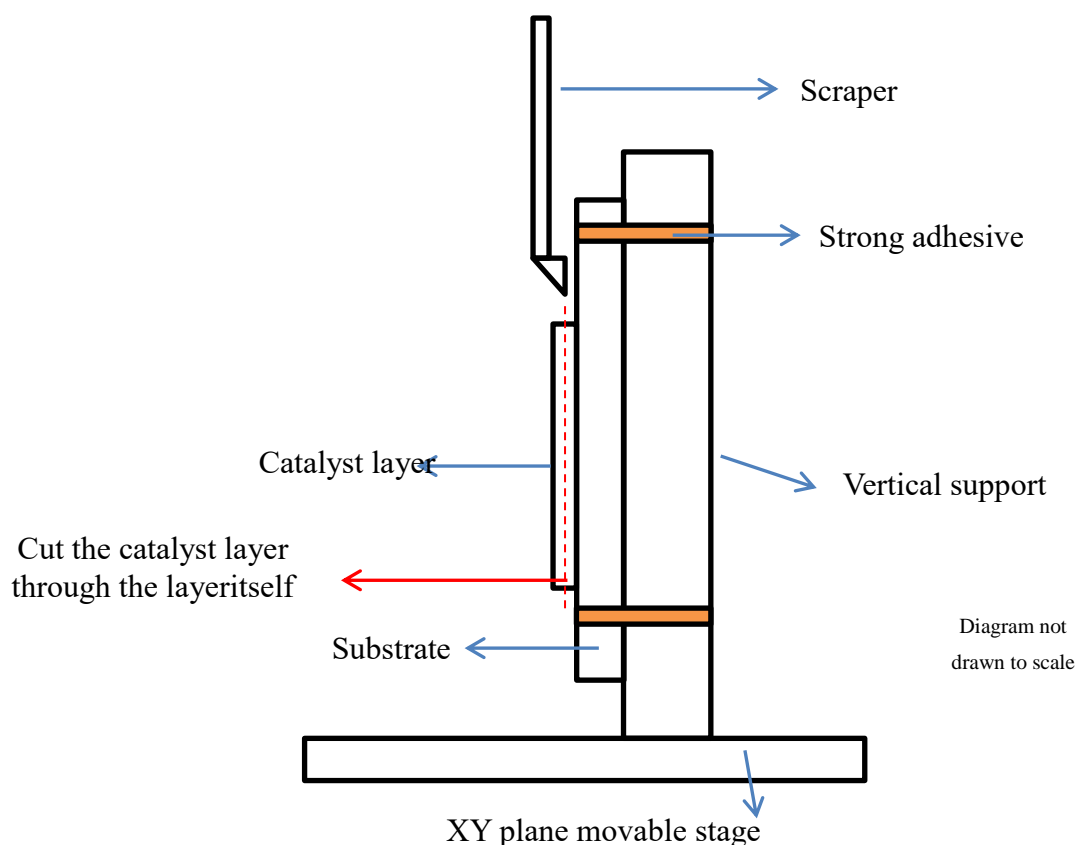
Figure 10.1 The proposed experimental setup to obtain cohesive strength of coating in a shearing nature

In order to further advance the utility of the techniques developed, it would also be useful to see how small the scraper can be made so that the testing device can be used in an actual catalytic converter straightaway.

10.6.2 Further work on scientific understanding

As the main line of the thesis in the area of catalyst layer focussed on developing understanding of fundamental particle behaviour in relation to the cohesive and adhesive strength resulted, one part of the future work to further advance this line could be to see the effect of additives on these strengths. The focus of the further work would be to apply the methodology already developed in this thesis to evaluate how different types of additives such as viscosity agent and dispersion agent and how their different concentrations would manipulate particle rearrangement process during suspension drying; thus the effect of the selected additives on the two strengths of catalyst layer can be found.

Following separate evaluation of cohesive and adhesive strength of a wide range of preparation parameters in unit of stress, a regime map can be made by designing physically meaningful dimensionless groups to incorporate all of the preparation parameters. The creation of such regime maps would offer guidance for researchers and industry to achieve optimum strength profile for their catalyst layers.

In the comparative study of dry-milled and wet-milled γ-alumina particles, it was determined that wet-milled γ-alumina possess more surface hydroxyl groups. It would be helpful to investigate how dry-milled γ-alumina particles can also be made to have such surface hydroxyl groups, e.g. by immersing them in water for a prolonged time. Understanding developed in respect of the mechanism of the formation of surface hydroxyl groups would then aid the design of wet-milling processes to produce wet-milled γ-alumina particles highly responsive to pH and drying rate influence.

In terms of the adhesive strength study specifically, the current thesis can still be expanded into more types of substrate, in particular alumina substrate. This is because adhesive strength work performed using alumina substrate could have an implication on how granular catalyst support behave in packed bed columns. As mentioned in the introduction (section 1.2.2) that many granular catalyst support would also be coated with a catalyst layer, adhesive strength measurement based on alumina substrate tailored to represent the surface of granular catalyst support actually in operation can be highly beneficial.

Nomenclature

Latin letters

Symbol	Meaning
d	diameter
d_{10}	the 10th percentile particle diameter
d_{50}	the 50th percentile particle diameter
d_{90}	the 90th percentile particle diameter
L	length
L/S	liquid solid ratio
p	pressure
PGM	precious group metal
SEM	scanning electron microscopy
u	velocity

Greek letters

Symbol	Meaning
ε	porosity
μ	viscosity
ρ	density

Subscript

Symbol	Meaning
p	particle
s	superficial

References

1. Caiazzo, F., et al., *Air pollution and early deaths in the United States. Part I: Quantifying the impact of major sectors in 2005.* Atmospheric Environment, 2013. **79**(0): p. 198-208.

2. Acres, G.J.K. and B. Harrison, *The Development of Catalysts for Emission Control from Motor Vehicles: Early Research at Johnson Matthey.* Topics in Catalysis, 2004. **28**(1-4): p. 3-11.

3. Georgios, N.P., *Modelling, reaction schemes and kinetic parameter estimation in automotive catalytic converters and diesel particulate filters*, in *Department of mechanical and industrial engineering*. 2003, Aristotle University Thessaloniki.

4. Islam, K.M.N., J. Hildenbrand, and M.M. Hossain, *Life cycle impacts of three-way ceramic honeycomb catalytic converter in terms of disability adjusted life year.* Journal of Cleaner Production, 2018.

5. Twigg, M.V., *Progress and future challenges in controlling automotive exhaust gas emissions.* Applied Catalysis B: Environmental, 2007. **70**(1–4): p. 2-15.

6. Cooper, J. and J. Beecham, *A Study of Platinum Group Metals in Three-Way Autocatalysts.* Platinum Metals Review, 2013. **57**(4): p. 281-288.

7. Berger, A., O. Hatling, and D. Rodriguez-Ortiz. *Three way catalytic converter*. 2009 [cited 2014 22]; Available from: http://www.cchem.berkeley.edu/molsim/teaching/fall2009/catalytic_converter/bkgcat con.html.

8. Avila, P., M. Montes, and E.E. Miró, *Monolithic reactors for environmental applications: A review on preparation technologies.* Chemical Engineering Journal, 2005. **109**(1–3): p. 11-36.

9. Cybulski, A. and J.A. Moulijn, *Structured catalysis and reactors*. 2nd ed. 2006, London: Taylor & Francis.

10. Holt, E.M., *The properties and forming of catalysts and absorbents by granulation.* Powder Technology, 2004. **140**(3): p. 194-202.

11. Santana, A., et al., *Vegetable fat hydrogenation in supercritical-fluid solvents: Melting behavior analysis by DSC and NMR.* The Journal of Supercritical Fluids, 2008. **46**(3): p. 322-328.

12. Agudelo, J.L., et al., *On the effect of EDTA treatment on the acidic properties of USY zeolite and its performance in vacuum gas oil hydrocracking.* Applied Catalysis A: General, 2014. **488**(0): p. 219-230.

13. Ahmad, R., J.-H. Ha, and I.-H. Song, *Enhancement of the compressive strength of highly porous Al2O3 foam through crack healing and improvement of the surface condition by dip-coating.* Ceramics International, 2014. **40**(2): p. 3679-3685.

14. Agrafiotis, C. and A. Tsetsekou, *The effect of powder characteristics on washcoat quality. Part I: Alumina washcoats.* Journal of the European Ceramic Society, 2000. **20**(7): p. 815-824.

15.   Agrafiotis, C., et al., *Evaluation of sol-gel methods for the synthesis of doped-ceria environmental catalysis systems. Part I: preparation of coatings.* Journal of the European Ceramic Society, 2002. **22**(1): p. 15-25.

16.   Degenstein, N.J., R. Subramanian, and L.D. Schmidt, *Partial oxidation of n-hexadecane at short contact times: Catalyst and washcoat loading and catalyst morphology.* Applied Catalysis A: General, 2006. **305**(2): p. 146-159.

17.   Fornasiero, P., et al., *Development of functionalized Fe–Al–Cr alloy fibers as innovative catalytic oxidation devices.* Catalysis Today, 2008. **137**(2–4): p. 475-482.

18.   Santos, P.S., H.S. Santos, and S.P. Toledo, *Standard transition aluminas. Electron microscopy studies.* Materials Research, 2000. **3**(4): p. 104-114.

19.   Chen, C. and W.-S. Ahn, *CO2 capture using mesoporous alumina prepared by a sol–gel process.* Chemical Engineering Journal, 2011. **166**(2): p. 646-651.

20.   Bauer, R., et al., *Transitional alumina particulate materials having controlled morphology and processing for forming same.* 2012, Google Patents.

21.   Osment, H.E., *Method of producing active alumina.* 1965, Google Patents.

22.   Adegbite, S., *Coating of catalyst supports: links between slurry characteristics, coating process and final coating quality.* 2010.

23.   Cheng, J.T. and P.D. Ellis, *Adsorption of rubidium (1+) to. gamma.-alumina as followed by solid-state rubidium-87 NMR spectroscopy.* The Journal of Physical Chemistry, 1989. **93**(6): p. 2549-2555.

24.   Deo, A.V., T.-T. Chuang, and I.G. Dalla Lana, *Infrared studies of adsorption and surface reactions of some secondary alcohols, C3 to C5, on. gamma.-alumina and. gamma.-alumina doped with sodium hydroxide.* The Journal of Physical Chemistry, 1971. **75**(2): p. 234-239.

25.   Peintinger, M.F., M.J. Kratz, and T. Bredow, *Quantum-chemical study of stable, meta-stable and high-pressure alumina polymorphs and aluminum hydroxides.* Journal of Materials Chemistry A, 2014. **2**(32): p. 13143-13158.

26.   Yazdanmehr, M., et al., *Electronic structure and bandgap of γ-Al 2 O 3 compound using mBJ exchange potential.* Nanoscale research letters, 2012. **7**(1): p. 488.

27.   Kumagai, M. and G.L. Messing, *Controlled transformation and sintering of a boehmite sol‐gel by α‐alumina seeding.* Journal of the American Ceramic Society, 1985. **68**(9): p. 500-505.

28.   Constantin, L.A., et al., *Semiclassical atom theory applied to solid-state physics.* Physical Review B, 2016. **93**(4): p. 045126.

29.   Housecroft, C.E. and E.C. Constable, *An Introduction to organic, inorganic and physical chemistry.* 2003, New York: Prentice Hall.

30.   Zhao, S., et al., *A method to form well-adhered γ-Al2O3 layers on FeCrAl metallic supports.* Surface and Coatings Technology, 2003. **167**(1): p. 97-105.

31.   Germani, G., et al., *Preparation and characterization of porous alumina-based catalyst coatings in microchannels.* Chemical Engineering Science, 2007. **62**(18–20): p. 5084-5091.

32. Ruhi, G., et al., *Wear and electrochemical characterization of sol-gel alumina coating on chemically pre-treated mild steel substrate.* Surface and Coatings Technology, 2006. **201**(3–4): p. 1866-1872.

33. Roth, T., K.H. Kloos, and E. Broszeit, *Structure, internal stresses, adhesion and wear resistance of sputtered alumina coatings.* Thin Solid Films, 1987. **153**(1–3): p. 123-133.

34. Kukolev, G.V. and A.G. Karaulov, *The properties of water suspensions of commercial alumina and rational conditions for slip casting.* Refractories, 1963. **4**(3-4): p. 184-191.

35. Giani, L., et al., *Washcoating method for Pd/γ-Al2O3 deposition on metallic foams.* Applied Catalysis B: Environmental, 2006. **62**(1–2): p. 121-131.

36. Jia, J., et al., *The influence of preparative parameters on the adhesion of alumina washcoats deposited on metallic supports.* Applied Surface Science, 2007. **253**(23): p. 9099-9104.

37. Valentini, M., et al., *The deposition of γ-Al2O3 layers on ceramic and metallic supports for the preparation of structured catalysts.* Catalysis Today, 2001. **69**(1–4): p. 307-314.

38. Sun, H., et al., *Preparation of well-adhered γ-Al2O3 washcoat on metallic wire mesh monoliths by electrophoretic deposition.* Applied Surface Science, 2007. **253**(6): p. 3303-3310.

39. Yang, K.S., Z. Jiang, and J. Shik Chung, *Electrophoretically Al-coated wire mesh and its application for catalytic oxidation of 1,2-dichlorobenzene.* Surface and Coatings Technology, 2003. **168**(2–3): p. 103-110.

40. Jiang, P., et al., *Preparation and properties of a γ-Al2O3 washcoat deposited on a ceramic honeycomb.* Surface and Coatings Technology, 2005. **190**(2-3): p. 314-320.

41. Livage, J., M. Henry, and C. Sanchez, *Sol-gel chemistry of transition metal oxides.* Progress in solid state chemistry, 1988. **18**(4): p. 259-341.

42. Agrafiotis, C. and A. Tsetsekou, *The effect of powder characteristics on washcoat quality. Part II: Zirconia, titania washcoats — multilayered structures.* Journal of the European Ceramic Society, 2000. **20**(7): p. 825-834.

43. Jia, L., M. Shen, and J. Wang, *Preparation and characterization of dip-coated γ-alumina based ceramic materials on FeCrAl foils.* Surface and Coatings Technology, 2007. **201**(16–17): p. 7159-7165.

44. Peela, N.R., A. Mubayi, and D. Kunzru, *Washcoating of γ-alumina on stainless steel microchannels.* Catalysis Today, 2009. **147, Supplement**(0): p. S17-S23.

45. Blachou, V., D. Goula, and C. Philippopoulos, *Wet milling of alumina and preparation of slurries for monolithic structures impregnation.* Industrial & Engineering Chemistry Research, 1992. **31**(1): p. 364-369.

46. Novak, S. and K. König, *Fabrication of alumina parts by electrophoretic deposition from ethanol and aqueous suspensions.* Ceramics International, 2009. **35**(7): p. 2823-2829.

47. Agrafiotis, C. and A. Tsetsekou, *The effect of processing parameters on the properties of γ-alumina washcoats deposited on ceramic honeycombs.* Journal of Materials Science, 2000. **35**(4): p. 951-960.

48.   Russel, W.B., D.A. Saville, and W.R. Schowalter, *Colloidal dispersions*. 1989: Cambridge university press.

49.   Abdelrasoul, A., H. Doan, and A. Lohi, *Fouling in Membrane Filtration and Remediation Methods*. 2013.

50.   Johnson, W.C. and P.T. Panousis, *The influence of Debye length on the CV measurement of doping profiles.* IEEE transactions on electron devices, 1971. **18**(10): p. 965-973.

51.   Meille, V., et al., *Deposition of -Al2O3 layers on structured supports for the design of new catalytic reactors.* Applied Catalysis A: General, 2005. **286**(2): p. 232-238.

52.   Wu, X., et al., *Structure and performance of γ-alumina washcoat deposited by plasma spraying.* Surface and Coatings Technology, 2001. **145**(1–3): p. 226-232.

53.   Fei, W., et al., *Sol Gel Alumina Coating On Fe–Cr–Al–Y Fibre Media for Catalytic Converters.* Surface engineering, 2003. **19**(3): p. 189-194.

54.   Maione, A., F. André, and P. Ruiz, *The effect of Rh addition on Pd/γ-Al2O3 catalysts deposited on FeCrAlloy fibers for total combustion of methane.* Applied Catalysis A: General, 2007. **333**(1): p. 1-10.

55.   Pérez, N.C., E.E. Miró, and J.M. Zamaro, *Cu, Ce/mordenite coatings on FeCrAl-alloy corrugated foils employed as catalytic microreactors for CO oxidation.* Catalysis Today, 2013. **213**: p. 183-191.

56.   Moseley, P.T., et al., *The microstructure of the scale formed during the high temperature oxidation of a fecralloy steel.* Corrosion Science, 1984. **24**(6): p. 547-565.

57.   Shafiee Afarani, M., A. Samimi, and E. Bahadori Yekta, *Synthesis of alumina granules by high shear mixer granulator: Processing and sintering.* Powder Technology, 2013. **237**(0): p. 32-40.

58.   Saleh, K., L. Vialatte, and P. Guigon, *Wet granulation in a batch high shear mixer.* Chemical Engineering Science, 2005. **60**(14): p. 3763-3775.

59.   Buelna, G. and Y.S. Lin, *Sol–gel-derived mesoporous γ-alumina granules.* Microporous and Mesoporous Materials, 1999. **30**(2–3): p. 359-369.

60.   Liu, P., et al., *Preparation of high purity spherical γ-alumina using a reduction-magnetic separation process.* Journal of Physics and Chemistry of Solids, 2008. **69**(4): p. 799-804.

61.   Lin, C.-S. and S.-T. Lin, *Effects of granule size and distribution on the cold isostatic pressed alumina.* Journal of Materials Processing Technology, 2008. **201**(1–3): p. 657-661.

62.   Twigg, M.V., *The Catalyst Handbook*. 2nd ed. 1996: Manson Publishing Ltd.

63.   Adams, M.J., M.A. Mullier, and J.P.K. Seville, *Agglomerate strength measurement using a uniaxial confined compression test.* Powder Technology, 1994. **78**(1): p. 5-13.

64.   Rajkumar, A.D., et al., *Investigating the effect of processing parameters on pharmaceutical tablet disintegration using a real-time particle imaging approach.* European Journal of Pharmaceutics and Biopharmaceutics, 2016. **106**: p. 88-96.

65.   Ai, Q., et al., *Developing a miniaturized approach for formulation development using twin screw granulation.* Powder Technology, 2016. **300**: p. 83-91.

66. Singh, B.P., et al., *Stability of dispersions of colloidal alumina particles in aqueous suspensions.* Journal of Colloid and Interface Science, 2005. **291**(1): p. 181-186.

67. López Valdivieso, A., et al., *Temperature effect on the zeta potential and fluoride adsorption at the α-Al2O3/aqueous solution interface.* Journal of Colloid and Interface Science, 2006. **298**(1): p. 1-5.

68. Dhenge, R.M., et al., *Twin screw granulation: effect of powder feed rate.* Advanced Powder Technology, 2011. **22**(2): p. 162-166.

69. Yokosawa, M.M., V.C. Pandolfelli, and E. Frollini, *Influence of pH and Time on the Stability of Aqueous Alumina Suspensions Containing Sodium Polyacrylates: A Revisited Process.* Journal of Dispersion Science and Technology, 2002. **23**(6): p. 827-836.

70. Franks, G.V. and Y. Gan, *Charging Behavior at the Alumina–Water Interface and Implications for Ceramic Processing.* Journal of the American Ceramic Society, 2007. **90**(11): p. 3373-3388.

71. Gadelmawla, E.S., et al., *Roughness parameters.* Journal of Materials Processing Technology, 2002. **123**(1): p. 133-145.

72. Bennett, R.B.N., D.E. , *Effect of Surface Chemical Reactions during Wet Milling of Alumina.* 1972.